Modelling Single Cell Dynamics of Protein Networks associated with Synaptic Plasticity

by

Yao He

A thesis submitted in partial fulfilment

of the requirements for the Degree of

Doctor of Philosophy

in Computational Systems Biology

at

Lincoln University

New Zealand

2015

Abstract of a thesis submitted in partial fulfilment of the

requirements for the Doctor of Philosophy

Modelling Single Cell Dynamics of Protein Networks associated with Synaptic Plasticity

by Yao He

Synaptic plasticity, an emergent property of the synaptic networks, has shown strong correlation to one of the essential functions of the brain, memory formation. Through understanding synaptic plasticity, we may discover the modulators and mechanisms which trigger memory formation. Mathematical models and computational methods show incredible potential in advancing the understanding of the complex behaviour of biological systems, which may be very difficult to understand using in vitro experiments. In this study, we develop the mathematical models of synaptic plasticity and analyse these models using computational methods to understand the dynamic behaviour of synaptic plasticity as well as the linkages to memory formation.

In the first part, we develop a simplified mathematical model of the NMDAR-mediated pathway of synaptic plasticity. The model is focused on the Ca^{2+} induced dynamics of modulators in the emergence of synaptic plasticity. The model is developed based on the essential synaptic modulators selected from the literature, but maintains the essential features of the modulators and the pathways. Importantly, this model shows the bidirectional behaviour of synaptic plasticity facilitated by the interactions among the modulators using the experimentally estimated kinetic parameters. Analysis of the dynamic behaviour of the model provides us with insights into the effective timescales of the modulators and an overall view of the main factors of the bidirectional behaviour. Using these information, we propose a hypothesised model of the memory system.

In the second part, we develop a theoretical model of the state transition of CaMKII, an important player for the induction of long term potentiation (LTP). This model includes the holoenzyme state transition of CaMKII and establishes a probabilistic framework

for the binding between CaMKII and NMDAR. Through the analysis of the model using computational methods, we gain insights into the relationships among the autophosphorylation of CaMKII, the formation of CaMKII-NMDAR complex and LTP. Moreover, we study the implication of the autophosphorylation in LTP, which has diverse conclusions in the literature.

Keywords: synaptic plasticity, long term potentiation, long term depression, bidirectional behaviour, CaMKII, autophosphorylation, CaMKII-NMDAR complex, mathematical model, ordinary differential equations, parameter estimation, parameter sensitivity analysis.

Publication and Presentations

Refereed Journal Papers Related to Synaptic Plasticity

- **He, Y.**, Kulasiri, D., Samarasinghe, S., 2014. Systems biology of synaptic plasticity: a review on N-methyl-D-aspartate receptor mediated biochemical pathways and related mathematical models. Biosystems. 122, 7–18.
- **He, Y.**, Kulasiri, D., Samarasinghe, S., 2015. Modelling the dynamics of CaMKII-NMDAR complex related to memory formation in synapses: The possible roles of threonine 286 autophosphorylation of CaMKII in long term potentiation. J. Theor. Biol. 365, 403–19.

Refereed Journal Papers Related to Methodology

- Kulasiri, D., **He, Y.**, Samarasinghe, S., 2011. Robustness of circadian rhythms in the presence of molecular fluctuations: an investigation based on a mechanistic, statistical theory and a simulation algorithm. Biosystems. 106, 57–66.

Conference Presentations

- Yao He and Don Kulasiri, "Dimensionless Modelling of Early Phase Synaptic Plasticity Based on the Calcium-Dependent Switch", BIT's 4th Annual World DNA and Genome Day 2013, page 053, Nanjing, China, April, 2013
- Lincoln University Postgraduate Conference, 2013
  Dimensionless Modelling of Early Phase Synaptic Plasticity Based on the Calcium-Dependent Switch

Acknowledgements

First and foremost, I would like to express profound gratitude to Professor Don Kulasiri, my supervisor, mentor and friend. This study could not have succeeded without his support, encouragement, supervision and suggestions. I would also express deepest thanks to my associate-supervisor Professor Sandhya Samarasinghe for sharing her invaluable ideas and suggestions during this study. Their comprehensive guidance makes me not only a better independent researcher, but also a better thinker beyond academics.

It is an enjoyable time sharing with the wonderful people in C-fACS (Centre for Advanced Computational Solutions) team and I would like to thank you all for your company and encouragement. Particularly, I would like to thank Dr. Hong Ling for her continued sharing of ideas and discussions as well as her help at the initiation of my study; Dr. Zhongkun Zhou for his friendship as well as the insightful lunch discussions every day; and Jingyi Liang for her trust and cooperation in accomplishing the challenging research tasks.

I would like to express my appreciation to Lincoln University for providing the Lincoln Postgraduate and Lincoln University Doctoral Scholarships.

Finally, I sincerely thank my parents and my girlfriend for their constant love, dedication and encouragement throughout my study and life, especially for the company and inspiration that kept me going during the hard time of Canterbury earthquake.

Table of Contents

Figures

Tables

Abbreviations

Terminology

AC	adenylyl cyclase
AKAP	A-kinase anchoring proteins
AMPAR	a-amino-3-hydroxy-5-methyl-4-isoxazole propionic acid
AMP	adenosine monophosphate
ATP	adenosine triphosphate
CaM	calmodulin
CaMKII	calcium/calmodulin-dependent protein kinase II
cAMP	cyclic adenosine monophosphate
CC	correlation coefficient
E-LTP	early phase long-term potentiation
I1	inhibitor 1
EPSC	excitatory postsynaptic current
EPSP	excitatory postsynaptic potential
HFS	high frequency stimulations
HS	holoenzyme states of CaMKII holoenzyme
HST	holoenzyme state transition of CaMKII holoenzyme
IS	inner states of CaMKII subunit
IST	inner state transition of CaMKII subunit
LFS	low frequency stimulations
LHS	Latin hypercube sampling
L-LTP	late phase long-term potentiation
LSA	local sensitivity analysis
LTP	long-term potentiation
LTD	long-term depression
MAGUK	membrane-associated guanylate kinase
MAPK	mitogen-activated protein kinase
MCMC	Markov chain Monte Carlo
NMDAR	N-methyl-D-aspartate receptor
NR1	NR1 subunit of NMDAR
NR2A/B	NR2A/NR2B subunit of NMDAR
pBS	potential binding sites
PCC	partial correlation coefficient
PDE	phosphodiesterase
PIP_2	acidic phospholipid phosphatidylinositol-4,5-bisphosphate
PKA	protein kinase A/cyclic AMP-dependent protein kinase
PKC	protein kinase C
PRCC	partial ranking correlation coefficient

PP1	protein phosphatase 1
PP2a	protein phosphatase 2a
PP2b	protein phosphatase 2b; calcinuerin
PSD	postsynaptic density
Ser831	serine 831 residue of AMPAR
Ser845	serine 845 residue of AMPAR
ST	state transition
T286	threonine 286 residue of CaMKII
T305/306	threonine 305/306 residues of CaMKII
TARP	transmembrane AMPAR regulatory protein
TBS	theta burst stimulation

Model variables

Ca^{2+}	intracellular calcium ion
CaCaM	one Ca^{2+} ion bound to CaM
Ca_2CaM	two Ca^{2+} ions bound to CaM
Ca_3CaM	three Ca^{2+} ions bound to CaM
Ca_4CaM	Ca^{2+}/CaM complex
CaM/iCaM	CaM without Ca^{2+} bound
CaMAC1	Ca^{2+}/CaM complex bound to AC isoform type 1
CaMAC8	Ca^{2+}/CaM complex bound to AC isoform type 8
CaMCaMKII	Ca^{2+}/CaM complex bound to CaMKII subunit
CaMCaMKII*	autophosphorylated CaMKII subunit
CaMKII*	CaM dissociated autophosphorylated CaMKII
CaMKIIS	CaMKII with NMDAR bound to S site of a CaMCaMKII
CaMKII*S	CaMKII with NMDAR bound to S site of a CaMCaMKII*
CaMKII*T	CaMKII with NMDAR bound to T site of any active subunit
Ca_4CaNB	small activated PP2b
CaMCaNA	full activated PP2b
cAMP	active cAMP
CaMPDE1	Ca^{2+}/CaM complex bound to PDE isoform type 1
EoPSD	CaMKII holoenzymes outside of PSD
EiPSD	NMDAR unbound CaMKII holoenzymes inside of PSD
iAC1	inhibited AC isofrom type 1
iAC8	inhibited AC isofrom type 8
iCaMKII	inhibited CaMKII subunit
iPDE1	inhibited PDE isoform type 1
iPP2b	inhibited PP2b
NMDARu	unbound NMDAR
PDE4B	unphosphorylated PDE isoform type 4B
PDE4D	unphosphorylated PDE isoform type 4D

$PDE4B^*$	phosphorylated PDE isoform type 4B by PKA
$PDE4D^*$	phosphorylated PDE isoform type 4D by PKA
PKAc	released PKA catalytic subunit
PP1	active PP1
R_2C_2	unreleased PKA complex
R_2cAMP_2	unreleased PKA complex bound to 2 cAMP
R_2cAMP_4	unreleased PKA complex bound to 4 cAMP
$I1^*PP1$	phosphorylated I1 bound to PP1

Chapter 1: Introduction

1.1 Characteristics of synaptic plasticity

A synapse, the transmission tunnel between two neurons, facilitates a one-way, unidirectional signal transduction, named synaptic transmission (see Section 2.1 for a brief description of or Appendix A for the details of the synaptic transmission), to deliver information from pre- to post- synaptic neurons in response to environmental stimulus. The transmission is accommodated by a simple synaptic structure (presynaptic axonal terminal; synaptic cleft; and postsynaptic dendritic spine) and mediated by neurotransmitters, which are released by the presynaptic neuron, diffuse across the synaptic cleft and trigger a response of the postsynaptic neuron. One marvellous ability of the synapse is the dynamical modulation of its synaptic strength, which reflects the degree of association between the environmental stimulus and the magnitude of the induced postsynaptic response by the synaptic transmission, by a complex synaptic process, called synaptic plasticity (Bliss and Collingridge, 1993).

Synaptic plasticity integrates the dynamics as well as the interactions of the three parts of the synapse that leads to alterations on the core components of synaptic transmission. The possible alterations by synaptic plasticity are related to the neurotransmitter release probability into the synaptic cleft and the efficiency of the postsynaptic neuron responding to neurotransmitters (Citri and Malenka, 2007). As a result, synaptic plasticity is a systematic process facilitated by the cooperation among several mechanisms including the neurotransmitter dynamics in the presynaptic neuron; the neurotransmitter/receptor interactions in the synaptic cleft; and the receptor trafficking, membrane dynamics, intracellular signalling transduction in the postsynaptic neuron.

Why is synaptic plasticity important? Direct evidence shows that antagonists or gene mutations related to synaptic plasticity impair memory formation (Bourtchuladze et al.,

1994; Chang et al., 1999; Davis et al., 1992; Giese et al., 1998; Morris, 1989; Silva et al., 1992a, 1992b). The exact relationship between synaptic plasticity and memory formation is far from completely understood. But, current understanding suggests that memory formation is experience dependent and has strong correlation to synaptic activities. Memory may store in the synaptic strength of the complex nervous network of the brain, which consists of billions of neurons connected by trillions of synapses (Anderson, 2000; Isaac et al., 1995). One hypothesis based on Hebbian theory (Hebb, 2002) states that the brain 'remembers' the experiences of an environmental stimulus as memory by selectively adapting synaptic strength of the synapses among the activated neurons in response to the stimulus (Lisman, 1989). As a result, the neurons are wired up as a cell assembly (Bear et al., 2007). The cell assembly recognises the environmental stimulus at the next occurrence. A good example is the hippocampal spatial neurons. Spatial neurons within a cell assembly fire together at a particular place to orient the location of the organism (Shapiro, 2001). Although the hypothesis may be too simple to account for different types of memories, it indicates, together with the experimental observations, neuronal functions rely on the connections (synapses) among the neurons within the cell assembly. Hence, synaptic plasticity, which participates in the synapse formation (Engert and Bonhoeffer, 1999; Morgado-Bernal, 2011), is critically important to neuronal functions.

The processes involved in synaptic plasticity have drawn wide interests from neuroscientists over the last two decades. Synaptic plasticity has multiple forms depending on the brain region and neuron type, while the mechanisms, expressing sites and expressing targets are different among them (reviewed in Citri and Malenka (2007)). The most studied form is hippocampal N-methyl-D-aspartate receptor (NMDAR)-dependent synaptic plasticity due to the extensive experimental investigations in this critical area of memory system. For this particular form, synaptic plasticity induces long lasting bidirectional modulations of the postsynaptic response when the area is stimulated by electrical stimulations (Bliss and Lømo, 1973; Bliss and Collingridge, 1993; Dudek and Bear, 1992). The postsynaptic response is defined as the magnitude

of the postsynaptic receptor mediated current (EPSC) or excitatory postsynaptic potential (EPSP), in relation to their basal levels in vivo (Bliss and Lømo, 1973; Dudek and Bear, 1992), and the major postsynaptic receptors in hippocampal neurons are glutamatergic receptors, including NMDAR and A-amino-3-hydroxy-5-methyl-4-isoxazole propionic acid receptor (AMPAR).

NMDAR-dependent synaptic plasticity requires the activation of NMDAR to induce a sequence of postsynaptic activities to alter the property of AMPAR (see Chapter 2 for the explanation), which controls the magnitude of the postsynaptic response induced by the synaptic transmission in hippocampal neurons (Ahmad et al., 2012; Lee et al., 2000; Lüscher and Malenka, 2012). The activated NMDAR triggers a rapid Ca^{2+} influx leading to an elevation in the intracellular Ca^{2+} level. The degree of the Ca^{2+} elevation determines the direction of the alteration on AMPAR and hence causes the corresponding increase or decrease of the magnitude of the postsynaptic response (Bear et al., 1987; Lisman, 1989; Yang et al., 1999). Specific terms are used to describe the bidirectional modulations: potentiation denotes an increase of the postsynaptic response, and depression denotes a decrease of the postsynaptic response.

Two sub forms of NMDAR-dependent synaptic plasticity contain the later stages that last very long from hours to days that are named long term potentiation (LTP) (Bliss and Lømo, 1973) and long term depression (LTD) (Dudek and Bear, 1992). The characteristic of the later stage is the outlasting activities after the vanishing of the Ca^{2+} signal. During the later stage, it is known that an alteration on gene expressions is required to retain the changes on synaptic system by the earlier stage and the alteration on gene expressions may remodel the structure of the synapse (Engert and Bonhoeffer, 1999), possibly through modulating actin dynamics (Shoji-Kasai et al., 2007). Therefore, the distinct periods, early phase and late phase, are defined to distinguish the time frames with or without alterations on gene expressions during synaptic plasticity (Abel et al., 1997; Bliss and Collingridge, 1993; Frey et al., 1993).

Recent investigation has shown a strong correlation between LTP/LTD and memory formation: (1) both memory formation and LTP trigger the formation of new synapses (Engert and Bonhoeffer, 1999; Morgado-Bernal, 2011); (2) blocking LTP diminishes spatial memory formation (Davis et al., 1992; Morris, 1989; Tsien et al., 1996); (3) the disruption of LTP by mutations impairs memory formation (Abel et al., 1997; Bourtchuladze et al., 1994; Chang et al., 1999; Grant and Silva, 1994; Huang and Lee, 1995; Silva et al., 1992a, 1992b); and (4) memory loss related brain diseases are associated with the enhanced LTD (Li et al., 2009; Shankar et al., 2008). Since the exact principles of memory system are far from completely understood, the emerging understanding of the protein networks associated with synaptic plasticity may provide insights into the biochemical basis of memory formation.

1.2 Modelling single cell dynamics associated with synaptic plasticity

A cell dynamically regulates its intracellular signalling, transcription, plasticity and fate (Spiller et al., 2010). The dynamics starts with the detection of extracellular signals by receptors at the cell surface. The consequent second messenger transmits through protein signalling pathways (usually involves feedback loops) and delivers the message to the nucleus, where the gene expression occurs. Resulting effects involve activations of specific proteins and alterations on multiple gene expressions (Spiller et al., 2010). Signalling pathways may have complex behaviours facilitated by the emergent properties of the interacting networks (Weng et al., 1999). However, understanding the complex behaviours is very challenging because the measurements of the interacting networks in real-time are difficult with current technology. Even if the measurements are feasible, the complexity of the protein interacting networks associated with the signalling pathway involves too much biological details that may be difficult for an unbiased human mind to comprehend. With the support from mathematical modelling and computational methods (Kotaleski and Blackwell, 2010; Spiller et al., 2010), we develop mathematical models based on hypotheses for the cell dynamics and validate

the hypotheses through the computations of the established model against available experimental data. Thoughtful interpretation of the computational results can help us to better understand the complex behaviour and develop further hypotheses to be tested experimentally.

The dynamic participation of the synaptic proteins in the sophisticated interacting networks gives rise to synaptic plasticity. In one facet of systems biology, we aim to understand the system level functions of synaptic proteins and the emergent properties of the protein interacting networks of synaptic plasticity through mathematical modelling based on biophysics. Thus, mathematical modelling based on biologically meaningful assumptions may provide insights into the dynamic behaviour of synaptic plasticity, which may be difficult to obtain through experiments. The models focus on three key aspects linking the synaptic components to the dynamic behaviour of synaptic plasticity (He et al., 2014): (1) the structural and functional properties of individual synaptic protein that show high correlation to the expression patterns of synaptic plasticity; (2) the emergent properties of the protein interacting networks that support the functionality of synaptic plasticity; and (3) the robustness of synaptic plasticity with respect to the low copy numbers of proteins. The models of these categories help us to identify the essential modulators of synaptic plasticity as well as to understand distinct and dynamic roles they play in the complex set of networks.

There are many questions of synaptic functioning that may be critical for understanding synaptic plasticity, which could be answered through mathematical modelling. The detail level of the synaptic system considered in each model maybe different depending on the specific question asked:

(1) What are the essential protein interacting networks underlying synaptic plasticity? Considering the distinct functions of LTP and LTD, which of the protein interacting networks induce the emergence of LTP and which of them induce the emergence of LTD?

    The answer should take into account the essential protein interacting networks in the emergence of synaptic plasticity. A minimal model integrating the

essential interacting networks of synaptic plasticity is necessary to analyse for the essential emergent properties underlying the dynamic behaviour of synaptic plasticity. The model development should be started with a careful selection of the indispensable synaptic proteins to be used as the variables of the model. As a result, the model development should provide insights into the essential modulators of synaptic plasticity and the simulation results of the model should gain insights into the dynamic roles that the modulators play in synaptic plasticity.

(2) How would the co-localisation of synaptic proteins impact synaptic plasticity?

This problem deals with the co-localisation of synaptic proteins and spatial movement of synaptic proteins among synaptic compartments. Hence, the models of this category need to be developed with the consideration of the spatial information and co-localisation of synaptic proteins. The simulating results of the models should provide a more precise prediction on the effective timescales of the synaptic proteins and hence allow us to link synaptic proteins to the phases of synaptic plasticity.

(3) What is the implication of interactions between modulators, specifically the binding between NMDAR and Ca^{2+}/CaM-dependent protein kinase II (CaMKII) (see Section 2.3.3 for the elaboration), in the dynamic behaviour of synaptic plasticity?

The answer should take into consideration of the biochemical details of the modulators, possibly expanding previous models of the modulator to include the latest understanding about the interaction. Then, the new model can be used to test the functionality of the particular modulator as well as its interaction to other modulators.

1.3 Motivations and objectives for this study

With the abundant experimental data of synaptic components, modelling of synaptic plasticity enables the integration of the fragmented information of the synaptic

components into a system level view to provide insights into the interactions and the roles of the main synaptic modulators contributing to synaptic plasticity (Kotaleski and Blackwell, 2010). The existing models related to synaptic plasticity help us to understand the structural and functional properties of synaptic proteins in the emergence of synaptic plasticity (Manninen et al., 2010).

This study develops mathematical models and computational methods to understand the protein interacting networks at different detail levels in the emergence of synaptic plasticity. This study has two major objectives: (1) to develop a simplified mathematical model of the NMDAR-mediated pathway to explore the bidirectional behaviour of synaptic plasticity. Specifically, we focus on understanding the essential modulators as well as the essential interactions among them, participated in the selective activation of the antithetic synaptic behaviours, LTP and LTD, by a common signalling upstream, the Ca^{2+} level. Analysis of the model reveals the main factors of the selectivity, which may be valuable to understand the important processes in different phases of synaptic plasticity and possibly uncover the biochemical mechanisms underlying the memory system; and (2) to develop a theoretical model of the state transitions of CaMKII, which have long lasting activity after the vanishing of the Ca^{2+} signal (Bayer et al., 2006) and play an important role in LTP as well as in memory formation (Lisman et al., 2012). CaMKII has several states and the state transitions among them during LTP can be simulated using this model. Understanding the relationship between the state transitions and LTP may not only give the knowledge for the roles of these states in LTP but also provide insights into memory formation. For instance, we use this model to understand the role of a particular state of CaMKII, the autophosphorylation, in the emergence of early phase LTP (E-LTP), which has diverse conclusions in the literature.

1.4 Overview of Chapters

This thesis contains six chapters.

The current chapter starts with an introduction on synaptic plasticity followed by a discussion on the importance of using mathematical modelling to understand the dynamical behaviour of synaptic plasticity. Then, some important questions of synaptic plasticity, which can be addressed through mathematical modelling, are highlighted. At the end, the motivations and objectives of this study are discussed.

Chapter two gives the necessary background for modelling synaptic plasticity, including the biochemical basis of synaptic plasticity, the potential modulators of synaptic plasticity, and the existing mathematical models of synaptic plasticity.

In Chapter three, we develop a mathematical model of the NMDAR-mediated pathways of synaptic plasticity. We use the model to explore the factors of the bidirectional behaviour of synaptic plasticity.

Chapter four gives the details on the development of a theoretical model of the state transitions of CaMKII in the emergence of E-LTP. Moreover, discussions are given on the parameter estimation and the parameter sensitivity of the model.

Chapter five extensively analyses the implication of the autophosphorylation of CaMKII in E-LTP, particularly on the autophosphorylation triggered dynamics of CaMKII in response to LTP induction signals.

Chapter six summarises this study as well as the major contributions, and outlines the directions for future research.

Chapter 2: Background for the Modelling of Synaptic Plasticity

In this chapter, we introduce the mechanisms underlying synaptic plasticity and the existing models of synaptic plasticity. The principles of the synapse are explained in detail in many books; Purves et al. (2008) and Bear et al. (2007) give excellent explanations not only on the synapse but also on the discoveries in neuroscience. In order to understand the specific proteins involved in synaptic plasticity, a brief description of the synaptic transmission is first given in Section 2.1 (see Appendix A for the details of synaptic transmission). Then, the mechanisms underlying synaptic plasticity is described in Section 2.2. The modulators of synaptic plasticity, in terms of their fundamental importance in facilitating the dynamic behaviour of synaptic plasticity, are described in detail in Section 2.3. At the end, the existing models of synaptic plasticity are summarised in Section 2.4.

2.1 Characteristics of synaptic transmission

A synapse is composed of three parts: a presynaptic terminal, a synaptic cleft, and a postsynaptic terminal (Fig. 2-1). Information is transmitted from the presynaptic terminal to the postsynaptic terminal through the synaptic cleft, a gap (20-40 nm in length) linking the pre- and post- synaptic terminals. The synaptic cleft is filled with a matrix of fibrous extracellular proteins to adhere the pre- and post- synaptic membranes.

The presynaptic terminal is the axon terminal of the sending neuron. The presynaptic terminal contains synaptic vesicles, which are membrane-enclosed spheres. Neurotransmitters are pumped into a synaptic vesicle by vesicular transporters embedded in the membrane of the synaptic vesicle. Synaptic vesicles are accumulated close to active zone, where neurotransmitters are released into the synaptic cleft in response to an action potential.

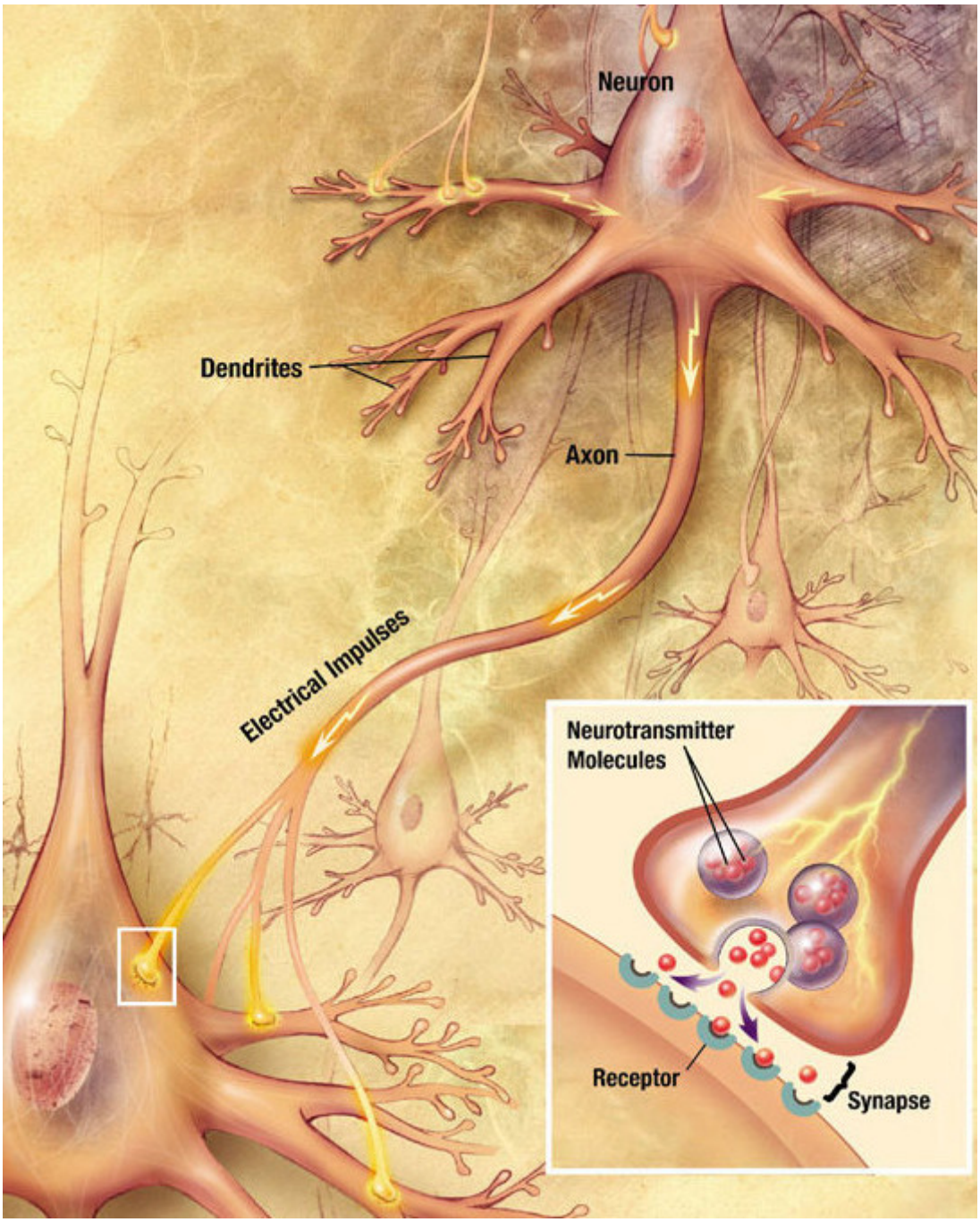

Figure 2-1 Synapse and synaptic transmission.

(**Source**: http://commons.wikimedia.org/wiki/File:Chemical_synapse_schema_cropped.jpg.

Copyright: no copyright, public domain in the United States)

The postsynaptic terminal is the dendrite or soma of the receiving neuron. At the distal tip of the dendritic spine (200 - 800 nm in diameter and 0.5 - 2 μm in length), a very small region (30 - 50 nm in length) called postsynaptic density (PSD) is directly exposed to the synaptic cleft (Sheng and Hoogenraad, 2007). PSD is constituted of approximately 10000 copies of proteins from more than 100 species, including receptors tyrosine kinases, G-protein-coupled receptors, ion channels and cell adhesion molecules (Sheng and Hoogenraad, 2007). The diverse groups of proteins are physiologically important in bridging and adapting the postsynaptic response to the presynaptic reaction induced by the environmental stimulus.

Ligand-gated receptors are densely distributed across PSD to sense the neurotransmitters in the synaptic cleft and trigger the response of the postsynaptic neuron; for instance, a postsynaptic potential (PSP) is generated. AMPAR is involved in the synaptic transmission of hippocampal neurons. PSD anchored AMPAR (PSD AMPAR) binds to neurotransmitters to open its embedded ion channel. The opening allows cations (mostly Na^+ and K^+) to enter and depolarise the postsynaptic membrane. An EPSP is induced as the consequence of the depolarisation and its magnitude is influenced by the AMPAR mediated EPSC (Citri and Malenka, 2007).

Two major factors regulating the AMPAR-mediated EPSC are the number of PSD AMPAR and the single channel conductance of AMPAR. AMPAR is a mobile receptor recycling between the cytoplasm and PSD of the synapse (Lüscher et al., 1999).The experimentally established data shows that the number of AMPAR is variable among synapses ranging from 0 to 200 (Ribrault et al., 2011). The insertion of AMPAR from the cytoplasmic reservation pool into PSD is governed by two independent steps (Fig. 2-2A): (1) externalisation into extrasynaptic sites by exocytosis, and lateral diffusion into PSD (Banke et al., 2000; Ehlers, 2000; He et al., 2009; Oh et al., 2006; Yang et al., 2008), and (2) binding to scaffolding proteins, such as PSD95, (Ehrlich et al., 2007; Garner et al., 2000; Hayashi et al., 2000) mediated by transmembrane AMPAR regulatory protein (TARP), the binding partner of AMPAR (Opazo et al., 2010; Tomita et al., 2005). The alterations on sites involved in either of the two steps can change the

number of PSD AMPAR and influence the overall receptor conductance without affecting the unitary channel conductance. The unitary channel conductance measures the conductance of a single AMPAR ion channel and an alteration of it would change the rate of which cations pass through the ion channel within a unit time.

2.2 NMDAR-dependent synaptic plasticity

NMDAR is blocked by a Mg^{2+} ion (Mayer et al., 1984; Nowak et al., 1984). A strong depolarisation of the postsynaptic membrane is required to repel the block and expose the embedded Ca^{2+} channel of NMDAR. With a glutamate molecule attached to NMDAR, the exposed ion channel opens and allows Ca^{2+} influx to diffuse across the postsynaptic membrane. The induced influx is rapid due to the high gradient of Ca^{2+} across the membrane (0.1 μM at intracellular volume and 1800 μM at extracellular volume) and leads to an elevation in the intracellular Ca^{2+} level. The Ca^{2+} elevation is the key to activate the subsequent pathways of synaptic plasticity.

Current evidence suggests that the Ca^{2+} elevation triggers postsynaptic cascades which modulate the phosphorylation levels on: (1) serine 831 residue (Ser831) of AMPAR to regulate the unitary channel conductance (Derkach et al., 1999); (2) serine 845 residue (Ser845) of AMPAR to regulate the rate of translocation of AMPAR into extrasynaptic sites (Banke et al., 2000; Ehlers, 2000; He et al., 2009; Oh et al., 2006; Yang et al., 2008); and (3) TARP to regulate the rate of binding of AMPAR to PSD-95 (Opazo et al., 2010; Tomita et al., 2005). The specific changes caused by the postsynaptic cascades are shown in Fig. 2-2.

First, intracellular Ca^{2+} forms a complex with calmodulin (CaM). CaM binds neurogranin, which inhibits and holds postsynaptic CaM. The elevation in the intracellular Ca^{2+} level activates protein kinase C (PKC) and PKC phosphorylates neurogranin to release the bound CaM (Baudier et al., 1991). The released CaM associates Ca^{2+} to form Ca^{2+}/CaM complex. The association causes a conformational change on CaM to expose its principle binding site, the hydrophobic domain, which increases the affinity of CaM to its binding proteins (LaPorte et al., 1980). Then,

Ca^{2+}/CaM complex selectively activates two pathways responsible for LTD or LTP (Table 2-1).

High Ca^{2+} elevation activates the LTP pathway, which triggers the activations of kinases, including CaMKII and protein kinase A (PKA) (Fig 2-2C). CaMKII phosphorylates: (1) Ser831 of AMPAR to increase the unitary channel conductance (Barria et al., 1997; Blitzer et al., 1998; Derkach et al., 1999); and (2) TARP to increase the surface expression of AMPAR (Opazo et al., 2010; Tomita et al., 2005). Meanwhile, PKA phosphorylates Ser845 of AMPAR to move more AMPAR into extrasynaptic sites through exocytosis (Esteban et al., 2003; Lee et al., 2010; Zheng and Keifer, 2009).

Moderate Ca^{2+} elevation activates the LTD pathway, which triggers the activations of phosphatases, including calcinuerin (PP2b) and protein phosphatase 1 (PP1) (Mulkey et al., 1994) (Fig. 2-2B). PP1 dephosphorylates both Ser831 and Ser845 of AMPAR to decrease the unitary channel conductance and to enhance the internalisation of AMPAR into cytoplasm by endocytosis (Beattie et al., 2000; Carroll et al., 2001; Mulkey et al., 1993; Snyder et al., 2003). Moreover, both PP2b and PP1 dephosphorylate TARP to reduce the surface expression of AMPAR (Snyder et al., 2003; Tomita et al., 2005). In addition, the latest evidence suggests that PP2b removes PKA out of dendritic spine or PSD to prevent the rephosphorylation on AMPAR (Gomez et al., 2002; Gorski et al., 2005).

The selection on which one of the two pathways to activate are regulated through the protein interacting networks of the essential modulators. The possible modulators and associated interacting networks underlying the mechanisms of synaptic plasticity are discussed in the following chapter.

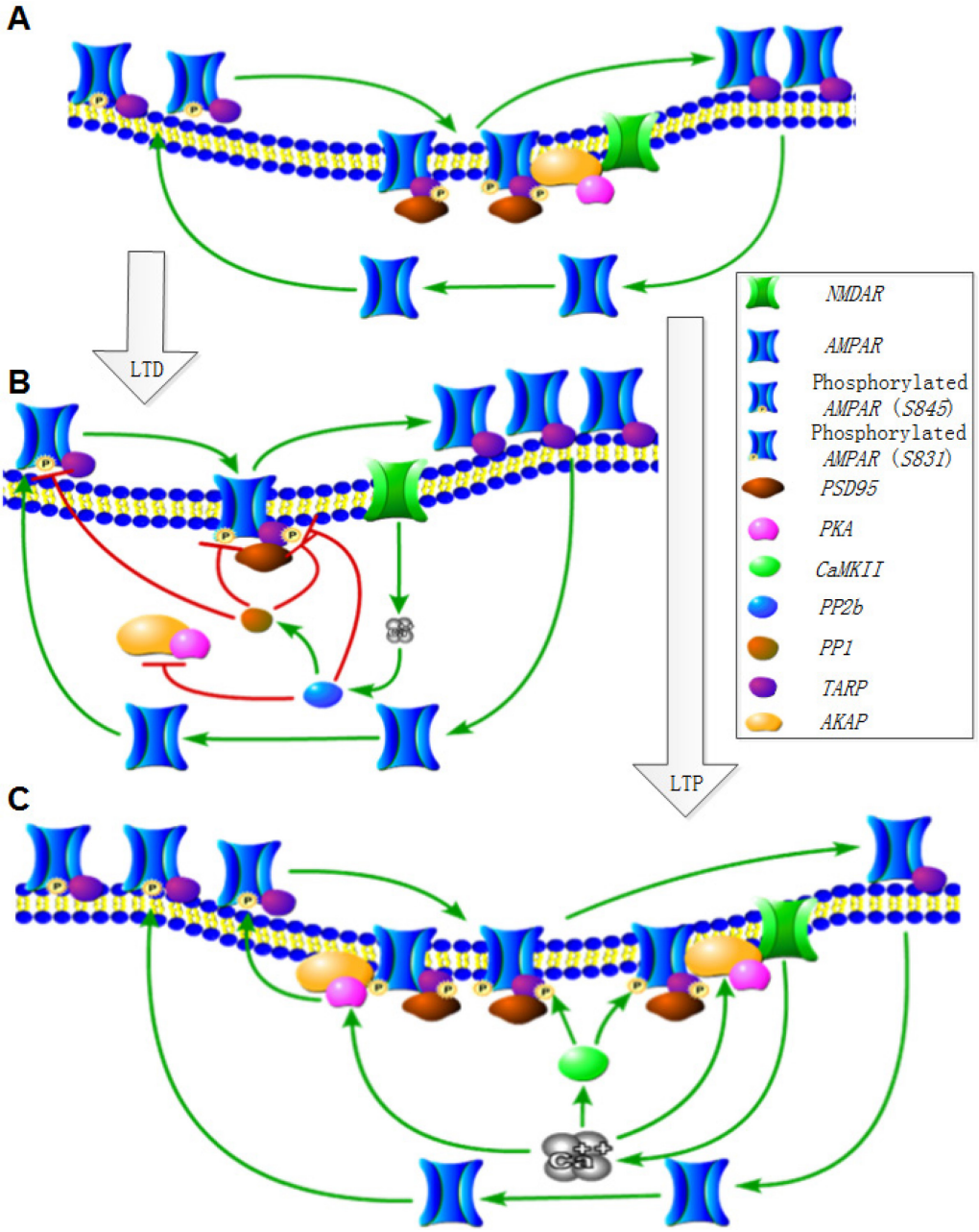

Figure 2-2 Specific changes of the postsynaptic neuron during LTP and LTD. Three states of the postsynaptic neuron are shown here: (A) basal, (B) LTD and (C) LTP. The details of the specific changes during LTP and LTD are summarised in Table 2-1.

Table 2-1

Specific changes of the postsynaptic neuron during LTP and LTD

States	*Ca^{2+} (μM)*	*Induction Frequency*	*Phosphorylation Level*			*AMPAR Number and Conductance*	*PKA Removal*
			Ser831	*Ser845*	*TARP*		
Basal	*0.1*	*NA*	*Low*	*Basal*	*Low*	*Basal*	*NA*
LTD	*<1*	*1Hz*	*/*	*-*	*-*	*-*	*Yes*
LTP	*>10*	*100-200Hz*	*+*	*+*	*+*	*+*	*NA*

(+ denotes increase, - denotes decrease, / denotes insignificant change, NA is not applicable or no report found)

2.3 Essential modulators of synaptic plasticity

The modulators of synaptic plasticity have fundamental importance in facilitating the dynamic behaviour of synaptic plasticity, including (1) the bidirectional behaviour in which two antithetic pathways share a single Ca^{2+} upstream; (2) the bi-stability in which the modulations are maintained much longer than the signal duration; and (3) the robustness with respect to the low copy numbers of proteins. Moreover, synaptic plasticity is dependent on the stimulation frequency as well as the intracellular Ca^{2+} level: the prolonged low frequency stimulations (LFS, 1Hz for 900s), which cause moderate elevations in the intracellular Ca^{2+} level, induce LTD; and the transient high frequency stimulations (HFS, 100 - 200Hz for 1s), which cause the high elevations in the intracellular Ca^{2+} level, induce LTP (Citri and Malenka, 2007). In this section, we describe the relevance of the modulators, in terms of their unique structures or functionalities, to the dynamic behaviour of synaptic plasticity.

2.3.1 NMDAR

NMDAR is a tetramer composed of two NR1 subunits and two NR2 subunits. The NR2 subunits are selected from either NR2A or NR2B subunits. NMDAR is anchored in PSD through binding to the PDZ domain of membrane-associated guanylate kinase protein family (MAGUKs), a well-known member is PSD-95 (Cho et al., 1992). Although the average number of NMDAR in PSD of a mature synapse is only 20 (Ribrault et al., 2011; Yashiro and Philpot, 2008), NMDAR is one of the major postsynaptic Ca^{2+} sources and has a critical role in the emergence of synaptic plasticity. Evidence shows an important role of NMDAR in the emergence of synaptic plasticity that dysfunctions of NMDAR impair synaptic plasticity as well as the formation of spatial memory (Davis et al., 1992; Morris, 1989; Morris et al., 1982; Tsien et al., 1996).

The difference in the current induction between NR2A-containing and NR2B-containing NMDARs may be important. Evidence shows that the current induced by NR2A is higher in amplitude and shorter in duration than that induced by NR2B (Erreger et al., 2005). As a direct effect, the pattern of the Ca^{2+} influx passing through

the receptor is different between NR2A- and NR2B- containing NMDARs. Moreover, LTP becomes dominant over LTD during the neuronal developmental period (Puyal et al., 2003) together with an increased NR2A/NR2B ratio of NMDARs (Liu et al., 2004). The number of NR2B-containing NMDARs is independent of the synaptic size (Shinohara et al., 2008), hence, the bidirectional behaviour of synaptic plasticity may be influenced by the NR2A/NR2B ratio.

2.3.2 Ca^{2+} and CaM interaction

The selectivity of Ca^{2+}/CaM complex stems from the unique Ca^{2+} sensitivities of the CaM binding proteins, some of which are key modulators of synaptic plasticity. In this thesis, "Ca^{2+}/CaM complex" refers to the fully Ca^{2+} bound CaM at all of its four Ca^{2+} binding sites (N terminus and C terminus of CaM each containing two Ca^{2+} binding sites). Filling these Ca^{2+} binding sites requires the following: (1) N terminus and C terminus carry different binding rates; (2) at the presence of CaM binding proteins, the affinity of CaM for Ca^{2+} is enhanced. The enhancement is in a heterotropic positive cooperative manner with respect to the numbers of unfilled Ca^{2+} binding sites (Keller et al., 1982; Olwin and Storm, 1985); and (3) the states of CaM binding proteins induce distinct degrees of the enhancement (Meyer et al., 1992). As a result, CaM binding proteins display unique Ca^{2+} sensitivities for the CaM binding and activation. For example, PP2b has a much higher Ca^{2+} sensitivity for CaM binding (Quintana et al., 2005). Having different Ca^{2+} sensitivities for CaM binding is physiologically important to distinguish the groups of proteins involved in LTP and LTD, respectively, and thus to facilitate the bidirectional behaviour of synaptic plasticity.

2.3.3 CaMKII

A CaMKII subunit has multiple isoforms and the dominant isoforms are expressed from α and β genes in hippocampus. Both isoforms are synthesised in the same location and they may form CaMKII hetero-oligomers (Shen et al., 1998). A CaMKII subunit consists of a kinase domain, a regulatory domain, and a hub domain with a linker linking the regulatory and hub domains. Twelve subunits are folded into two hexametric

rings and each ring contains six subunits with their six hub domains attached one by one to form a central hub (Fig. 2-3A) (Chao et al., 2011). The functionality of CaMKII relies on a few critical sites (Fig. 2-3B): (1) substrate binding site (S site) in the kinase domain for the catalytic activity; (2) pseudosubstrate segment in the regulatory domain (contains CaM footprint which is critical for Ca^{2+}/CaM complex binding and CaMKII activation); (3) T site in the kinase domain for NMDAR binding; (4) threonine 286 site (abbreviation: T286 for α isoform or T287 for β isoform) in the regulatory domain for autonomous activity, the autophosphorylation; and (5) threonine 305/306 sites (T305/T306) in the pseudosubstrate segment for regulation of CaMKII activity (but the exact mechanism is unknown).

The inhibited subunits of CaMKII have the regulatory domain attached to the kinase domain; the S site binds to the pseudosubstrate segment and the T site binds to the T286 site (Fig. 2-3B (a)) (Chao et al., 2011). All the critical sites are blocked and the kinase is inactive. However, inactive CaMKII subunits are dynamically switching between two inhibited states: autoinhibited compact and autoinhibited extended states (Fig. 2-3A). The critical sites are completely blocked in the autoinhibited compact state, while the autoinhibited extended state exposes some critical sites for the activation (Stratton et al., 2013). The major factor determining the rate of switching is the length of the linker, which varies among CaMKII isoforms (Chao et al., 2011).

A CaMKII subunit is activated when a Ca^{2+}/CaM complex binds to the CaM footprint leading to a conformational change which exposes the S site for the catalytic processes (Fig. 2-3B (b)) (Chao et al., 2011; Lisman et al., 2002). Together with the exposure of the S site, the T286 site is exposed and can be trans-autophosphorylated by the adjacent active subunits (autophosphorylation) to prevent the rebinding between the kinase and the regulatory domains (Fig. 2-3B(c)) (Chao et al., 2011; Lou et al., 1986; Miller and Kennedy, 1986; Saitoh and Schwartz, 1985; Yang and Schulman, 1999). As a result, the autophosphorylated CaMKII subunit remains at least partially active even when the CaM dissociates. Moreover, the autophosphorylation increases the affinity of a subunit for Ca^{2+}/CaM complex binding (Meyer et al., 1992). Hence, the autophosphorylation

prevents the reverting of the active CaMKII subunits into the inhibited state when the Ca^{2+} level decreases (Fong et al., 1989; Miller et al., 1988; Waxham et al., 1990). After CaM dissociation, T305/T306 becomes autophosphorylated (inhibitory autophosphorylation) to prevent the rebinding of Ca^{2+}/CaM complex (Elgersma et al., 2002; Goh and Manahan-Vaughan, 2014).

CaMKII is held away from PSD by F-actin (Shen et al., 1998) and Ca^{2+}/CaM dependent activation releases the kinase that allows it to translocate into PSD (Shen and Meyer, 1999). CaMKII binds to NR2B subunit of NMDAR and the binding anchors CaMKII in PSD (Gardoni et al., 1998; Leonard et al., 1999; Strack and Colbran, 1998). The binding locks CaMKII in an active conformation independent of the autophosphorylation (Bayer et al., 2001).

The difference in CaMKII isoforms may be important for synaptic plasticity. β isoform translocates much slower than α isoform (Shen and Meyer, 1999). The slower translocation rate may be caused by two factors: (1) F-actin binds to β isoform, but not α isoform (Shen and Meyer, 1999; Shen et al., 1998); and (2) the rates of the switching between the autoinhibition states are different among CaMKII isoforms (Chao et al., 2011). As a result, the slower translocation rate of β isoform subunit may be unable to keep up with the transient signal of the LTP induction. On the other hand, β isoform has a higher catalytic property than that of α isoform (Huynh and Pagratis, 2011), which may enhance the phosphorylation on the substrates. Moreover, the binding between β isoform and F-actin may facilitate the structural changes in the late phase (Okamoto et al., 2009). Further evidence shows that the α/β isoforms ratio of a CaMKII is actively regulated in hippocampal neurons which could be an important factor of LTP induction (Shen et al., 1998; Thiagarajan et al., 2002).

The prolonged activity of CaMKII may be critical for the long-lasting activity of LTP. Two processes maintain the activity of CaMKII: (1) the autophosphorylation maintains the activity of CaMKII for up to one minute after the Ca^{2+} level decreases (Lee et al., 2009), and (2) the NMDAR binding maintains the staying of CaMKII in PSD for at least 30 minutes (Bayer et al., 2006), and potentially maintains CaMKII in an active

conformation (Bayer et al., 2001). The prolonged activity of CaMKII potentially maintains the phosphorylation level of AMPAR and TARP, both of which are critical for LTP.

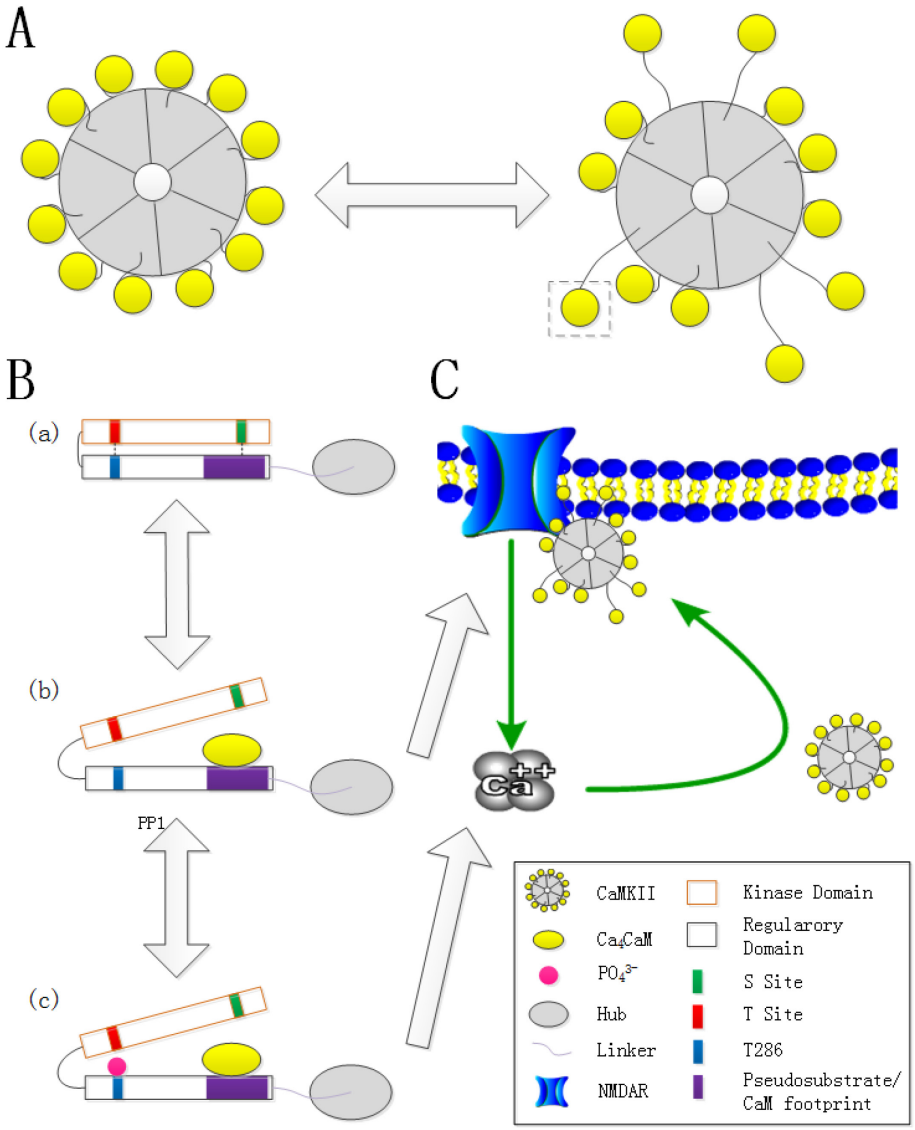

Figure 2-3 Structure and conformational changes of CaMKII. (A) Inhibited CaMKII is switching between two states: autoinhibited compact (left) and autoinhibited extended (right). The rate of the switching is dependent on the length of the linker. **(B)** A schematic of a CaMKII subunit (dashed rectangle of Fig. A): (a) Inhibited subunit: the S site binds to the pseudosegment and the T site binds to the T286 site (dashed lines); (b) Ca^{2+}/CaM complex attaches to the CaM footprint to cause a conformational change where the kinase domain detaches from the regulatory domain. At this state, the subunit is active; and (c) the activated subunit is autophosphorylated at the T286 site to retain the opening between the kinase and regulatory domains. At this state, the subunit is at least partially active. *Phosphorylation can be reverted by protein phosphatase 1 (PP1)-dependent dephosphorylation* (Stemmer and Klee, 1991). **(C)** Activated subunits can bind to NMDAR in a Ca^{2+} dependent manner that anchors the holoenzyme in PSD.

2.3.4 Cyclic adenosine monophosphate (cAMP) and PKA

PKA holoenzyme is composed of two catalytic subunits and a regulatory dimer; the regulatory dimer binds to and inhibits the catalytic subunits (Zawadzki and Taylor, 2004). The activation of PKA requires cAMP binding to the regulatory dimer to trigger the release of the catalytic subunits allowing the catalytic subunits to phosphorylate the substrates. Furthermore, cAMP-PKA signalling pathway may be involved in the activation of the gene expression pathway for further maintenance of LTP (Mayford et al., 2012).

The regulation of PKA may facilitate the bidirectional behaviour of synaptic plasticity. The regulation involves interactions among adenylyl cyclase (AC), cAMP and phosphodiesterase (PDE) (Fig. 2-4). AC catalyses the conversion of adenosine triphosphate (ATP) into cAMP in response to a few signals, i.e. Ca^{2+}/CaM complex, dopamine, G-proteins. Among 8 types of ACs, two are Ca^{2+}/CaM complex dependent in neuron. Meanwhile, PDE converts cAMP into adenosine monophosphate (AMP) and both Ca^{2+}/CaM complex and PKA promote the activity of PDE (Lugnier, 2006; Stanton et al., 2005). As a result, cAMP may be dual inhibited by: (1) Ca^{2+}/CaM complex through a direct inhibitory circuit; and (2) PKA through an inhibitory feedback loop. Such inhibition loop forms a switch on the activation of PKA with respect to the Ca^{2+} level: the moderate elevation in the Ca^{2+} level leads to a stronger PDE-inhibition than the AC-dependent activation resulting in the low cAMP levels to prevent the activation of PKA and LTP; and the high elevation in the Ca^{2+} level saturates the PDE-dependent inhibition so that the AC-dependent activation is dominant to promote the activation of PKA and LTP.

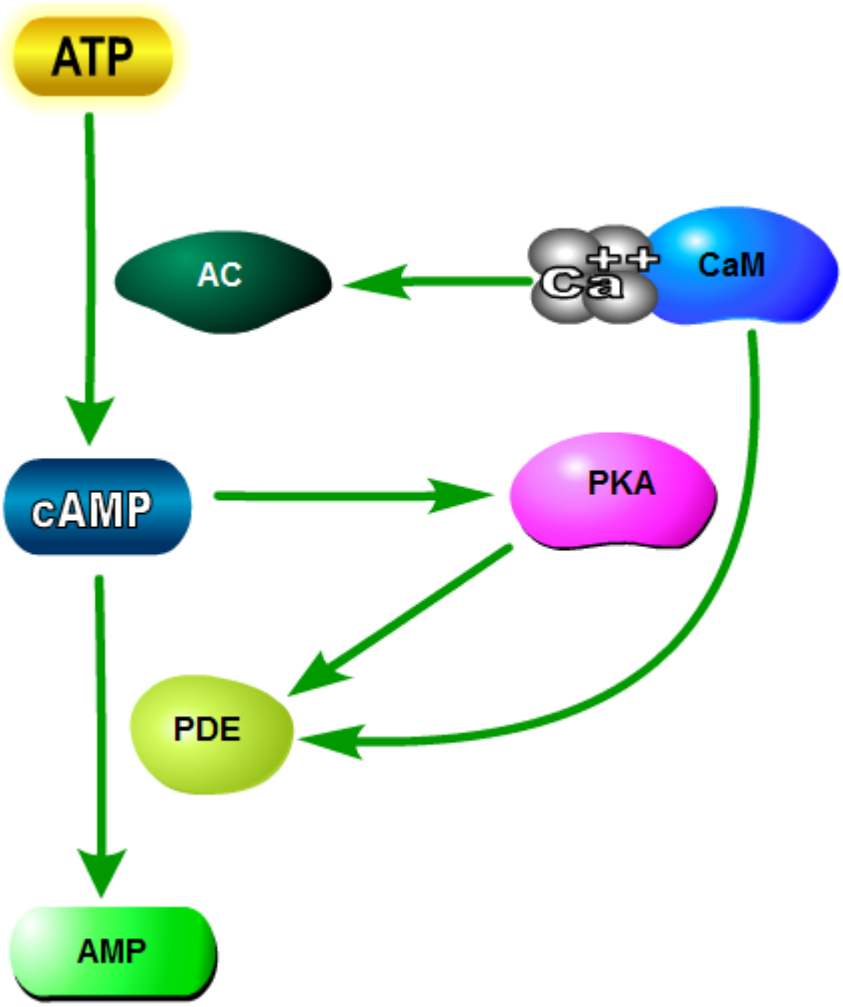

Figure 2-4 Regulation of PKA through PDE-depndent cAMP inhibiton. Ca^{2+}/CaM complex stimulates AC, which converts ATP into cAMP. cAMP further activates PKA. Meawhile, cAMP is inhibted by PDE by converting into AMP and the activity of PDE is promoted by both PKA and Ca^{2+}/CaM complex. As a result, there is a strong inhibition of cAMP by PDE and a high level of Ca^{2+}/CaM complex is required to activate cAMP as well as PKA.

2.3.5 A-kinase anchoring proteins

While a lot of synaptic proteins undergo spatial movements between synaptic compartments, the targeting and the spatial specificity of synaptic proteins become important for synaptic plasticity. One protein family involved in the processes is A-kinase anchoring proteins (AKAPs) (reviewed in Sanderson and Dell'Acqua (2011)), which bind and translocate PKA into dendritic spine and PSD (Carr et al., 1992). Moreover, AKAPs can bind to many other proteins, some of which are critical to synaptic plasticity.

The most studied type of AKAPs is AKAP150 in mouse, and its homologue, AKAP79, in human. The translocation of AKAP79/150 into dendritic spine and PSD is enabled by its targeting domain near the N-terminus through binding to proteins in the specific synaptic compartment, including F-actin (Gomez et al., 2002), acidic phospholipid phosphatidylinositol-4,5-bisphosphate (PIP_2) (Dell'Acqua et al., 1998) and cadherin cell adhesion molecule (Gorski et al., 2005). AKAP79/150 binds to PKC, AC, PP2b and MAGUKs other than PKA (Bhattacharyya et al., 2009; Coghlan et al., 1995; Colledge et al., 2000; Dell'Acqua et al., 2002; Efendiev et al., 2010; Klauck et al., 1996; Oliveria et al., 2003; Robertson et al., 2009; Tavalin et al., 2002; Willoughby et al., 2010). The diverse binding ability of AKAP79/150 establishes links among the modulators and facilitates critical interactions among them in the emergence of synaptic plasticity. Many other types of AKAPs may contribute to synaptic plasticity as well. For example, Yotiao binds to PP1, instead of PP2b, and regulates the activity of NMDAR (Lin et al., 1998; Westphal et al., 1999). In conclusion, AKAP allows synaptic proteins to be co-localised for their optimal functioning. Such an arrangement promotes the targeting of modulators of synaptic plasticity to critical sites of the synaptic transmission. The exact co-localisations of synaptic proteins are important and require further investigations.

Removal of AKAP away from dendritic spine or PSD is critical for LTD (Fig. 2-2B) (Gomez et al., 2002; Gorski et al., 2005). The removal, caused by PP2b-dependent actin depolymerisation and phospholipase C cleavage of PIP_2 (Gomez et al., 2002; Horne and

Dell'Acqua, 2007; Keith et al., 2012), diminishes the activity of PKA suggesting that the functionality of PKA relies on the binding to AKAP79/150 and translocation into dendritic spine and PSD (Smith et al., 2006). Moreover, the removal slightly lags behind the occurring of the dephosphorylation of target substrate by phosphatases (Sanderson et al., 2012; Smith et al., 2006), which may indicate that the removal is a potential mechanism to prevent the rephosphorylation of substrates by PKA. Particularly, the rephosphorylation may cause AMPAR to re-enter extrasynaptic sites. There is no evidence showing the involvement of the removal in LTP.

2.3.6 Interactions among modulators

The interaction between kinases and phosphatases may be important to differentiate LTP and LTD. Current understanding indicates two places of the interaction: (1) the regulation of PP1 and (2) potentially the removal of AKAP (Mulkey et al., 1994; Sanderson and Dell'Acqua, 2011).

PP1 strongly prevents the LTP induction; it dephosphorylates all the critical sites of synaptic proteins related to LTP: Ser831, Ser845, TARP and CaMKII. The phosphorylated inhibitor 1 (I1) binds to and inhibits PP1. It is understood that I1 is phosphorylated by PKA (Blitzer et al., 1998), while PP2b dephosphorylates I1 to release PP1 (Mulkey et al., 1994) (Fig. 2-5). As a result, the activation of PP2b triggers the activation of PP1 to dephosphorylate these critical sites. On the other hand, the activation of PKA prevents the PP1-depednent dephosphorylation of these critical sites, which may be another reason for the removal of PKA during LTD discussed previously.

However, the mechanism to prevent the PP2b-dependent removal of AKAPs as well as PKA is not well understood. One possible mechanism is the phosphorylation of ADF/cofilin by kinases, which suppresses the F-actin depolymerisation (Carlier and Pantaloni, 1997; Chen et al., 2000; Pantaloni et al., 2001). The suppression increases the level of F-actin and thus stabilises AKAPs in the dendritic spine. Moreover, evidence shows the elevation in the actin level during LTP (Fukazawa et al., 2003).

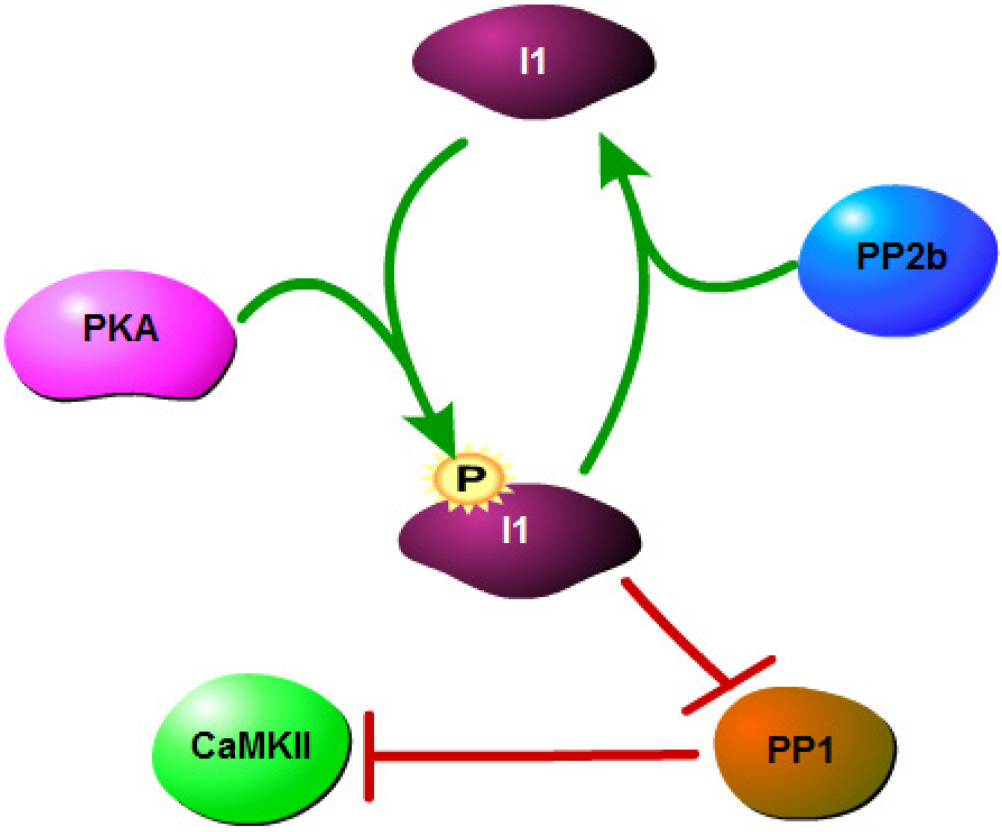

Figure 2-5 Regulation of PP1. Active PP1 dephosphorylates a number of substrates, including the T286 site of CaMKII subunits for the autophosphorylation. The phosphorylated I1 binds to and inhibits PP1. The phosphorylation of I1 is driven by PKA and some other kinases. PP2b activates PP1 by dephosphorylating I1 to release PP1 from the I1 binding.

2.4 Existing models of synaptic plasticity

There are a number of models and they approach the core of synaptic plasticity differently (Fig. 2-6). A single component model (Fig. 2-6A) studies a single synaptic component and highlights its potential structural and functional properties linking it to the dynamic behaviour of synaptic plasticity. Simplified models (SMs) (Fig. 2-6B) focus on the interactions among a few synaptic proteins (often selected from Ca^{2+}, CaM, cAMP, CaMKII, PKA, PP2b, PP1 and AMPAR) that form simplified synaptic circuits. The selected synaptic proteins are claimed to be critical for synaptic plasticity. SMs are theoretical frameworks and the encapsulated relationships among synaptic proteins may not have direct biochemical relationships to experimentally discovered interactions. However, the results of simulations are useful to understand the essentiality and to investigate the potential roles that a synaptic protein plays in the interacting networks of synaptic plasticity. Moreover, SMs look into the important emergent properties of the synaptic circuits that compare well to the dynamic behaviour of synaptic plasticity. Although SMs carry limitations to the experimentally established data, SMs provide valuable insights into the complexity of synaptic interactions. Complete pathway models (CPMs) (Fig. 2-6C) also look at the emergent properties of the synaptic networks, but they are different from SMs in some ways: (1) CPMs contain the full spectrum of synaptic proteins of a (or a part of a) functional synapse and the mathematical frameworks of the relationships among these proteins are developed based on their experimentally revealed biochemical reactions or plausible biochemical reactions; and (2) the results of CPMs tend to explain the experimental data better; so that, the predictions made by CPMs have a high level of believability.

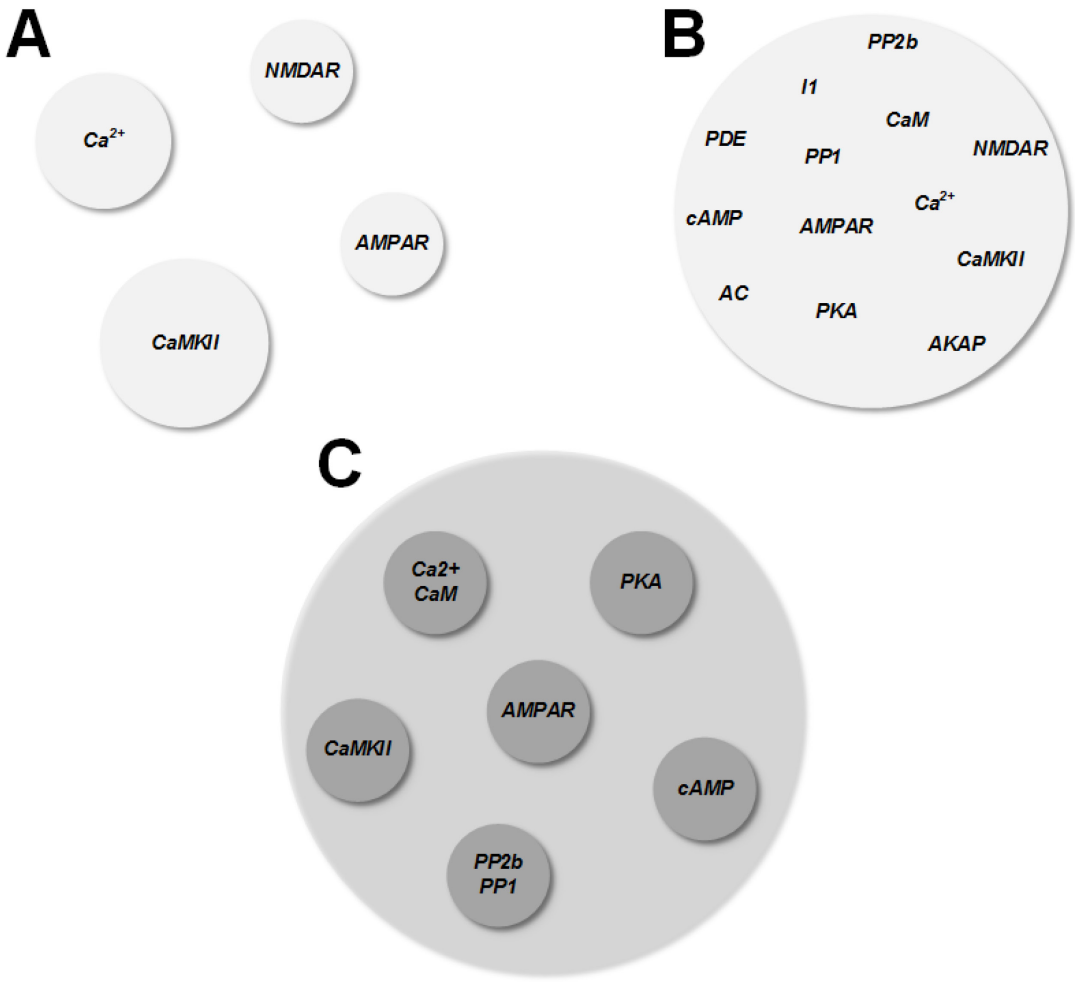

Figure 2-6 Scopes of models related to synaptic plasticity. A circle represents a model related to synaptic plasticity and the text inside represents the scope of the model. Three parts of the figures represent: **(A)** single component models; **(B)** simplified models; and **(C)** complete pathway models.

2.4.1 Single component models

Single component models are often applied to study the essence of Ca^{2+} dynamics, CaMKII autophosphorylation and AMPAR trafficking during synaptic plasticity.

2.4.1.1 Ca^{2+} dynamics

Modelling Ca^{2+} dynamics investigates the relationships between the changes of intracellular Ca^{2+} levels and the dynamic behaviour of synaptic plasticity. The existing models of Ca^{2+} dynamics mainly focus on the propagation of the Ca^{2+} influx to synaptic compartments during synaptic plasticity (Holmes and Levy, 1990; Naoki et al., 2005; Zador et al., 1990). Considering the fast diffusion rate of the Ca^{2+} ions (0.3-1 μm^2/ms) and the small size of the dendritic spine (0.03-0.8 μm^3), the Ca^{2+} ions should be instantaneously spread over and evenly distributed across the synapse. However, evidence shows distinct behaviours of Ca^{2+} dynamics between the areas close to (local) and far away (global) from Ca^{2+} sources (Augustine et al., 2003). Hence, the propagation of the Ca^{2+} signal across postsynaptic compartments may contain motifs of the Ca^{2+} selectivity.

Naoki et al. (2005) model the intracellular Ca^{2+} dynamics and comment on its relationship to the bidirectional behaviour of synaptic plasticity. They not only investigate the difference between the local and global Ca^{2+} dynamics in response to the Ca^{2+} influx as well as the subsequent diffusive processes, but also try to understand the implications of: (1) the diffusible CaM as shown in vivo, and (2) the Ca^{2+} influx from NR2A-containing and NR2B-containing NMDARs. The results of the simulation suggest that the frequency of the stimulus and the influx rate of NMDAR subunits can be dual decoded by the local/global Ca^{2+} dynamics and the diffusible CaM. The dual decoding supports further postsynaptic decisions for the functional direction of synaptic plasticity and allows errors to some extent. Moreover, the results of the simulation propose a hypothesis that: (1) HFS paired with the influx through NR2A induces LTP; and (2) LFS paired with the influx through NR2B induces LTD. This interpretation is consistent with the experimental observations (Liu et al., 2004).

2.4.1.2 CaMKII autophosphorylation

The existing models of CaMKII state transitions investigate the complicated dynamics and structural changes among the twelve subunits during the induction of LTP and predict relationships among the Ca^{2+} levels, the formation of Ca^{2+}/CaM complex, and the autophosphorylation.

A number of approaches are applied to study the CaMKII state transitions. The deterministic approaches are used to study the general levels of the autophosphorylation with respect to different stimulus frequencies and multiple-pulse stimulations (Dosemeci and Albers, 1996; Kubota and Bower, 2001; Pepke et al., 2010). The conclusions drawn from these studies are that the frequency of the stimulus is decoded through a bi-stable switch of the autophosphorylation between the low (induced by LFS) and high (induced by HFS) levels of the autophosphorylation (Dosemeci and Albers, 1996; Kubota and Bower, 2001); and the high levels of the autophosphorylation in response to HFS may be important for both induction and maintenance of LTP (Aslam et al., 2009; Graupner and Brunel, 2007; Lisman and Zhabotinsky, 2001). Stochastic approaches are used to study the robustness of the autophosphorylation against the low number of subunits and the protein turnover of CaMKII (one per 30 h on average) (Miller et al., 2005). The results of stochastic studies suggest that the stability of the autophosphorylation increases as the number of the subunits of CaMKII increases and the persistent activation time span could reach from a few years to the whole life time.

2.4.1.3 AMPAR trafficking

AMPAR trafficking involves interactions among synaptic proteins to drive the exocytosis and endocytosis of AMPAR at the extrasynaptic sites, and to drive the anchoring or removal of AMPAR in PSD. The models of AMPAR trafficking try to understand the protein interactions governing the translocation of AMPAR between the cytoplasm and PSD, and the timescales of these interactions to explain the experimental observations. One model (Holcman and Triller, 2006) uses Markovian approach to look at the stochastic spatial movement of AMPAR into and out of PSD. The results of the

simulation provide some clues of the timescales of the lateral movement of AMPAR and suggest that the number of scaffolding proteins (such as PSD95) in PSD is important in the regulation of the number of the functional AMPAR.

2.4.2 Simplified models

The dynamic behaviour of synaptic plasticity may have contributions from many small interacting networks, including but not limited to the CaMKII/PP1 interacting network; the PKA/PP1 interacting network; the PKA/PP2b interacting network; the cAMP-dependent PKA regulation network; the AKAPs dependent co-localisation of PKA; and the multiple phosphorylation states of AMPAR. Modelling of these small interacting networks provides insights into the relationships between the functions of the small networks and patterns of the dynamic behaviour of synaptic plasticity. Thus, the roles of synaptic proteins in the emergence of synaptic plasticity can be better understood by interpreting them with the small networks. Moreover, the integration of small interacting networks would possibly describe dynamic behaviours of larger systems.

The phosphorylation/dephosphorylation of AMPAR is a good example of SM in investigating the contribution of protein interactions to the dynamic behaviour of synaptic plasticity. The bidirectional behaviour of synaptic plasticity is interpreted through the dynamics of modulators and their interactions (d'Alcantara et al., 2003) or is reflected by a 'U shape' in the quantities in terms of the AMPAR, such as the AMPAR conductance (Castellani et al., 2005), having Ca^{2+} level as the control parameter. The bidirectional behaviour of synaptic plasticity is facilitated by the different cooperativity of Ca^{2+} between kinases and phosphatases and may have to obey some criteria in basal conditions (d'Alcantara et al., 2003). In addition, the neuronal decision in the functional direction of synaptic plasticity may be encoded in the stimulus frequency. The decision is transduced by the Ca^{2+}-CaM interacting network and decoded by the autophosphorylation (Bradshaw et al., 2003; Castellani et al., 2005; Chiba et al., 2008; Dupont et al., 2003). Moreover, SMs are developed for other areas of the brain. A synaptic plasticity model in cerebellum (Kitagawa et al., 2009) suggests that the PDE1-mediated regulation of cAMP sets the threshold for the cerebellar

inhibitory synaptic plasticity that may be applicable in hippocampal synaptic plasticity as well.

2.4.3 Complete pathway models

CPMs contain far more synaptic proteins than the other two categories of models. In addition to the essential modulators of synaptic plasticity, the synaptic proteins involved in the production, maintenance, and communication among the essential modulators, which do not have direct implications to synaptic plasticity, are also included. These features make CPMs appear more realistic and accurate against experiments, but they are difficult to develop and the estimation of parameters is very challenging. Good examples of CMPs are model of kinases and phosphatase interactions by Hayer and Bhalla (2005), and model of PKA and cAMP interactions by Kim et al. (2011).

2.4.3.1 Model of kinases and phosphatase interactions

The model developed by Hayer and Bhalla (2005) is an expansion of the 1999 model (Bhalla and Iyengar, 1999) with remarkable additions: (1) the two compartments for the cytoplasm and PSD of the postsynaptic neuron; (2) involvement of the AMPAR recycling between the two compartments; (3) a single model with both LTP and LTD; and (4) stochastic analyses of the robustness of the bi-stability of synaptic plasticity.

The model describes the detailed cascade from the NMDAR induced Ca^{2+} influx to the phosphorylation/dephosphorylation on AMPAR. It is a comprehensive model with 256 variables and is divided into many small sub-models, where each sub-model describes the dynamics of a modulator. The sub-models include CaMKII reactions, CaM reactions, PP1 reactions, PP2b reactions, PKA reactions, cAMP reactions and AMPAR trafficking reactions. Many elementary reactions are modelled in the sub-models according to mass action rate law to describe the state transitions of the modulators into the functional state. The interactions among the sub-models, as the elementary reactions among the functional state of the modulators, formulate the interaction of the larger network to induce synaptic plasticity.

The model investigates the bi-stability of the postsynaptic responses under different network environments which may be existed in the synaptic system (network 0-5), where network 0 formulates the original model used for the parameter estimation and network 1-5 make specific modifications on the original model (as well as the sub-models) to answer specific questions asked. Analyses of networks 1 and 2 propose a new bi-stable switch with respect to the number of the functional AMPAR (AMPAR switch) that may be the mechanisms underlying the structural changes for a silent synapse to become active. Network 3 shows a bi-stable switch with respect to the level of CaMKII autophosphorylation (CaMKII switch), which has been proposed in many models (Dosemeci and Albers, 1996; Kubota and Bower, 2001; Zhabotinsky, 2000) and the experimental literature (Lisman and McIntyre, 2001). Moreover, the coupling between the AMPAR switch and the CaMKII switch are investigated under two situations: (1) Network 4: tight coupling, where a common pool of PP1 participates in dephosphorylating both AMPAR and CaMKII; and (2) Network 5: weak coupling, where the dephosphorylation of AMPAR and CaMKII are processed by independent PP1 pools. The above situations may be coexisting because the AKAPs mediated protein cluster has the local dynamics among the proteins in the cluster (model 4) and the global dynamics to other clusters (model 5). The results of the simulation show that the AMPAR switch is dominant for LTP induction to drive AMPAR into PSD and the CaMKII switch fine tunes the conductance of AMPAR based on the frequency of the stimulus. In addition, the results show that turning on of the CaMKII switch along also induces slow turning on of the AMPAR switch possibly through saturating the PP1-dependent dephosphorylation, which is consistent with the experimental observations (Tomita et al., 2005). With this ability of the CaMKII switch, the role of cAMP-PKA pathway may be to enhance: (1) the CaMKII switch through inhibiting PP1 to decrease the threshold of Ca^{2+} levels for induction of the autophosphorylation; and (2) the movement of as much AMPAR as possible into extrasynaptic sites. The importance of this role of cAMP-PKA pathway is highlighted in the situation where a single train of HFS is unable to induce LTP without PKA (Otmakhova et al., 2000; Zhang et al., 2011). Moreover, turning on both switches would extend the high state duration even to life

time that is unlikely with turning on of individual switch alone. Further investigation on robustness of the switches suggests that it is difficult to turn on both switches, but it is very robust against stochasticity when both switches are on.

2.4.3.2 Model of PKA and cAMP interactions

The model developed by Kim et al. (2011) is an expansion from the 2010 work (Kim et al., 2010) and evaluates into a multi-compartmental stochastic reaction-diffusion model of the Ca^{2+} dependent cAMP/PKA interaction pathway. Kim et al. (2011) use this model to understand the significance of the spatial specificity of PKA by AKAPs in the emergence of synaptic plasticity. The approach is extraordinarily important because that the spatial movement and targeting of synaptic proteins are essential elements of synaptic plasticity, but very few works have looked at this direction (Kotaleski and Blackwell, 2010). The approach is also applied to study spatial specificity of PKA in striatal synaptic plasticity (Oliveira et al., 2012).

Kim et al. (2011) model the detailed synaptic interactions related to cAMP/PKA pathway. The model includes a Ca^{2+} and dopamine (activates AC) sub-model which describes dynamics of Ca^{2+} and dopamine; a cAMP signalling sub-model which describes the regulation of cAMP as well as the production of PKA in response to Ca^{2+} and dopamine elevations; a Ca^{2+} activated signalling sub-model which describes the activation of CaMKII and the activation of phosphatases, including PP2b and PP1, as well as the interactions between phosphatases and PKA through the phosphorylation of I1; and an AMPAR signalling sub-model which describes the phosphorylation states of Ser845/Ser831 of AMPAR. Interactions among the sub-models formulate the complex signalling pathway from Ca^{2+} influx to the alterations on AMPAR.

In Kim et al.'s work, the diffusible molecules are randomly diffused among many sub volumes towards their targets. The dendrite is divided into many rectangular sub volumes and allows two dimensional diffusion for molecules to move around the dendrite, while the dendritic spine, which is a bulge on the dendrite, is divided into a few cylindrical or conical sub volumes and allows one dimensional diffusion for

molecules to move either towards or away from PSD. The diffusible molecules included in the model are cAMP, ATP, all forms of CaM, CaMKII, I1 and the catalytic subunit of PKA. The diffusions of them are simulated based on the modelling-morphology described above and their diffusion constants.

The results of the simulation suggest that anchoring of PKA near its targets (AMPAR and I1 in the model) or near AC, the source of cAMP, both enhances the activity of PKA; however, the enhancement is larger when PKA is anchored near AC. Moreover, the larger enhancement is regardless of the location of AC; although there is a much greater distance to PSD if AC is in dendrite, anchoring PKA near AC still gains larger enhancement of its activity than anchoring PKA near its targets. Further analysis shows that cAMP is less diffusible because of the strong PDE inactivation, although the diffusibility of cAMP itself is greater than PKA. As a result, microdomains of cAMP are formed near AC. Therefore, the PKA anchored near the microdomains gains greater activation since the inactivation of PKA catalytic subunits is low. The conclusion drawn is that the co-localisation of PKA by AKAPs is crucial for synaptic plasticity. The conclusion is confirmed in mice expressing Ht31 peptide, which disrupts the PKA anchoring, and LTP is impaired in these mice (Kim et al., 2011).

Chapter 3: Mathematical Modelling and Analysis of the Bidirectional Behaviour of Synaptic Plasticity

The emergent properties of the protein interacting networks of the NMDAR-mediated pathway of synaptic plasticity (Fig. 3-1) facilitate the dynamic behaviour of synaptic plasticity (He et al., 2014). In this chapter, we explore the emergent properties in facilitating the bidirectional behaviour of synaptic plasticity in which the antithetic synaptic behaviours, LTP and LTD, are triggered by a common signalling upstream, the Ca^{2+} level. The bidirectional behaviour, as an essential participant of the early phase synaptic plasticity, is facilitated by Ca^{2+} and CaM sensitive modulators and expressed through the interactions among them. Thus, by investigating the emergent properties involved in the bidirectional behaviour, we can gain deeper understanding of the main factors of the bidirectional behaviour as well as the roles of modulators play in the early phase. Moreover, these investigations may provide insights into the gene expression related to the late phase as well as the biochemical pathways underlying memory formation.

As discussed in Section 2.4.3, many models successfully describe the protein interacting networks of synaptic plasticity and investigate the emergent properties of the pathways. However, these models focus on mimicking the exact dynamics of the modulators for the emergence of synaptic plasticity and do not simplify the interactions or variables. As a result, it is difficult to track down the essential processes for a particular dynamical behaviour of synaptic plasticity, the bidirectional behaviour of synaptic plasticity in this case. This problem can be solved by developing a simplified model which includes the indispensable modulators, as reported in the literature, to be the variables. Analysis of the simplified model will reveal the essential processes as the most sensitive interactions to the bidirectional behaviour.

We develop a new mathematical model of the NMDAR-mediated pathway of synaptic plasticity (MoNP) using Ca^{2+} level as the input. The development of MoNP is driven by the critical question: what are the essential processes required for the bidirectional behaviour of synaptic plasticity? The essential processes of the bidirectional behaviour are defined as the synaptic protein interactions which are strongly correlated to the bidirectional behaviour. Alterations on these interactions should significantly influence the bidirectional behaviour. These essential interactions can lead to the understanding of the roles of the essential modulators play in facilitating the bidirectional behaviour. However, identifying these interactions is very challenging, because it is difficult to predict the function of a synaptic protein interaction when it is interacting in a complex set of synaptic protein interacting networks.

We take a few steps to track down these essential processes: (1) we search the literature for the experimentally reported Ca^{2+} driven processes that reveal strong correlation to either LTP or LTD; (2) we develop sub-models for these Ca^{2+} driven processes to validate and understand their potential roles in the dynamical behaviour of synaptic plasticity. One criteria for the development of the sub-model is to use minimal states of the synaptic proteins, while maintaining the essential features of the process; and (3) we integrate the established sub-models to form the whole synaptic protein interacting network to analyse the processes most sensitive to the bidirectional behaviour of synaptic plasticity.

Consequently, MoNP has a considerably small number of variables determined by experimentally reported critical synaptic modulators. Moreover, the model development is based on up to date biological meaningful interactions and the experimentally determined kinetic properties of the modulators. The main contribution of MoNP is the establishment of a new model of synaptic plasticity based on a considerably small number of modulators, but integrating: (1) the essential features of the synaptic modulators/pathway as discussed in Section 2.3; (2) the latest experimentally determined kinetic parameters of the modulators; and (3) the latest

biochemical interactions among synaptic modulators. Most importantly, MoNP exhibits the bidirectional behaviour of synaptic plasticity.

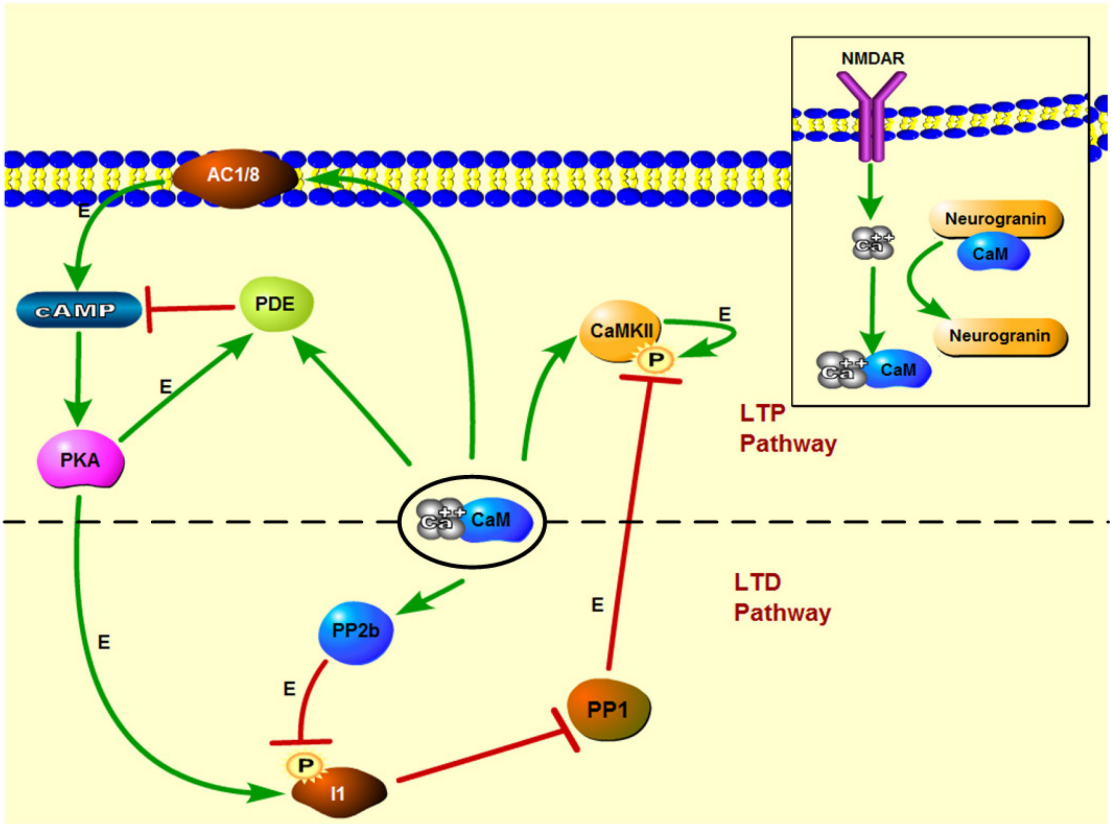

Figure 3-1 NMDAR-mediated pathway of synaptic plasticity. Inset: the activated NMDAR triggers transient Ca^{2+} influx that frees CaM from the neurogranin binding. Ca^{2+} binds to CaM to form Ca^{2+}/CaM complex. **Main**: A moderate elevation of the Ca^{2+} level activates the LTD pathway leading to the activation of PP2b, which dephosphorylates I1 to release PP1. A high elevation of the Ca^{2+} level activates the LTP pathway leading to the activation of CaMKII and AC. AC further activates cAMP, which then activates PKA. The activity of cAMP is inhibited by PDE, whose activity is promoted by both PKA and Ca^{2+}/CaM complex. The two sub pathways also interact with each other. PP1 reverses the autophosphorylation of CaMKII, while PKA inhibits the activation of PP1 through phosphorylating I1. (E denotes an enzymatic reaction).

The sub-models included in MoNP are Ca^{2+}-CaM interaction (see Section 3.2.1 for the explanation of the pathway, derivation and analysis), CaM competition dynamics (see Section 3.2.2), PKA activation pathway (see Section 3.3.1), PP2b activation pathway (see Section 3.3.2), PP1 activation pathway (see Section 3.3.3), and CaMKII activation pathway (see Section 3.3.4). The variables included in these sub-models are reported critical in the literature and have the similar or moderately slower effective timescales to the timescale of Ca^{2+}-CaM interaction in forming Ca^{2+}/CaM complex, which initiates the signalling cascade of synaptic plasticity (Xia and Storm, 2005) (see Appendix B.1.1 for the reason for comparing the effective timescales).

We ignore the AMPAR trafficking and the NMDAR activation. Although AMPAR trafficking is the main target of the protein interacting networks of synaptic plasticity, it has a much slower timescale than the protein interactions of the pathway (Ehlers, 2000). Since our focus is the dynamic behaviour of the synaptic protein interacting networks, and is not particularly on the resulting alterations on AMPAR caused by the protein interactions, the alteration on AMPAR trafficking can be represented by the similar phosphorylation on other substrates, such as the phosphorylation of I1. The activation of NMDAR has an impact on the Ca^{2+} influx as well as the resulting elevation, but the process is extensively modelled previously. We take the approach by Zhabotinsky (2000) to model the Ca^{2+} dynamics following the Ca^{2+} influx (see Appendix G for the detailed explanation).

The general assumptions on which the sub-models are based include:

(1) We only consider a single compartment as the dendritic spine (approximately 0.1 fL = 10^{-16} L = 10^{-19} m^3), and assume the biochemical reactions taken place in a well-mixed volume such that the concentrations of modulators are even across the compartment. We ignore the possible local dynamics of the modulators as well as the dynamics in PSD.

(2) For those indispensable biochemical reactions which are Ca^{2+} independent, or much faster than the Ca^{2+}-CaM interaction, we assume that they are always in the

equilibrium. The associated dynamics of proteins involved in these reactions are expressed by the equilibrium rate.

(3) The bidirectional behaviour of synaptic plasticity is an essential element of the early phase synaptic plasticity, where gene expression is not altered. Hence, we assume the total numbers of modulators are at steady states, i.e., new syntheses of modulators remain at a rate that exactly balances their degradations.

(4) Phosphorylation and dephosphorylation are catalytic reactions to be described by Michaelis-Menten kinetics. All other reactions are assumed to obey mass action kinetics (see Appendix B for the explanation).

The general assumptions are applied to all the sub-models and may couple with more specific assumptions for each case.

This chapter contains 5 sections: a discussion and summary of the experimentally estimated kinetic characteristics of the modulators is given in Section 3.1 to support the model development; then we demonstrate the development of the sub-models based on biochemical interactions (ordinary differential equation (ODE); see Appendix B for the explanation and derivation) and analyse their steady states in response to Ca^{2+} levels to highlight the essential features of the modulators for the bidirectional behaviour of synaptic plasticity. The discussion of the features is separated into two sections: (1) features related to Ca^{2+}/CaM complex formation and competition in Section 3.2, and (2) features related to Ca^{2+} and CaM sensitive modulators in Section 3.3. In Section 3.4, we analyse the dynamics of the integrated model, MoNP, to understand the factors of the bidirectional behaviour of synaptic plasticity. Lastly, we summarise the results in Section 3.5.

3.1 Kinetic characteristics of essential modulators

In this section, the kinetic characteristics of the modulators are summarised. The kinetic characteristics include the affinities of bindings, mainly to Ca^{2+} or CaM; the enzymatic properties of kinases and phosphatases; the approximate concentrations in the neuron;

and other relevant to the development of MoNP. Most kinetic characteristics of the modulators are estimated experimentally (Brenda: http://www.brenda-enzymes.info, or DOQCS: http://doqcs.ncbs.res.in/) while only a few remain unknown, but are estimated by computational procedures (Chiba et al., 2008; Hayer and Bhalla, 2005; Kim et al., 2011). When both experimental and computational estimations exist, we obtain the ranges of the experimentally estimated kinetic characteristics and compare them to the computational estimations. If they match (within 30% margin of difference), we use the computational estimations; otherwise, we use the mean of experimental estimations.

3.1.1 Determining turnover rate of enzymatic reactions

The enzymatic activity of an enzyme is usually estimated experimentally based on Michaelis–Menten kinetics and the estimation establishes two parameters, K_m and V_{max} (see Appendix B.2). V_{max} is the maximum reaction rate of the enzymatic reaction to turn a substrate into a product and K_m is the concentration of the substrate when the reaction rate is half of V_{max} (see Fig. B-4). V_{max} can be approximated by a function in terms of the concentration of the active enzyme, $[E_a]$, given as $V_{max} = K_{cat}[E_a]$, where K_{cat} is called the turnover rate of the reaction equivalent to the rate constant of turning the substrate into the product (see Appendix B.2).

Since $[E_a]$ is dynamically changing due to the dynamic protein interaction, determination of K_{cat} is essential for estimating the reaction rate. The unified V_{max} unit is mol/(min.mg), expressed as the number of moles of the product formed per milligram of the enzyme over one minute. (mol/(min.mg) is convertible to the usual unit of the reaction rate, mol L^{-1} s^{-1}, given the volume of the reaction and the mass of the enzyme). To calculate K_{cat} from V_{max}, the atomic mass of the enzyme, m_a (in Dalton), must be known. Hence, the K_{cat} (s^{-1}) can be calculated as given by Eq. (3.1):

$$K_{cat} = 1000 V_{\max} m_a / 60 . \tag{3.1}$$

The K_m and K_{cat} of enzymatic reactions associated with the essential modulators are summarised in Table 3-1.

3.1.2 Determining dissociation constant of bindings

The dissociation constant, K_d, of a binding between two proteins can be determined by the quotient of their dissociation rate constant, k_{off}, divided by their association rate constant, k_{on}, given as $K_d = k_{off}/k_{on}$. K_d is a good indicator of the binding strength (or the affinity of the binding) between two proteins (the lower the stronger) and provides further information for the competitive dynamics among a mixture of proteins, which have the same binding partner. The modulators of synaptic plasticity usually require the binding to their activators to induce a conformational change for the activation and the CaM binding modulators may bind competitively to CaM for the activation. The kinetic properties of the bindings are summarised in Table 3-2. As shown in the table, PP2b has the strongest affinity (28 pM) for the CaM binding among the CaM binding proteins listed; however, the autophosphorylation of CaMKII strengthens the binding affinity between CaMKII and CaM (52 pM) to the same level of PP2b. While PP2b and CaMKII are critical for the induction of LTD and LTP, respectively, the CaM competition may have a role in the bidirectional behaviour of synaptic plasticity. Furthermore, the binding affinity between PKA regulatory (PKAr) and catalytic (PKAc) subunits is strong, suggesting a low level of the PKA catalytic subunits existing alone.

Table 3-1

Summary of the enzymatic characteristics of the modulators

Substrate	*Product*	*Enzyme*	K_{cat} (s^{-1})	K_m (μM)	*Source*
I1	*I1**	*PKA*	*1.4*	*5*	[4],[6]
*I1**	*I1*	*PP2a*	*2*	*16*	[3]
		PP2b	*2.8*	*3*	[8],[9]
CaMKII	*CaMKII**	*CaMKII*	*1.2~10*	*19*	[2],[7]
*CaMKII**	*CaMKII*	*PP2a*	*2*	*16*	[3]
		PP1	*1.72*	*11*	[2]
ATP	*cAMP*	*AC1/AC8*	*2.843*	*230*	[3],[8]
		Ca^{2+} *ind. AC*	*2*	*230*	[3],[8]
cAMP	*AMP*	*PDE1*	*1.7*	*10*	[10]
		CaM-PDE1	*10*	*10*	[10]
		PDE4B	*1.56*	*4.5*	[11]
		PDE4D	*5.4*	*1.5*	[11]
		*PDE4B**	*3.12*	*4.5*	[5]
		*PDE4D**	*10.8*	*1.5*	[5]
PDE4	*PDE4**	*PKA*	*18*	*25*	[1]

* phosphorylated; [1] Bastidas et al. (2012); [2] Chiba et al. (2008); [3] Hayer & Bhalla (2005); [4] Hemmings et al. (1984); [5] Hoffmann et al. (1998); [6] Huang & Paudel (2000); [7] Huynh & Pagratis (2011) [8] Kim et al. (2011); [9] Klee et al. (1998); [10] Sharma & Wang (1986); [11] Wang et al.(2007).

Table 3-2

Summary of the binding affinities between the modulators

Prot. A	***Prot. B***	k_{on} ($\mu M^{-1}s^{-1}$)	k_{off} (s^{-1})	K_d	***Source***
Ca^{2+}/*CaM Complex*	*PP2b (CaNA)*	*46*	$0.0012^{H}/0.2\sim2^{L}$	*28 pM/≈5 nM*	[4]
	PDE1	*100*	*1*	*10 nM*	[3]
	AC1	*50*	*1*	*20 nM*	[2]
	AC8	*20*	*1*	*50 nM*	[1]
	CaMKII	*21*	$1.1/0.0011^{A}$	*51 nM/52 pM*	[4]
PKAr	*PKAc*	*0.17*	*0.0016*	*9 nM*	[6]

^{L} low [Ca^{2+}]; ^{H} high [Ca^{2+}]; ^{A} autophosphorylated. [1] Cali et al. (1994); [2] Hayer & Bhalla (2005); [3] Kim et al. (2011); [4] Quintana et al. (2005); [5] Stemmer and Klee (1994); [6] Zawadzki & Taylor, (2004).

3.1.3 The concentrations of modulators in brain

Most of the modulators have their brain concentration measured in the unit of μM. But the concentrations of PP2b, ACs and CaM dependent PDEs are given in the units of μg per mg proteins (Su et al., 1995), percentage of total membrane proteins (Gomperts et al., 2009), and percentage of total cellular proteins (Polli and Kincaid, 1994), respectively. However, the concentration of CaM is given in both units of μg per mg proteins and μM (Kakiuchi et al., 1982) that gives us an estimated concentration, 2.1μM, of PP2b. For ACs and PDEs, we take the values used by a previous computational study (Kim et al., 2010), since the exact total amount of synaptic proteins is unclear. There are two types of ACs in hippocampus: Ca^{2+} dependent ACs, including isoform type 1/8 (AC1 and AC8); and Ca^{2+} independent ACs. AC8 accounts for less than 20% of Ca^{2+} dependent ACs in hippocampus (Wang et al., 2003). The previous computational study uses 2.5μM for the concentration of AC1, so that the concentration of AC8 is 0.625μM (25% of 2.5 μM). The concentration of Ca^{2+} independent ACs is assumed to be 2.5μM. We also assume equal concentrations between the PDE isoforms type 4B (PDE4B) and type 4D (PDE4D). The concentrations of the modulators are summarised in Table 3-3.

Table 3-3
Summary of the concentrations of the modulators

Prot.	*Con. (μM)*	*Source*
CaM	*17*	[4]
PKA	*1.2*	[3]
PP2b	*2.1*	[7]
PP2A	*0.1111*	[2]
PP1	*3.5*	[5]
I1	*1.5*	[5]
CaMKII	*20*	[2]
PDE1	*4*	[5],[6]
PDE4	*2*	[5]
Ca^{2+} ind. AC	*2.5*	
AC1	*2.5*	[1]
AC8	*0.625*	[8]

[1] Gomperts et al. (2009); [2] Hayer and Bhalla (2005); [3] Hofmann et al. (1977); [4] Kakiuchi et al. (1982); [5] Kim et al. (2010); [6] Polli and Kincaid (1994); [7] Su et al. (1995); [8] Wang et al. (2003)

3.2 Features of Ca^{2+}/CaM complex

In Section 2.3.2, we review the ability of Ca^{2+}/CaM complex to selectively activate CaM binding proteins for different purposes during synaptic plasticity. In this section, we discuss the remarkable features of Ca^{2+}/CaM complex through mathematical analyses regarding: (1) the enhancement of the affinity of CaM for Ca^{2+} by CaM binding proteins, and (2) the competition among CaM binding proteins for the Ca^{2+}/CaM binding.

3.2.1 Enhancement of the affinity of CaM for Ca^{2+} binding

CaM binds to Ca^{2+} by four sequential binding processes; each of the processes attaches one Ca^{2+} ion to CaM. One key point of the binding processes is that CaM binding proteins enhance the affinity of CaM for Ca^{2+} binding (Xia and Storm, 2005). The reaction schema of the sequential bindings to form Ca^{2+}/CaM complex are given as follows:

$$iCaM + Ca^{2+} \underset{k_{1b}}{\overset{k_{1f}}{\rightleftharpoons}} CaCaM\,, \tag{3.2}$$

$$CaCaM + Ca^{2+} \underset{k_{2b}}{\overset{k_{2f}}{\rightleftharpoons}} Ca_2CaM\ , \tag{3.3}$$

$$Ca_2CaM + Ca^{2+} \underset{k_{3b}}{\overset{k_{3f}}{\rightleftharpoons}} Ca_3CaM\ , \text{ and} \tag{3.4}$$

$$Ca_3CaM + Ca^{2+} \underset{k_{4b}}{\overset{k_{4f}}{\rightleftharpoons}} Ca_4CaM\ , \tag{3.5}$$

where iCaM denotes the unbound CaM, Ca_nCaM denotes the CaM complex with n number of Ca^{2+} ions attached and Ca_4CaM is the Ca^{2+}/CaM complex. k_{1f}, k_{2f}, k_{3f} and k_{4f} are association rate constants and k_{1b}, k_{2b}, k_{3b} and k_{4b} are dissociation rate constants. The concentration of Ca^{2+}/CaM complex, $[Ca_4CaM]$, is given by Eq. (3.6) (see appendix B.3 and Eq. (B39) for the derivation):

$$\left[Ca_4CaM\right] = \frac{\left[CaM_T\right]\left[Ca^{2+}\right]^4}{K_{d1}K_{d2}K_{d3}K_{d4} + K_{d2}K_{d3}K_{d4}\left[Ca^{2+}\right] + K_{d3}K_{d4}\left[Ca^{2+}\right]^2 + K_{d4}\left[Ca^{2+}\right]^3 + \left[Ca^{2+}\right]^4}, \tag{3.6}$$

where $[CaM_T]$ is the total concentration of CaM, $K_{d1} = k_{1b}/k_{1f}$, $K_{d2} = k_{2b}/k_{2f}$, $K_{d3} = k_{3b}/k_{3f}$, and $K_{d4} = k_{4b}/k_{4f}$, CaM has an average dissociation constant (K_d) of 14 μM for Ca^{2+} (Olwin et al., 1984) and the concentration of intracellular Ca^{2+} of the neuron ranges from 0.1μM to 10μM (Xia and Storm, 2005). Hence, Eq. (3.6) can be approximated as $\left[Ca_4CaM\right] = \frac{\left[CaM_T\right]\left[Ca^{2+}\right]^4}{K_{d1}K_{d2}K_{d3}K_{d4} + \left[Ca^{2+}\right]^4}$, where $K_{d1}\,K_{d2}\,K_{d3}\,K_{d4} = 14^4 = 38416\ \mu M^4$.

The affinity of CaM for Ca^{2+} binding is enhanced with the presence of CaM binding proteins, which bind to Ca^{2+}/CaM complex for the activation, and the enhancement is in a heterotropic positive cooperative manner with respect to the numbers of unfilled Ca^{2+} binding sites (Keller et al., 1982; Olwin and Storm, 1985). We consider a simple representation of the enhancement by assuming that CaM binding proteins increase the association rate constants for the binding between Ca^{2+} and CaM by a fixed proportion, ø, which is dependent on the properties of CaM binding proteins. Therefore, the enhanced rates are: $k_{4f\_en}=(1+ø)k_{4f}$, $k_{3f\_en}=(1+ø)k_{3f}$, $k_{2f\_en}=(1+ø)k_{2f}$, and $k_{1f\_en}=(1+ø)k_{1f}$. The concentration of Ca^{2+}/CaM complex with the enhancement is given by Eq. (3.7):

$$[Ca_4CaM] = \frac{[CaM_T][Ca^{2+}]^4}{\frac{K_1K_2K_3K_4}{(1+\phi)^4} + [Ca^{2+}]^4}. \tag{3.7}$$

So that, the ratio of [Ca_4CaM] to [CaM_T] is:

$$\frac{[Ca_4CaM]}{[CaM_T]} = \frac{[Ca^{2+}]^4}{\frac{K_1K_2K_3K_4}{(1+\phi)^4} + [Ca^{2+}]^4}. \tag{3.8}$$

As shown in Fig. 3-2, without the enhancement, the accumulation of Ca^{2+}/CaM complex is minor over the normal range of Ca^{2+} levels, while the enhancement decreases the Ca^{2+} level required for the build-up of Ca^{2+}/CaM complex. With a greater enhancement, the formation of Ca^{2+}/CaM complex is initialised at a much lower Ca^{2+} levels. Moreover, a clear difference exists in the build-up of Ca^{2+}/CaM complex among no enhancement, 20% enhancement, 50% enhancement and 100% enhancement. Hence, the formation rate of Ca^{2+}/CaM complex in a local domain is determined by the distinct nature of CaM binding proteins surrounding the CaM molecule. As a result, the distinct nature of the CaM binding protein controls the pattern of the enclosing CaM molecule to form Ca^{2+}/CaM complex having the Ca^{2+} as the parameter. In other words, the CaM binding protein controls the activation of itself, by binding to Ca^{2+}/CaM complex, having the Ca^{2+} as the parameter. Therefore, the CaM binding proteins display distinct Ca^{2+} affinities for their activations (Xia and Storm, 2005). However, instead of considering different enhancements over many local domains of the dendritic spine, we ignore local dynamics and assume a fixed enhancement of the affinity of CaM for Ca^{2+} across the dendritic spine in the derivation of sub-models (assumption (1)).

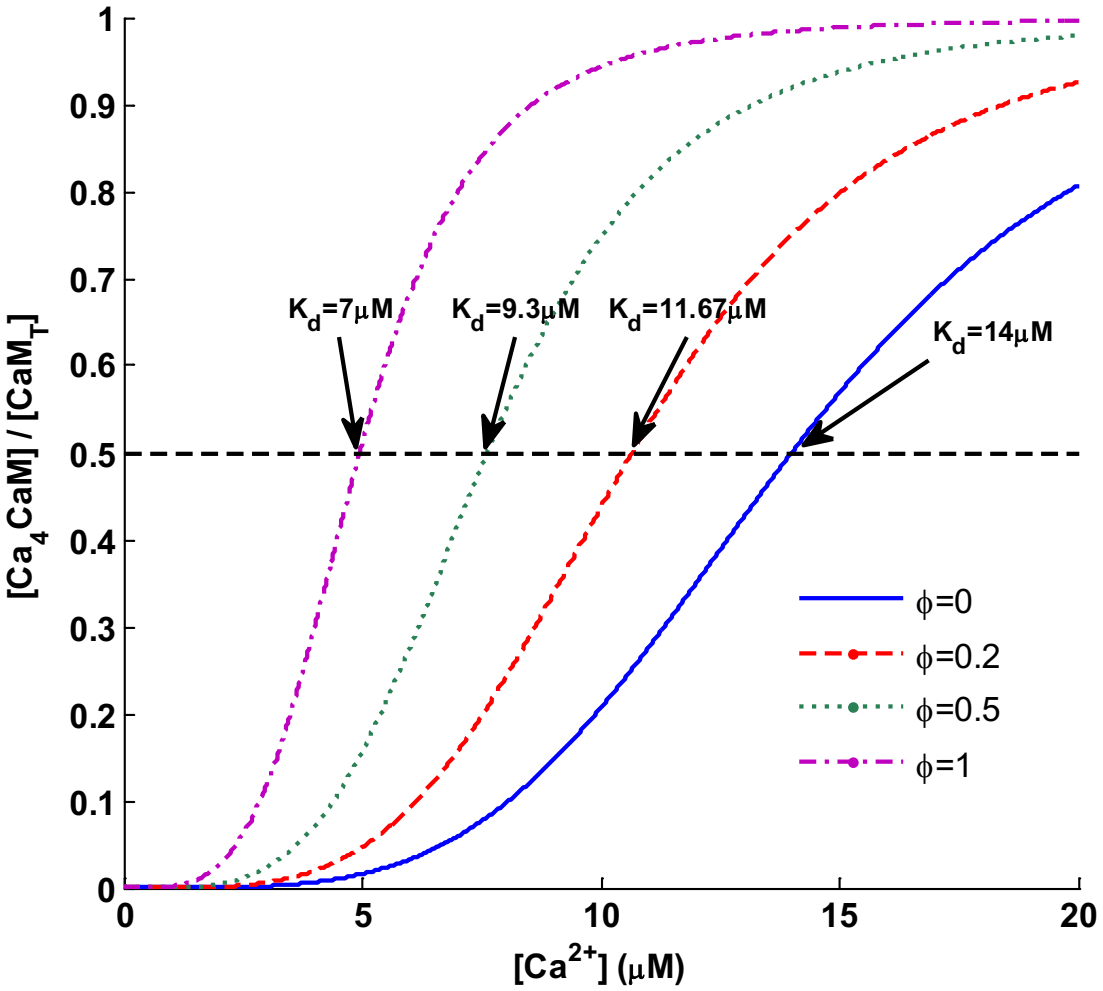

Figure 3-2 The ratio of [*Ca₄CaM*] to [*CaM_T*] with respect to different [Ca^{2+}]. Four ***ø*** are tested: 0, 0.2, 0.5 and 1. At a greater enhancement of the CaM affinifty for Ca^{2+} (larger ***ø*** value), the formation of Ca^{2+}/CaM complex becomes more rapid.

3.2.2 Competitive binding of CaM binding proteins to Ca^{2+}/CaM complex

A number of the modulators bind to Ca^{2+}/CaM for the activation resulting in a competition for Ca^{2+}/CaM complex binding, especially at low levels of Ca^{2+}/CaM complex. The competition may trigger distinct behaviours of proteins in a Ca^{2+} level dependent manner that may be correlated to the bidirectional behaviour of synaptic plasticity.

Four of the selected modulators participate in the competition: (1) PP2b; (2) Ca^{2+}/CaM complex dependent ACs (AC1 and AC8); (3) Ca^{2+}/CaM complex dependent PDE (PDE1); and (4) CaMKII. Importantly, the activation of all the modulators are influenced by the competition, including the direct activation of PP2b and CaMKII, and the indirect activation of PP1 and PKA through activation of PP2b, ACs, and PDE.

Considering the following reaction schema of the competition among CaM binding proteins for the Ca^{2+}/CaM complex (Ca_4CaM) binding:

$$Ca_4CaM + iAC1 \underset{k_{c1b}}{\overset{k_{c1f}}{\rightleftarrows}} CaMAC1, \tag{3.9}$$

$$Ca_4CaM + iAC8 \underset{k_{c2b}}{\overset{k_{c2f}}{\rightleftarrows}} CaMAC8, \tag{3.10}$$

$$Ca_4CaM + iPDE1 \underset{k_{c3b}}{\overset{k_{c3f}}{\rightleftarrows}} CaMPDE1, \tag{3.11}$$

$$Ca_4CaM + iPP2b \underset{k_{c4b}}{\overset{k_{c4f}}{\rightleftarrows}} CaMPP2b, \text{ and} \tag{3.12}$$

$$Ca_4CaM + iCaMKII \underset{k_{c5b}}{\overset{k_{c5f}}{\rightleftarrows}} CaMCaMKII, \tag{3.13}$$

where CaMX denotes the bound complex in which a Ca^{2+}/CaM complex binding to a CaM binding protein, X, and iX denotes the inhibited form of the CaM binding protein.

To understand the effects of the competition, we compare the difference between non-competitiveness and competitiveness of the bindings. For independent compartment (non-competitive binding) mixing Ca^{2+}/CaM complex with one of the CaM binding

proteins, the equilibrium level of the bound complex, denoted by [$CaMX_e$], can be expressed as an equation in terms of the initial concentration of Ca^{2+}/CaM complex (or the total concentration of Ca^{2+}/CaM complex in the system), [Ca_4CaM_0] (Hulme and Trevethick, 2010):

$$[CaMX_e] = \frac{\Delta - \sqrt{\Delta^2 - 4[X_T][Ca_4CaM_0]}}{2} \quad , \tag{3.14}$$

where $K_d = k_b/k_f$, [X_T] is the total concentration of X expressed as [X_T] = [X_e] + [$CaMX_e$] and Δ=[X_T] + [Ca_4CaM_0] + K_d (subscripts e denotes equilibrium, 0 denotes initial and T denotes total). Meanwhile, we have ODEs based on mass action rate law to describe the competitive dynamics among the CaM binding proteins mixing in a common compartment. Numerical solution of the ODEs gives the competitive dynamics among CaM binding proteins for the Ca^{2+}/CaM binding. The ODEs are given by Eqs. (3.15 – 3.19):

$$\frac{d[CaMAC1]}{dt} = k_{c1f}[Ca_4CaM][iAC1] - k_{c1b}[CaMAC1], \tag{3.15}$$

$$\frac{d[CaMAC8]}{dt} = k_{c2f}[Ca_4CaM][iAC8] - k_{c2b}[CaMAC8], \tag{3.16}$$

$$\frac{d[CaMPDE1]}{dt} = k_{c3f}[Ca_4CaM][iPDE1] - k_{c3b}[CaMPDE1], \tag{3.17}$$

$$\frac{d[CaMPP2b]}{dt} = k_{c4f}[Ca_4CaM][iPP2b] - k_{c4b}[CaMPP2b], \tag{3.18}$$

$$\frac{d[CaMCaMKII]}{dt} = k_{c5f}[Ca_4CaM][iCaMKII] - k_{c5b}[CaMCaMKII], \tag{3.19}$$

where [$iAC1$] = [$AC1_T$] - [$CaMAC1$], [$iAC8$] = [$AC8_T$] - [$CaMAC8$], [$iPDE1$] = [$PDE1_T$] - [$CaMPDE1$], [$iPP2b$] = [$PP2b_T$] - [$CaMPP2b$] and [$iCaMKII$] = [$CaMKII_T$] - [$CaMCaMKII$] according to the mass conservation law.

The comparison of the bound portions of CaM binding proteins between non-competitiveness and competitiveness of the bindings is shown in Fig. 3-3. Without the competition, AC1, AC8, PDE1 and PP2b can be activated by very low levels of Ca^{2+}/CaM complex (Fig. 3-3A – 3-3D), while CaMKII requires a high level of Ca^{2+}/CaM complex for the complete activation due to its large concentration in the

synapse (Fig. 3-3E). The competition triggers different behaviours among these proteins, indicated by the changes of their $K_{0.5}$ values ($K_{0.5}$ measures the [Ca_4CaM] at which the bound portion of the CaM binding protein reaches half). Only the build-up of PP2b ($K_{0.5}$ changes from 1.05μM to 1.11μM) is slightly influenced by the competitiveness of the binding, while the build-ups of PDE1 ($K_{0.5}$ changes from 2.01μM to 8.25μM), AC1 ($K_{0.5}$ changes from 1.27μM to 11.74μM), AC8 ($K_{0.5}$ changes from 0.365μM to 17.34μM) and CaMKII ($K_{0.5}$ changes from 10.06μM to 17.64μM) are strongly influenced. The reason is that PP2b binds to Ca^{2+}/CaM complex at a much higher affinity than other CaM binding proteins (K_d: 28pM for PP2b, 10nM for PDE1, 20nM for AC1, 50nM for AC8 and 51nM for CaMKII; see Table 3-2) . Hence, PP2b binds to Ca^{2+}/CaM complex under a minor competition from other CaM binding proteins. PDE1 is less influenced than ACs and CaMKII, because PDE1 binds the strongest to Ca^{2+}/CaM among them. As a result, the binding of PDE1 to Ca^{2+}/CaM complex suffers a strong competition from PP2b and a weaker competition from others. Meanwhile, ACs and CaMKII bind to Ca^{2+}/CaM complex against the strong competitions from both PP2b and PDE1. Another finding is that the competitiveness arranges CaM binding proteins, in terms of their $K_{0.5}$, in a Ca^{2+} activation order which is biological meaningful against their specific roles in synaptic plasticity: (1) moderate Ca^{2+}/CaM complex activated for LTD, including PP2b (1.11μM) and PDE1 (8.25μM); and (2) high Ca^{2+}/CaM complex activated for LTP, including AC1 (11.74μM), AC8 (17.34μM) and CaMKII (17.64μM). Moreover, the two groups of CaM binding proteins, related to LTP or LTD, are separated by a relative large $K_{0.5}$ of 3.5μM. The arrangement by the non-competitiveness is mixed: AC8 (0.365 μM), PP2b (1.05μM), AC1 (1.27μM), PDE1 (2.01μM), and CaMKII (10.06μM).

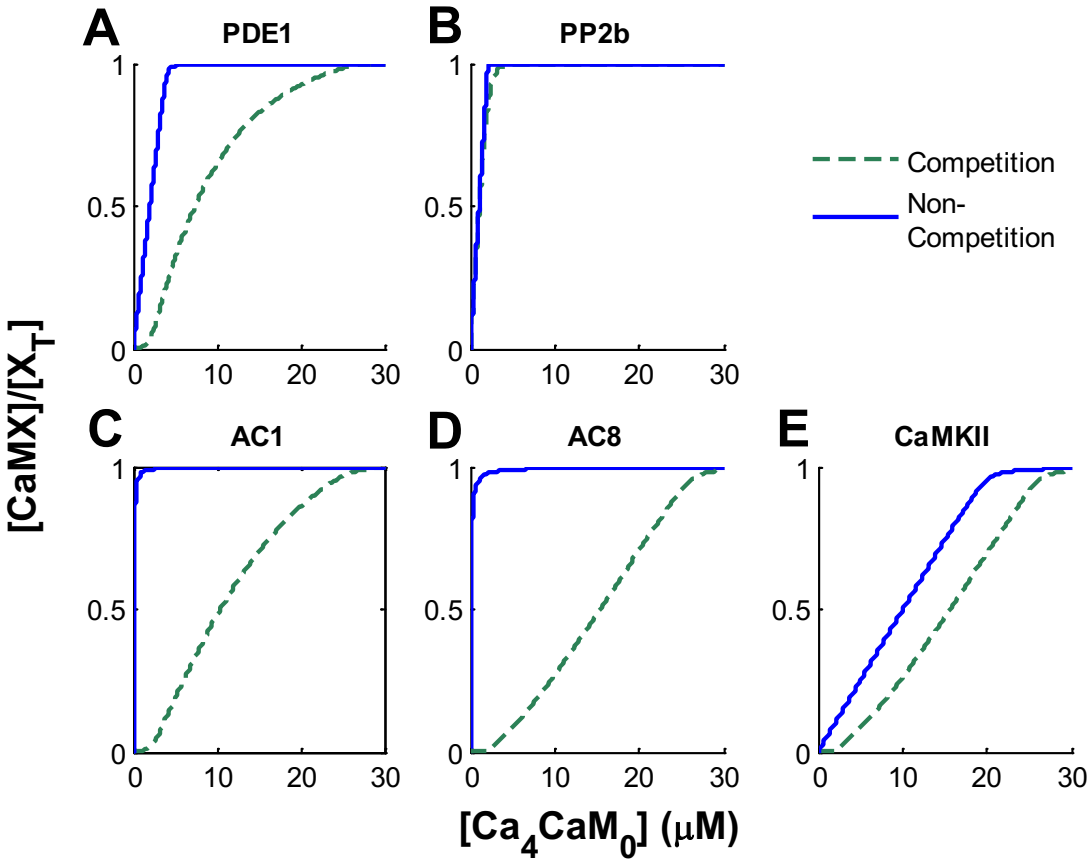

Figure 3-3 The bound portion of CaM binding proteins under non-competitiveness and competitiveness of the bindings. Parameters used are shown in Table 3-2 and the total concentrations of proteins are shown in Table 3-3. Figures show the bound portions of CaM binding proteins at steady state with respect to different initial concentrations of Ca^{2+}/CaM complex under both the non-competitiveness (blue solid lines) and competitiveness (green dahsed lines) of the bindings to Ca^{2+}/CaM complex. Five CaM binding proteins are involved in the competitive binding: (**A**) PDE1, (**B**) PP2b, (**C**) AC1, (**D**) AC8, and (**E**) CaMKII.

Interestingly, when CaMKII is removed, other CaM binding proteins bind to Ca^{2+}/CaM complex rapidly (Fig. 3-4). The explanation is that CaMKII is abundant in synapses (Sheng and Hoogenraad, 2007), so that the activation of CaMKII consumes a large amount of Ca^{2+}/CaM complex that restricts the binding of Ca^{2+}/CaM complex to other CaM binding proteins. Moreover, without CaMKII, the Ca^{2+} activation order remains, but the separation between two groups of CaM binding proteins narrows to 1.16μM (PDE1 (5.05μM) and AC1 (6.21μM)). Hence, it is unclear whether the concentration of CaMKII has a critical role in the bidirectional behaviour of synaptic plasticity. We analyse further the implication of the CaMKII concentration in the dynamical behaviour of synaptic plasticity using MoNP in Section 3.4.1.

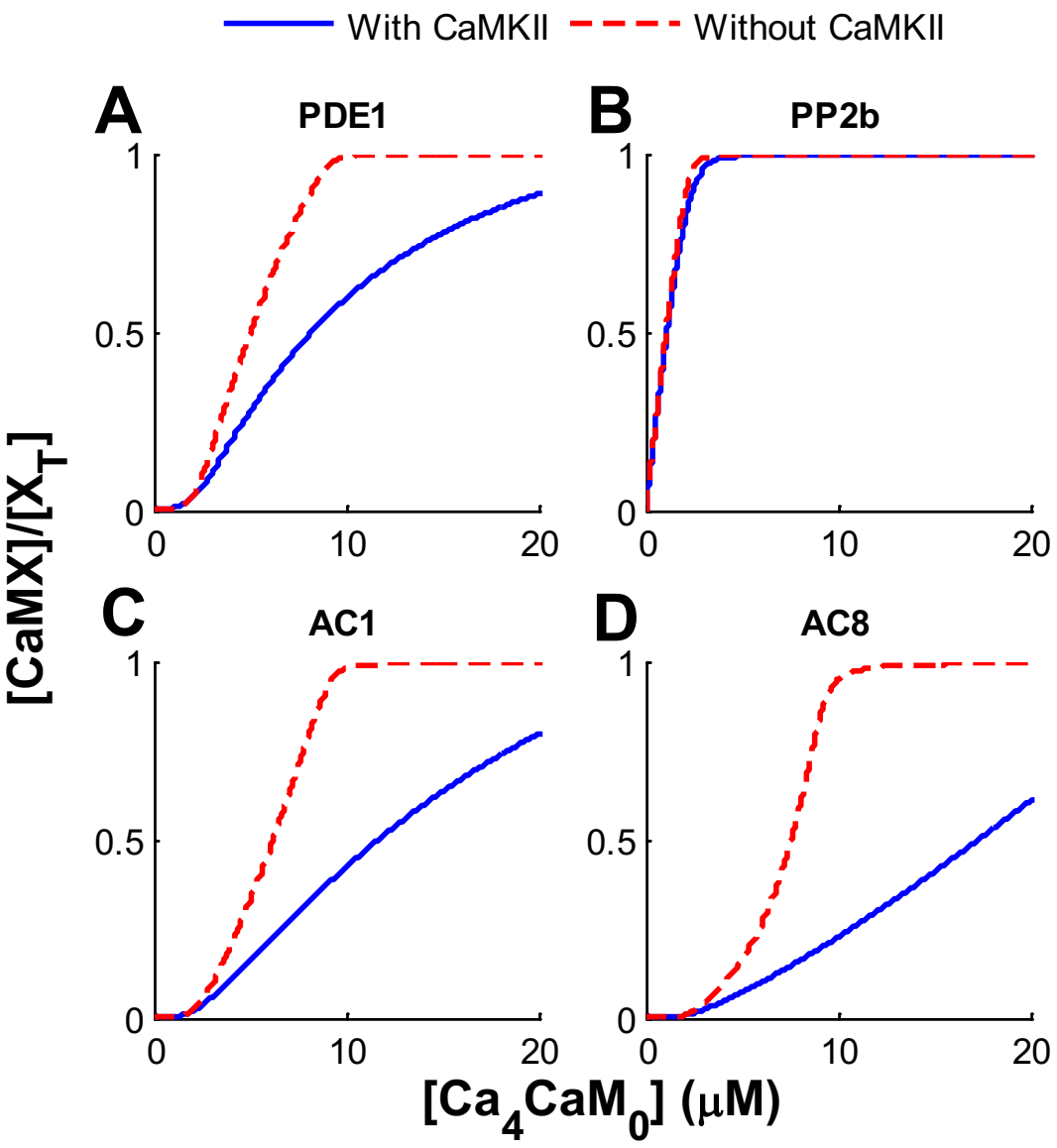

Figure 3-4 The bound portion of CaM binding proteins under the competitioness of the bindings with or without CaMKII. Figures show the bound portions of CaM binding proteins with the competitiveness of the bindings at steady state with respect to different initial concentrations of Ca^{2+}/CaM complex with (blue solid lines) or without (red dahsed lines) CaMKII. CaM binding proteins shown are: (**A**) PDE1, (**B**) PP2b, (**C**) AC1, and (**D**) AC8.

3.3 Ca^{2+} dependent activation of modulators

In this section, we discuss the Ca^{2+} dependent activation of the modulators, including cAMP, PKA, PP2b, PP1 and CaMKII. We develop sub-models for the activation pathway of these modulators based on reaction schema summarised in varies databases, including Brenda and DOQCS as previously mentioned, and analyse the steady states of the established models in isolation to understand the emergent properties of the pathways that contribute to the bidirectional behaviour of synaptic plasticity. This section has four parts: (1) PKA activation pathway, (2) PP2b activation pathway, (3) regulation of PP1 by phosphorylating I1, and (4) regulation of CaMKII autophosphorylation by PP1.

3.3.1 PKA activation pathway

The PKA activation pathway involves the activations of cAMP through stimulating ACs by Ca^{2+} or G-proteins and, the regulation of cAMP by PDEs, and the binding of cAMP to the regulatory dimmer of PKA as introduced in Section 2.3.4 (Ferguson and Storm, 2004; Wang and Strom, 2003). The major function of this pathway is to modulate the activity of PKA, which has a critical role in LTP, through regulating the activity of cAMP. We model this pathway as three parts: (1) activation of cAMP; (2) inhibition of cAMP; and (3) cAMP dependent activation of PKA and the estimation of unknown parameters. Then, we analyse the pathway and highlight the critical behaviour of the pathway.

3.3.1.1 Activation of cAMP

A number of proteins can stimulate AC to produce cAMP, i.e. Ca^{2+}/CaM and G-proteins. Our main focus is the critical Ca^{2+} dependent processes during synaptic plasticity, hence we assume that the activity of Ca^{2+} independent pathways remains at equilibrium (assumption 2). As a result, the activity of Ca^{2+} independent ACs (denoted by AC2) is expressed at the equilibrium rate. The process of activating cAMP is described by the reaction schema as follows:

$$iAC2 \underset{k_{5b}}{\overset{k_{5f}}{\rightleftarrows}} AC2\,, \tag{3.20}$$

$$Ca_4CaM + iAC1 \underset{k_{c1b}}{\overset{k_{c1f}}{\rightleftarrows}} CaMAC1\,, \tag{3.21}$$

$$Ca_4CaM + iAC8 \underset{k_{c2b}}{\overset{k_{c2f}}{\rightleftarrows}} CaMAC8\,, \tag{3.22}$$

$$ATP + CaMAC1 \underset{k_{6b}}{\overset{k_{6f}}{\rightleftarrows}} CaMAC1ATP \xrightarrow{K_{cat1}} cAMP + CaMAC1\,, \tag{3.23}$$

$$ATP + CaMAC8 \underset{k_{7b}}{\overset{k_{7f}}{\rightleftarrows}} CaMAC1ATP \xrightarrow{K_{cat2}} cAMP + CaMAC8\,, \text{ and} \tag{3.24}$$

$$ATP + AC2 \underset{k_{8b}}{\overset{k_{8f}}{\rightleftarrows}} AC2ATP \xrightarrow{K_{cat3}} cAMP + AC2\,. \tag{3.25}$$

Reactions (3.20 – 3.22) are elementary reactions for the state transition of Ca^{2+} independent ACs and the binding between Ca^{2+}/CaM complex and AC1/AC8 (see Eqs. (3.15 and 3.16) for the binding dynamics). Reactions (3.23 - 3.25) are enzymatic catalysed reactions to convert ATP into cAMP by AC1, AC8 and AC2, respectively.

The equilibrium concentration of active Ca^{2+} independent ACs, [*AC2*], is given by Eq. (3.26):

$$[AC2] = \frac{[AC2_T]}{1+K}, \tag{3.26}$$

where [$AC2_T$] is the total concentration of AC2 and $K = k_{5b}/k_{5f}$.

Based on Michaelis and Menten rate law, the conversion rates (the same unit, micro molar per second (μM/s), applies for all the reaction rates in Chapter 3) of ATP into cAMP catalysed by AC1 (V_1), AC8 (V_2) and AC2 (V_3) are given by Eqs. (3.27 - 3.29):

$$V_1 = \frac{K_{cat1}[CaMAC1][ATP]}{K_{m1} + [ATP]}, \tag{3.27}$$

$$V_2 = \frac{K_{cat2}[CaMAC8][ATP]}{K_{m2} + [ATP]}, \text{ and} \tag{3.28}$$

$$V_3 = \frac{K_{cat3}[AC2][ATP]}{K_{m3} + [ATP]}\,, \tag{3.29}$$

where $K_{m1} = (k_{6b} + K_{cat1})/k_{6f}$, $K_{m2} = (k_{7b} + K_{cat2})/k_{7f}$, and $K_{m3} = (k_{8b} + K_{cat3})/k_{8f}$. Since ATP is abundant in all cells (ATP >> K_{mi}, i =1, 2, 3), we assume that the concentration

of ATP is a very large constant, such that $\frac{[ATP]}{K_m + [ATP]} \approx 1$. Hence, the production rate of cAMP, V_{cAMP_prod}, is given by Eq. (3.30):

$$V_{cAMP\_prod.} = V_1 + V_2 + V_3 = K_{cat1}[CaMAC1] + K_{cat2}[CaMAC8] + \frac{K_{cat3}[AC2_T]}{1+K} \quad . \tag{3.30}$$

3.3.1.2 Inhibition of cAMP

PDEs convert cAMP into AMP, but the conversion rates are different among PDE isoforms and are promoted by different proteins. For instance, PDE1 is promoted by Ca^{2+}/CaM complex and PDE4 is phosphorylated and promoted by PKA catalytic subunits, PKAc. Such interactions dynamically regulate the concentration of cAMP as given by the reaction schema as follows:

$$PDE4B + PKAc \underset{k_{9b}}{\overset{k_{9f}}{\rightleftarrows}} PDE4BPKAc \xrightarrow{K_{cat4}} PDE4B^* + PKAc, \quad PDE4B^* \xrightarrow{k_{10}} PDE4B, \tag{3.31}$$

$$PDE4D + PKAc \underset{k_{9b}}{\overset{k_{9f}}{\rightleftarrows}} PDE4DPKAc \xrightarrow{K_{cat4}} PDE4D^* + PKAc, \quad PDE4D^* \xrightarrow{k_{10}} PDE4D, \tag{3.32}$$

$$iPDE1 + Ca_4CaM \underset{k_{c3b}}{\overset{k_{c3f}}{\rightleftarrows}} CaMPDE1, \tag{3.33}$$

$$cAMP + iPDE1 \underset{k_{11b}}{\overset{k_{11f}}{\rightleftarrows}} cAMPiPDE1 \xrightarrow{K_{cat5}} AMP + iPDE1, \tag{3.34}$$

$$cAMP + CaMPDE1 \underset{k_{12b}}{\overset{k_{12f}}{\rightleftarrows}} cAMPCaMPDE1 \xrightarrow{K_{cat6}} AMP + CaMPDE1, \tag{3.35}$$

$$cAMP + PDE4B \underset{k_{13b}}{\overset{k_{13f}}{\rightleftarrows}} cAMPPDE4B \xrightarrow{K_{cat7}} AMP + PDE4B, \tag{3.36}$$

$$cAMP + PDE4B^* \underset{k_{14b}}{\overset{k_{14f}}{\rightleftarrows}} cAMPPDE4B^* \xrightarrow{K_{cat8}} AMP + PDE4B^*, \tag{3.37}$$

$$cAMP + PDE4D \underset{k_{15b}}{\overset{k_{15f}}{\rightleftarrows}} cAMPPDE4D \xrightarrow{K_{cat9}} AMP + PDE4D \text{, and} \tag{3.38}$$

$$cAMP + PDE4D^* \underset{k_{16b}}{\overset{k_{16f}}{\rightleftarrows}} cAMPPDE4D^* \xrightarrow{K_{cat10}} AMP + PDE4D^*, \tag{3.39}$$

Reaction (3.33) is an elementary reaction for the binding between PDE1 and Ca^{2+}/CaM complex, and other reactions are enzyme-catalysed reactions: reactions (3.31 and 3.32)

describe the PKA-dependent phosphorylation and promotion of PDE4 activity and reactions (3.34 – 3.39) describe the PDEs-dependent inhibition of cAMP by converting cAMP into AMP.

Since $k_{9b} + K_{cat4} \gg k_{9f}[PDE4B_T][cAMP_T] = \frac{k_{9b} + K_{cat4}}{K_{m4}}[PDE4B_T][cAMP_T]$ ($k_b \approx 4K_{cat}$ (Bhalla and Iyengar, 1999)), there is negligible [*PDE4PKAc*] during the phosphorylation of PDE4. The ODEs for the dynamics of the phosphorylated form of type 4 PDEs by PKAc, [$PDE4B^*$] and [$PDE4D^*$], are given by Eqs. (3.40 and 3.41):

$$\frac{d[PDE4B^*]}{dt} = \frac{K_{cat4}PKAc([PDE4B_T] - [PDE4B^*])}{K_{m4} + ([PDE4B_T] - [PDE4B^*])} - k_{10}[PDE4B^*], \text{ and} \quad (3.40)$$

$$\frac{d[PDE4D^*]}{dt} = \frac{K_{cat4}PKAc([PDE4D_T] - [PDE4D^*])}{K_{m4} + ([PDE4D_T] - [PDE4D^*])} - k_{10}[PDE4D^*], \quad (3.41)$$

where [$PDE4B_T$] is the total concentration of PDE4B: [$PDE4B_T$] = [*PDE4B*] + [$PDE4B^*$], [$PDE4D_T$] is the total concentration of PDE4D: [$PDE4D_T$] = [*PDE4D*] + [$PDE4D^*$], and $K_{m4} = (k_{9b} + K_{cat4})/k_{9f}$.

Based on Michaelis and Menten rate law, the conversion rates of cAMP into AMP catalysed by PDE1 (V_4), CaMPDE1 (V_5), PDE4B (V_6), PDE4B* (V_7), PDE4D (V_8), and PDE4D* (V_9) are given by Eqs. (3.42-3.47):

$$V_4 = \frac{K_{cat5}[PDE1][cAMP]}{K_{m5} + [cAMP]} = ([PDE1_T] - [CaMPDE1])\frac{K_{cat5}[cAMP]}{K_{m5} + [cAMP]}, \quad (3.42)$$

$$V_5 = \frac{K_{cat6}[CaMPDE1][cAMP]}{K_{m6} + [cAMP]}, \quad (3.43)$$

$$V_6 = \frac{K_{cat7}[PDE4B][cAMP]}{K_{m7} + [cAMP]} = ([PDE4B_T] - [PDE4B^*])\frac{K_{cat7}[cAMP]}{K_{m7} + [cAMP]}, \quad (3.44)$$

$$V_7 = \frac{K_{cat8}[PDE4B^*][cAMP]}{K_{m8} + [cAMP]}, \quad (3.45)$$

$$V_8 = \frac{K_{cat9}[PDE4D][cAMP]}{K_{m9} + [cAMP]} = ([PDE4D_T] - [PDE4D^*])\frac{K_{cat9}[cAMP]}{K_{m9} + [cAMP]}, \text{and} \quad (3.46)$$

$$V_9 = \frac{K_{cat10}\left[PDE4D^*\right][cAMP]}{K_{m10} + [cAMP]}, \tag{3.47}$$

where $K_{m5} = (k_{11b} + K_{cat5})/k_{11f}$, $K_{m6} = (k_{12b} + K_{cat6})/k_{12f}$, $K_{m7} = (k_{13b} + K_{cat7})/k_{13f}$, $K_{m8} = (k_{14b} + K_{cat8})/k_{14f}$, $K_{m9} = (k_{15b} + K_{cat9})/k_{15f}$, and $K_{m10} = (k_{16b} + K_{cat10})/k_{16f}$.

The promoted activity of PDE1 remains the same K_m (i.e. $K_{m5} = K_{m6}$), but significantly increases V_{max} (i.e. $K_{cat6} \gg K_{cat5}$) (Bender and Beavo, 2006). Similar information related to PDE4 are not found from the literature, but previous computational studies use an unchanged or a slightly changed K_m between phosphorylated and unphosphorylated PDE4 (Hayer and Bhalla, 2005; Kim et al., 2011). Hence, we assume that the phosphorylation on PDE4 significantly increases V_{max} without changing K_m. Now, we can combine Eqs. (3.42 and 3.43), Eqs. (3.44 and 3.45) and Eqs. (3.46 and 3.47) into V_{10}, V_{11} and V_{12}, respectively, as given by Eqs (3.48 - 3.50):

$$V_{10} = V_4 + V_5 = \frac{K_{cat5}\left[PDE1_T\right][cAMP]}{K_{m5} + [cAMP]}\left(1 + \left(K_{cat6}/K_{cat5} - 1\right)\frac{[CaMPDE1]}{\left[PDE1_T\right]}\right), \tag{3.48}$$

$$V_{11} = V_6 + V_7 = \frac{K_{cat7}\left[PDE4B_T\right][cAMP]}{K_{m7} + [cAMP]}\left(1 + \left(K_{cat8}/K_{cat7} - 1\right)\frac{\left[PDE4B^*\right]}{\left[PDE4B_T\right]}\right), \text{ and} \tag{3.49}$$

$$V_{12} = V_8 + V_9 = \frac{K_{cat9}\left[PDE4D_T\right][cAMP]}{K_{m9} + [cAMP]}\left(1 + \left(K_{cat10}/K_{cat9} - 1\right)\frac{\left[PDE4D^*\right]}{\left[PDE4D_T\right]}\right). \tag{3.50}$$

The inhibition rate of cAMP, V_{cAMP_inhib}, is given by Eq. (3.51):

$$\begin{aligned} V_{cAMP\_inhib.} &= V_{10} + V_{11} + V_{12} \\ &= \frac{K_{cat5}\left[PDE1_T\right][cAMP]}{K_{m5} + [cAMP]}\left(1 + \left(K_{cat6}/K_{cat5} - 1\right)\frac{[CaMPDE1]}{\left[PDE1_T\right]}\right) \\ &\quad + \frac{K_{cat7}\left[PDE4B_T\right][cAMP]}{K_{m7} + [cAMP]}\left(1 + \left(K_{cat8}/K_{cat7} - 1\right)\frac{\left[PDE4B^*\right]}{\left[PDE4B_T\right]}\right) \\ &\quad + \frac{K_{cat9}\left[PDE4D_T\right][cAMP]}{K_{m9} + [cAMP]}\left(1 + \left(K_{cat10}/K_{cat9} - 1\right)\frac{\left[PDE4D^*\right]}{\left[PDE4D_T\right]}\right) \end{aligned}. \tag{3.51}$$

3.3.1.3 Activation of PKA

A PKA holoenzyme contains a regulatory dimmer binding to two catalytic subunits. The regulatory subunit has multiple isoforms and RIIβ is the dominant isoform expressed in the brain. Each regulatory subunit contains two tandem cAMP-binding domains (denoted by A and B). During the activation, cAMP first binds to the domain B and then binds to the domain A to trigger the release of the catalytic subunit. The binding of cAMP to the domain A is essential for the PKA activation (Zawadzki and Taylor, 2004; Zhang et al., 2012) and the domain B seems to inhibit the activation in RIIβ (Zawadzki and Taylor, 2004). However, cAMP is not involved in the catalytic subunit release, but enhances the rate of the release. The experimentally estimated binding affinity (denoted by their dissociation constant, K_d) between the regulatory dimmer and catalytic subunits is 0.6nM while cAMP binding decreases the affinity by more than 10 folds to 9nM (Zawadzki and Taylor, 2004). Therefore, one of the foundation for the maximum PKA activity is that the regulatory dimmer is fully bound by cAMP through two sequential bindings to the domain B and domain A. We simplify the process to have an approximation of the PKA activation by making the following assumptions: (1) a two-step mechanism governs the binding of cAMP to the regulatory dimmer that two cAMP bind to the domain B followed by binding of the other two cAMP to the domain A. The inhibition of the cAMP activation by the domain B is a structural feature of RIIβ and the inhibition is encapsulated by the rates of the bindings; (2) two PKA catalytic subunits are released from the regulatory dimmer simultaneously, and (3) the release occurs at a negligible rate without fully cAMP bound and at a significant rate when four cAMP are attached. The pathway is given by the reaction schema as follows:

$$R_2C_2 + 2cAMP \underset{k_{17b}}{\overset{k_{17f}}{\rightleftarrows}} R_2C_2cAMP_2 \quad , \tag{3.52}$$

$$R_2C_2cAMP_2 + 2cAMP \underset{k_{18b}}{\overset{k_{18f}}{\rightleftarrows}} R_2C_2cAMP_4 \text{ , and} \tag{3.53}$$

$$R_2C_2cAMP_4 \underset{k_{19f}}{\overset{k_{19b}}{\rightleftarrows}} 2PKAc + R_2cAMP_4 \text{ ,} \tag{3.54}$$

where R_2C_2 denotes the PKA complex with a regulatory subunits dimmer binding to two catalytic subunits, PKAc denotes the released PKA catalytic subunit and R_2cAMP_2/R_2cAMP_4 denote unreleased PKA complexes associated with 2/4 cAMP molecules. The rates (V_{13}-V_{15}) of reactions (3.52 – 3.54) based on mass action rate law are given by Eqs. (3.55 – 3.57):

$$V_{13} = k_{17f}\left[R_2C_2\right]\left[cAMP\right]^2 - k_{17b}\left[R_2C_2cAMP_2\right], \tag{3.55}$$

$$V_{14} = k_{18f}\left[R_2C_2cAMP_2\right]\left[cAMP\right]^2 - k_{18b}\left[R_2C_2cAMP_4\right], \text{ and} \tag{3.56}$$

$$V_{15} = k_{19b}\left[R_2C_2cAMP_4\right] - k_{19f}\left[PKAc\right]^3 \Big/ 2, \tag{3.57}$$

where the total concentration of PKA, $[R_2C_{2T}]$, is conserved, which expresses as $[R_2C_{2T}] = [R_2C_2] + [R_2C_2cAMP_2] + [R_2C_2cAMP_4] + [R_2cAMP_4]$ based on the conserved regulatory dimers or $[R_2C_{2T}] = [R_2C_2] + [R_2C_2cAMP_2] + [R_2C_2cAMP_4] + 2[PKAc]$ based on the conserved catalytic subunits. Further calculation shows that $[R_2cAMP_4] = [PKAc]/2$.

The ODEs for dynamics of the proteins involved in the PKA activation are given by Eqs. (3.58 – 3.62):

$$\frac{d\left[R_2C_2\right]}{dt} = -V_{13}, \tag{3.58}$$

$$\frac{d\left[R_2C_2cAMP_2\right]}{dt} = V_{13} - V_{14}, \tag{3.59}$$

$$\frac{d\left[R_2C_2cAMP_4\right]}{dt} = V_{14} - V_{15}, \tag{3.60}$$

$$\frac{d\left[cAMP\right]}{dt} = -2V_{13} - 2V_{14}, \text{ and} \tag{3.61}$$

$$\frac{d\left[PKAc\right]}{dt} = 2V_{15}. \tag{3.62}$$

However, the association rate constants, k_{17f}, k_{18f}, and k_{19f} are unclear for this simplified mathematical framework. The values of the association constant given in the literature or used by previous computational studies were in the unit of $\mu M^{-1}s^{-1}$, which is

inconsistent to the unit of $\mu M^{-2}s^{-1}$ used here according to mass action rate law. We estimate these parameters using Markov chain Monte Carlo (MCMC) (see Appendix E.1 for the procedure) with respect to the experimental data found from the literature. We found two sets of data for the normalised activation of PKA with respect to different levels of cAMP (Zawadzki and Taylor, 2004; Zhang et al., 2012). Both sets are measured under the same procedure: incubates 10nM PKA with different levels of cAMP for 2 minutes and normalises the measures by the level of activated PKA at the maximum concentration of cAMP. We use one set for the parameter estimation and the other set for the validation. The activation of PKA (same procedure as the experiment) based on the estimated parameters is shown in Fig. 3-5.

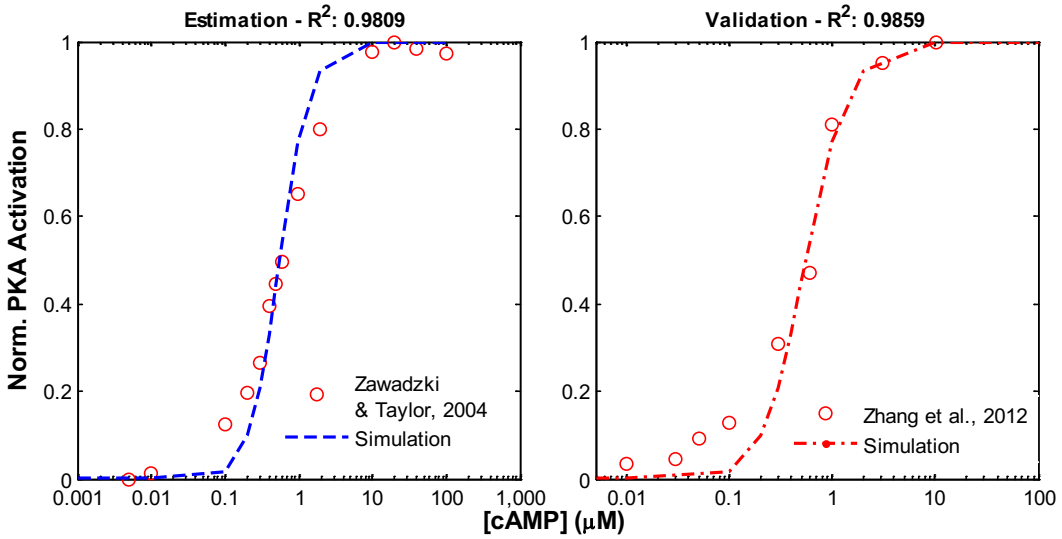

Figure 3-5 Estimation of parameters for the activation of PKA. Activation of PKA (normalised by the level of PKA activity at maximum [*cAMP*]) with respect to different [*cAMP*] are recorded at the end of 2 min simulation. (**A**) Estimation of the unknown parameters (blue dashed line) based on the experimental data (Zawadzki and Taylor, 2004). (**B**) Validation of the estimated parameter by another set of experimental data (Zhang et al., 2012). The R^2 of the estimation and the validation are shown in the title of the corresponding figure. The known parameters are k_{17b} ($0.02s^{-1}$), k_{18b} ($0.2s^{-1}$) and k_{19b} ($0.0016s^{-1}$) (Kim et al., 2011; Zawadzki and Taylor, 2004). The estimated parameters are k_{17f} ($8\ \mu M^{-2}s^{-1}$), k_{18f} ($0.7\ \mu M^{-2}s^{-1}$), and k_{19f} ($0.25\ \mu M^{-2}s^{-1}$).

3.3.1.4 Analysis of the pathway

The ODE of the dynamics of [*cAMP*] for the overall pathway is given by Eq. (3.63):

$$\frac{d[cAMP]}{dt} = V_{cAMP\_prod.} - V_{cAMP\_inhib.} - 2V_{13} - 2V_{14}\,. \tag{3.63}$$

The ODEs of the dynamics of other proteins, including PKA, PDE1, PDE4, AC1 and AC8, remain the same as described previously.

We numerically solve the ODEs and the dynamics of [*cAMP*] and [*PKA*] are shown in Fig 3-6. Both cAMP and PKA have switch like behaviours with respect to the increasing levels of Ca^{2+} or Ca^{2+}/CaM complex. The switch prevents the growth of cAMP or PKAc at the low levels of Ca^{2+} or Ca^{2+}/CaM complex, but induces rapid growth of cAMP or PKAc at the high levels of Ca^{2+} or Ca^{2+}/CaM complex. The level of PKAc reaches a plateau of only 0.25μM (2.4μM in total) due to the high binding affinity between the PKA catalytic subunits and the PKA regulatory dimmer.

We further analyse the contributions of PDE1 and PDE4 to the dynamics of cAMP and PKA by using three modified circuits: (1) removing PDE1-dependent inhibition; (2) removing PDE4-dependent inhibition; and (3) removing inhibitions by both isoforms of PDE. In all circumstances, [$PDE1_T$] remains the same to rule out the effects of the alteration on the CaM competition. We gain insights into the different roles of PDEs in regulating the dynamics of cAMP and the significance of the comprehensive inhibition of cAMP through comparing the difference between the original circuit and the modified circuits.

As shown in Fig. 3-7A, without the PDE-dependent inhibition of cAMP, the level of cAMP outbreaks, starting from 40μM at basal, and reaches 900μM at 30μM of Ca^{2+} within 100s. The accumulation of cAMP continues after the first 100s until all ATP is converted to cAMP due to the lack of cAMP inhibition (results not shown). In comparison, the level of cAMP reaches only 1.4μM in the steady state at 30μM of Ca^{2+} with the PDE-dependent inhibition. Meanwhile, without the PDE-dependent inhibition, PKAc starts to accumulate from very low level of Ca^{2+} and rapidly reaches the plateau (Fig. 3-7B). Although this result may be imprecise since we have simplified the Michaelis constant of cAMP activation, it gives an indication of the significance of PDEs in the regulation of cAMP.

Removing of either PDE1 or PDE4 alone, the level of cAMP is higher (Fig. 3-8A), but are significantly lower than removing both of them (Fig. 3-7A). cAMP reaches a much higher level by removing PDE1 than removing PDE4. Moreover, removing PDE1 accelerates the accumulation of cAMP and PKAc at high Ca^{2+} levels (Fig.3-8). These results suggest that PDE1 prevents the "outbreak" of the cAMP production as it is activated in parallel to the activation of CaM-dependent ACs. On the other hand, removing PDE4 results in a higher basal levels of cAMP and PKA (Fig.3-8). Hence, PDE4 is effective at low Ca^{2+} levels where the activity of PDE1 is low. In conclusion, PDE4 moderately inhibits cAMP and prevents growth of cAMP at basal levels, while PDE1 strongly inhibits cAMP in parallel to the activation of Ca^{2+} dependent ACs.

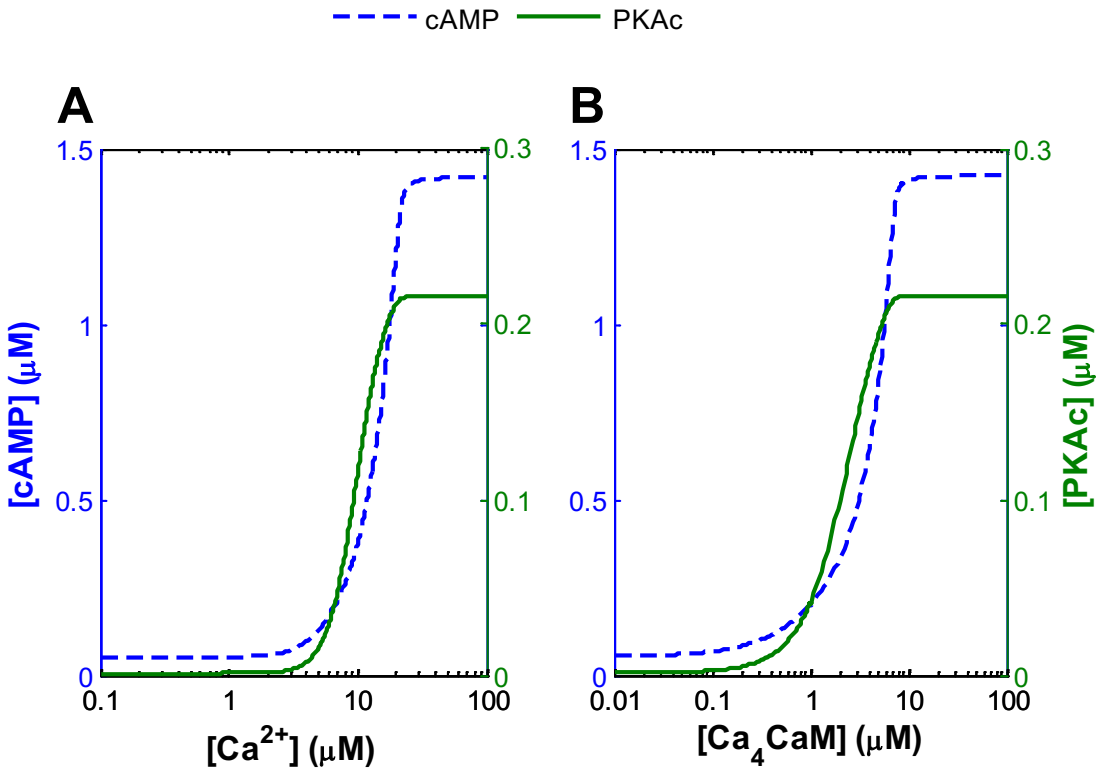

Figure 3-6 The steady levels of cAMP and PKA mixing with different levels of Ca^{2+} and Ca^{2+}/CaM complex. The levels of cAMP (blue dashed lines) and PKA (green solid lines) are recorded at the end of 100s simulation. (**A**) the steady levels of cAMP and PKA mixing with different Ca^{2+} levels (in log scale). The initial concentration of Ca^{2+}/CaM complex is expressed by Eq.(3.6) with the parameters: $[CaM_T]$=17μM, K_1=20μM, K_2=0.56μM, K_3=100μM, K_4=5μM (Chiba et al., 2008); and (**B**) the steady levels of cAMP and PKA mixing with different Ca^{2+}/CaM complex levels. Parameters are given in Tables (3-1 — 3-3) except K=20, k_{10}=0.25s^{-1}, k_{17f} =8$\mu M^{-2}s^{-1}$, k_{17b}=0.02s^{-1}, k_{18f} =0.7$\mu M^{-2}s^{-1}$, k_{18b}=0.2s^{-1}, k_{19f} =0.25$\mu M^{-2}s^{-1}$, and k_{19b}=0.0016s^{-1}.

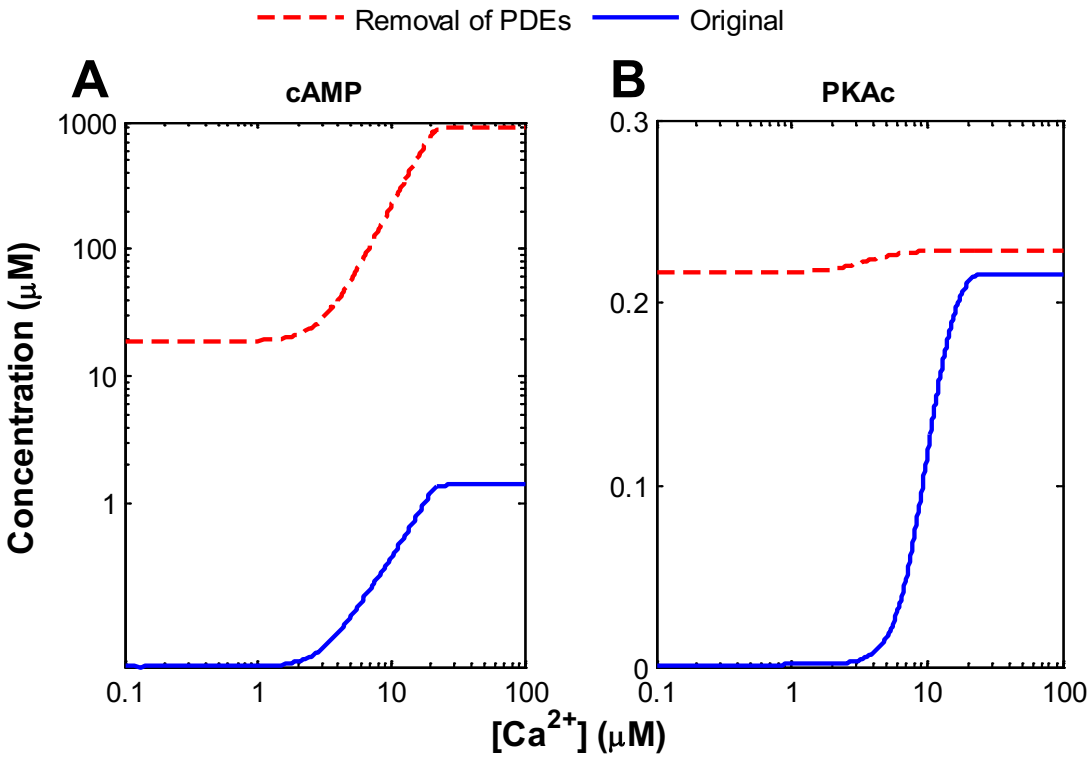

Figure 3-7 Influence of removal of PDEs to dynamics of [*cAMP*] and [*PKA*]. The levels of cAMP and PKA are recorded at the end of 100s simulation at different Ca^{2+} levels (in log scale). The results are compared between the original circuit (blue solid lines) and the modified circuit (red dashed lines). The results are represented as: (**A**) the level of cAMP (in log scale) and (**B**) the level of PKA.

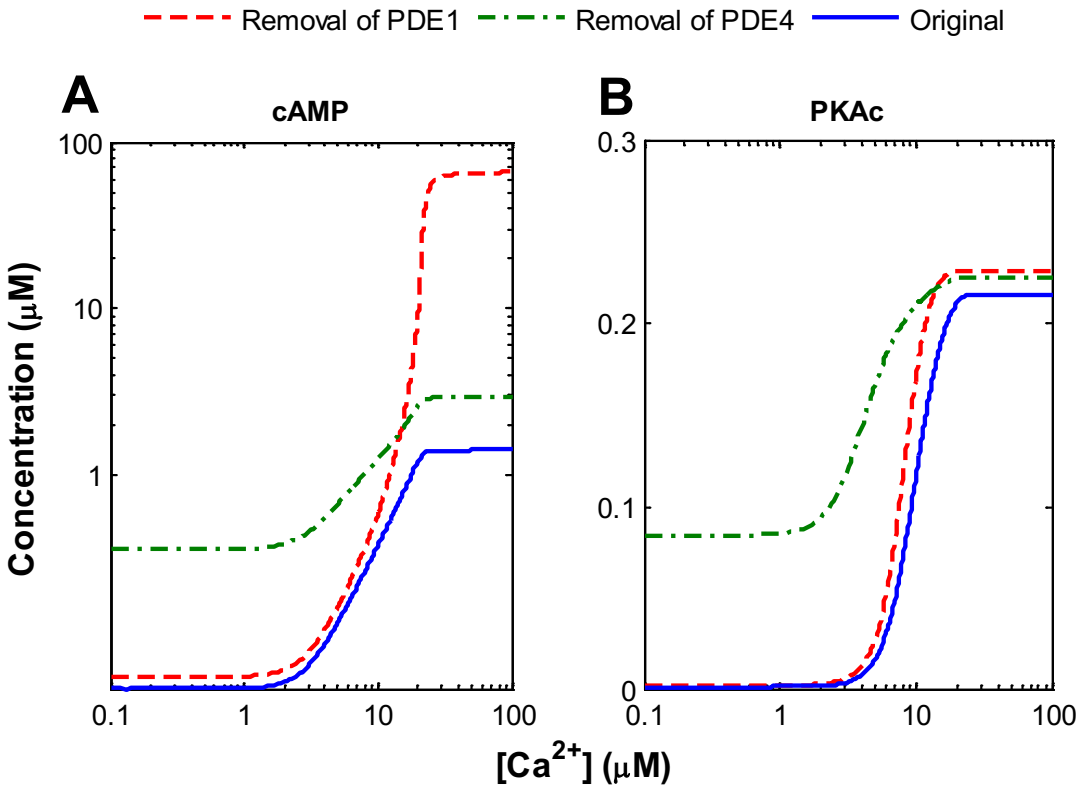

Figure 3-8 Influence of removals of either PDE1 or PDE4 alone to dynamics of [*cAMP*] and [*PKA*]. The levels of cAMP and PKA are recorded at the end of 100s simulation at different Ca^{2+} levels (in log scale). The results are compared between the original circuit (blue solid lines) and the removal of either PDE1 (red dashed lines) or PDE4 (green dashed and dotted lines) alone. The results are represented as: (**A**) the levels of cAMP (in log scale) and (**B**) the levels of PKA.

3.3.2 PP2b activation pathway

PP2b is a heterodimer composed of a CaM binding regulatory subunit, calcinuerin A (CaNA), which tightly binds to a Ca^{2+} binding regulatory subunit, calcinuerin B (CaNB) (Klee et al., 1998). CaNA contains a catalytic domain that is essential for the enzymatic activity. During the activation, CaNB first binds to four Ca^{2+} ions (two sites have a high Ca^{2+} affinity for less than 0.07 μM and the other two have a low affinity for greater than 0.5~1μM) allowing CaNA to bind to Ca^{2+}/CaM complex (Stemmer and Klee, 1994). The binding to CaM triggers a conformational change of CaNA to expose the catalytic domain. PP2b has two levels of activation: (1) a basal activity with a small activation when the low affinity sites of CaNB binds to Ca^{2+} with a Hill coefficient of 1.8 (Stemmer and Klee, 1994); and (2) a full activation which increases the basal activity by 20 folds without changing the K_m when Ca^{2+}/CaM complex attaches to CaNA (Klee et al., 1998).

According to the above information, we model the dynamics of PP2b in transition among three states: inactive state (iPP2b), small activation (Ca_4CaNB) and full activation (CaMCaNA). We assume that all four Ca^{2+} binding sites of CaNB are occupied during the small activation, but the rate of the small activation depends on the binding of Ca^{2+} to the low affinity sites. Moreover, CaNB binds to Ca^{2+} at a very fast rate based on the rate constants used in the previous computational study (Hayer and Bhalla, 2005). Hence, we approximate the level of Ca_4CaNB at the equilibrium (assumption 2) based on Hill equations in terms of Ca^{2+} level and the level of free CaNA, as given by Eq. (3.64):

$$[\mathrm{Ca}_4\ CaNB] = \frac{\left([\mathrm{PP}\,2b_T] - [CaMCaNA]\right)\left[Ca^{2+}\right]^{n1}}{{K_{d1}}^{n1} + \left[Ca^{2+}\right]^{n1}}, \tag{3.64}$$

where $[PP2b_T]$ is the total concentration of PP2b: $[PP2b_T] = [iPP2b] + [Ca_4CaNB] + [CaMCaNA]$, $n1$ is the Hill coefficient and K_{d1} is the dissociation constant. The reaction schema of the full activation is given by:

$$\mathrm{Ca}_4\mathrm{CaM} + \mathrm{Ca}_4\ CaNB \xrightarrow{k_{c4f}} CaMCaNA\,. \tag{3.65}$$

At low levels of Ca^{2+}, CaM may be dissociated from both Ca^{2+} and CaNA and the dissociation rate is much faster than that at high levels of Ca^{2+} (Quintana et al., 2005). Hence, we model the CaM dissociation from CaNA by two pathways and the deciding factor is the Ca^{2+} level. The two pathways are given by the following reaction schema:

$$\text{Pathway 1: } CaMCaNA \xrightarrow{k_{c4b1}} \text{Ca}_4\text{CaM} + \text{Ca}_4\, CaNB \text{, and} \tag{3.66}$$

$$\text{Pathway 2: } CaMCaNA \xrightarrow{k_{c4b2}} \text{CaM} + iPP2b \text{,} \tag{3.67}$$

and the probability of CaM dissociating by pathway 1 is determined by a Hill equation in terms of $[Ca^{2+}]$ given by Eq. (3.68):

$$\frac{\left[Ca^{2+}\right]^{n2}}{K_{d2}{}^{n2} + \left[Ca^{2+}\right]^{n2}}, \tag{3.68}$$

where *n1* is the Hill coefficient and K_{d2} is the dissociation constant. The ODE for the dynamics of $[CaMCaNA]$ is given by Eq. (3.69):

$$\begin{aligned}\frac{d\left[CaMCaNA\right]}{dt} = {} & k_{c4f}\left[Ca_4CaM\right]\frac{\left(\left[\text{PP}2b_T\right]-\left[CaMCaNA\right]\right)\left[Ca^{2+}\right]^{n1}}{K_{d1}{}^{n1}+\left[Ca^{2+}\right]^{n1}} \\ & -\left[CaMCaNA\right]\left(k_{c4b1}\frac{\left[Ca^{2+}\right]^{n2}}{K_{d2}{}^{n2}+\left[Ca^{2+}\right]^{n2}} + k_{c4b2}\left(1-\frac{\left[Ca^{2+}\right]^{n2}}{K_{d2}{}^{n2}+\left[Ca^{2+}\right]^{n2}}\right)\right).\end{aligned} \tag{3.69}$$

As shown in Fig. 3-9, PP2b is small activated at a very low Ca^{2+} level and transited to the full activation at a moderate Ca^{2+} level. Comparing with Fig. 3-6A, PP2b is completely activated when the activation of cAMP and PKA are just initiated. Moreover, the small activation of cAMP reaches the maximum while the activity of PKA remains at an extremely low level that is sufficient to drive the equilibrium of the phosphorylation towards the dephosphorylation. In the next section, we investigate the dynamics of the phosphorylation of I1 to regulate the activity of PP1.

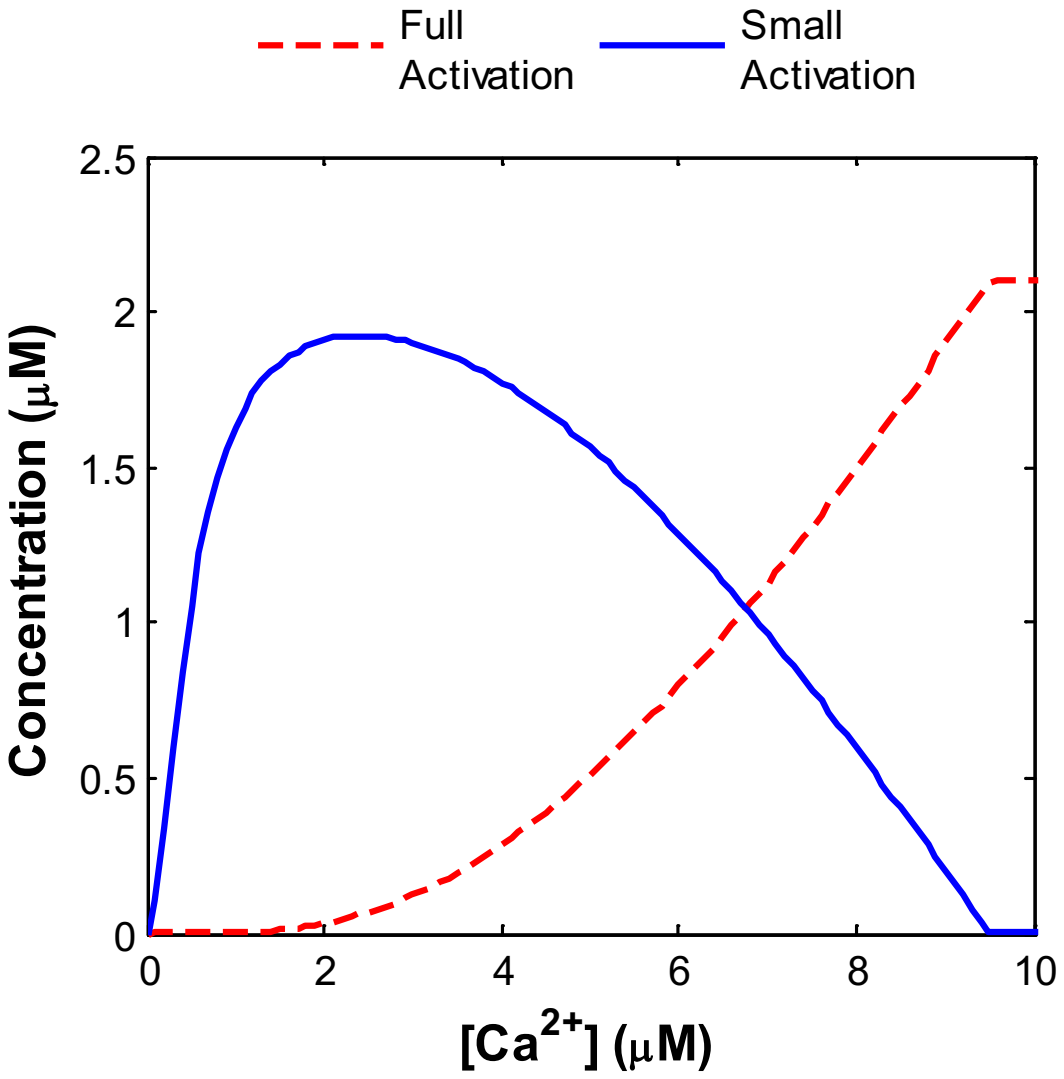

Figure 3-9 The steady levels of the two activated states of PP2b with respect to different levels of Ca^{2+}. The levels of the small activation (blue solid line) and the full activation (red dashed line) of PP2b are recorded at the end of 100s simulation and presented with respect to different Ca^{2+} levels. The initial concentration of Ca^{2+}/CaM complex is expressed by Eq.(3.6) with the parameters: $[CaM_T]$=17μM, K_1=20μM, K_2=0.56μM, K_3=100μM, K_4=5μM (Chiba et al., 2008); Parameters used in the simulation are given in Tables 3-2 and 3-3 except K_{d1}=0.5μM, K_{d2} = 0.6μM, $n1$=1.8, and $n2$ =3 (Stemmer and Klee, 1994).

3.3.3 Regulation of PP1 by phosphorylating I1

As discussed in Section 2.3.6, the phosphorylated I1 binds and inhibits PP1 (Mulkey et al., 1994). The phosphorylation is driven by PKA and reverted by protein phosphatases including PP2a and PP2b. To simplify the interaction, we consider two states of I1, phosphorylated and bound, I1*PP1, or unphosphorylated and unbound, I1 + PP1. This is valid if the phosphorylation makes a large change in the binding affinity between I1 and PP1: from extreme low of the unphosphorylated case to extreme high of the phosphorylated case. As given by previous computational studies, the binding affinities between I1 and PP1 are high (< 1nM) for the phosphorylated case and extreme low (does not bind) for the unphosphorylated case (Hayer and Bhalla, 2005; Kim et al., 2011). Therefore, the phosphorylated I1 binds immediately to PP1 and the unphosphorylated I1 dissociates immediately from PP1, leaving negligible concentrations for cases of phosphorylated unbound and unphosphorylated bound. The theoretical interaction is described by the following reaction schema:

$$I1 + PKAc \underset{k_{20b}}{\overset{k_{20f}}{\rightleftarrows}} I1 + PKAc \xrightarrow{K_{cat11}} I1^* PP1 + PKAc\,, \tag{3.70}$$

$$I1^* PP1 + PP2a \underset{k_{21b}}{\overset{k_{21f}}{\rightleftarrows}} I1^* PP1PP2a \xrightarrow{K_{cat12}} I1 + PP1 + PP2a\,, \tag{3.71}$$

$$I1^* PP1 + Ca_4CaNB \rightleftarrows I1^* PP1Ca_4CaNB \xrightarrow{K_{cat13}/20} I1 + PP1 + Ca_4CaNB\,, \text{ and} \tag{3.72}$$

$$I1^* PP1 + CaMCaNA \underset{k_{22b}}{\overset{k_{22f}}{\rightleftarrows}} I1^* PP1CaMCaNA \xrightarrow{K_{cat13}} I1 + PP1 + CaMCaNA\,. \tag{3.73}$$

Based on Michaelis and Menten rate law, the ODE for the dynamics of [I1**PP1*] is given by Eq. (3.74) (valid if [$PP1_T$] > [$I1_T$]):

$$\begin{aligned}\frac{d\left[I1^* PP1\right]}{dt} = &\frac{K_{cat11}\left[PKAc\right]\left(\left[I1_T\right]-\left[I1^* PP1\right]\right)}{K_{m11}+\left(\left[I1_T\right]-\left[I1^* PP1\right]\right)} \\ &-\frac{K_{cat12}\left[PP2a\right]\left[I1^* PP1\right]}{K_{m12}+\left[I1^* PP1\right]} \\ &-\frac{K_{cat13}\left(\left[CaMCaNA\right]+\frac{1}{20}\left[Ca_4CaNB\right]\right)\left[I1^* PP1\right]}{K_{m13}+\left[I1^* PP1\right]}\end{aligned}\,, \tag{3.74}$$

where $[I1_T]$ is the total concentration of I1: $[I1_T] = [I1] + [I1^*PP1]$, $[PP1_T]$ is the total concentration of PP1: $[PP1_T] = [PP1] + [I1^*PP1]$, $K_{m11} = (k_{20b} + K_{cat11})/k_{20f}$, $K_{m12} = (k_{21b} + K_{cat12})/k_{21f}$ and $K_{m13} = (k_{22b} + K_{cat13})/k_{22f}$. The level of active PP1 is calculated by $[PP1] = [PP1_T] - [I1^*PP1]$.

As shown in Fig. 3-10, the concentration of bound PP1, $[I1^*PP1]$ (blue solid line), first declines to a trough and then slightly recovers for the increasing Ca^{2+} level. Before $[I1^*PP1]$ reaches the trough, an intermediate state of $[I1^*PP1]$ exists, where PP2b is exchanging between the small and full activation states. $[I1^*PP1]$ reaches trough at approximately 9 μM of Ca^{2+}, when the activity of PP2b approaches the peak (red dashed line). PKA is activated just before trough and the activation induce only a slight rise of $[I1^*PP1]$. The reason for the slight rise is that PP2b has both higher kinetic characteristics and higher active level than those of PKA. On the other hand, $[I1^*PP1]$ is high at basal due to the higher basal activity of PKA triggered by Ca^{2+}-independent ACs while the activation of PP2b purely depends on Ca^{2+} and CaM.

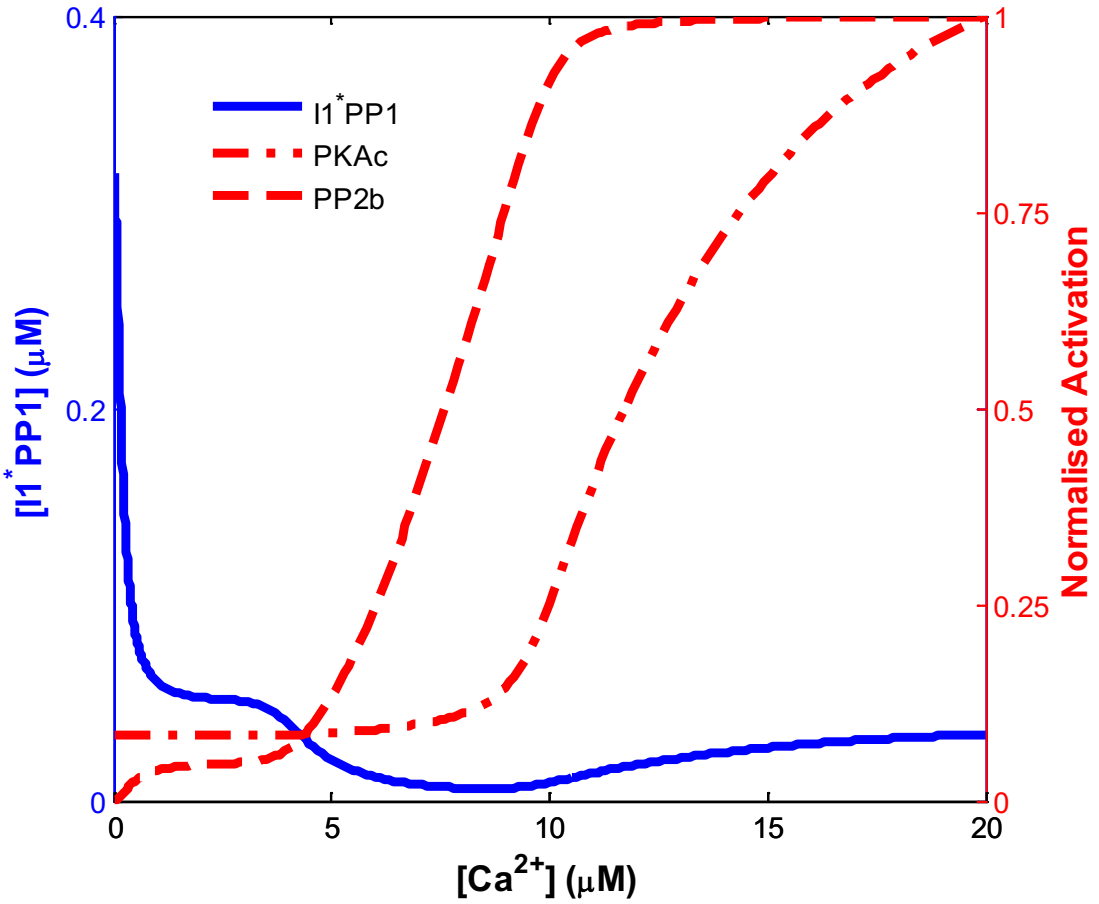

Figure 3-10 Steady levels of bound PP1 with respect to different Ca^{2+} levels. The [$I1^*PP1$] is recorded at the end of 1000s simulation and presented with respect to different [Ca^{2+}]. The initial concentration of Ca^{2+}/CaM complex is expressed by Eq.(3.6) with the parameters: [CaM_T]=17μM, K_1=20μM, K_2=0.56μM, K_3=100μM, K_4=5μM (Chiba et al., 2008). Red lines show the activity levels of PKA and PP2b ([$CaMCaNA$] + [Ca_4CaNB]/20) normalised by their maximum activities. Parameters used are given in Table 3-1.

3.3.4 Regulation of CaMKII autophosphorylation by PP1

An active CaMKII subunit can be autophosphorylated by its active neighbouring subunits and the autophosphorylation is reversed by PP1-dependent dephosphorylation. Autophosphorylated subunits have a much slower CaM dissociation rate (Hudmon and Schulman, 2002). We formulate the dynamics of CaMKII autophosphorylation based on a previous model (Chiba et al., 2008) with modifications to implement the dephosphorylation by PP2a. The transitions among four states of CaMKII are modelled: inhibited CaMKII (iCaMKII), Ca^{2+}/CaM bound CaMKII (CaMCaMKII), autophosphorylated CaMKII (CaMCaMKII*) and CaM dissociated autophosphorylated CaMKII (CaMKII*). The ODEs of the dynamics of the CaMKII states are given by Eqs (3.75 – 3.77) (Chiba et al., 2008):

$$\begin{aligned}\frac{d[CaMCaMKII]}{dt} &= k_{c5f}[iCaMKII][Ca_4CaM] - k_{c5b1}[CaMCaMKII] \\ &\quad - \frac{K_{cat14}P[CaMCaMKII][ATP]}{K_{m14}+[ATP]} + \frac{K_{cat15}[PP1][CaMCaMKII^*]}{K_{m15}+[CaMCaMKII^*]}, \\ &\quad + \frac{K_{cat16}[PP2a][CaMCaMKII^*]}{K_{m16}+[CaMCaMKII^*]}\end{aligned} \tag{3.75}$$

$$\begin{aligned}\frac{d[CaMCaMKII^*]}{dt} &= k_{c5f}[CaMKII^*][Ca_4CaM] - k_{c5b2}[CaMCaMKII^*] \\ &\quad + \frac{K_{cat14}P[CaMCaMKII][ATP]}{K_{m14}+[ATP]} - \frac{K_{cat15}[PP1][CaMCaMKII^*]}{K_{m15}+[CaMCaMKII^*]}, \text{ and} \\ &\quad - \frac{K_{cat16}[PP2a][CaMCaMKII^*]}{K_{m16}+[CaMCaMKII^*]}\end{aligned} \tag{3.76}$$

$$\begin{aligned}\frac{d[CaMKII^*]}{dt} &= -k_{c5f}[CaMKII^*][Ca_4CaM] + k_{c5b2}[CaMCaMKII^*] \\ &\quad - \frac{K_{cat15}[PP1][CaMKII^*]}{K_{m15}+[CaMKII^*]} - \frac{K_{cat16}[PP2a][CaMKII^*]}{K_{m16}+[CaMKII^*]},\end{aligned} \tag{3.77}$$

where $[iCaMKII] = [CaMKII_T] - [CaMCaMKII] - [CaMCaMKII^*] - [CaMKII^*]$, $[CaMKII_T]$ is the total concentration of CaMKII, and P is defined as the probability that either or both sides of a neighbouring subunit are active (Chiba et al., 2008). Following the same assumption as in Section 3.3.1.1, we assume $\frac{[ATP]}{K_{m14}+[ATP]} \approx 1$.

3.4 Emergent properties of the NMDAR-mediated pathway

We analyse the emergent properties of the NMDAR-mediated protein interacting pathway using MoNP. MoNP integrates the sub-models developed in the previous sections (see Appendix F for the complete model of MoNP and the parameters) and maintains the essential features of the network as we have discussed in each individual case. MoNP is numerically solved using Matlab ODE solver, ode15s, to conduct computational experiments for our analysis. Different from the analysis in Sections 3.2 and 3.3, where total amount of Ca^{2+}/CaM complex is steady and expressed by Eq. (3.6), the total amount of Ca^{2+}/CaM complex in MoNP is dynamically changing. We first study the steady state of CaM binding proteins in Section 3.4.1. Then we analyse the temporal pattern of the pathway in response to transient Ca^{2+} stimulation in Section 3.4.2. At the end, we briefly investigate the implication of PP2b-dependent removal of AKAP and PKA during LTD in Section 3.4.3.

3.4.1 Ca^{2+} regulated CaM competition

We quantify the CaM competition by calculating the portions of LTP related (ACs and CaMKII) or LTD related (PDE1 and PP2b) Ca^{2+}/CaM complex bindings at steady state with respect to different levels of Ca^{2+}. We then use an index, kinase related CaM binding index (KBI), to present the portion of bound Ca^{2+}/CaM complex trapped by LTP related proteins. KBI ranges from 0 to 1, and is given by Eq. (3.78):

$$KBI = \frac{[Kinase - Ca_4CaM]}{[Kinase - Ca_4CaM] + [Phosphatase - Ca_4CaM]}, \tag{3.78}$$

where [*Kinase-Ca₄CaM*] = [*CaMAC1*] + [*CaMAC8*] + [*CaMCaMKII*] + [*CaMCaMKII**], and [*Phosphatse-Ca₄CaM*] = [*CaMPDE1*] + [*CaMCaNA*]. We run MoNP with different Ca^{2+} levels from 0.07μM (rest) to 3μM and calculate KBI for each Ca^{2+} level. Using the value of KBI recorded at the rest Ca^{2+} as the base, we calculate the net change of KBI from the base and normalise the change by the base. The normalised net change of KBI, $\widehat{\Delta KBI}$, is given by Eq. (3.79):

$$\widehat{\Delta KBI} = \frac{KBI - KBI_{base}}{KBI_{base}} . \quad (3.79)$$

Therefore, a decrease from the base (a negative value for $\widehat{\Delta KBI}$) indicates an enhanced LTD related CaM binding and an increase from the base (a positive value for $\widehat{\Delta KBI}$) indicates an enhanced LTP related CaM binding. This interpretation is consistent with the experimental measure of synaptic plasticity, which uses the percentage of EPSP measured at the rest Ca^{2+} level (Bliss and Collingridge, 1993).

As shown in Fig. 3-11, the normalised net change of KBI, simulated with CaMKIIα isoform (K_{cat} = 1.2s^{-1}), forms a U-shape curve with respect to the increasing Ca^{2+} level. The curve decreases first and reaches the bottom at 1μM of Ca^{2+} indicating an enhanced LTD related CaM binding. The result shows a potential Ca^{2+} range, 0.5μM - 1μM, for the induction of LTD by taking the Ca^{2+} range from the 20% decrease (-0.2) to the bottom. Then, it rapidly recovers to the base at about 1.5μM of Ca^{2+} and reaches the top at 3μM of Ca^{2+} indicating the enhanced LTP related CaM binding occurring after 1.5μM of Ca^{2+}. Moreover, the most of CaM is consumed at 3μM of Ca^{2+} and the competition should reach the steady state.

CaMKII isoforms have different K_{cat} for the enzymatic activity; the dominant hippocampal isoform, α and β, have K_{cat} of 1.2s^{-1} and 9.8s^{-1}, respectively (Huynh and Pagratis, 2011). We know that the autophosphorylation decreases the CaM dissociation, hence, we test four K_{cat} of the autophosphorylation: 0s^{-1} (without the autophosphorylation), 1.2s^{-1}, 5s^{-1} (mixed) and 9.8s^{-1} to understand the role of the autophosphorylation in the CaM-competition. As shown in Fig 3-11, the faster rate of the autophosphorylation narrows the LTD induction range and enhances the LTP related CaM bindings. Moreover, the faster rate of the autophosphorylation traps more Ca^{2+}/CaM complex faster. On the other hand, without the autophosphorylation, the LTD induction range is wider; $\widehat{\Delta KBI}$ recovers slowly to the base and the top of $\widehat{\Delta KBI}$ is reduced indicating the reduced LTP related CaM bindings. Moreover, the amount of bound Ca^{2+}/CaM complex is much smaller than the cases with the autophosphorylation.

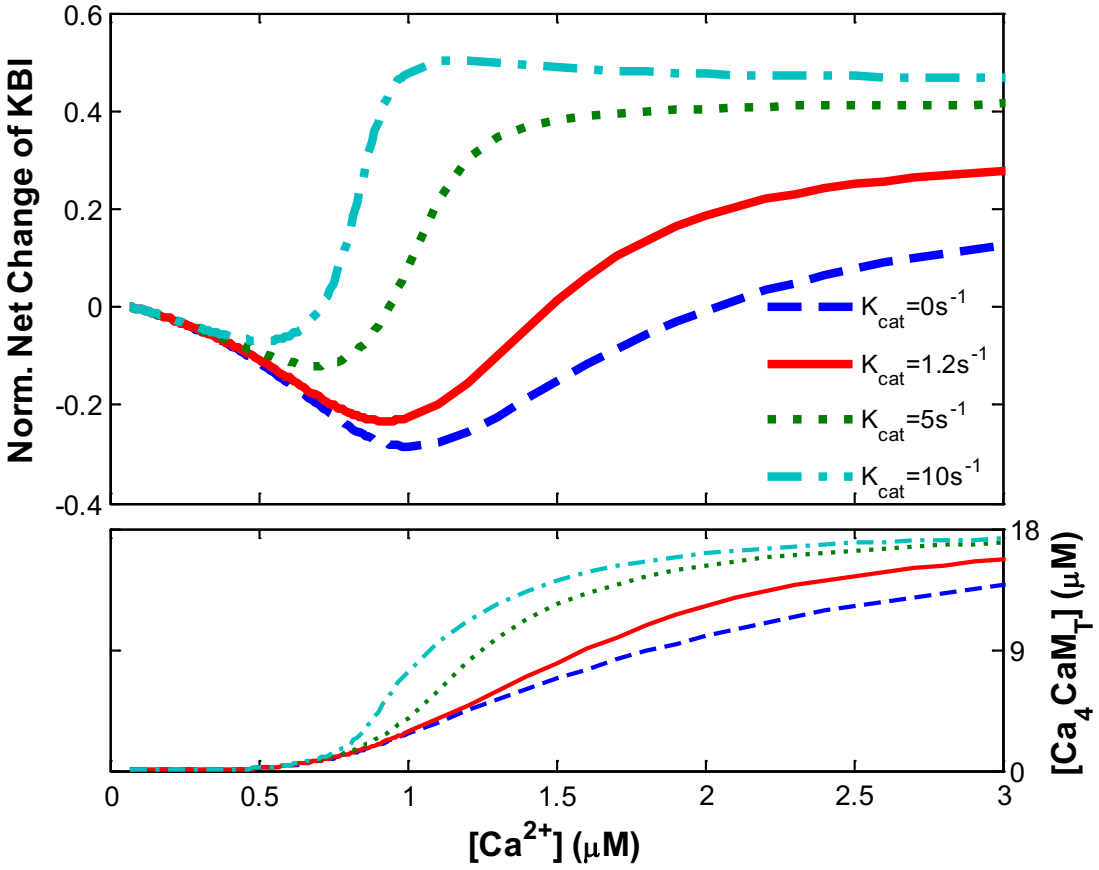

Figure 3-11 The normalised net change of KBI with respect to different K_{cat} of the autophosphorylation. MoNP is run for 1000s using different [Ca^{2+}], KBI is calculated at the end of the simulation. The upper panel shows the normalised net change of KBI with respect to different [Ca^{2+}]. The lower panel shows the total concentration of the bound Ca^{2+}/CaM complex with respect to different [Ca^{2+}]. Four different turnover rates of the autophosphorylation are tested: $0s^{-1}$ (blue dahsed line), $1.2s^{-1}$ (red solid line), $5s^{-1}$ (green dotted line), and $10s^{-1}$ (cyan blue dashed and dotted line).

CaMKII and CaM concentrations are abundant in hippocampal neurons (20μM and 17.7μM used here), hence, we test the relation between their concentrations and the CaM competition. Interestingly, lower concentrations of CaM significantly influence the pattern of $\widehat{\Delta KBI}$ (Fig. 3-12), while the pattern maintains in all concentrations of CaMKII tested (Fig. 3-13). The reason is that the concentration of CaMKII changes the basal consumption of CaM by CaMKII and thus affects the basal value of KBI (Fig. 3-13), while the concentration of CaM does not (Fig. 3-12). Hence, it gets harder for LTP related proteins to compete for CaM against LTD related proteins at a lower concentration of CaM because LTP related proteins have much weaker affinity for CaM than that of LTD related proteins. On the other hand, a lower KBI basal value is associated with the lower CaMKII concentration, so that the pattern can be maintained. Hence, the abundance of CaM maybe important for the induction of LTP.

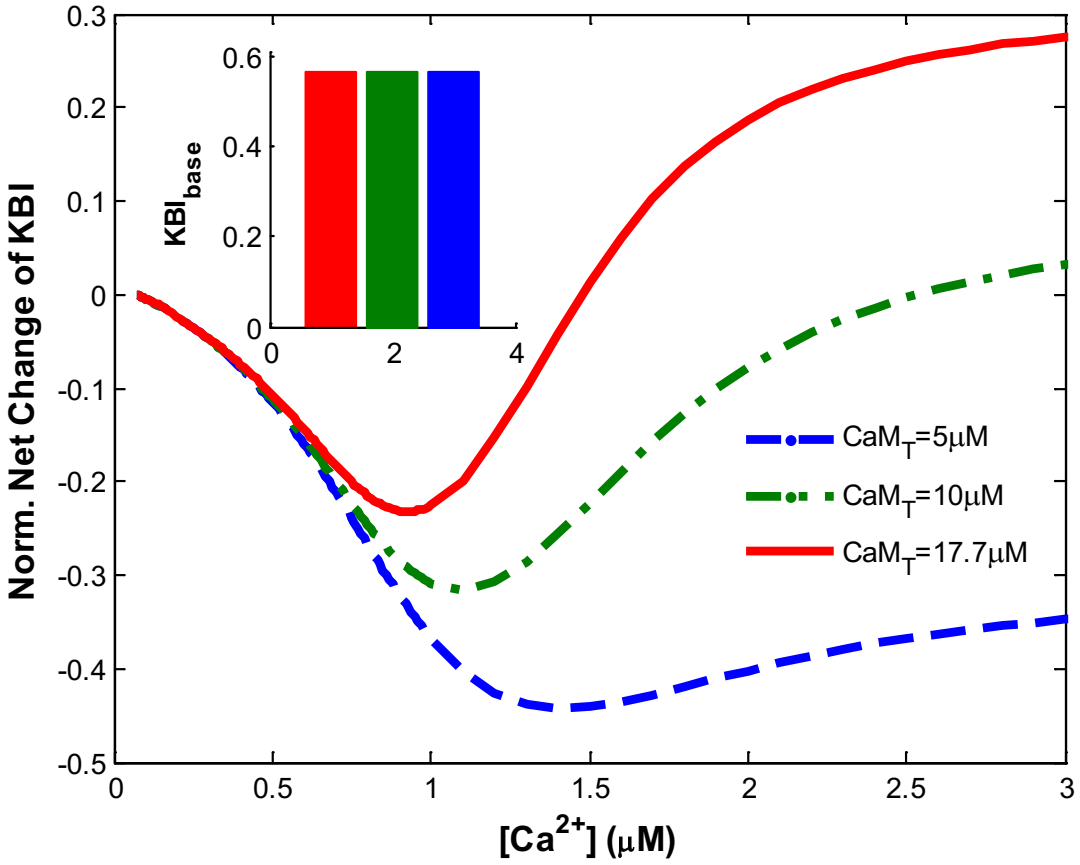

Figure 3-12 The normalised net change of KBI with respect to different [CaM_T]. MoNP is run for 1000s using different [Ca^{2+}], KBI is calculated at the end of the simulation. The figure shows the normalised net change of KBI with respect to different [Ca^{2+}]. Inset: the basal values of KBI for different [CaM_T]. Three different [CaM_T] are tested: 5μM (blue dashed line), 10μM (green dashed and dotted line) and 17.7μM (red solid line).

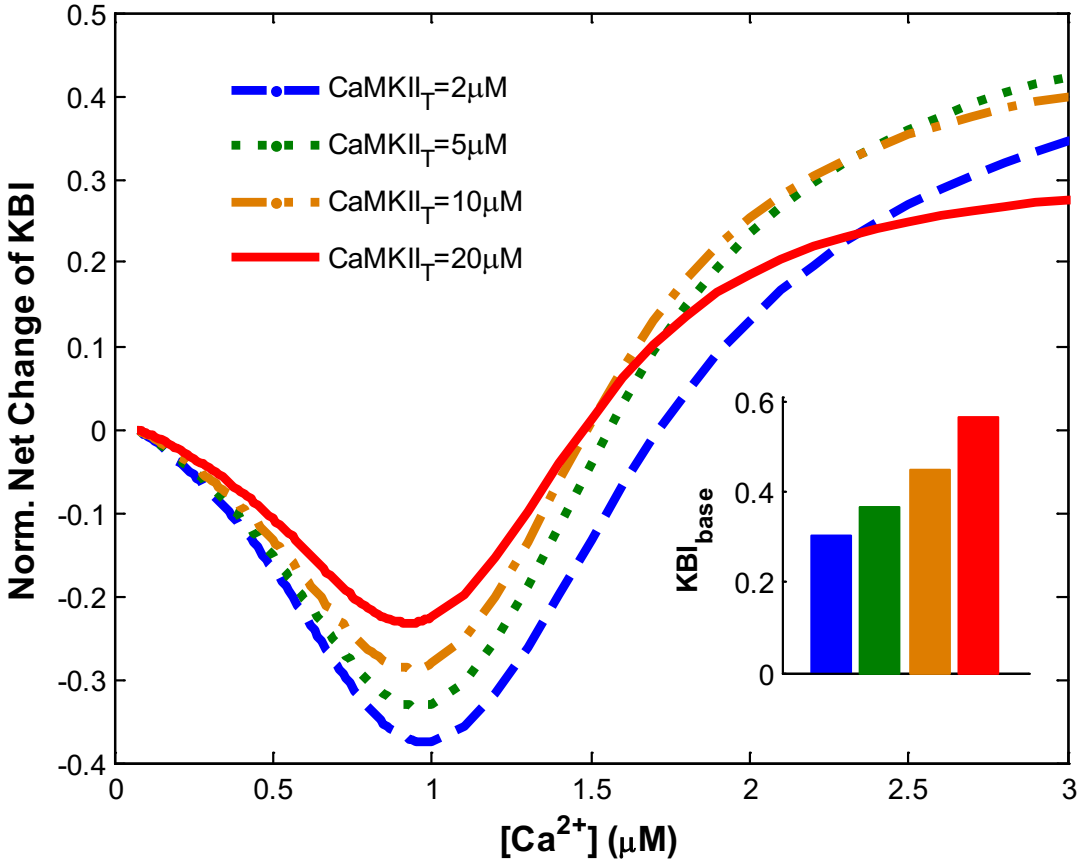

Figure 3-13 The normalised net change of KBI with respect to different [*CaMKII*$_T$]. MoNP is run for 1000s using different [Ca^{2+}], KBI is calculated at the end of the simulation. The figure shows the normalised net change of KBI with respect to different [Ca^{2+}]. Inset: the basal values of KBI for different [*CaMKII*$_T$]. Four different [*CaMKII*$_T$] are tested: 2μM (blue dashed line), 5μM (green dotted line), 10μM (orange dashed and dotted line) and 20μM (red solid line).

3.4.2 Temporal pattern of modulators

LTP and LTD are induced by transient Ca^{2+} signals, which may trigger temporal activation of modulators far from their steady states. We conduct computational experiments using MoNP to understand the temporal activation of modulators and their implications in the bidirectional behaviour of synaptic plasticity. We simulate MoNP with the rest Ca^{2+} level (0.07μM) until all the variables reach their steady level and record their values as the base. Then, we apply three patterns of Ca^{2+} signal to stimulate MoNP: (1) tetanus contains 900 pulses at 1Hz (LFS), (2) tetanus contains 100 pulses at 100Hz (HFS), and (3) theta burst stimulation (TBS) (see Appendix G for the explanation). HFS and TBS are common protocols for LTP induction and LFS induces LTD (Bliss and Collingridge, 1993; Dudek and Bear, 1993; Kumar, 2011). We then calculate $\widehat{\Delta KBI}_t$ at a given time, *t*, as well the normalised net change of the concentration of bound PP1, $\widehat{\Delta\left[I1^{*}PP1\right]}_t$, at the same time to indicate the PP1 regulation as given by Eq. (3.80):

$$\widehat{\Delta\left[I1^{*}PP1\right]}_t = \frac{\left[I1^{*}PP1\right]_t - \left[I1^{*}PP1\right]_{base}}{\left[I1^{*}PP1\right]_{base}}, \tag{3.80}$$

where $[I1^{*}PP1]_{base}$ is $[I1^{*}PP1]$ measured at the rest Ca^{2+} level. Using these indicators, we investigate the timescales of the activation of modulators as well as their effectiveness in the emergence of synaptic plasticity.

We first analyse the dynamics of the modulators in response to HFS and TBS. During HFS, $\widehat{\Delta KBI}$ drops slightly at the beginning and elevates afterwards. Then, $\widehat{\Delta KBI}$ increases smoothly after the Ca^{2+} signal disappeared for a few seconds and returns to the base (Fig. 3-14). The drop is due to the high affinity of PP2b for CaM and the elevation is due to the turn on of the autophosphorylation that enhances the affinity of CaMKII for the CaM binding to the same level of PP2b. The smooth increase is due to the slightly longer activity of CaMKII than that of PP2b after the disappearing of the Ca^{2+} signal (Fig. 3-14). $\widehat{\Delta\left[I1^{*}PP1\right]}$ behaves differently in response to HFS. $\widehat{\Delta\left[I1^{*}PP1\right]}$ drops rapidly during the Ca^{2+} signal, and slowly recovers and increases after the

disappearing of the Ca^{2+} signal (Fig. 3-15). At the end, $\widehat{\Delta[I1^{*}PP1]}$ reaches a maximum of 0.2. The delayed phosphorylation is due to the slow activation, as well as the slow deactivation, of PKA. As a result, PKA maintains a moderate activity when the activity of PP2b is eliminated (Fig. 3-15) and rephosphorylates the substrate above the base.

TBS contains three trains of tetanus, and each train contains less pulses (40 pulses) than that of HFS (100 pulses) while the total is similar (120 to 100 pulses). The temporal dynamics in response to each of the trains is similar to HFS, but is different when the trains are coupled. As shown in Fig. 3-16, each of the trains induces a pattern of $\widehat{\Delta KBI}$ similar to that of HFS, but when the trains are coupled by increasing the turnover rate of the autophosphorylation, the latter trains do not induce the initial drop. Moreover, the activation of PKA is greater and induces a much higher rephosphorylation of I1 above the base than that of HFS in the same timescale (Fig. 3-17). The coupling relies on the longer activities of kinases, facilitated by the autophosphorylation and the slow deactivation of PKA. As a result, the activities of kinases can be elevated higher by subsequent tetanus applied before their activities are completely eliminated. The higher activities of kinases can either induce a stronger phosphorylation or prevent the effects induced by phosphatases.

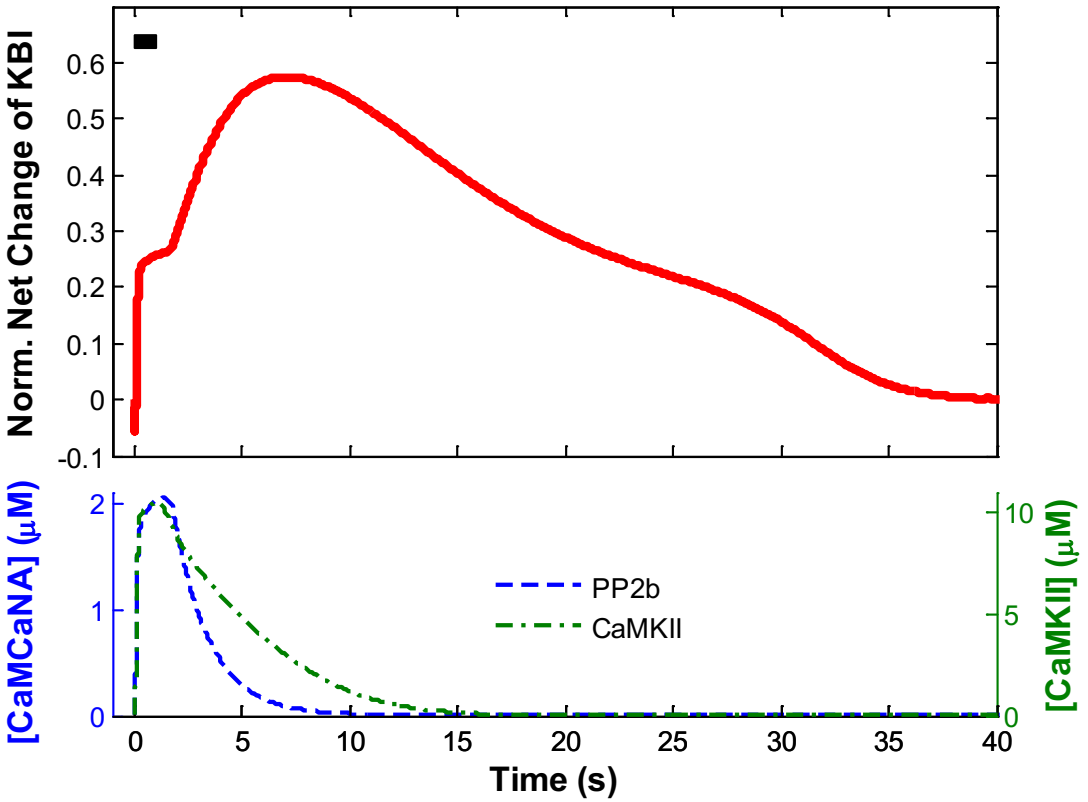

Figure 3-14 The dynamics of the normalised net change of KBI in response to HFS. MoNP is run in response to HFS initiated at t = 0s (black bar). The upper panel shows the dynamics of the normalised net change of KBI and the lower panel shows the dynmics of [*CaMCaNA*] and [*CaMKII*].

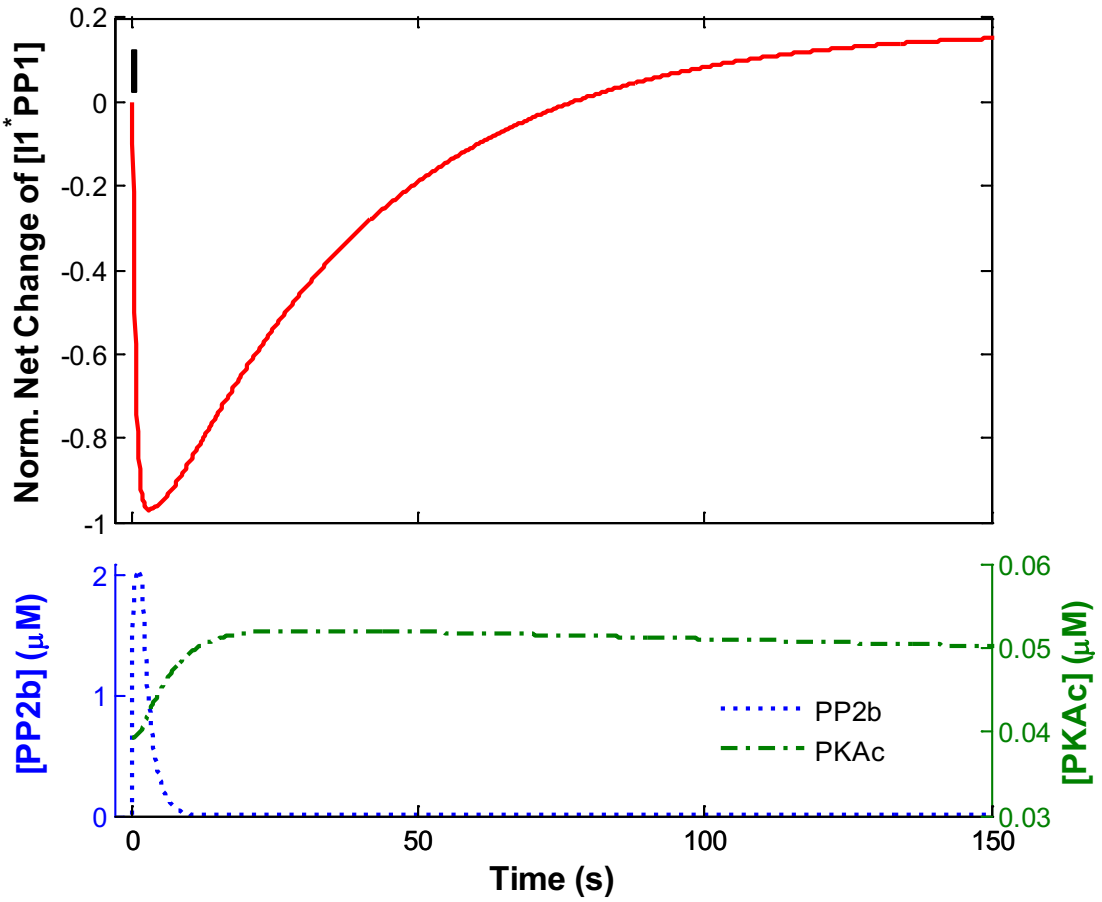

Figure 3-15 The dynamicas of the normalised net change of [*I1*PP1*] in response to HFS. MoNP is run in response to HFS initiated at t = 0s (black bar). The upper panel shows the dynamics of the normalised net change of [*I1*PP1*] and the lower panel shows the dynmics of [*PP2b*] ([*CaMCaNA*] + [Ca_4*CaNB*]/20) and [*PKAc*].

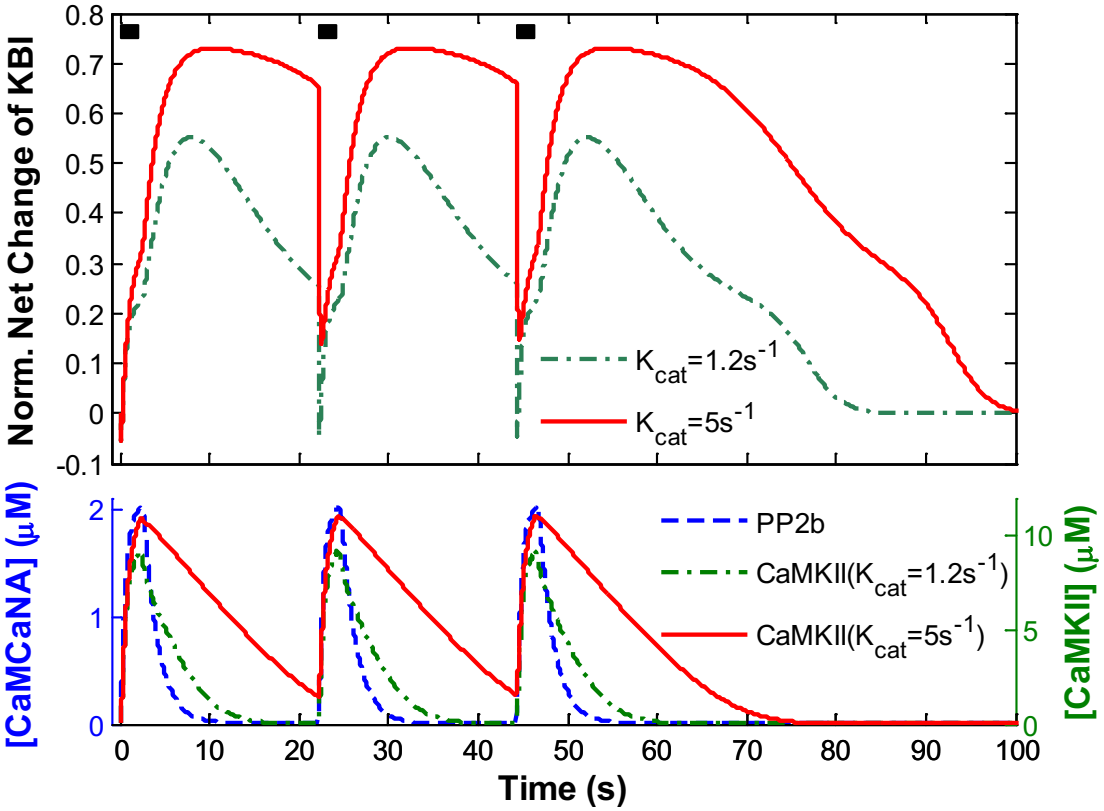

Figure 3-16 The dynamics of the normalised net change of KBI in response to TBS. MoNP is run in response to TBS with the first train initiated at t = 0s (black bars). The upper panel shows the dynamics of the normalised net change of KBI and the lower panel shows the dynmics of [*CaMCaNA*] and [*CaMKII*]. Two turnover rates of the autophosphrylation are used: (1) $1.2s^{-1}$, and (2) $5s^{-1}$.

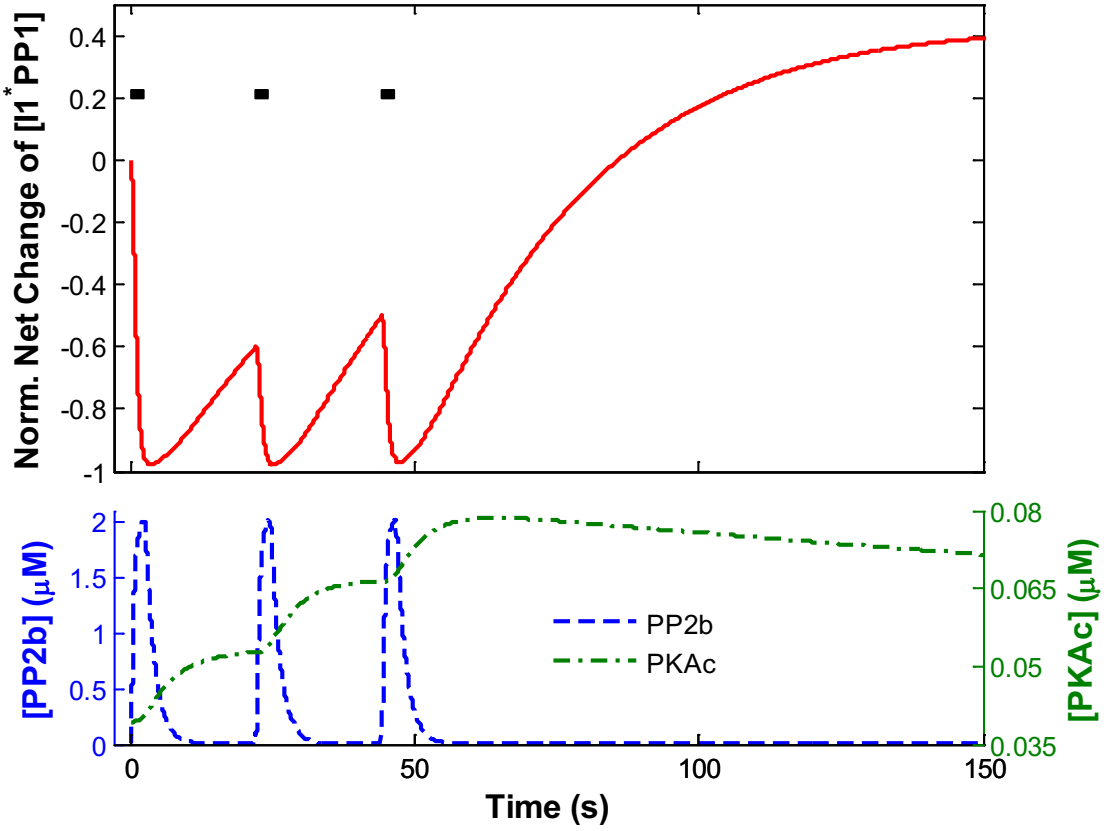

Figure 3-17 The dynamics of the normalised net change of [*I1*PP1*] in response to TBS. MoNP is is run in response to TBS with the first train initiated at t = 0s (black bars). The upper panel shows the dynamics of the normalised net change of [*I1*PP1*] and the lower panel shows the dynmics of [*PP2b*] ([*CaMCaNA*] + [Ca_4CaNB]/20) and [*PKAc*].

In response to LFS, $\widehat{\Delta KBI}$ slightly decreases and fluctuates around -0.05 (Fig. 3-18). The activation of PP2b and CaMKII are both low, which indicates a minor contribution of CaM-competition to LTD. Meanwhile, the phosphorylation of I1 is significantly affected in response to LFS (Fig. 3-19). $\widehat{\Delta\left[I1^{*}PP1\right]}$ rapidly decreases and maintains at a low level during LFS for both kinetic parameters of the Ca^{2+} influx tested (the parameters induces $[Ca^{2+}]$ on the borders of 0.5~1μM for LTD). The decrease is due to the small activation of PP2b over the extreme low activity of PKA at the same time. As a result, I1 can be dephosphorylated by PP2b much faster than rephosphorylated by PKA. However, we notice that PKA does rephosphorylate I1 above the base after the disappearing of the Ca^{2+} signal (Fig. 3-19) due to the slow deactivation of PKA, although the activity of PKA is increased by an extremely small amount. This finding leads to the discussion of the removal of AKPA, as well as PKA, in the next section.

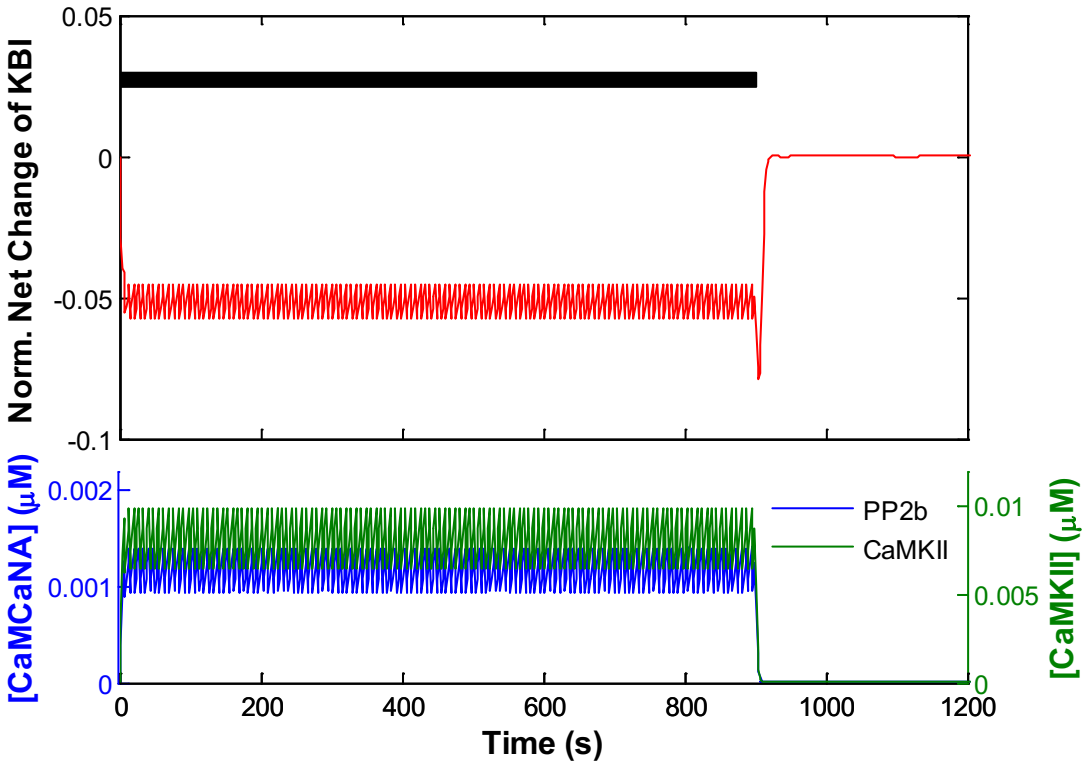

Figure 3-18 The dynamics of the normalised net change of KBI in response to LFS. MoNP is run in response to LFS initiated at t = 0s (black bar). The upper panel shows the dynamics of the normalised net change of KBI and the lower panel shows the dynmics of [*CaMCaNA*] and [*CaMKII*].

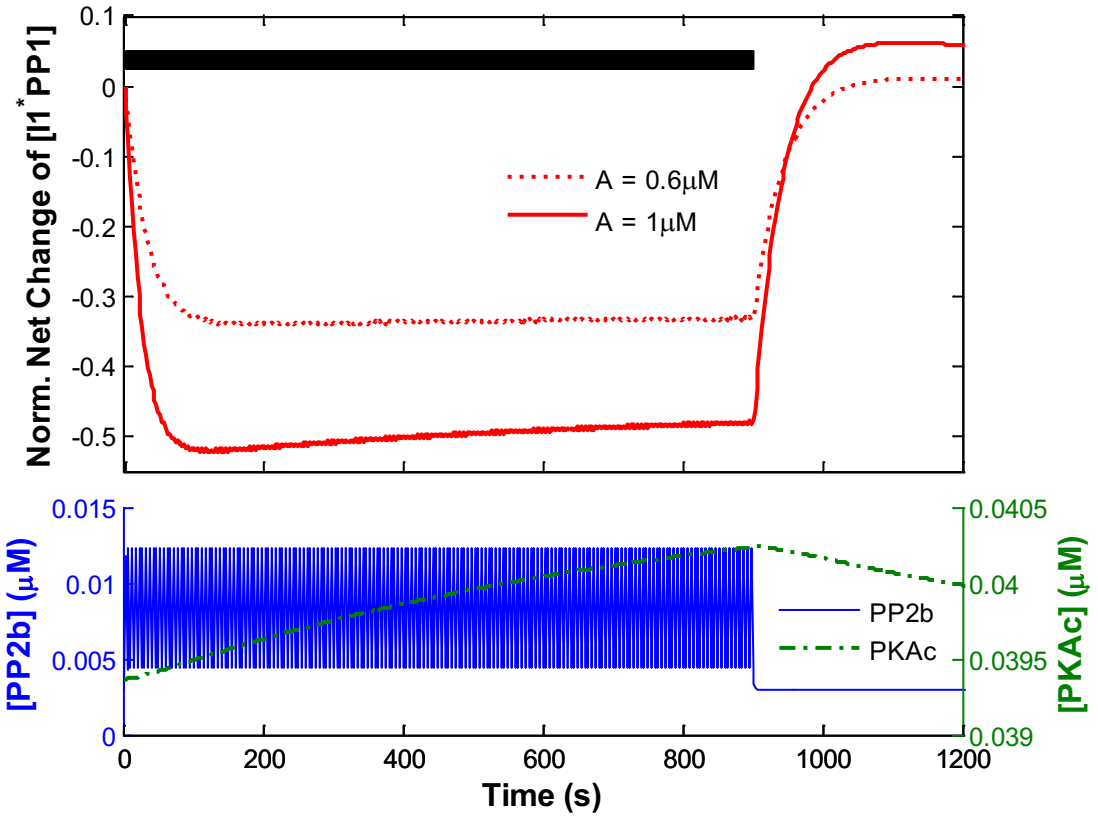

Figure 3-19 The dynamics of the normalised net change of [*I1*PP1*] in response to LFS. MoNP is run in response to LFS initiated at t = 0s (black bar). The upper panel shows the dynamics of the normalised net change of [*I1*PP1*] and the lower panel shows the dynamics of [*PP2b*] ([*CaMCaNA*] + [Ca_4CaNB]/20) and [*PKAc*]. Two kinetic parameters of the Ca^{2+} influx (see Appendix G for the explaination) are used: (1) A=0.6μM, and (2) A=1μM.

3.4.3 Computational study on the removal of PKA by PP2b

As discussed in Section 2.3.5, one of the possible mechanisms to prevent the rephosphorylation by PKA during LTD is the PP2b dependent removal of AKAP and PKA. However, the exact mechanism of the removal is unclear. In the previous section, we have shown that PKA does rephosphorylate I1 above the base even at low Ca^{2+} levels. Hence, we modify MoNP to include the removal and conduct computational experiments to test the implication of the removal in the prevention of the PKA rephosphorylation during LTD.

The activation of PKA is modelled as the state transitions among four states in MoNP: R_2C_2, R_2cAMP_2, R_2cAMP_4 and the released PKAc. AKAP binds to the regulatory dimmer (Gold et al., 2006), so that we assume PP2b removes the unreleased PKA complex, R_2C_2, R_2cAMP_2, and R_2cAMP_4, far away from the cAMP sources. We model the removal of PKA complex by mass action law and the PP2b regulation of the removal by a Hill equation. We ignore the binding of the removed regulatory dimmer to cAMP since it is far away from cAMP sources. Hence, the removal rate of R_2C_2, R_2cAMP_2, R_2cAMP_4 (V_{r1}, V_{r2} and V_{r3}) and state transition rate among them (V_{17} and V_{18}) are given by Eqs. (3.81 – 3.85):

$$V_{r1} = k_{rf}\left[R_2C_2\right]\frac{\left[ActivePP2b\right]}{K_{m17}+\left[ActivePP2b\right]} - k_{rb}\left[R_2C_2\right]_r, \tag{3.81}$$

$$V_{r2} = k_{rf}\left[R_2C_2cAMP_2\right]\frac{\left[ActivePP2b\right]}{K_{m17}+\left[ActivePP2b\right]} - k_{rb}\left[R_2C_2cAMP_2\right]_r, \tag{3.82}$$

$$V_{r3} = k_{rf}\left[R_2C_2cAMP_4\right]\frac{\left[ActivePP2b\right]}{K_{m17}+\left[ActivePP2b\right]} - k_{rb}\left[R_2C_2cAMP_4\right]_r, \tag{3.83}$$

$$V_{17} = -k_{17b}\left[R_2C_2cAMP_2\right]_r, \text{ and} \tag{3.84}$$

$$V_{18} = -k_{18b}\left[R_2C_2cAMP_4\right]_r, \tag{3.85}$$

where [*ActivePP2b*] = [Ca_4CaNB]/20 + [*CaMCaNA*], [R_2C_2]$_r$, [$R_2C_2cAMP_2$]$_r$, and [$R_2C_2cAMP_4$]$_r$ are the corresponding concentrations of the removed states of PKA complex, k_{rf} is the rate constant for the removal of PKA, k_{rb} is the rate constant for the re-association of PKA complex to cAMP sources, K_{m17} is the concentration of [*ActivePP2b*] where the removal reaches half maximum, k_{17b} and k_{18b} are dissociation rate constant of cAMP from $R_2C_2cAMP_2$ and $R_2C_2cAMP_4$, respectively. The modified ODEs for the dynamics of [R_2C_2], [$R_2C_2cAMP_2$], [$R_2C_2cAMP_4$], as well as their corresponding removed forms are given by Eqs. (3.86-3.91):

$$\frac{d[R_2C_2]}{dt} = -V_{13} - V_{r1}, \tag{3.86}$$

$$\frac{d[R_2C_2cAMP_2]}{dt} = V_{13} - V_{14} - V_{r2}, \tag{3.87}$$

$$\frac{d[R_2C_2cAMP_4]}{dt} = V_{14} - V_{15} - V_{r3}, \tag{3.88}$$

$$\frac{d[R_2C_2]_r}{dt} = V_{r1} + V_{17}, \tag{3.89}$$

$$\frac{d[R_2C_2cAMP_2]_r}{dt} = V_{r2} - V_{17} + V_{18}, \tag{3.90}$$

$$\frac{d[R_2C_2cAMP_4]_r}{dt} = V_{r3} - V_{18}. \tag{3.91}$$

As shown in Fig. 3-20, the PKA removal reduces the rephosphorylation of I1. PP2b slowly removes PKA and the removal lags behind the drop of $\widehat{\Delta[I1^* PP1]}$ due to the slow deactivation of PKA. This may be an explanation for the experimentally observed lag of the PKA removal (Sanderson et al., 2012; Smith et al., 2006). Furthermore, the rephosphorylation of I1 by PKA reaches a maximum below the base without altering the time taken to reach the maximum compared to that of no PKA removal. There is no direct experimental evidence on I1 rephosphorylation for this observation. However, an experiment on the phosphorylation of S845 of AMPAR (different substrates, but involve similar sets of kinases and phosphatases), observes unaltered time taken for the rephosphorylation of S845 to reach the maximum when the PKA removal rate is altered by altering the activity of PP2b (Sanderson et al., 2012). The same paper also shows

that synaptic strength (indicated by EPSP slope) recovers above the base in response to LFS when the PP2b removal of PKA is reduced.

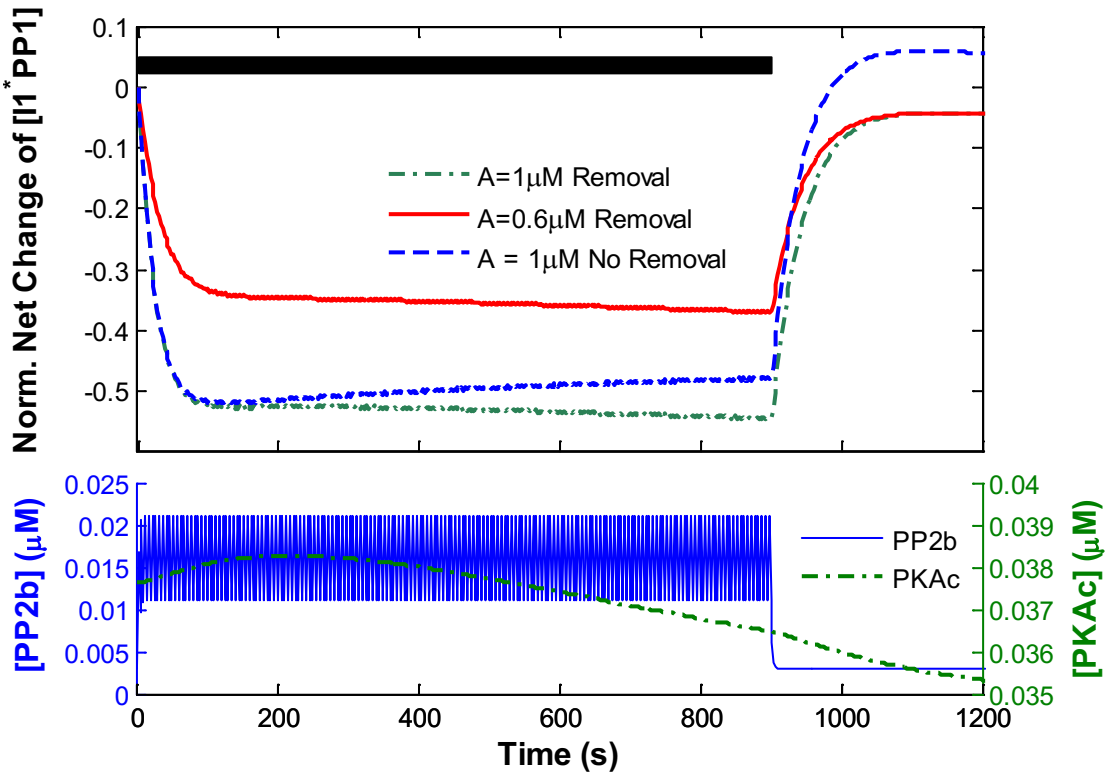

Figure 3-20 The dynamics of the normalised net change of [*I1*PP1*] in response to LFS with the PKA removal. The modified MoNP with the PKA removal is run in response to LFS initiated at t = 0s (black bar). The upper panel shows the dynamics of the normalised net change of [*I1*PP1*] and the lower panel shows the dynamics of [*PP2b*] ([*CaMCaNA*] + [Ca_4CaNB]/20) and [*PKAc*]. Two kinetic parameters of the Ca^{2+} influx are used: (1) A=0.6μM, and (2) A=1μM. The dynamics without the PKA removal is retrieved from Fig. 3-19. Parameter used are: k_{rf} = 0.25s^{-1}, k_{rb} = 1/600s^{-1}, K_{m17} = 3μM.

3.5 Discussion and summary

We develop a new model of the NMDAR mediated pathway of synaptic plasticity (MoNP) based on the essential modulators using Ca^{2+} concentration as the input. MoNP is developed based on carefully selected modulators of synaptic plasticity from the literature and the experimentally estimated kinetic characteristics of these modulators. The main contribution of MoNP is the establishment of a simplified model of NMDAR mediated pathway of synaptic plasticity, which integrates: (1) the essential features of the modulators/pathways; (2) the latest experimentally estimated kinetic parameters of the modulators; and (3) the latest findings of the biochemical interactions among modulators.

The steady state analysis of MoNP shows that the competition among CaM binding proteins for Ca^{2+}/CaM complex binding behaves bidirectionally having the Ca^{2+} level as the control parameter. The LTD related binding is stronger at low Ca^{2+} levels, while the LTP related binding is stronger at high Ca^{2+} levels. Two factors may be important for modulating the strength of LTP related bindings: (1) the rate of the autophosphorylation, and (2) the concentration of CaM. The fast rate of the autophosphorylation narrows the LTD induction range and enhances the LTP related CaM binding. The rate may be modulated by controlling the ratio of CaMKII isoforms, which is actively regulated (Shen et al., 1998; Thiagarajan et al., 2002). Moreover, high concentrations of CaM is required for the recovery and further enhance of KBI above the base, which may be the reason for the higher accumulation of CaM in the brain tissue (Kakiuchi et al., 1982) as well as the essential roles of CaM play in LTP (Malenka et al., 1989).

Analysis of the temporal patterns of the modulators in response to transient Ca^{2+} signals provide insights into the effective timescales of the modulators during synaptic plasticity. The activation and deactivation of PP2b are fast, while those are slightly slower for CaMKII and the slowest for PKA. As a result, the activities of CaMKII and PKA are low for weak signals or are retained longer when strong signals disappear.

Hence, both $\widehat{\Delta[I1^{*}PP1]}$ and $\widehat{\Delta KBI}$ decrease and recover rapidly in response to LFS, while they drop initially and rise above the base afterwards in response to HFS. Moreover, the coupling among multiple trains further enhances the activities of CaMKII and PKA that increase $\widehat{\Delta[I1^{*}PP1]}$ and $\widehat{\Delta KBI}$.

At the end, we test the implication of PKA removal through a computational experiment. The results show that the removal does prevent the PKA rephosphorylation above the base without altering the timescale of the rephosphorylation. The removal lags behind the dephosphorylation that may be due to the slow deactivation of PKA.

Why does the bidirectional behaviour exist in two synaptic processes, the CaM competition and the PP1 regulation, facilitated by different kinases including CaMKII and PKA? Analysis of the temporal pattern of the system may indicate the different roles of kinases play in LTP. Activation of CaMKII is fast, and persists for a moderate period facilitated by the autophosphorylation. Once autophosphorylated, CaMKII binds to CaM in a similar level of affinity to that of PP2b. Therefore, activation of CaMKII following a strong Ca^{2+} signal balances the phosphatase induced decrease of synaptic strength and facilitates a short, but strong increase of synaptic strength in the early phase. On the other hand, activation of PKA is slow, but persists for a much longer period. The strong binding affinity between the PKA regulatory dimmer and catalytic subunits results in a low level of the released PKA catalytic subunits. As a result, the PKA dependent phosphorylation is weak against the PP2b-dependent dephosphorylation. So that PKA requires designated signals, like TBS, to have itself accumulated a significant amount. Due to the slow deactivation, the accumulated amount maintains for a much longer period than PP2b to rephosphorylate the substrate to a higher level. Considering PKA may be involved in gene expression pathways (Mayford et al., 2012), the slow deactivation of PKA may trigger the gene expression in late phase to maintain the changes in early phase. On the other hand, PP2b removes PKA to revert the permanent modification. Therefore, the designated pattern is transient to minimise the PP2b-dependent removal.

Hence, we now have a hypothesised model for the memory system. Learning first triggers activation of CaMKII to form a short term memory and the lasting of the short term memory is modulated by the ratio of CaMKII isoforms. Following designated signals, PKA is activated, and triggers gene expression pathways to maintain the short term memory by inducing a growth of the synapse. After that, a long term memory is formed. Forgetting of the long term memory is induced by PP2b to remove PKA resulting in a shrinkage of the synapse.

Chapter 4: A Theoretical Model of State Transition of CaMKII

CaMKII plays a very important role in the induction of synaptic plasticity as well as the associated phenomena, such as memory formation. Two states of CaMKII, the autophosphorylation and the CaMKII-NMDAR binding, both show strong correlation to synaptic plasticity and memory formation (Barria et al., 1997; Buard et al., 2010; Giese et al., 1998; Halt et al., 2012; Irvine et al., 2006; Otmakhov et al., 2004; Sanhueza et al., 2011; Vest et al., 2007; Zhang et al., 2008; Zhou et al., 2007). Especially, the CaMKII-NMDAR complex, formed by associating the T site of CaMKII to NMDAR, has outstanding contributions to synaptic plasticity: (1) the complex maintains the staying of CaMKII in PSD for more than 30 minutes (Bayer et al., 2006) that may be a potential mechanism underlying the connection between E-LTP and late phase LTP (L-LTP); (2) the induction of LTP displays high associativity to the formation of CaMKII-NMDAR complex (Appleby et al., 2011; Otmakhov et al., 2004; Zhang et al., 2008); and (3) inhibiting the formation of CaMKII-NMDAR complex impairs LTP (Barria et al., 1997; Halt et al., 2012; Zhou et al., 2007).

Modelling the state transition (ST) of CaMKII has been a predominant path to understand the dynamic behaviour of synaptic plasticity. Inner state transitions of CaMKII (ISTs) refer to state transitions of a single subunit, which has no direct impact to the state of other subunits in the same holoenzyme, for example, the Ca^{2+}/CaM complex binding and the autophosphorylation; holoenzyme state transitions of CaMKII (HSTs) refer to state transitions impacting the state of a holoenzyme as well as all of its constituting subunits, for example, the translocation and the NMDAR binding. As discussed in Section 2.4.1.2, many models successfully describe ISTs and investigate the potential roles of the autophosphorylation play in decoding the frequency of the stimulation. However, they neither include the HSTs nor provide insight into the relationships among the autophosphorylation, CaMKII-NMDAR complex and LTP.

HSTs are important for the formation of CaMKII-NMDAR complex; the holoenzyme structure of CaMKII is experimentally shown crucial for its binding to NMDAR (Strack et al., 2000). We hope to understand the relationships among the autophosphorylation, the CaMKII-NMDAR complex and LTP by developing a dynamic model of the HSTs (MoHST) of CaMKII and using MoHST to understand the dynamic behaviour of CaMKII, especially the formation of CaMKII-NMDAR complex, in response to Ca^{2+} signals. The main contributions of this model development are the inclusion of the ISTs based on the conformation of CaMKII subunits, the inclusion of translocation of the CaMKII holoenzyme between dendritic spine and PSD, and the development of a probabilistic framework for the binding between NMDAR and the CaMKII holoenzyme. To the best of our knowledge, this is the first attempt to model the HSTs and provide insights into the factors of CaMKII-NMDAR complex formation.

In this chapter, we present the detailed information of MoHST: the development of MoHST is described in Section 4.1; Section 4.2 gives the details related to the simulation with MoHST, including generation of Ca^{2+} signals, parameter estimation, and computational experiments; Section 4.3 gives the details of parameter perturbation and the associated results; and a brief discussion/summary is given in Section 4.4.

4.1 Model development

This section elaborates the development of MoHST, including the assumptions on which MoHST is based, the probabilistic framework, the conceptual models, and the equations.

4.1.1 Model assumptions

(1) As the translocation of CaMKII into PSD and the formation of CaMKII-NMDAR complex in response to LTP induction signal are important processes, PSD and dendritic spine are treated as two-compartments in the model. The mean volumes of PSD and dendritic spine are approximately 0.01 fL (cylinder

of 200 - 800 nm diameter and 30 – 50 nm height) and 0.1fL (cylinder of 200 - 800 nm diameter and 0.5 - 2 μm height), respectively (1 fL= 10^{-15} L = 10^{-18} m^3).

(2) The dynamics of the switching between the autoinhibited states of the CaMKII subunit are ignored. The reason is that the switching rate is different among the isoforms of CaMKII subunits, which is not a consideration of MoHST. Hence, we assume that the switching instantaneously reach a constant ratio in comparison to the slower binding process between Ca^{2+}/CaM complex and CaMKII subunits, which involves spatial movement and targeting. Hence, the constant ratio can be encapsulated by the binding rate between Ca^{2+}/CaM complex and CaMKII subunits.

(3) We assume that the total number of CaMKII subunits and CaMKII holoenzymes are at steady states to reflect the situation where gene expression is not altered during E-LTP. New CaMKII synthesis remains at a rate that exactly balances the degradation of CaMKII.

(4) Phosphorylation and dephosphorylation are catalytic reactions to be described by Michaelis-Menten kinetics. All other reactions are assumed to obey mass action kinetics.

(5) Ca^{2+}, CaM, ATP (supports the autophosphorylation) and PP1 (dephosphorylates T286) are evenly distributed across the whole synapse. We ignore the local Ca^{2+} dynamics around Ca^{2+} sources (Augustine et al., 2003) which are assumed to be insignificant in order to simplify the model.

(6) The translocation of CaMKII is assumed to be dependent on the levels of the CaM bound and the autophosphorylated CaMKII subunits (see (Shen and Meyer, 1999)).

(7) We considers S site mediated T site binding as the only mechanism for binding between CaMKII and NMDAR (Fig. 4-3A). We assume that one NR2B of NMDAR binds to only one active CaMKII subunit; this is a plausible assumption given that a CaMKII subunit is 475 amino acids long that covers the

binding region, amino acids 839~1303, of NR2B. Therefore, one CaMKII holoenzyme is able to bind only one NR2B subunit. (Based on the work reported by Shinohara et al., (2008), we assume that NMDAR has only one NR2B subunit.)

(8) The experimental observations indicate that PP1 is inaccessible to CaMKII in PSD (Mullasseril et al., 2007). Since the model only considers the NMDAR bound case of anchoring CaMKII in PSD, we assume that PP1 does not dephosphorylate the NMDAR bound CaMKII.

(9) We assume that T site binding between CaMKII and NMDAR is irreversible at least for the duration of the simulation of E-LTP.

(10) We assume CaM is always attached to the autophosphorylated or the NR2B bound CaMKII subunits. The dissociation of CaM from the CaMKII subunit is prevented by the autophosphorylation and the NR2B binding. The autophosphorylation and NR2B binding decrease the CaM dissociation rate by 1000 folds and 20 folds, respectively (Bayer et al., 2001; Hudmon and Schulman, 2002). Hence, the dissociation rate of CaM is negligible in these CaMKII subunits.

4.1.2 States of CaMKII

Eight states of CaMKII are considered as important which are involved either in the ISTs or HSTs. There are three inner states (IS) of a subunit (from Chiba et al., (2008)): (1) inhibited CaMKII subunit (variable iCaMKII is the number of subunits in this state), (2) CaM bound CaMKII subunit (variable: CaMCaMKII), and (3) autophosphorylated CaMKII subunit (variable: CaMCaMKII*).

There are five holoenzyme states (HS) of CaMKII: (1) CaMKII outside of PSD (variable EoPSD is the number of holoenzymes outside of PSD); (2) NMDAR unbound CaMKII inside of PSD (variable: EiPSD); (3) CaMKII with NMDAR bound to (S site of) a CaM bound subunit (variable: CaMKIIS); (4) CaMKII with NMDAR bound to (S site of) an autophosphorylated subunit (variable: CaMKII*S); and (5) CaMKII with

NMDAR bound to (T site of) any active subunit (CaMKII*T) (An active subunit could be either a CaMCaMKII or a CaMCaMKII *).

HSs are composed of different ISs: (1) EoPSD and EiPSD have all of their subunits (12 subunits) belonging to the three groups of ISs, and (2) CaMKIIS, CaMKII*S and CaMKII*T have exactly 1 subunit bound to a NR2B according to assumption 7 (the bound subunit is denoted by the same variable name as the holoenzyme: CaMKIIS, CaMKII*S or CaMKII*T) and others (11 subunits) belonging to the three groups of ISs. Therefore, based on assumption (3), the total number of CaMKII subunits, $CaMKII_{Total}$, is conserved during E-LTP and given as follows:

$$CaMKII_{Total} = iCaMKII + CaMCaMKII + CaMCaMKII^{*} + CaMKIIS + CaMKII^{*}S + CaMKII^{*}T \text{ , or}$$

$$CaMKII_{Total} = 12\left(EoPSD + EiPSD + CaMKIIS + CaMKII^{*}S + CaMKII^{*}T\right).$$

4.1.3 A probabilistic framework of the CaMKII-NMDAR binding

The difficulty of modelling the formation of CaMKII-NMDAR complex stems from the twelve subunits that constitute CaMKII. Each subunit can be in any one of the three possible conformations discussed above, resulting in 91 possible conformations of the holoenzyme. (To select 12 subunits from 3 possible conformations, there are, $C_2^{12+3-1} = \frac{14!}{2!(14-12)!} = 91$ possible ways (Benjamin and Quinn, 2003)). Moreover, CaMKII may contain subunits which could potentially bind to NMDAR (we call them potential binding subunit (pBS); see section 4.1.3.2 for the explanation), but NMDAR can only bind to one of them (assumption (7)). To avoid having a reaction rate constant for each specific conformation -there are 91 of them- we develop a probabilistic framework in modelling the formation of CaMKII-NMDAR complex and the rates of bindings are multiplied by the modifiers given by this framework (Fig. 4-1). The symbols of the probabilities or modifiers used in the model are listed and defined in Table 4-1. (Note that we use variable names to identify the states in Fig. 4-1 and Table 4-1 for brevity.)

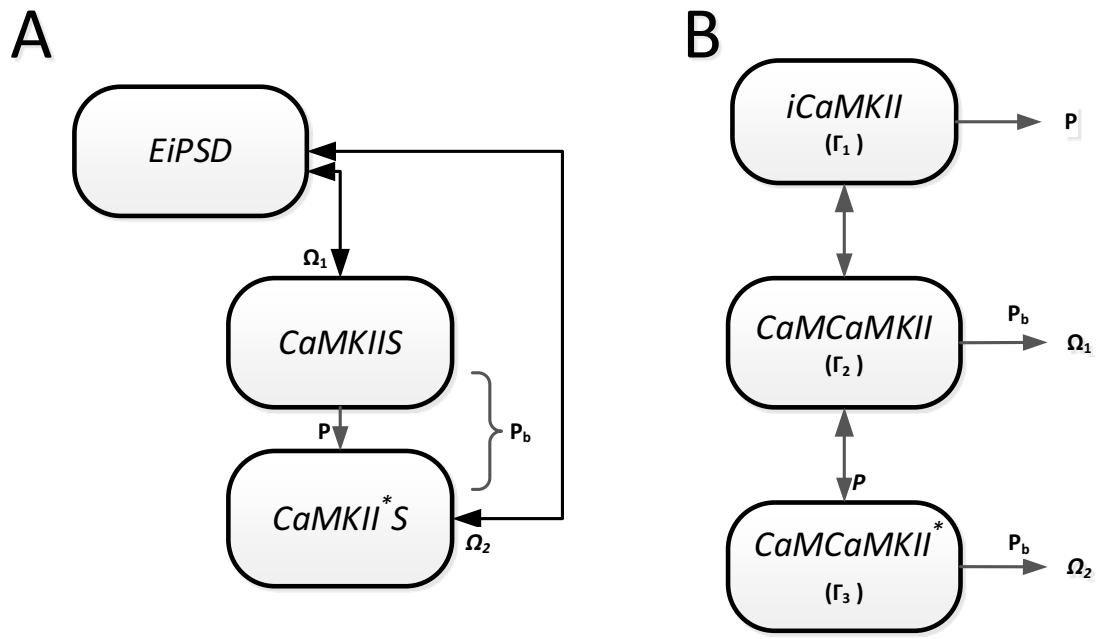

Figure 4-1 Schematic diagram of the probabilistic framework. (**A**) The framework of CaMKII-NMDAR binding: NMDAR binds the S site of an active subunit of EiPSD to form CaMKIIS or CaMKII*S. The rates of the bindings are modified by Ω_1 or Ω_2, respectively, to reflect the average binding rates to NMDAR with respect to 91 possible conformations of CaMKII holoenzyme. (**B**) ISs of CaMKII determine Γ_s (s = 1, 2, 3) which represent the fractions of the three potential ISs in constituting CaMKII. Ωs are dependent on Γs and P_b (see Section 4.1.3.2).

Table 4-1

Definition of the probabilities and modifiers used in the model

Group	*Symbol*	*Definition*
IS	Γ_1	*fraction of iCaMKII to the total number of unbound subunits*
	Γ_2	*fraction of CaMCaMKII to the total number of unbound subunits*
	Γ_3	*fraction of CaMCaMKII* to the total number of unbound subunits*
	P	*probability that either or both sides of a neighbouring subunit are active*
HS	P_b	*probability of S site mediated binding between CaMKII and NMDAR*
	Ω_1	*modifier for average formation rate of CaMKIIS with respect to 91 possible conformations of CaMKII*
	Ω_2	*modifier for average formation rate of CaMKII*S with respect to 91 possible conformations of CaMKII*

4.1.3.1 Composition of CaMKII

The probability that a CaMKII is constituted by a given conformation is expressed as a function of three ratios, Γ_1, Γ_2 and Γ_3 (Fig. 4-1B). Γ_1, Γ_2 and Γ_3 represent the fractions of iCaMKII, CaMCaMKII and CaMCaMKII* subunits that constitute the twelve subunits of CaMKII, respectively. Since the bound subunits are governed by different state fractions (assumption (8)), hence, Γs are calculated by dividing the number of corresponding subunits by the total number of unbound subunits (Eqs. (4.1 – 4.3)):

$$\Gamma_1 = \frac{iCaMKII}{CaMKII_{Total} - \left(CaMKIIS + CaMKII^*S + CaMKII^*T\right)}, \tag{4.1}$$

$$\Gamma_2 = \frac{CaMCaMKII}{CaMKII_{Total} - \left(CaMKIIS + CaMKII^*S + CaMKII^*T\right)}, \tag{4.2}$$

$$\Gamma_3 = \frac{CaMCaMKII^*}{CaMKII_{Total} - \left(CaMKIIS + CaMKII^*S + CaMKII^*T\right)}, \text{ and} \tag{4.3}$$

$$\Gamma_1 + \Gamma_2 + \Gamma_3 = 1 .$$

Then, the probability of a particular conformation can be obtained based on Γs; for example, the probability that CaMKII contains exactly n CaMCaMKII* is given by Eq. (4.4):

$$\beta \cdot \Gamma_3^{\,n} \left(1 - \Gamma_3\right)^{12-n}, \qquad (\text{n} = 0, 1, \ldots, 12) \tag{4.4}$$

where β is the binomial coefficient: $\beta = \frac{12!}{n!(12-n)!}$ (Goldberg, 1986).

The probability of S site mediated binding between CaMKII and NMDAR, P_b, is calculated by dividing the sum of CaMKIIS and CaMKII*S by the total number of NMDAR, $NMDAR_{Total}$ (Fig. 4-1A):

$$P_b = \frac{CaMKIIS + CaMKII^*S}{NMDAR_{Total}}. \tag{4.5}$$

4.1.3.2 Formation of CaMKII-NMDAR complex - Calculation of Ω

pBS is a CaMKII subunit that both: (1) belongs to an unbound holoenzyme in PSD (subunits of EiPSD), and (2) is active. In terms of the active state of the subunit, pBS can be categorised as: CaMCaMKII pBS (CaM-pBS), and CaMCaMKII* pBS (T286-

pBS). The two groups are considered separately because of the difference in their dissociation rates from NMDAR binding (Bayer et al., 2006). Considering an EiPSD with n CaM-pBS and m T286-pBS, the formation of CaMKIIS is the event that NMDAR binds to one of the n CaM-pBS and does not bind to other subunit which is not a CaM-pBS (assumption 7). Since EiPSD only contains 3 types of subunits (CaM-pBS, T286-pBS and iCaMKII) and iCaMKII never binds to NMDAR, so that the statement "NMDAR does not bind to other subunit which is not a CaM-pBS" is simply a statement of "NMDAR does not bind to any of the m T286-pBS". The probability that NMDAR binds to one of the n CaM-pBS, $P_{\text{CaM-pBS}}$, is given by (see Appendix D for the details of the derivation):

$$P_{\text{CaM-pBS}} = \frac{nP_b}{(n-1)P_b + 1}, \tag{4.6}$$

where $P_b = \frac{CaMKIIS + CaMKII^* S}{NMDAR_{Total}}$.

The probability that NMDAR does not bind to any of the m T286-pBS, $P_{\overline{\text{T286-pBS}}}$, is given by:

$$P_{\overline{\text{T286-pBS}}} = \frac{1-P_b}{(m-1)P_b + 1}. \tag{4.7}$$

Since pBSs are independent from each other, the probability of the formation of CaMKIIS, $P_{CaMKIIS}$, is given by:

$$P_{CaMKIIS} = \left(P_{\text{CaM-pBS}} \cap P_{\overline{\text{T286-pBS}}}\right) = \frac{1-P_b}{(m-1)P_b + 1} \cdot \frac{nP_b}{(n-1)P_b + 1}. \tag{4.8}$$

We define an elementary CaMKII which contains 1 CaM-pBS and 0 T286-pBS. The probability of the formation of CaMKIIS based on the elementary CaMKII is P_b. If the rate of the formation of CaMKIIS based on the elementary CaMKII is k_{3f}, then the rate of formation of CaMKIIS based on other conformations of CaMKII can be expressed by a unified format: k_{3f} multiplies a coefficient. The coefficient can be expressed as the ratio of the probability of the formation of CaMKIIS based on the particular conformation to that based on the elementary CaMKII, P_b, and is given by Eq. (4.9):

$$\frac{1-P_b}{(m-1)P_b + 1} \cdot \frac{n}{(n-1)P_b + 1}. \tag{4.9}$$

It may be feasible to have a comprehensive model to mimic the exact formation rate of CaMKIIS (with 91 kinetic parameters). Alternatively, we use the mean rate of the formation based on the possible conformations of CaMKII holoenzyme. This approach determines an approximate formation rate of CaMKIIS. So, Ω_1 is given by Eq. (4.10):

$$\Omega_1 = \sum_{n=1}^{12} \frac{12!}{n!(12-n)!} \Gamma_2^{\,n} \sum_{m=0}^{12-n} \frac{(12-n)!}{m!(12-n-m)!} \Gamma_3^{\,m} \Gamma_1^{\,12-m-n} \frac{1-P_b}{(m-1)P_b+1} \cdot \frac{n}{(n-1)P_b+1}, \quad (4.10)$$

where $\sum_{n=1}^{12} \frac{12!}{n!(12-n)!} \sum_{m=0}^{12-n} \frac{(12-n)!}{m!(12-n-m)!}$ determines the probabilities for specific numbers of CaM-pBS (n) and T286-pBS (m) based on binomial distribution (Goldberg, 1986). Therefore, the mean rate of the formation of CaMKIIS is $k_{3f} \cdot \Omega_1$.

Similarly, we define Ω_2 as the mean coefficient of the formation of CaMKII*S with respect to 91 possible conformations of CaMKII holoenzyme. The only difference is that the elementary CaMKII becomes the holoenzyme containing 1 T286-pBS and 0 CaM-pBS. The expression of Ω_2 is given by Eq. (4.11):

$$\Omega_2 = \sum_{m=1}^{12} \frac{12!}{m!(12-m)!} \Gamma_3^{\,m} \sum_{n=0}^{12-m} \frac{(12-m)!}{n!(12-n-m)!} \Gamma_2^{\,n} \Gamma_1^{\,12-m-n} \frac{1-P_b}{(n-1)P_b+1} \cdot \frac{m}{(m-1)P_b+1}. \quad (4.11)$$

4.1.4 Previous models of IST of CaMKII

We use Holmes's model of the CaM dynamics (Holmes, 2000) and its successor (Chiba et al., 2008) to model ISTs of CaMKII in response to the Ca^{2+} influx. The deciding factor for this choice is the relative simplicity of Holmes's approach without compromising the agreement to the experimental data (Chiba et al., 2008). Holmes's model describes the binding of Ca^{2+} to CaM to form Ca^{2+}/CaM complex as four steps by attaching four Ca^{2+} ions to a CaM molecule sequentially (Fig. 4-2A). In addition, Holmes (2000) assumes that the bindings to the sites of the C-terminus of CaM occur first. Chiba et al. (2008) formulate a model that describes ISTs of CaMKII among inhibited, CaM-bound, autophosphorylated and CaM dissociated autophosphorylated states of CaMKII subunits, and this model has the level of Ca^{2+}/CaM complex as the input. We ignore the CaM dissociated autophosphorylated state based on assumption 9 (Fig. 4-2B). The variables associated with ISTs of CaMKII are listed in Table 4-2.

Table 4-2

Definition of the states/variables associated with IST of CaMKII

States (#)	*Definition*
Ca^{2+}	*Intracellular calcium ion*
CaCaM	*one Ca^{2+} ion binds to CaM*
Ca_2CaM	*two Ca^{2+} ions bind to CaM*
Ca_3CaM	*three Ca^{2+} ions bind to CaM*
Ca_4CaM	*Ca^{2+}/CaM complex*

The equations for the reaction rates (R1~R7, unit: molecular number (#) per sec, abbreviated as # s^{-1}) are given by Holmes (2000) and Chiba et al. (2008) and we reproduce them in the following equations:

(1) Ca^{2+} attaches to CaM to form CaCaM (Holmes, 2000),

$$R_1 = k_{6f} Ca^{2+} \cdot CaM - k_{6b} CaCaM \ . \tag{4.12}$$

(2) Ca^{2+} attaches to CaCaM to form Ca_2CaM (Holmes, 2000),

$$R_2 = k_{7f} Ca^{2+} \cdot CaCaM - k_{7b} Ca_2 CaM \ . \tag{4.13}$$

(3) Ca^{2+} attaches to Ca_2CaM to form Ca_3CaM (Holmes, 2000),

$$R_3 = k_{8f} Ca^{2+} \cdot Ca_2 CaM - k_{8b} Ca_3 CaM \ . \tag{4.14}$$

(4) Ca^{2+} attaches to Ca_3CaM to form Ca^{2+}/CaM complex (Holmes, 2000),

$$R_4 = k_{9f} Ca^{2+} \cdot Ca_3 CaM - k_{9b} Ca_4 CaM \ . \tag{4.15}$$

(5) *We* simplify *the reaction rate of Ca^{2+}/CaM complex binding to iCaMKII to form CaMCaMKII*.

In the original model, two pathways of Ca^{2+}/CaM complex dissociation are modelled (Chiba et al., 2008); in the pathway one the whole Ca^{2+}/CaM complex dissociates from CaMKII subunit and, in the pathway two, Ca^{2+} dissociates from Ca^{2+}/CaM complex first and then the remaining CaM dissociates from CaMKII subunit (Peersen et al., 1997). The percentage of Ca^{2+}/CaM dissociates by the pathway two is determined by a Hill function; based on the parameter values of the original model and the rest Ca^{2+} levels measured from a normal hippocampal

neuron (0.07~0.11μM), it can be shown that 99% of the Ca^{2+}/CaM complex dissociates by the pathway one. Therefore, we ignore the pathway two and the modified R_5 is given in Eq. (4.16):

$$R_5 = k_{1f} Ca_4 CaM \cdot iCaMKII - k_{1b} CaMCaMKII \ . \tag{4.16}$$

(6) Autophosphorylation of CaMCaMKII to form CaMCaMKII* (Chiba et al., 2008),

$$R_6 = \frac{K_{cat1} CaMCaMKII \cdot P \cdot ATP}{K_{m1} + ATP}, \tag{4.17}$$

where P is defined by Chiba et al., (2008) as the probability that either or both sides of a neighbouring subunit are active and is given by the expression, 1 - Γ_1^2. ATP is a constant (the number of ATP in the synapse).

(7) Dephosphorylation of CaMKII* into CaMKIICaM by PP1 (Chiba et al., 2008),

$$R_7 = \frac{K_{cat2} CaMCaMKII^* \cdot PP1}{K_{m2} + CaMCaMKII^*}, \tag{4.18}$$

where $PP1$ is a constant (the number of PP1 in the synapse).

The values of rate constants (k_{1f}, k_{1b}, k_{6f}, k_{6b}, k_{7f}, k_{7b}, k_{8f}, k_{8b}, k_{9f}, k_{9b}, K_{cat1}, K_{cat2}) and Michaelis constants (K_{m1}, K_{m2}) are obtained from the original model at 37°C (Chiba et al., 2008) and converted into the values based on molecular numbers (the values of parameters are shown in Table 4-4, and see Appendix C for the details of the conversion). Other conditions, such as the total numbers of CaM and CaMKII, are modified to reflect the hippocampal synapses; these are discussed in Section 4.2.

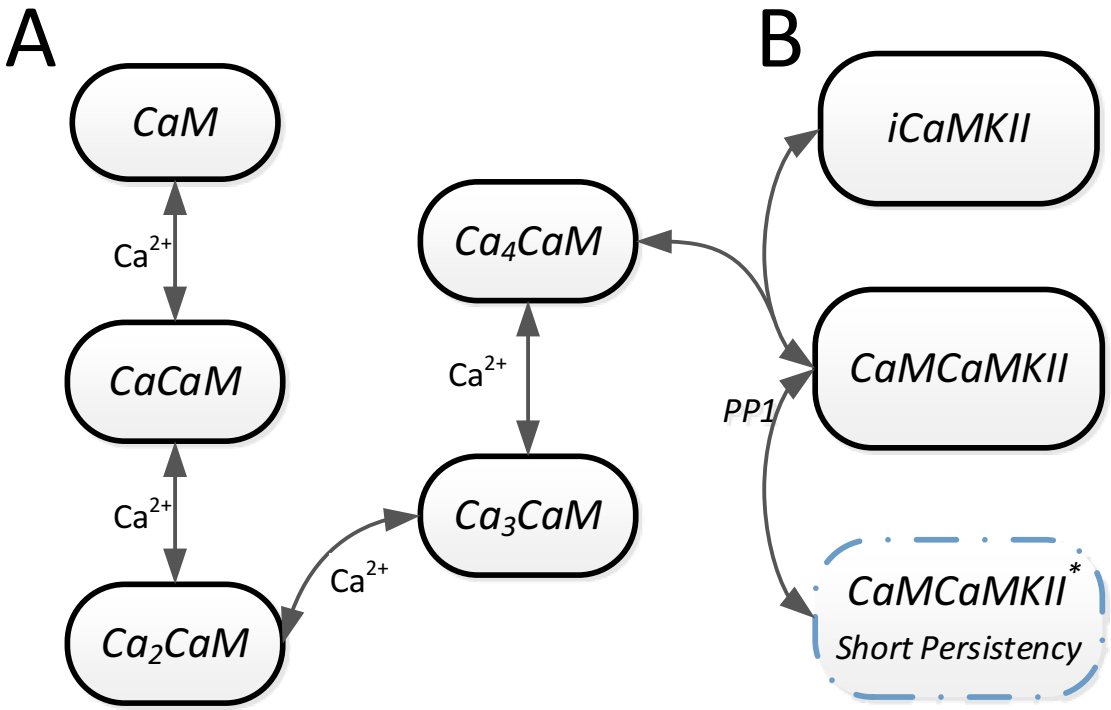

Figure 4-2 Ca^{2+}- CaM interactions and the ISTs. (**A**) Ca^{2+} attaches to all four Ca^{2+} binding sites of CaM by four sequential steps (Holmes, 2000). (**B**) An inhibited CaMKII subunit (iCaMKII) binds to a Ca^{2+}/CaM complex (Ca_4CaM) to form a Ca_4CaM bound CaMKII subunit (CaMCaMKII). A CaMCaMKII is autophosphorylated by its active neighbour to form an autophosphorylated CaMKII subunit (CaMCaMKII*). Both CaMCaMKII and CaMCaMKII* are active CaMKII subunits, but CaMCaMKII* has a prolonged activity for up to 1 minute after the disappearance of signal (Ca^{2+}) (Lee et al., 2009). Dephosphorylating CaMCaMKII* by PP1 reverts CaMCaMKII* into CaMCaMKII. When Ca_4CaM dissociates CaMCaMKII, the CaMKII subunit becomes inactive (iCaMKII).

4.1.5 A new model of HST of CaMKII

In this section, we develop MoHST which encapsulates the HSTs (R_8~R_{19}, unit: molecular number (#) per second, abbreviated as # s^{-1}). The schematic diagram of MoHST is given below (Fig. 4-3).

4.1.5.1 Translocation of CaMKII into PSD

The translocation of CaMKII into PSD is CaM-bound dependent and the dissociation of CaMKII from PSD is decreased by the autophosphorylation (Shen and Meyer, 1999). Both the active states of CaMKII subunit have a CaM molecule attached (assumption (10)), so that we assume the translocation of CaMKII into PSD is positively correlated to the fraction of active CaMKII subunits ($\Gamma_2+\Gamma_3$) and the dissociation of CaMKII from PSD is inversely correlated to the fraction of CaMKII* (Γ_3). The correlations are formulated by Hill functions and the reaction rate of the CaMKII translocation rate into PSD (V_1) and dissociation rate away from PSD (V_2) are given by Eqs. (4.19 and 4.20):

$$V_1 = V_{\max 1}\frac{\Gamma_2+\Gamma_3}{K_{m3}+\Gamma_2+\Gamma_3}, \text{ and} \tag{4.19}$$

$$V_2 = V_{\max 2}\frac{K_{m4}}{K_{m4}+\Gamma_3}, \tag{4.20}$$

where V_{max1} is the maximum translocation rate of CaMKII into PSD and V_{max2} is the maximum dissociation rate of CaMKII away from PSD. According to mass action law, the max translocation rate of the CaMKII into PSD is k_{2f}EoPSD, where k_{2f} is the translocation rate constant, and the max translocation occurs when all the subunits of EoPSD are active. Similarly, the dissociation rate of CaMKII from PSD is k_{2b}EiPSD, where k_{2b} is the dissociation rate constant, and the max dissociation occurs when none of the subunits of EiPSD are autophosphorylated. Hence, the reaction rate (R_8) of the CaMKII translocation is given by Eq. (4.21):

$$R_8 = k_{2f}EoPSD\frac{\Gamma_2+\Gamma_3}{K_{m3}+\Gamma_2+\Gamma_3} - k_{2b}EiPSD\frac{K_{m4}}{K_{m4}+\Gamma_3}, \tag{4.21}$$

where K_{m3} is the $\Gamma_2+\Gamma_3$ value at which the translocation rate of EoPSD into PSD is half of its maximum and K_{m4} is the Γ_3 value at which the dissociation rate of EiPSD from PSD is half of its maximum.

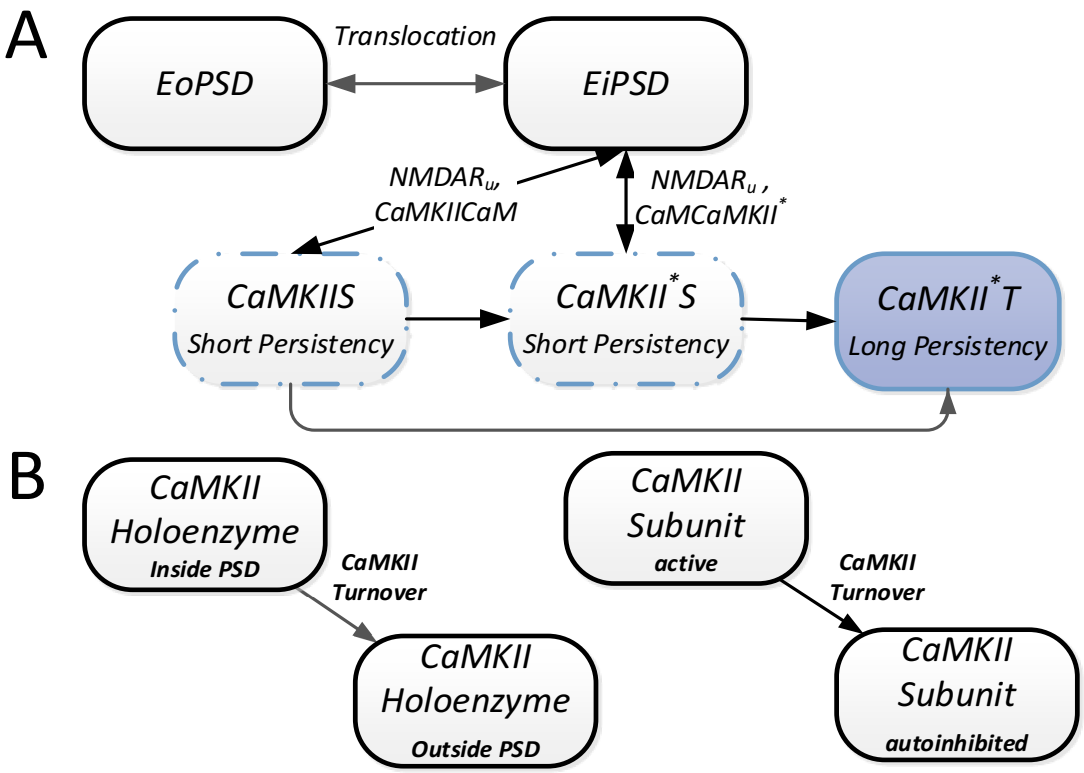

Figure 4-3 The HSTs. (A) CaMKII holoenzyme in dendritic spine (EoPSD) is translocated into PSD. Unbound CaMKII in PSD (EiPSD) binds to NMDAR through S site mediated T site binding (Bayer et al., 2006), where a reversible binding is established first at the S site (CaMKIIS and CaMKII*S) and then is transferred to a long persisting binding at the T site (CaMKII*T). CaMKIIS can be phosphorylated to become CaMKII*S, which has a slower dissociation rate from NMDAR binding. **(B)** CaMKII turnover is modelled as a simple conversion process that CaMKII inside of PSD is converted into CaMKII outside of PSD. Similarly, active CaMKII subunits are converted into inhibited CaMKII subunits.

4.1.5.2 Formation of CaMKII-NMDAR complex

The formation of CaMKIIS requires that NMDAR binds to a CaM-pBS and the reaction rate (R_9) of the binding is given by Eq. (4.22):

$$R_9 = k_{3f}\Omega_1 EiPSD \cdot NMDAR_u - k_{3ba} CaMKIIS \,, \tag{4.22}$$

where k_{3f} is the formation rate of CaMKIIS based on an elementary CaMKII, k_{3b} is the dissociation rate constant of CaMKII from NMDAR (k_{3b} is different for CaMKIIS, k_{3ba}, and CaMKII*S, k_{3bb}), and $NMDAR_u$ denotes the number of unbound NMDAR.

Similarly, the formation of CaMKII*S requires that NMDAR binds to a T286-pBS and the reaction rate (R_{10}) for this binding is given by Eq. (4.23):

$$R_{10} = k_{3f}\Omega_2 EiPSD \cdot NMDAR_u - k_{3bb} CaMKII^*S \,, \tag{4.23}$$

where we assume the rates of the formation of CaMKIIS and CaMKII*S based on the elementary forms of CaMKII is the same, k_{3f}. Next, the transfers of the S site binding to the T site are modelled as first order irreversible reactions and their reaction rates (R_{11} and R_{12}) are given by Eqs. (4.24 and 4.25):

$$R_{11} = k_4 CaMKIIS \,, \quad \text{and} \tag{4.24}$$

$$R_{12} = k_4 CaMKII^*S \,, \tag{4.25}$$

where k_4 is the rate of transferring the binding at the S site to the T site.

CaMKIIS can be autophosphorylated to become CaMKII*S, the reaction rate (R_{13}) of autophosphorylating CaMKIIS into CaMKII*S is (see Eq. (4.18)):

$$R_{13} = \frac{K_{cat1} CaMKIIS \cdot P \cdot ATP}{K_{m1} + ATP} \,. \tag{4.26}$$

4.1.5.3 CaMKII turnover

CaMKII turnover is the process that the newly synthesised CaMKII replaces the old CaMKII (Ehlers, 2003). It is caused by two concurrent processes: degradation of old CaMKII and synthesis of new CaMKII. Since the total number of CaMKII is conserved (assumption (3)), we model the turnover as an exchange process which converts

CaMKII inside of PSD (EiPSD, CaMKIIS, CaMKII*S and CaMKII*T) into EoPSD or active subunits (CaMCaMKII and CaMCaMKII*) into iCaMKII, both at a constant rate, k_5. Therefore, the reaction kinetics of CaMKII turnover is a set of first order reactions and the reaction rates (R_{14}~R_{19}) are given by Eqs. (4.27 – 4.32):

$$R_{14} = k_5 CaMCaMKII \,, \tag{4.27}$$

$$R_{15} = k_5 CaMCaMKII^* \,, \tag{4.28}$$

$$R_{16} = k_5 EiPSD \,, \tag{4.29}$$

$$R_{17} = k_5 CaMKIIS \,, \tag{4.30}$$

$$R_{18} = k_5 CaMKII^* S \text{ , and} \tag{4.31}$$

$$R_{19} = k_5 CaMKII^* T \,. \tag{4.32}$$

4.1.6 Complete model, and constraints

The reaction rates of the reactions governing the ISTs and HSTs are given in R_1~R_{19} (Unit: # s^{-1}). The time-dependent changes of the states of CaMKII can be formulated based on R_1~R_{19} as given by Eqs. (4.33 – 4.46):

(1) Ca^{2+}/CaM complex formation:

$$\frac{dCaCaM}{dt} = R_1 - R_2 \,, \tag{4.33}$$

$$\frac{dCa_2CaM}{dt} = R_2 - R_3 \,, \tag{4.34}$$

$$\frac{dCa_3CaM}{dt} = R_3 - R_4 \text{ , and} \tag{4.35}$$

$$\frac{dCa_4CaM}{dt} = R_4 - R_5 \,. \tag{4.36}$$

(2) Changes in IS of CaMKII:

$$\frac{dCaMCaMKII}{dt} = R_5 - R_6 + R_7 - R_9 - R_{14} \text{ , and} \tag{4.37}$$

$$\frac{dCaMCaMKII^*}{dt} = R_6 - R_7 - R_{10} - R_{15}\,. \tag{4.38}$$

(3) CaMKII-NMDAR formation – Changes in HS of CaMKII

$$\frac{dEiPSD}{dt} = R_8 - R_9 - R_{10} - R_{16}\,, \tag{4.39}$$

$$\frac{dCaMKIIS}{dt} = R_9 - R_{11} - R_{13} - R_{17}\,, \tag{4.40}$$

$$\frac{dCaMKII^*S}{dt} = R_{10} - R_{12} + R_{13} - R_{18}\,, \text{ and} \tag{4.41}$$

$$\frac{dCaMKII^*T}{dt} = R_{11} + R_{12} - R_{19}\,. \tag{4.42}$$

(4) Constraints due to the conserved molecular numbers:

$$iCaMKII = CaMKII_{Total} - CaMCaMKII - CaMCaMKII^* - CaMKIIS - CaMKII^*S - CaMKII^*T\,, \tag{4.43}$$

$$CaM = CaM_{Total} - CaCaM - Ca_2CaM - Ca_3CaM - Ca_4CaM - \left(CaMKII_{Total} - iCaMKII\right), \tag{4.44}$$

$$NMDAR_u = NMDAR_{Total} - CaMKIIS - CaMKII^*S - CaMKII^*T\,, \text{ and} \tag{4.45}$$

$$EoPSD = CaMKII_{Total}/12 - EiPSD - \left(NMDAR_{Total} - NMDAR\right). \tag{4.46}$$

The values of the estimated parameters and those obtained from the literature, and the constants used in MoHST are listed in Table 4-4.

4.2 Simulations with MoHST

In this section, we discuss the procedure of simulating MoHST, including the generation of Ca^{2+} signals at different frequencies, the parameter estimation according to experimental data, and conducting meaningful computational experiments.

4.2.1 Modelling the input: generation of Ca^{2+}

Three patterns of Ca^{2+} have been used to test the model: (1) steady Ca^{2+} levels, (2) low frequency tetanus induced Ca^{2+} waves, and (3) high frequency tetanus induced Ca^{2+} waves. The steady Ca^{2+} levels represent rest Ca^{2+} level (0.07 μM) or a period of steady

Ca^{2+} level following a gentle stimulation. Low frequency tetanus (1Hz) is experimentally used to induce LTD (Bliss and Collingridge, 1993; Mayford et al., 2012); therefore the model response following the low frequency tetanus can be a good contrast to understand the critical system behaviours in the emergence of LTP by the high frequency tetanus. The Ca^{2+} input is generated by a framework described by Zhabotinsky (2000) (see Appendix G for the details).

4.2.2 Estimation of parameters

Most of the parameters have been estimated in the literature and there are only eight new parameters (k_{2f}, k_{2b}, K_{m3}, K_{m4}, k_{3f}, k_4, k_{3ba}, k_{3bb}) related to the HSTs to be estimated. Markov Chain Monte Carlo (MCMC) method (Haario et al., 2006, 2001) was used to estimate these parameters (see Appendix E.1 for the details). The goodness-of-fit of the parameters is determined by mean square error (MSE) of the normalised model output from the normalised experimentally established data (Shen and Meyer, 1999), and MCMC converges to a set of parameters that gives minimum MSE. (The normalisation of a variable x at time t, $\hat{x}_t$, is based on Eq. (4.47):

$$\hat{x}_t = (x_t - x_{\min})/(x_{\max} - x_{\min}), \tag{4.47}$$

where x_{min} and x_{max} are the minimum and maximum of the data, respectively, from the model or experiment. Since the experimental data is normalised from fluorescence intensity and does not contain quantitative information, the normalisation enables comparison of the trends in the experimentally observed CaMKII translocations to those predicted by the model.)

The ranges of parameters for MCMC (Table 4-3) are decided based on the following information: (1) k_{2f} is between $0.00625s^{-1}$ and $0.075s^{-1}$ (with 50% uncertainty), because the half-maximal times required for the translocation of CaMKII into PSD are approximately 20s (alpha isoform) and 80s (alpha/beta isoforms 1:1) (Shen and Meyer, 1999); (2) k_{2b} is between $0.01s^{-1}$ and $0.3s^{-1}$ (with 50% uncertainty), because the half-life times for the dissociation of CaMKII from PSD are approximately 5s (T286A mutant) and 50s (wild type) (Shen and Meyer, 1999; Shen et al., 2000); (3) K_{m3} is between 0

and 0.5, because half of the CaMKII holoenzyme (alpha/beta isoforms 1:1) are free from the F-actin binding when the probability of Ca^{2+}/CaM complex binding to a CaMKII subunit is at 0.46 based on binomial probability; (3) K_{m4} is between 0 to 0.1, where 0.1 is slight higher than 1/12, which represents one autophosphorylated subunit per holoenzyme on average; (4) the ranges of k_{3ba} and k_{3bb} are assumed to be between $0.001s^{-1}$ to $0.5s^{-1}$ and $0.001s^{-1}$ to $0.1s^{-1}$, respectively (Bayer et al., 2006); and (5) the range of k_{3f} is assumed to be between $0.001\#^{-1}s^{-1}$ and $0.02\#^{-1}s^{-1}$, because K_d of the binding between the elementary CaMKII and NMDAR (quotient of dividing k_{2bb} by k_{3f}) should be approximately 1# or less due to the multiple pBS enhancement of the binding affinity between CaMKII and NMDAR. The K_d in molecular number is calculated based on the estimated K_d of 138 ± 60 nM for the CaMKII-NMDAR binding (Strack and Colbran, 1998), and the assumed volume of 0.01 fL for PSD (assumption 1).

Table 4-3
Ranges of the parameter for MCMC

Parameter	*Low*	*High*
k_{2f}	$0.00625\ s^{-1}$	$0.075\ s^{-1}$
k_{2b}	$0.01\ s^{-1}$	$0.3\ s^{-1}$
K_{m3}	0	0.5
K_{m4}	0	0.1
k_{3f}	$0.001\ \#^{-1}s^{-1}$	$0.02\ \#^{-1}s^{-1}$
k_{3ba}	$0.001\ s^{-1}$	$0.5\ s^{-1}$
k_{3bb}	$0.001\ s^{-1}$	$0.1\ s^{-1}$
k_4	$0.001\ s^{-1}$	$0.02\ s^{-1}$

The molecular numbers of the CaMKII holoenzyme and CaMKII subunit are set to 100 and 1200, respectively (Ribrault et al., 2011). The molecular number of NMDAR is set to 20 (Ribrault et al., 2011; Sheng and Hoogenraad, 2007). The concentration of CaM in hippocampus is 17 μM (Kakiuchi et al., 1982), which is equivalent to 1000 molecules per synapse. Since there are a large number of other CaM binding proteins in the synapse, the number of CaM dedicated to CaMKII is set to 500. The number of PP1 is fitted by MCMC within the range 0 to 200.

The values of the estimated parameters by MCMC and those obtained from the literature, and the constants used in the model are summarised in Table 4-4.

4.2.3 Computational implementation and experiments with MoHST

MoHST is solved using Matlab ode solver: ode15s and the following methods are used to set up meaningful computational experiments.

4.2.3.1 Time courses of CaMKII translocation

First, MoHST is run for long enough time under rest Ca^{2+} level until all variables reach their steady levels. Then, a strong Ca^{2+} is applied for 600s to induce a pulse of CaMKII into PSD. The Ca^{2+} application is set at a steady level of 20μM to induce the maximum CaMKII translocation and we assume that experimental data were measured under the maximum CaMKII translocation. During the translocation of CaMKII into PSD, the number of CaMKII in PSD (EiPSD + CaMKIIS + $CaMKII^*S$ + $CaMKII^*T$) is recorded and normalised based on Eq. (4.47). After that, Ca^{2+} is fixed to the rest level. As a result, CaMKII is dissociated from PSD. (Again, the number of CaMKII in PSD during the dissociation is recorded and normalised based on Eq. (4.47)). As shown in Fig. 4-4, the simulated time courses of CaMKII translocation based on the model values are similar to the normalised experimental data obtained by Shen and Meyer (1999).

4.2.3.2 Formation of CaMKII-NMDAR complex following a tetanus

First, the model is run for long enough time under rest Ca^{2+} level until all variables reach their steady levels. Then, a Ca^{2+} signal following a tetanus stimulation is applied and the time of the application is marked as t = 0. The duration of the signal is dependent on the number of pulses carried by the tetanus and the frequency of which the pulses is applied. For example, 100 pulses at 1Hz, 10Hz and 100Hz take 100s, 10s and 1s, respectively. The simulation stops at 30 minutes after the disappearing of the Ca^{2+} signal, the number of CaMKII-NMDAR complex ($CaMKII^*T$) is recorded.

Table 4-4

Parameters and constants: their biological meaning, values and sources

Parameter	***Biological Meaning***	***Value***	***Source***
k_{1f}	*Binding rate of Ca_4CaM and iCaMKII*	$0.035\#^{-1}s^{-1}$	[1]
k_{1b}	*Dissociation rate of CaMCaMKII into Ca_4CaM and iCaMKII*	$0.14s^{-1}$	[1]
k_{2f}	*Translocation rate of EoPSD into PSD*	$0.0088s^{-1}$	MCMC estimated
k_{2b}	*Dissociation rate of EiPSD out of PSD*	$0.247s^{-1}$	MCMC estimated
k_{3f}	*Binding rate of elementary CaMKII to NMDAR at the S site*	$0.008\#^{-1}s^{-1}$	MCMC estimated
k_{3ba}	*Dissociation rate of CaMKIIS into EiPSD and NMDAR*	$0.38\ s^{-1}$	MCMC estimated
k_{3bb}	*Dissociation rate of CaMKII*S into EiPSD and NMDAR*	$0.024\ s^{-1}$	MCMC estimated
k_4	*Transfer rate of NMDAR binding from S site to T site*	$0.01\ s^{-1}$	MCMC estimated
k_5	*Turnover rate of CaMKII*	$1/108000\ s^{-1}$	[2]
k_{6f}	*Binding rate of Ca^{2+} and CaM to form CaCaM*	$0.0415\ \#^{-1}s^{-1}$	[1]
k_{6b}	*Dissociation rate of CaCaM into Ca^{2+} and CaM*	$50\ s^{-1}$	[1]
k_{7f}	*Binding rate of Ca^{2+} and CaCaM to form Ca_2CaM*	$1.45\ \#^{-1}s^{-1}$	[1]
k_{7b}	*Dissociation rate of Ca_2CaM into Ca^{2+} and CaCaM*	$50\ s^{-1}$	[1]
k_{8f}	*Binding rate of Ca^{2+} and CaCaM to form Ca_3CaM*	$0.2\ \#^{-1}s^{-1}$	[1]
k_{8b}	*Dissociation rate of Ca_3CaM into Ca^{2+} and Ca_2CaM*	$1250\ s^{-1}$	[1]
k_{9f}	*Binding rate of Ca^{2+} and CaCaM to form Ca_4CaM*	$4.15\ \#^{-1}s^{-1}$	[1]
k_{9b}	*Dissociation rate of Ca_4CaM into Ca^{2+} and Ca_3CaM*	$1250\ s^{-1}$	[1]
K_{cat1}	*Autophosphorylation rate of CaMCaMKII into CaMCaMKII**	$0.9s^{-1}$	[1]
K_{cat2}	*Dephosphorylation rate of CaMCaMKII* by PP1*	$1.72s^{-1}$	[1]
K_{m1}	*Michaelis constant of the autophosphorylation*	1150#	[1]
K_{m2}	*Michaelis constant of the dephosphorylation by PP1*	660#	[1]
K_{m3}	*Fraction of active CaMKII subunits at half maximal translocation rate*	0.39	MCMC estimated
K_{m4}	*Fraction of autophosphorylated CaMKII subunits at half maximal dissociation rate*	0.019	MCMC estimated
Constant	***Biological Meaning***	***Value (#)***	***Source***
$CaMKII_{Total}$	*Total number of CaMKII subunits*	*1200*	[3]
CaM_{Total}	*Total number of CaM molecule*	*500*	MCMC estimated
$NMDAR_{Total}$	*Total number of NMDAR (or NR2B)*	*20*	[3],[4]
ATP	*Total number of ATP*	*240000*	[5]
PP1	*Total number of PP1*	*145*	MCMC estimated

[1] Chiba et al., (2008); [2] Ehlers, (2003); [3] Ribrault et al., (2011);

[4] Sheng and Hoogenraad, (2007); [5] Coultrap et al., (2012)

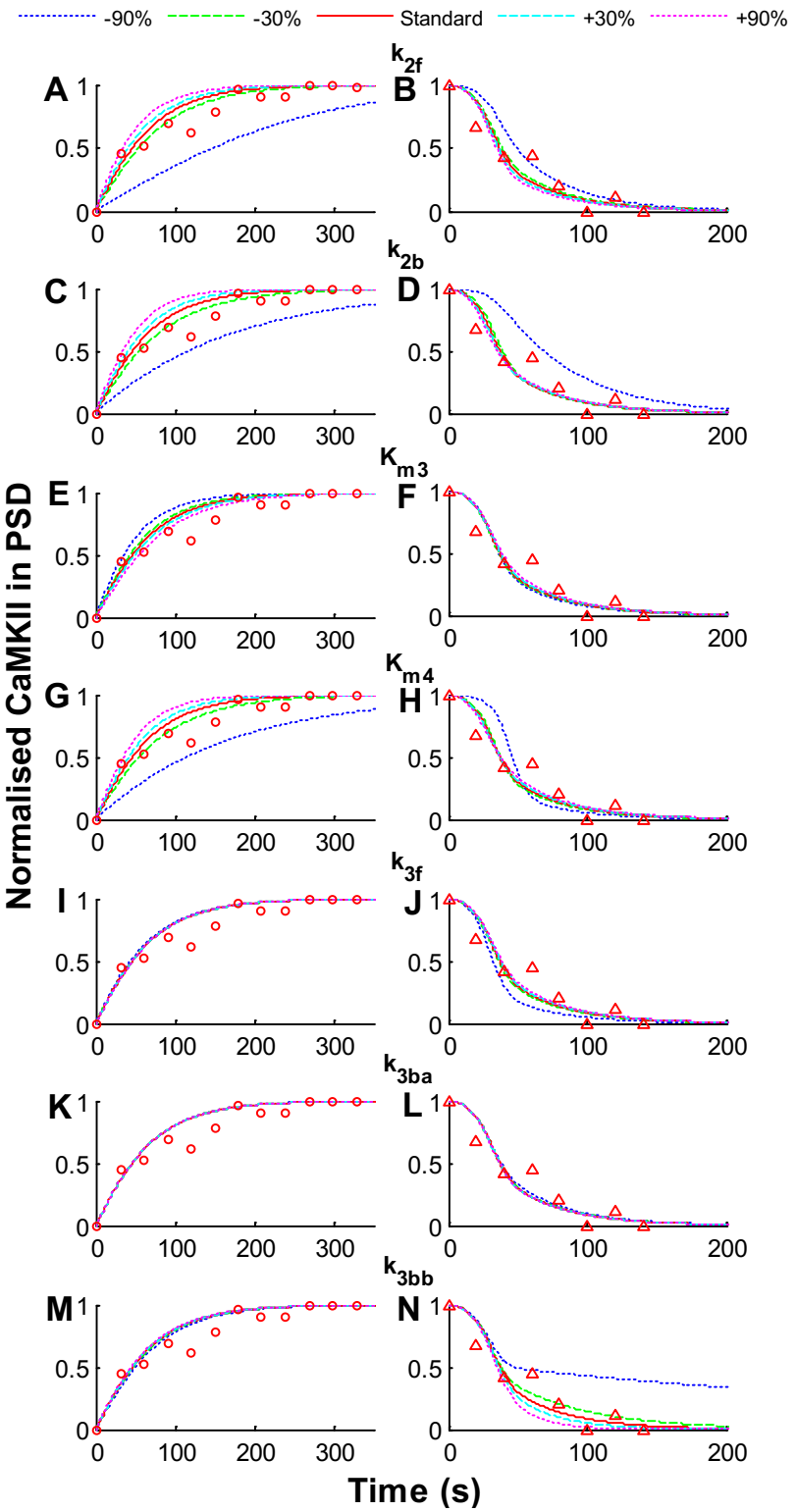

Figure 4-4 Parameter sensitivity related to CaMKII translocation. The figures in the left hand side (A, C, E, G, I, K and M) show the changes in time courses of the CaMKII translocation into PSD and figures in the right hand side (B, D, F, H, J, L and N) show the changes in time course of the CaMKII dissociation from PSD. The red solid lines are based on standard values of the parameters used by the model. The dashed and dotted lines are 30% and 90% perturbations from the standard value, respectively. Circles and triangles are the corresponding time courses retrieved from the experiments (Shen and Meyer, 1999).

4.3 Parameter perturbation

We analyse the variation in model output with respect to perturbation of eight parameters (k_{2f}, k_{2b}, K_{m3}, K_{m4}, k_{3f}, k_4, k_{3ba}, and k_{3bb}), all of which are related to the HSTs. The analysis is based on local sensitivity analysis (LSA) and partial rank correlation coefficient (PRCC) (Marino et al., 2008). Two model outputs are selected: (1) CaMKII translocation (LSA only), and (2) the formation of CaMKII-NMDAR complex (both LSA and PRCC).

4.3.1 Methods of parameter perturbation

4.3.1.1 LSA

In LSA, we vary one parameter at a time, from 10% to 190% of its standard value, and the other parameters are kept at their standard values. The results of LSA are shown in Fig. 4-4 (the CaMKII translocation) and Fig. 4-5 (the formation of CaMKII-NMDAR complex).

We calculate the variation of CaMKII-NMDAR complex formation with respect to the perturbation of the *j*th parameter (j=1 to 8), V_j, by Eq. (4.48) (Ling et al., 2010):

$$V_j = \left| \frac{\left(C_j^{130\%} - C^{\text{Standard}}\right) / C^{\text{Standard}}}{\left(P_j^{130\%} - P_j^{\text{Standard}}\right) / P_j^{\text{Standard}}} \right|, \tag{4.48}$$

where P_j^{Standard} is the value of parameter *j* under the standard condition and C^{Standard} is the number of CaMKII-NMDAR complex formed under the standard condition. $P_j^{130\%}$ is the value of parameter *j* with 30% increase from its standard value and $C_j^{130\%}$ is the corresponding number of CaMKII-NMDAR complex formed. The eight parameters are ranked based on their V_j from the highest to the lowest (Fig. 4-6).

4.3.1.2 PRCC

We randomly generate 1000 sets of the eight parameters with a predefined range (50% to 150% of the standard value) using Latin hypercube sampling (LHS) (McKay et al.,

1979), which gives simultaneously varied and evenly distributed and minimally correlated sets of parameters. We run the model for each of the 1000 sets of parameters as inputs and other parameters are kept at the standard values. We record the number of CaMKII-NMDAR complex formed for each set of parameters. At the end, we calculate $PRCC_j$ (j = 1 to 8), the absolute value of PRCC (see Appendix E.2 for the details) between the number of CaMKII-NMDAR complex formed and parameter j, as well as the corresponding p-value to reject the null hypothesis stating that no relationship exists between parameter j and the number of CaMKII-NMDAR formed. The eight parameters are ranked based on their $PRCC_j$ from the highest to the lowest (Fig. 4-6).

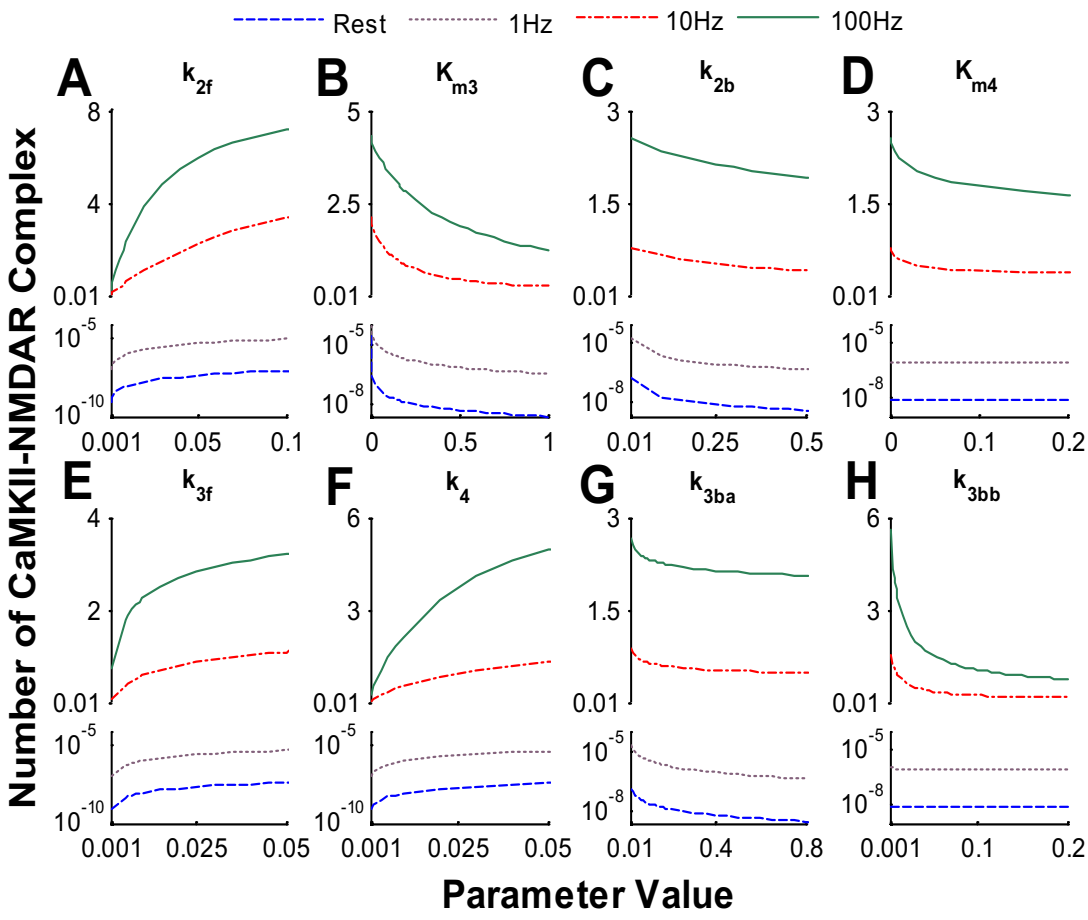

Figure 4-5 Parameter sensitivity related to CaMKII-NMDAR complex formation in the wild type CaMKII. Four patterns of Ca^{2+} inputs (rest, 1Hz, 10Hz and 100Hz) are tested for each parameter selected. The parameters are perturbed from 10% to 190% of its standard value and the results shown are the number of CaMKII-NMDAR complex at the end of the simulation (30 minutes after the end of the Ca^{2+} elevation). The lower panels are in the log scale and the upper panels are in the decimal scale. The parameters selected are: (**A**) k_{2f}, (**B**) K_{m3}, (**C**) $k2_b$, (**D**) K_{m4}, (**E**) k_{3f}, (**F**) k_4, (**G**) k_{3ba} and (**H**) k_{3bb}.

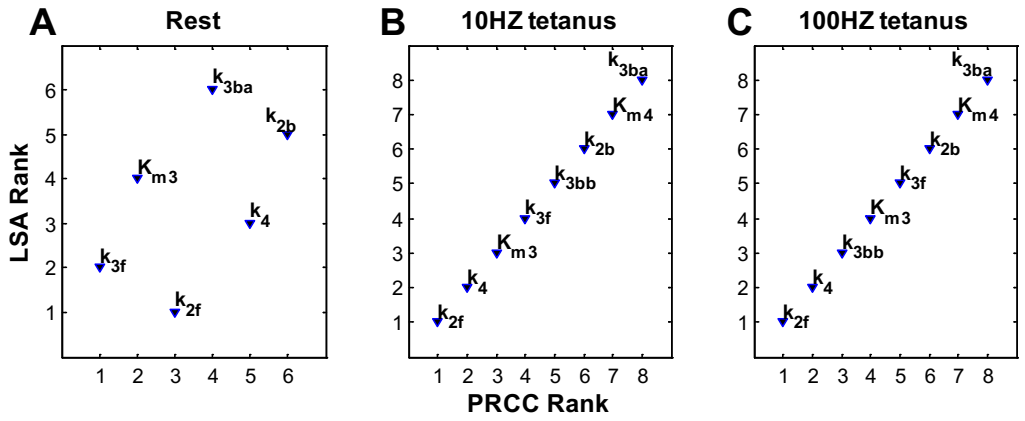

Figure 4-6 Parameter sensitivity rank. The sensitivity of eight parameters (k_{2f}, k_{2b}, K_{m3}, K_{m4}, k_{3f}, k_4, k_{3ba}, k_{3bb}) to the variation in the formation of CaMKII-NMDAR complex are ranked by LSA and PRCC as discussed in Section 4.8 (lower rank denotes higher sensitivity). The insensitive parameters based on the p-value from PRCC (0.05 significant level) are removed from the ranking.

4.3.2 Factors related to the formation of CaMKII-NMDAR complex

First of all, we test the potential frequency dependence of CaMKII-NMDAR complex formation since LTP is strongly correlated to the frequency of the induction signal (Kandel, 2009; Mayford et al., 2012). MoHST is simulated with four patterns of Ca^{2+} inputs: (1) rest level (70 nM), (2) tetanus contains 100 pulses at 1Hz (peak at 0.4μM), (3) tetanus contains 100 pulses at 10Hz (peak at 2.5μM) and (4) tetanus contains 100 pulses at 100Hz (peak at 20μM). (Giese et al. (1998) used these patterns of Ca^{2+} inputs in their experiments. However the peaks of Ca^{2+} inputs are not given by the experiments; the peaks are from simulations by the theoretical framework given in Appendix G). At each pattern, the parameters related to the HSTs are perturbed to understand their effects on the binding (Fig. 4-5).

Under the rest and 1Hz tetanus, there are no signs of the formation of CaMKII-NMDAR complex for any parameter regions (Fig. 4-5). Meanwhile, the high rates of change of CaMKII-NMDAR complex in response to 10Hz and 100Hz tetanus are shown within certain parameter regions in each case and more importantly, the levels of the CaMKII-NMDAR complex display significant differences between 10Hz and 100Hz tetanus. These results are consistent with the experimental observations (Giese et al., 1998).

Then, we rank the parameters related to the HSTs (Fig. 4-6) by both LSA and PRCC. The most sensitive parameters with respect to the formation of CaMKII-NMDAR complex are related to the CaMKII translocation (k_{2f} and K_{m3}) and the CaMKII binding (k_{3f} and k_4) in all three cases (1Hz is not shown). Interestingly, the parameters related to the autophosphorylation (k_{3bb} and K_{m4}) are insensitive at rest, but are very sensitive at both 10Hz and 100Hz tetanus. The behaviours suggest the important roles the autophosphorylation play during the transient signals which induce LTP.

4.4 Discussion and summary

We develop a theoretical model of the formation of CaMKII-NMDAR complex which has the following novel contributions in comparison to the previously published studies :

(1) the conformations of CaMKII subunits are expressed as ratios of the total number of CaMKII subunits, and the compositions of CaMKII are formulated by binomial distribution based on these ratios; (2) the probability of the binding between CaMKII and NMDAR is dynamically changing with respect to the STs of CaMKII; (3) the time courses of the CaMKII translocation predicted by using the parameters are in good agreement with the experimental data; and (4) the model is able to clearly distinguish the levels of the formation of CaMKII-NMDAR complex in response to the frequencies of the stimulation.

MoHST provides insights into the formation of CaMKII-NMDAR complex which is regulated not only by the binding affinity between CaMKII and NMDAR as expected, but also by the rate of the CaMKII translocation into PSD (Fig. 4-6). This result is important because the rate of the CaMKII translocation is different between its isoforms where CaMKIIα subunit translocates much faster than CaMKIIβ subunit (Shen and Meyer, 1999; Shen et al., 1998). The ratio between the levels of α and β isoforms of CaMKII is actively regulated in hippocampal neurons and may be important for LTP (Shen et al., 1998; Thiagarajan et al., 2002).

The parameter perturbation suggests the important roles of the autophosphorylation play in the formation of CaMKII-NMDAR complex during the transient signal. One possible explanation is that the translocation of CaMKII into PSD takes a relatively long time (Fig. 4-4), therefore, transient signals which induce LTP would only give a very small amount of the CaMKII translocation. As a result, the decrease of the dissociation of CaMKII from PSD by the autophosphorylation (Shen and Meyer, 1999; Shen et al., 1998) may be crucial to prolong the interaction between CaMKII and NMDAR during the transient signals. However, the level of the autophosphorylation is low at rest (data not shown), therefore more specific details of the autophosphorylation induced dynamics of CaMKII is needed and is discussed in Chapter 5.

There are some limitations: (1) MoHST does not include inhibitory autophosphorylation on residues threonine 305/306 of CaMKII subunit. The inhibitory autophosphorylation is shown to have a role in the CaMKII dissociation and LTP

(Elgersma et al., 2002; Goh and Manahan-Vaughan, 2014; Shen et al., 2000); (2) MoHST does not test other mechanisms of the CaMKII-NMDAR binding: NR2B contains two CaMKII binding sites, one is the autophosphorylation dependent and the other is not (Bayer et al., 2001). However, the S site mediated T site binding does not have the specific dependence on the autophosphorylation, so it is likely to have another mechanism of CaMKII-NMDAR binding which is specific to the autophosphorylation; (3) other CaMKII binding partners in PSD are not considered: these temporary anchoring of CaMKII in PSD may influence the CaMKII translocation into PSD (Robison et al., 2005); (4) the inhibitors targeting CaMKII-NMDAR binding (Scozzari et al., 2012; Vest et al., 2007) are not considered: these inhibitors should increase the threshold for initiating formation of CaMKII-NMDAR complex leading to tight regulation of LTP; and (5) the switching between CaMKII autoinhibited compact and autoinhibited extended is not considered; however, the switching might be an important factor studying the CaMKII isoform related dynamics in regulating the formation of CaMKII-NMDAR complex.

Chapter 5: Implication of the Autophosphorylation in LTP

Disparate experimental evidence exists on the significance of the autophosphorylation for the formation of CaMKII-NMDAR complex and the induction of E-LTP. Some studies state that the formation of CaMKII-NMDAR complex does not require the autophosphorylation (Barcomb et al., 2013; Bayer et al., 2006, 2001): T286A mutant (Bayer et al., 2006), which lacks the autophosphorylation, and the autophosphorylation repressors (Barcomb et al., 2013) do not block the formation of CaMKII-NMDAR complex, although the strength of CaMKII and NMDAR binding decreases. On the other hand, a set of studies shows that the autophosphorylation is required for LTP and spatial memory formation (Giese et al., 1998; Irvine et al., 2006), especially during E-LTP (Buard et al., 2010). Furthermore, a study reports that the autophosphorylation is irreversible in PSD (Mullasseril et al., 2007). The irreversibility of the autophosphorylation in PSD may have a critical role in LTP. Overall, it is unclear about the roles that the autophosphorylation plays in the formation of CaMKII-NMDAR complex as well as the linkage to the induction of E-LTP.

A better understanding of the autophosphorylation can be obtained by comparing the dynamic behaviours of the system between T286A mutant and the wild type studies (Bayer et al., 2006; Giese et al., 1998; Lee et al., 2009). T286A mutant CaMKII is obtained by replacing the threonine residue at position 286 (T286 site) with an alanine residue (Fong et al., 1989). As a result, the T286 site is no longer allowing the attaching of the phosphate group and thus the subunit lacks the autophosphorylation. We analyse MoHST to gain insights into the roles that the autophosphorylation plays in the formation of CaMKII-NMDAR complex as well as the linkage to the induction of E-LTP. We study the difference in CaMKII dynamics, specifically the CaMKII translocation time course and the formation of CaMKII-NMDAR complex, between the wide type and the T286A mutant CaMKII.

MoHST predicts well the alteration on the CaMKII translocation by T286A mutant in comparison to the experimental observation. In addition, the model predicts the formation of CaMKII-NMDAR complex under T286A mutant well: in particular, the model predicts that T286A mutant is not able to distinguish the frequency of tetanus; this prediction is consistent with the experimental observation. With regard to the autophosphorylation, the model shows that (1) the autophosphorylation amplifies the postsynaptic responses in reaction to the stimulation signals; (2) the autophosphorylation decodes the frequency of the stimulation to trigger appropriate postsynaptic response as reported frequently by previous modelling studies of CaMKII (Dosemeci and Albers, 1996; Kubota and Bower, 2001); and (3) the autophosphorylation can couple multiple trains of tetanus that are separated by relatively long inter-train intervals.

This chapter contains four sections: Section 5.1 briefly introduces the setup of computational experiments; Section 5.2 analyses the role of the autophosphorylation related to CaMKII translocation; Section 5.3 analyses the role of the autophosphorylation related to the formation of CaMKII-NMDAR complex; and Section 5.4 gives a brief discussion/summary.

5.1 Computational experiments

We set up two sets of computational experiments as described in Section 4.2.3 and in each set, we simulated twice, one by the wild type CaMKII and one by T286A mutant, with exactly the same pattern of Ca^{2+} input. The computational T286A mutant study is performed by fixing ATP level at 0 since ATP is the essential requirement for the autophosphorylation. We compare the CaMKII dynamics between the wild type and T286A mutant in terms of: (1) the CaMKII translocation, and (2) the formation of CaMKII-Complex. We then comment on the difference to understand its biological meaning.

5.2 Role of the autophosphorylation related to CaMKII translocation

MoHST predicts well the alteration on the CaMKII translocation by T286A mutant in comparison to the experimental observation. As shown in Fig. 5-1A, the time course of the CaMKII translocation into PSD agrees well with the wild type data (no T286A mutant data found); the simulated time courses of the CaMKII dissociation from PSD have reasonable agreements to both the wild type and T286A mutant data (Shen and Meyer, 1999; Shen et al., 2000). The wild type CaMKII takes about 1 min to have complete CaM dissociation from CaMKII subunit (Fig. 5-1B) which is consistent with the experimentally reported time duration (data not shown; see Fig. 2 in Lee et al., (2009)). The simulated T286A mutant dissociation agrees well with the experimental results as well (Fig. 5-1C).

The autophosphorylation delays the CaMKII inactivation and the dissociation of CaMKII from PSD as observed in experiments (Lee et al., 2009; Shen and Meyer, 1999; Shen et al., 2000). As a result, the peak translocation of T286A mutant into PSD is much smaller (Fig. 5-1A inset) and the translocation of T286A mutant into PSD takes less time to reach the peak (Fig. 5-1A). Moreover, the T286A mutant dissociates much faster from PSD (Fig. 5-1C) that may be a consequence from the faster CaM dissociation from CaMKII subunits (Fig. 5-1B).

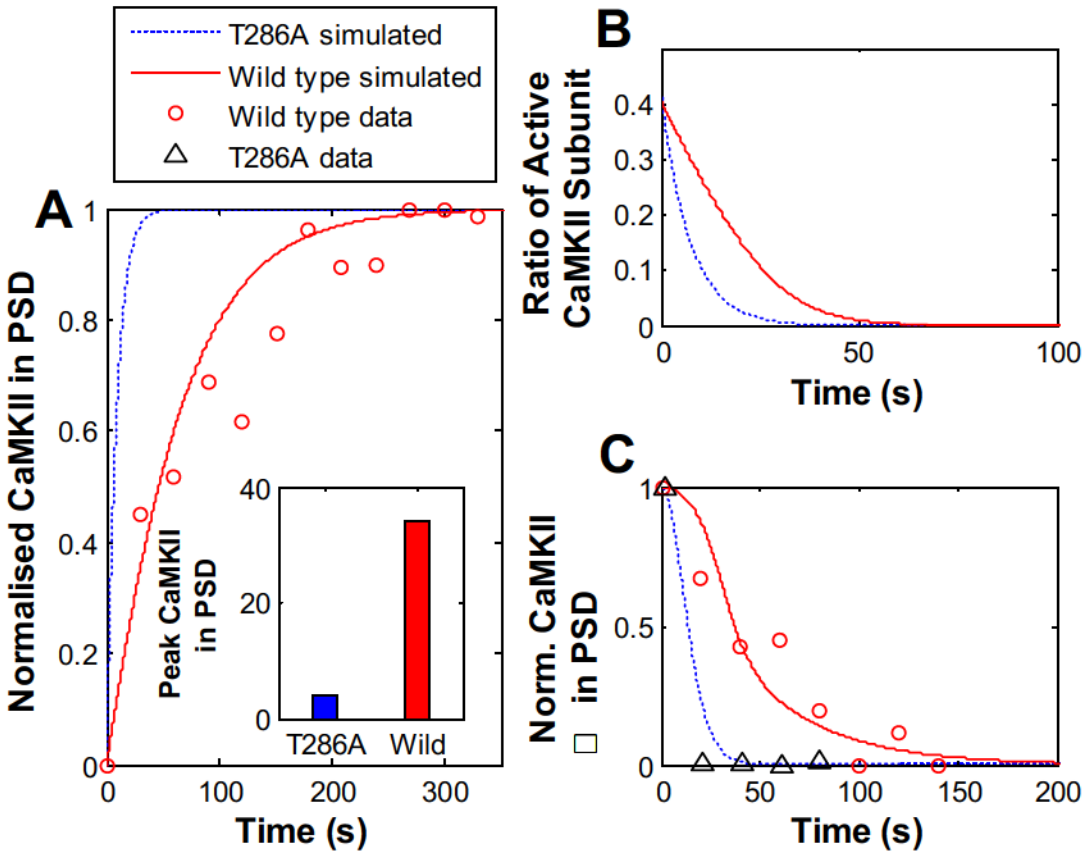

Figure 5-1 The autophosphorylation in CaMKII translocation into PSD. (**A**) Time course of the CaMKII translocation into PSD. Inset: peak number of CaMKII in PSD. (**B**) Time course of the CaM dissociation from CaMKII. The level of CaM-bound (active) subunits is shown as a ratio against the total number of CaMKII subunits. (**C**) Time course of the CaMKII dissociation from PSD. Circles and triangles are corresponding time courses of CaMKII translocation into PSD and dissociation from PSD for the wild type and T286A mutant CaMKII, respectively, from the experiments (Shen and Meyer, 1999).

5.3 Role of the autophosphorylation related to the formation of CaMKII-NMDAR complex

5.3.1 Frequency dependence

T286A mutant impairs the frequency dependence of the formation of CaMKII-NMDAR complex. As shown in Fig. 5-2, T286A mutant shows a much lower capability in discriminating 10Hz and 100Hz tetanus. Testing the 1000 sets of parameters generated, T286A mutant only reaches 1% to 10% of the capability of the wild type (Fig. 5-2I) which implies very weak ability of T286A mutant to discriminate between the two frequencies. This weakness of T286A mutant in discriminating 10Hz and 100Hz tetanus captured by the model is very similar to the experimental observations of the impairment in LTP by T286A mutant (Fig. 2C in Giese et al., (1998)).

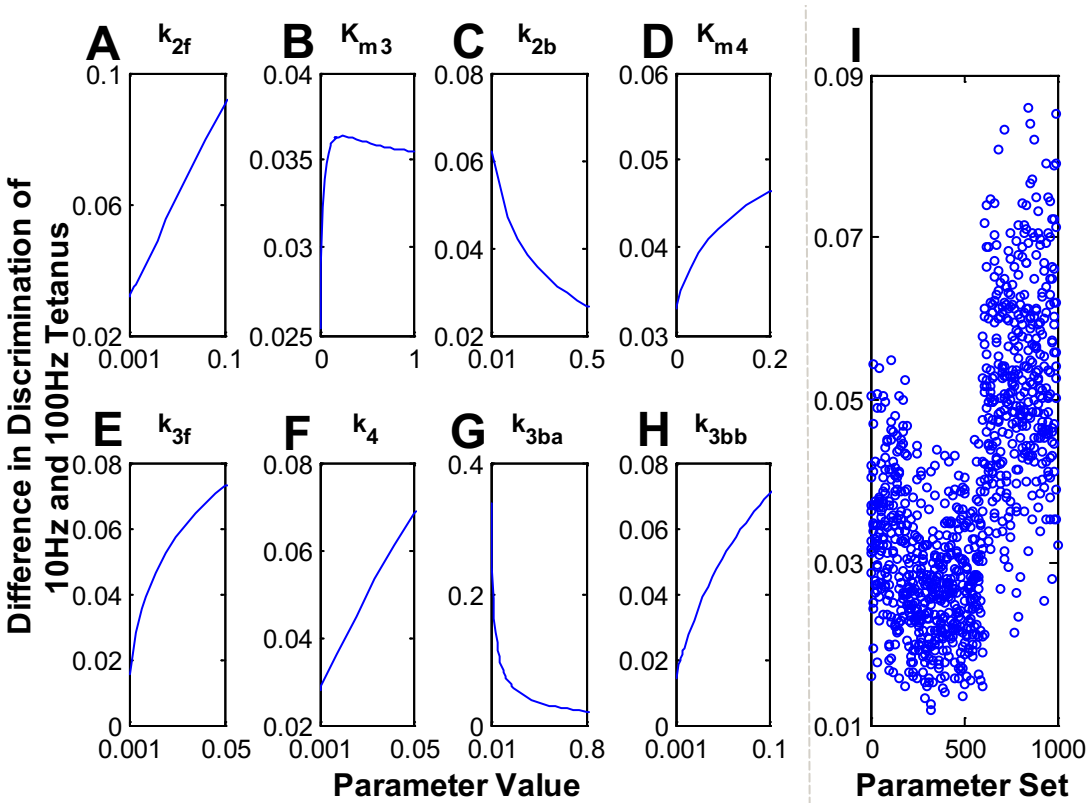

Figure 5-2 Comparison of the capabilities in discrimination of 10HZ and 100Hz tetanus between T286A mutant and the wild type CaMKII. We compare between T286A mutant and the wild type CaMKII for the difference in the 10Hz and 100Hz induced formation of CaMKII-NMDAR complex. The results are presented as a quotient of dividing the difference for the T286A mutant by the difference for the wild type. We perturb parameters to search for the entire possible space of the quotient based on: (**1**) LSA (**A- H**); and (**2**) LHS (**I**).

5.3.2 The autophosphorylation in response to a single tetanus

The maximum numbers of active CaMKII subunits in response to the single tetanus are similar between T286A mutant and the wild type CaMKII, but the wild type delays CaMKII inactivation as expected (Fig. 5-3A). When this delay of CaMKII inactivation affects the formation of CaMKII-NMDAR complex downstream, a significant difference in the model behaviour is observed between T286A mutant and the wild type CaMKII (Fig. 5-3B). First, less T286A mutant is translocated into PSD in response to the tetanus. The peak of the CaMKII translocation is 7 in the wild type compared to 4 in T286A mutant. As a result, the time to reach the peak translocation is shorter for T286A mutant. Secondly, T286A mutant dissociates much faster and lastly, the formation of CaMKII-NMDAR complex is decreased for T286A mutant. The overall patterns of the CaMKII dynamics as well as the phase shift between T286A mutant and the wild type (Fig. 5-3B inset) are very similar to the experimental observation (Fig. 2B in Bayer et al., (2006)). As a conclusion, the autophosphorylation amplifies the postsynaptic response (formation of CaMKII-NMDAR complex in this case) to a single tetanus.

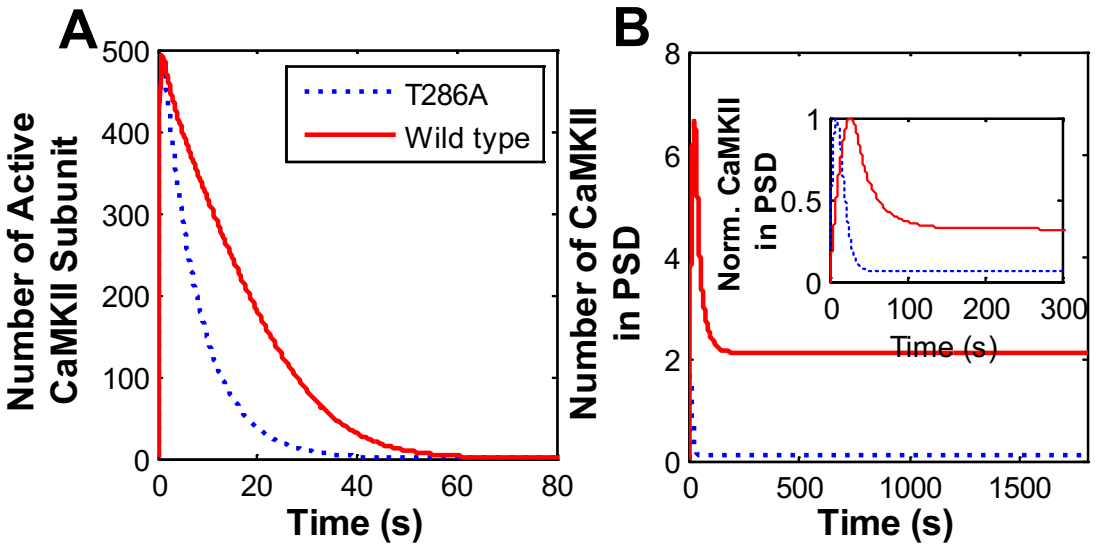

Figure 5-3 Dynamics triggered by the autophosphorylation in response to a single tetanus. A single tetanus of 100 pulses at 100Hz is applied at t=0s. The model is simulated for 30 minutes under two types of CaMKII: T286A mutant and the wild type. (**A**) The number of active CaMKII subunits over the first 100s. (**B**) The CaMKII translocation and the formation of CaMKII-NMDAR complex over the 30 minutes simulation. Inset: normalised CaMKII in PSD over the first 300s of the simulation.

5.3.3 The autophosphorylation in response to multiple trains of tetanus

Multiple trains of tetanus sequentially activate the wild type CaMKII (Fig. 5-4A); the translocation of CaMKII into PSD is enhanced significantly (Fig. 5-4B). Moreover, the formation of CaMKII-NMDAR complex increases with the increased number of tetanus applied, but reaches a plateau because of the limited number of NMDAR in PSD (Fig. 5-4C). In T286A mutant, the CaMKII translocation and the CaMKII-NMDAR complex formation are much lower than those of the wild type (Figs. 5-4B and 5-4C). Quantitatively, the number of CaMKII-NMDAR complex formed after 20 trains of tetanus for T286A mutant is smaller than those formed after a single train of tetanus for the wild type (Fig. 5-4C).

The inter-train interval between the successive tetanus is another important factor that affects LTP. The approximate inter-train intervals required to obtain sustained formation of CaMKII-NMDAR complex (Fig. 5-4D), predicted by the model, are greater than 10s for T286 and 20s for wild type. (There are no experimental evidence to verify these values but the general protocol to experimentally induce E-LTP requires an inter-train interval within 10-20s (Bhalla, 2013).)

The autophosphorylation may improve the response-coupling among multiple trains. As shown in Fig. 5-4D, a range of inter-train intervals exists where the formation of CaMKII-NMDAR complex is larger than that of completely separated trains; within this range, a train enhances the CaMKII-NMDAR complex formed by the following train. This range is wider in the wild type CaMKII (66s, from 22s to 88s) compared to T286A mutant (32s, from 10s to 42s).

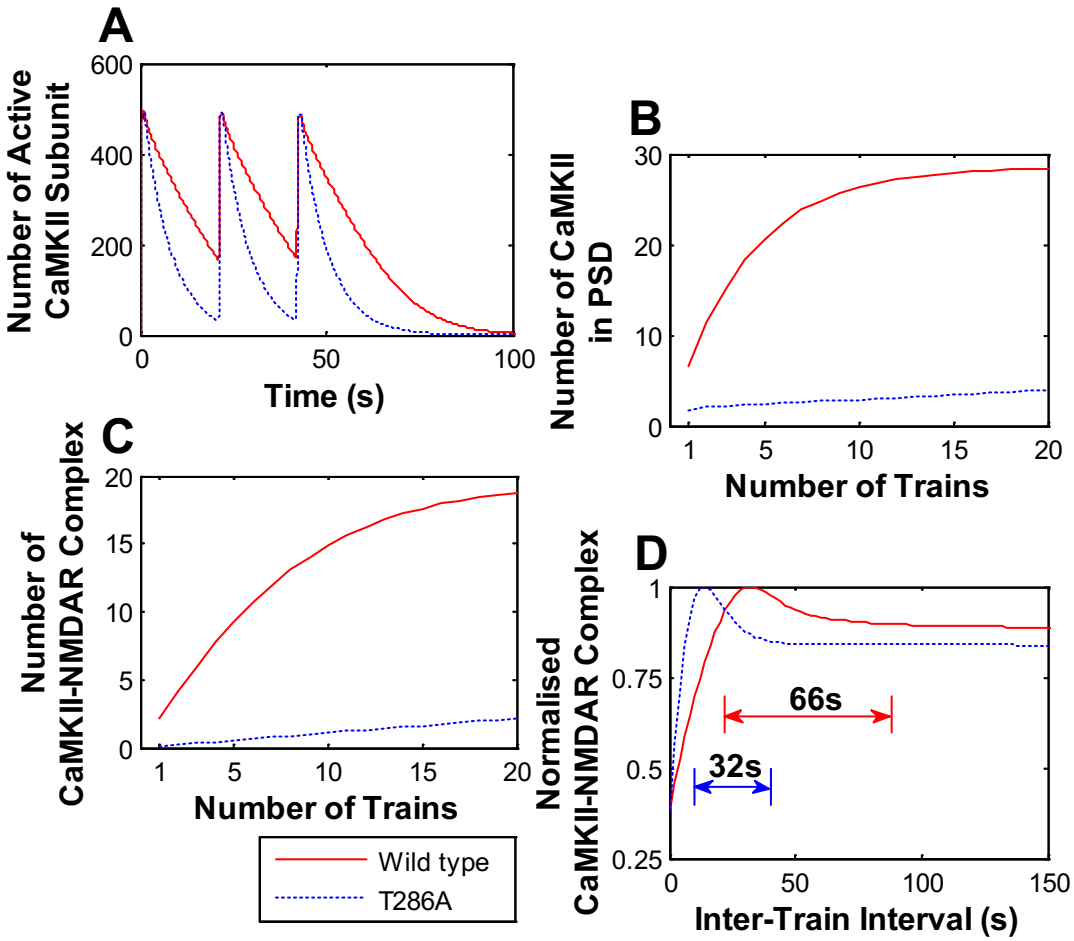

Figure 5-4 Dynamics triggered by the autophosphorylation in response to multiple trains of tetanus. (**A**) Number of active CaMKII subunits over the simulation of 100s in response to 3 trains of tetanus. 3 trains of tetanus are applied at t = 0s with an inter-train interval of 20s. Each tetanus lasts for 1s and contains 100 pulses at 100Hz. (**B**) The peak translocation of CaMKII in response to different number of tetanus in succession. (**C**) The formation of CaMKII-NMDAR complex in response to different numbers of tetanus in succession. The number of CaMKII-NMDAR complex presented is measured at the end of the simulation (simulation continues for 30min after the signal is disappeared). (**D**) Normalised number of CaMKII-NMDAR complex in response to 3 trains of tetanus with different inter-train intervals. The number of CaMKII-NMDAR complex presented is recorded at the end of the simulation (simulation continues for 30min after the signal is disappeared) and normalised by the maximum CaMKII-NMDAR complex formed among the different inter-train intervals. Arrows show the range of inter-train intervals in which the formation of CaMKII-NMDAR complex is greater than that of 3 completely separated trains (CaMKII-NMDAR complex formed in response to 3 completely separated trains is recorded at inter-train interval of 150s. A 1% up-adjustment is added to the record to balance the CaMKII turnover for the additional signal duration).

5.4 Discussion and summary

In this chapter, we analyse MoHST to bring insights into the roles of the autophosphorylation play in the formation of CaMKII-NMDAR complex as well as the linkage to the induction of E-LTP. We select the CaMKII translocation and the formation of CaMKII-NMDAR complex as the model outputs and compare their behaviours between the wild type and T286A mutant CaMKII.

MoHST predicts well the alteration on the CaMKII translocation by T286A mutant in comparison to the experimental observation (Fig. 5-1). In addition, the model predicts the formation of CaMKII-NMDAR complex under T286A mutant well: in particular, the model predicts that T286A mutant is not able to distinguish the frequency of tetanus: this prediction is consistent with the experimental observation. (Fig. 5-2 and Fig. 2C in Giese et al., (1998)). The impairment may be a consequence of the faster dissociation of T286A mutant CaMKII from PSD (Fig. 5-1C), so that the much shorter duration in PSD is insufficient to bind to NMDAR to from CaMKII-NMDAR complex during the transient 10Hz and 100Hz tetanus.

With regard to the autophosphorylation, MoHST shows that (1) the autophosphorylation amplifies the postsynaptic responses in reaction to the stimulation signals; (2) the autophosphorylation decodes the frequency of the stimulation to trigger appropriate postsynaptic response as reported frequently by previous modelling studies of CaMKII (Dosemeci and Albers, 1996; Kubota and Bower, 2001); and (3) the autophosphorylation can couple multiple trains of tetanus that are separated by relatively long inter-train intervals. Furthermore, Mullasseril et al. (2007) reports that the autophosphorylation is irreversible in PSD. This irreversibility implies that the autophosphorylated CaMKII can persist and remain active in PSD for a much longer period that extends the range of the inter-train interval in coupling the trains of tetanus. This observation links the autophosphorylation to repetitive learning where a learning activity is repeated for several times with a relative long time separated between successive repeats. Because repetitive learning is a common protocol in triggering

memory formation, the autophosphorylation may have a role in coupling the successive leaning activities to form memories. To support this argument, according to Giese et al. (1998), mice with T286A mutant CaMKII have an impairment in forming the spatial memory in searching the hidden platform (see Fig.4 in Giese et al. (1998)).

Chapter 6: Conclusion and Future Directions

This study advances our knowledge of synaptic plasticity by using mathematical models and computational methods to understand the complex behaviour of synaptic plasticity, which may be difficult for an unbiased human mind to comprehend. The system level understanding of the emergence of synaptic plasticity is essential to provide insights for the biochemical basis of memory formation. We develop two mathematical models (MoNP and MoHST) depending on the detail level of the synaptic system required to answer the specific research questions asked. The simulated results at different levels, one at the level of the protein interacting networks of the complete pathway while the other at the level of the state transition of one important protein, successfully provide new insights into the dynamic behaviour of synaptic plasticity. In this section, we summarise our major achievements and the associated contributions, and outline future directions following this study.

6.1 Summary of the study

The first objective is to develop a simplified model of the protein interacting networks of the NMDAR-mediated pathway of synaptic plasticity (MoNP) (Chapter 3). The purposes of MoNP are: (1) to understand the essential modulators required in the emergence of synaptic plasticity; (2) to understand the factors of the bidirectional behaviour of synaptic plasticity; and (3) to advance our knowledge in the relationship between synaptic plasticity and memory formation.

We select the essential modulators of synaptic plasticity based on the latest experimental finding. We first develop sub-models of the activations of the modulators. The key criteria of the development is to maintain the essential features of the modulators as discussed in Section 2.3 and specific assumptions are made to simplify

the unrelated interactions. Moreover, we collect the experimentally estimated kinetic parameters to be used in the sub-models and estimate unknown parameters based on the experimental data found from the literature. At the end, the integration of these sub-models gives us a simplified model of the NMDAR-mediated pathway of synaptic plasticity.

We use MoNP to understand the effective timescales of the modulators and to predict factors of the bidirectional behaviour of synaptic plasticity. We analyse both the steady state and the transient Ca^{2+} signal induced temporal patterns of MoNP that reveal two processes which behave bi-directionally with respect to the Ca^{2+} level. The competition for the CaM binding between LTP and LTD related proteins (CaM competition) shows a U-shape behaviour in the steady state having the Ca^{2+} level as the control parameter. The shape of the switch is sensitive to the rate of the autophosphorylation and the concentration of CaM. The temporal pattern of CaM competition shows a slight decrease in response to LFS, while a short, but strong increase during HFS and TBS. The coupling between trains of TBS can be modulated through the autophosphorylation. Meanwhile, the phosphorylation on I1, which formulates a competition between PP2b and PKA (phosphorylation competition) only shows bidirectional behaviours in response to temporal pattern of Ca^{2+} signal indicating the requirement of the designated signal for this process. PP2b strongly dephosphorylates I1 during the signal because the moderate activation of PKA, but PKA rephosphorylates I1 after the disappearing of the signal due to the slow deactivation of PKA. At the end, the modified MoNP confirms that PP2b-depndent removal of PKA prevents the rephosphorylation.

The second objective is to develop a theoretical model of state transitions of CaMKII (MoHST), which is critical in the emergence of LTP (Chapter 4). The purposes of this model are: (1) to model the holoenzyme state transition of CaMKII; (2) to formulate a mathematical framework for the binding between CaMKII and NMDAR; (3) to understand the relationship between the autophosphorylation, formation of CaMKII-NMDAR complex, and LTP.

MoHST is developed based on two critical HSTs of CaMKII: the translocation between PSD and dendritic spine and the binding to NMDAR to form CaMKII-NMDAR complex. The composition of CaMKII holoenzyme is formulated by binomial distribution based on ratios of CaMKII subunit conformations. The binding to NMDAR is formulated based on a probabilistic framework with the binding rates modified by the composition of CaMKII holoenzyme and the binding probability. The time courses of the CaMKII translocation predicted are in good agreement to the experimental data. Moreover, the model is able to clearly distinguish the frequencies of the Ca^{2+} signal through the levels of the formation of CaMKII-NMDAR complex.

We analyse the sensitivity of parameters related to HSTs by two method: (1) LSA, and (2) PRCC. The results show that the formation of CaMKII-NMDAR complex is not only controlled by the binding rates to NMDAR but also the translocation rate of CaMKII holoenzyme. Furthermore, the parameters related to the autophosphorylation show strong sensitivity under transient signals. Since the rates of the autophosphorylation and the translocation are different among CaMKII isoforms, CaMKII-NMDAR binding may be regulated in an isoform specific manner.

At the end, we use MoHST to understand the role of the autophosphorylation in the formation of CaMKII-NMDAR complex by comparing the wild type and the autophosphorylation impaired mutation, T286A (Chapter 5). MoHST predicts well the impairment of T286A mutant from the wild type and the predictions are consistent with the experimental observation. Deeper into the dynamics of the autophosphorylation, MoHST predicts that (1) the autophosphorylation amplifies the postsynaptic responses in reaction to the stimulation signals; (2) the autophosphorylation decodes the frequency of the stimulation to trigger appropriate postsynaptic response; and (3) the autophosphorylation can couple multiple trains of tetanus that are separated by relatively long inter-train intervals.

6.2 Contributions

The major contributions of the study are:

- Developed a simplified model of NMDAR-mediated pathway of synaptic plasticity (MoNP) which integrates: (1) the essential features of modulators and the pathway; (2) the latest experimentally estimated kinetic parameters of the modulators; and (3) the latest finding of the biochemical interactions among the modulators.
- Advanced our understanding of the protein interacting networks involved in the emergence of synaptic plasticity through analysing the behaviour of MoNP in steady state and the associated temporal pattern in response to transient Ca^{2+} signals. The analysis reveals the effective timescales of modulators that is important to understand the roles of modulators as well as the dynamical interactions among them in the emergence of synaptic plasticity leading to a hypothesised model of memory system.
- Predicted the major factors of the bidirectional behaviour of synaptic plasticity by comparing behaviours of MoNP with variations in parameters.
- Tested the implication of the PP2b-dependent removal of PKA by comparing the dynamics of rephosphorylation by PKA between MoNP and modified MoNP which includes the removal.
- Developed a theoretical model of the holoenzyme state transition of CaMKII (MoHST). Comparing to previous computational studies, MoHST includes the holoenzyme level state transitions, including the translocation between PSD and dendritic spine and the binding to NMDAR.
- Revealed the factors for the formation of CaMKII-NMDAR complex using parameter sensitivity analysis methods. The factors are the translocation rate into PSD and the binding rate to NMDAR. Moreover, the autophosphorylation of CaMKII is shown to be critical for the formation during transient signals.

- Advanced our understanding of the implication of the autophosphorylation in the formation of CaMKII-NMDAR complex as well as LTP by comparing the behaviour of MoHST between the wild type and T286A mutation. We highlighted the ability of the autophosphorylation in coupling multiple trains of tetanus.

6.3 Future directions

We propose several directions to extend this study for future works:

General

- A consistent conclusion drawn from both MoNP and MoHST is the significance of the CaMKII isoform specific regulation of synaptic plasticity. However, neither MoNP nor MoHST include the necessary information regarding CaMKII isoforms. Therefore, it is important to accommodate the differences in CaMKII isoforms as well as the regulation of the ratio between CaMKII isoforms in future studies.
- Both MoNP and MoHST are analysed based on deterministic approaches. However, the low copy number of proteins in the synapse induces stochastic effects resulting undesirable levels of some species in the system. Therefore, the application of stochastic approaches to MoNP and MoHST are necessary to understand the implications of stochastic effects onto the dynamic behaviour of synaptic plasticity. The understanding of the most sensitive factors to noise and their implication to the dynamic behaviour of synaptic plasticity may provide insights into the possible role of stochastic effects in memory formation.
- To understand the alteration on AMPAR trafficking associated with synaptic plasticity, a new model of AMPAR trafficking is required. The new model should include: (1) the complete pathway of AMPAR recycling between PSD and cytoplasmic pool; and (2) the critical phosphorylation sites of AMPAR and the associated mechanisms of the alterations on the AMPAR trafficking. The

new model can be used to gain insights into the critical sites of AMPAR involved in LTP and LTD, respectively.

- We only analysed the sensitivity of parameters related to HSTs of MoHST. In order to gain an overall understanding of the critical processes in the systems of MoNP and MoHST, comprehensive parameter sensitivity analyses are required to all the parameters of MoNP and MoHST.

MoNP

- In Section 2.4.3.2, we point out that the spatial movement and targeting of synaptic proteins are essential elements of synaptic plasticity. However, in the development of MoNP, we ignore these elements to simplify MoNP. To increase the accuracy of the prediction of MoNP, the spatial movement and co-localisation need to be considered. For example, PKA is removed much faster by AKAP anchored PP2b (Sanderson et al., 2012), and PP1 may not dephosphorylate PSD CaMKII (Mullasseril et al., 2007). With the spatial information considered, the emphasis shifts to the local dynamics of modulators instead of the global dynamics of MoNP.

MoHST

- As listed in the limitation, MoHST needs to include the inhibitory autophosphorylation on T305/306, the CaMKII binding partners other than NR2B and the possible CaMKII inhibitor specific to the NR2B binding, such as CaMKIIN. These processes may have significant impacts on the formation of CaMKII-NMDAR complex.
- It is proposed that the binding between CaMKII β isoform and F-actin may have a critical role in the structural switch of dendritic spine in the L- LTP (Okamoto et al., 2009). The number of F-actin determines the postsynaptic protein binding capacity and the binding to CaMKII helps stabilising F-actin in the synapse. In MoHST, the binding between CaMKII and F-actin is interpreted as a regulator for the translocation and formulated by Hill equations. To test the hypothesis of

the involvement of CaMKII and F-actin in the structural switch, MoHST can be modified to include the binding between CaMKII and F-actin. Then, we can test the new model for conditions on which the hypothesis stands and validate the conditions against the real situation.

6.4 Conclusion

The biochemical basis of memory formation may be correlated with the mechanisms underlying synaptic plasticity, which are now emerging. However, understanding the complex behaviour of synaptic plasticity is very challenging; the complexity couples too much biological details that may be difficult to comprehend. Mathematical models and computational methods bring the potential to explore, understand and interpret the detailed biological information that allow our research to penetrate through the complexity and understand the principles of synaptic plasticity. In this thesis, we have demonstrated the development of two mathematical models and the ways of using the models to understand the complex behaviour of synaptic plasticity at different detail levels. For instance, we use MoNP to investigate the dynamic protein interactions in the emergence of synaptic plasticity and to propose the main factors of the bidirectional behaviour of synaptic plasticity; we then use MoHST to investigate the state transition of CaMKII in the induction of LTP, particularly to understand the relationship among the autophosphorylation, the formation of CaMKII-NMDAR complex and LTP. Importantly, although the models are developed at different levels of detail, the understanding regarding the same process is consistent indicating the reliable role that mathematical models and computational methods play in revealing the complexity of a biological system.

Appendices

Appendix A: Synaptic Transmission

Synaptic transmission is a neurotransmitter driven process (Fig. A-1). The process involves a few sequential steps, including neurotransmitter synthesis; neurotransmitters release into the synaptic cleft; binding between neurotransmitters and postsynaptic ligand-gated receptors, as well as induction of postsynaptic response; and clearance of neurotransmitters out of synaptic cleft.

Among the different types of neurotransmitters, amino acids and amines are involved in the fast synaptic transmission. Both amino acids and amines are released from synaptic vesicles. Moreover, both of them are synthesised in the axon terminal by their synthesizing enzymes and are taken up shortly after the synthesis into the synaptic vesicle (Südhof, 2004). However, amino acids, as the elementary blocks of proteins, are abundant in all cells; while amines are only synthesised by the neuron which releases them.

Action potential triggers the neurotransmitter release through depolarising the presynaptic membrane. Action potential can be generated in many ways: by sensory nerves in response to environmental stimuli or by inter-neurons in response to the synaptic transmission from their presynaptic neurons. Action potential depolarises the presynaptic membrane at the active zone, where many voltage-gated Ca^{2+} channels lie (Südhof, 2004). The depolarisation opens these Ca^{2+} channels and triggers Ca^{2+} influx to increase the intracellular Ca^{2+} level. The increased intracellular Ca^{2} level further triggers the neurotransmitter release (de Jong and Verhage, 2009).

The neurotransmitter release occurs rapidly through exocytosis, which fuses the synaptic vesicle membrane with the presynaptic membrane and releases its contents, neurotransmitters, into the synaptic cleft. The release is triggered by a vesicle protein called synaptotagmin 1, which senses Ca^{2+} and triggers the exocytosis (Stevens, 2004;

Südhof, 2004). After the release, the empty synaptic vesicle re-enters the axonal terminal.

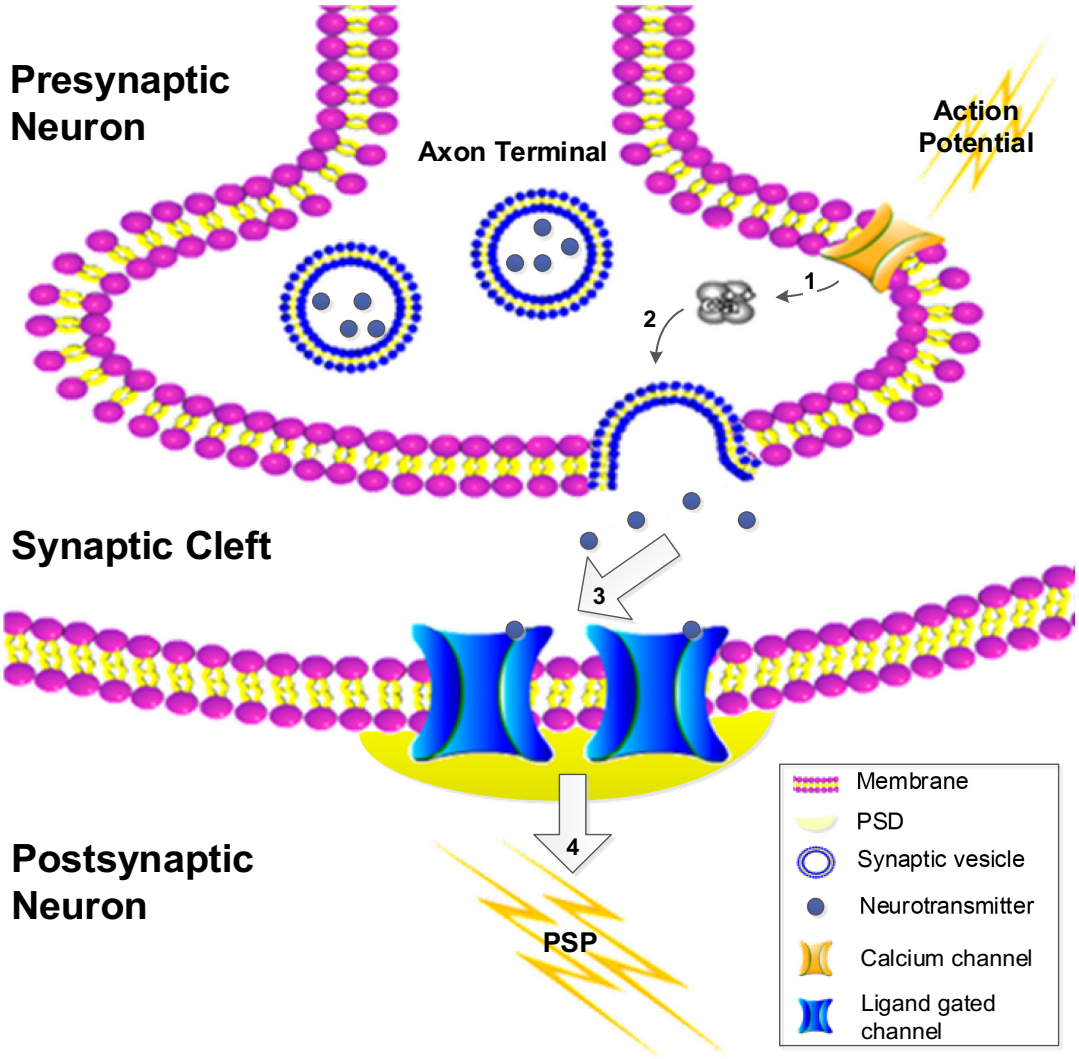

Figure A-1 Synaptic transmission. (1) Action potential depolarises the presynaptic membrane to open the calcium channel, which allows an influx of Ca^{2+} ions. **(2)** Ca^{2+} ions trigger the release of neurotransmitters into the synaptic cleft by exocytosis at the active zone. **(3)** The released neurotransmitters diffuse across the synaptic cleft and bind to ligand-gated receptors at PSD. The binding opens the embedded ion channels of the receptors. **(4)** The opening of the ligand-gated ion channels allows an influx of ions to induce a postsynaptic potential (PSP).

The released neurotransmitters bind to ligand-gated receptors in PSD and induce PSP. The ligand-gated receptor is composed of 4 or 5 subunits with an embedded ion channel. With a neurotransmitter bound, the subunits are twisted to expose the ion channel (Wollmuth and Sobolevsky, 2004). An ion influx through the exposed ion channel induces PSP as a result of the great ion gradient across the membrane. Depending on ion permeability of the ion channel, two types of PSP can be induced: (1) EPSP: the membrane of the postsynaptic neuron would be depolarised towards the threshold of generating an action potential if the channels are permeable to cations; and (2) inhibitory postsynaptic potential (IPSP): the membrane would be hyperpolarised away from the threshold of generating an action potential if the channels are permeable to anions. Large enough EPSP would cause a current to generate the action potential in spike-initiation zone, which usually locates in the axon hillock, of the postsynaptic cell.

The neurotransmitters in the synaptic cleft are cleared at the end of the transmission in order to prepare for the next transmission. There are two ways to remove the neurotransmitters out of the synaptic cleft: (1) presynaptic reuptake to transport the neurotransmitters back into the presynaptic terminal by the membrane transporter proteins in the presynaptic membrane. Once back into the presynaptic terminal, the neurotransmitters are either degraded or reloaded into the synaptic vesicle; and (2) enzymatic destruction in the synaptic cleft to inactivate or destroy the neurotransmitters. Once the neurotransmitters are cleared, one cycle of synaptic transmission is completed.

Appendix B: Mathematical Concepts

The model of a biological system is often constructed based on biochemical reactions among the proteins of the biological system, which facilitate the functionality of the biological system. These biochemical reactions are modelled through mathematical representations based on their reaction rates (or reaction velocities), which determine the change of the concentrations of the proteins of the biological system. The reaction rate depends both on the chemical nature and on the quantity of the participating reactants in the reaction mixture (Waage and Gulberg, 1986). These mathematical representations are rate laws describing the relationships between the reaction rate and the quantity of the participating reactants and are different among different types of reaction mechanisms. The rate laws express that the rate of the i^{th} reaction, V_i, is expressed as a function, f_i, in terms of the concentrations of the participating reactants, x_1~x_n, as given by Eq. (B1):

$$V_i = f_i\left(x_1, x_2 \ldots x_n\right). \tag{B1}$$

As specific to synaptic plasticity, three rate laws are usually applied: (1) mass action rate law (Waage and Gulberg, 1986); (2) Michaelis-Menten rate law (Michaelis and Menten, 1913); and (3) Hill rate law (Hill, 1910).

B.1 Mass action rate law

Mass action rate law describes the reaction rate of an elementary reaction, which involves a single mechanistic step/state transition to form the product. Mass action rate law generally states that the rate of a biochemical reaction is proportional to the quantity of the participating reactants (Waage and Gulberg, 1986). For a sample elementary reaction as shown in the following reaction scheme:

$$aA + \beta B \xrightarrow{k} \sigma S + \tau T\ , \tag{B2}$$

where A and B are the reactants, S and T are the products. α, β, σ and τ are the numbers of corresponding molecules involved in the reaction, and k is the reaction rate constant

indicating the pace of the reaction. The corresponding reaction rate (V) is given by Eq. (B3):

$$V = k[A]^{\alpha}[B]^{\beta}, \tag{B3}$$

where [A] is the concentration of A and [B] is the concentration of B ([x] denotes the concentration of substance x). The order of a reaction defines the relationship between the concentrations of substances in the reaction and the rate of the reaction. For the above reaction, α and β are the orders of reaction with respect to reactants A and B, respectively. The overall reaction order is $\alpha+\beta$. A first order reaction has an overall reaction order of 1 and a second order reaction has an overall reaction order of 2. The dynamic change of the concentrations of A, B, S and T is described by a set of ordinary differential equations (ODEs) in terms of V as given by Eqs. (B4 – B7):

$$\frac{d[A]}{dt} = -\alpha V, \tag{B4}$$

$$\frac{d[B]}{dt} = -\beta V, \tag{B5}$$

$$\frac{d[S]}{dt} = \sigma V, \text{ and} \tag{B6}$$

$$\frac{d[T]}{dt} = \tau V. \tag{B7}$$

As shown in Fig. B-1, the solution of Eqs. (B4 – B7) shows that [A], as the reactant, decreases and [S], as the product, increases over the first 5 seconds of the reaction. The result means A (and B) is consumed to produce S (and T). The slopes of the decrease and the increase depend on the rate constant, k. For faster reactions, the slopes are steeper.

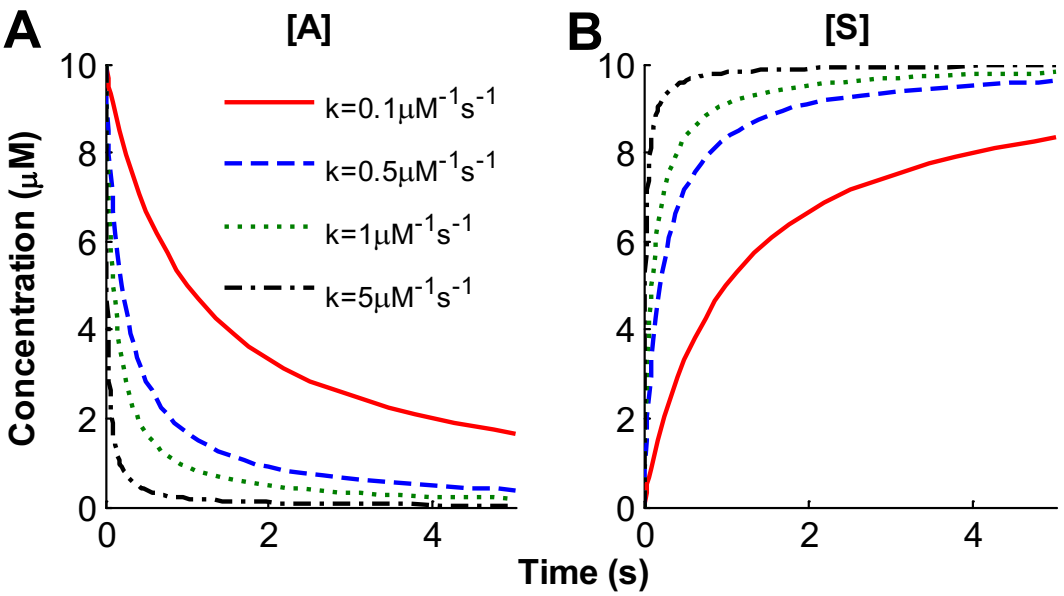

Figure B-1 The solution of reaction in Eq. (3.2) assuming it is a second order reaction. Based on the assumption, α, β, σ and τ are set to 1. The initial concentration for A, B, S and T are 10, 10, 0 and 0 μM, repsectively. The results of the first 5 seconds of the reaction are shown as: **(A)** $[A]$, and **(B)** $[S]$.

B.1.1 Factors for the final product of a elementary reaction cascade

Consider a sequential elementary reaction cascade shown in the following reaction scheme:

$$A \xrightarrow{k_1} B \xrightarrow{k_2} P. \tag{B8}$$

The reaction involves two first order reactions; one converts substance A into substance B (reaction 1 with rate constant k_1) and the other converts substance B into the final product P (reaction 2 with rate constant k_2). Therefore, the reaction rates for reaction 1 (V_1) and for reaction 2 (V_2), are given by Eqs. (B9 and B10)

$$V_1 = k_1[A], \text{ and} \tag{B9}$$

$$V_2 = k_2[B]. \tag{B10}$$

The ODEs for the dynamics of [A], [B] and [P] are given by Eqs. (B11 – B13):

$$\frac{d[A]}{dt} = -V_1, \tag{B11}$$

$$\frac{d[B]}{dt} = V_1 - V_2, \text{ and} \tag{B12}$$

$$\frac{d[P]}{dt} = V_2. \tag{B13}$$

To understand the factors regulating the production of P, we solve the ODEs with respect to different rate constants. The results (with the initial concentrations of A, B and P to be 10, 0, and 0 μM, respectively) are shown in Figs. B-2 and B-3. The red solid lines shows the slope of the growth of [P] with respect to time when the rates of the reactions are equal, and are used as the control for the further analysis. We fix k_1 and perturb k_2 for the first set of tests. As shown in Fig. B-2, there is insignificant impact on the slope of the growth of [P] from the control when k_2 is greater than k_1. However, significant impact on the slope of the growth of [P] from the control is observed when k_2 is smaller than k_1. Both observations are independent of k_1. The similar observations are obtained when we fix k_2 and perturb k_1. As shown in Fig B-3, a greater k_1 than k_2 has insignificant impact on the slope of the growth of [P], while a significant impact on

the slope of the growth of [P] is caused when k_1 is smaller than k_2. Both effects are independent of k_2. The observations indicate that the production of P is not dependent on a particular reaction, but limited by the slowest reaction along its upstream reaction cascade. Hence, the reaction in a slower timescale is dominating the cascade to produce the final product. Based on this property, a number of approximate descriptions of biochemical system are formulated, i.e. Michaelis-Menten rate law and Hill rate law.

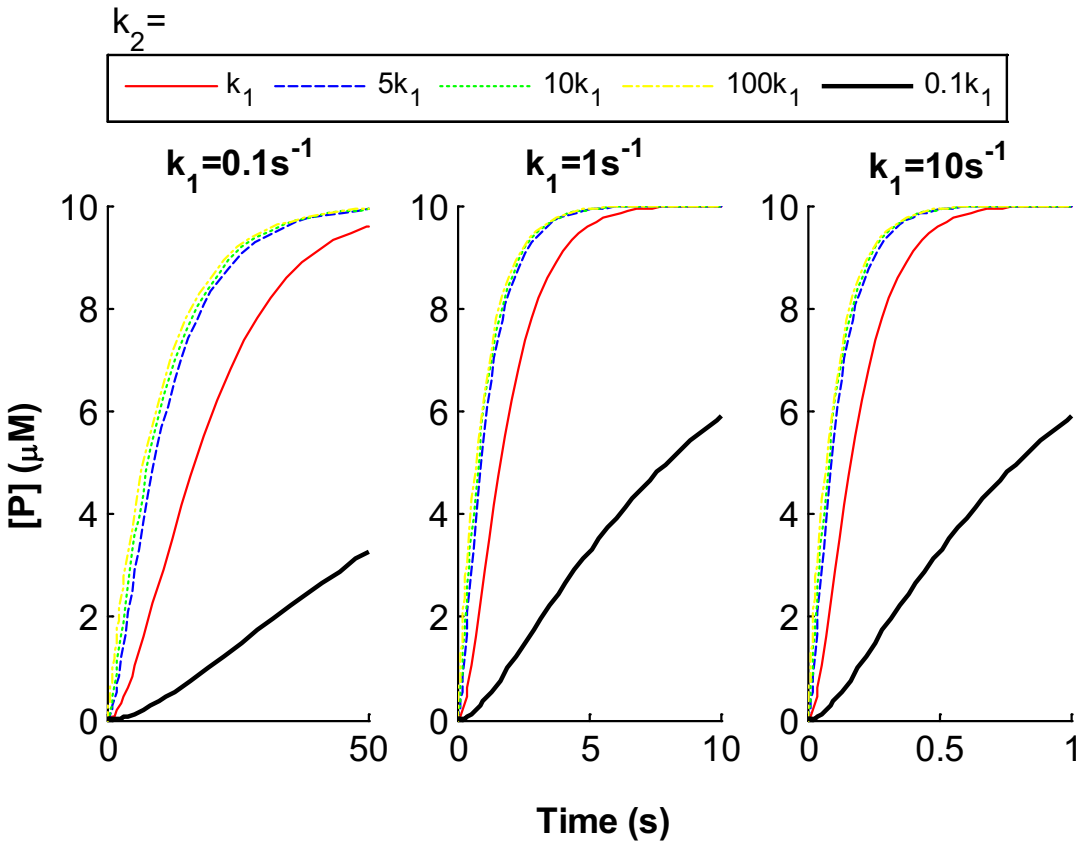

Figure B-2 The [*P*] growth with respect to different k_2. Three figures from left to right consider three cases of k_1 values: $0.1s^{-1}$, $1s^{-1}$ and $10s^{-1}$. In each case, 5 values of k_2 are tested: same as k_1; 5 times greater than k_1; 10 times greater than k_1; 100 times greater than k_1; and a tenth of k_1.

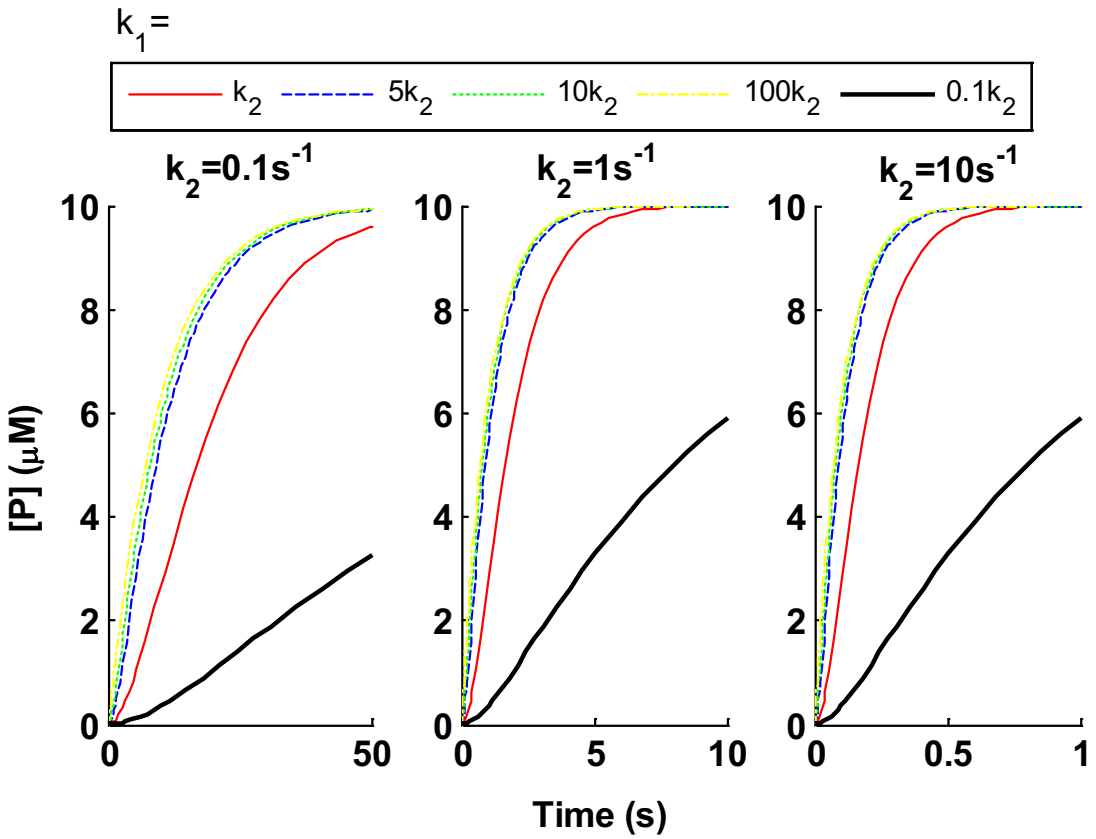

Figure B-3 The [*P*] growth with respect to different k_1. Three figures from left to right consider three cases of k_2 values: $0.1s^{-1}$, $1s^{-1}$ and $10s^{-1}$. In each case, 5 values of k_1 are tested: same as k_2; 5 times greater than k_2; 10 times greater than k_2; 100 times greater than k_2; and a tenth of k_2.

B.2 Michaelis-Menten rate law

Michaelis-Menten rate law provides an approximate description of enzyme-catalysed reactions (Michaelis and Menten, 1913) of the following reaction scheme:

$$S + E \underset{k_b}{\overset{k_f}{\rightleftarrows}} ES \xrightarrow{K_{cat}} P + E \quad , \tag{B14}$$

where S is the substrate, E is the enzyme, ES is the substrate-enzyme complex or intermediate complex, and P is the final product. The reaction involves: (1) a reversible reaction to mix S and E to form a complex, ES. The reaction rate constants are k_f for the forward reaction to form ES and k_b for the backward reaction to decompose ES into S and E; and (2) an irreversible reaction to convert ES into P and releasing E. The reaction rate constant is K_{cat} for the irreversible reaction. Hence, the ODEs of the dynamics of [S], [E], [ES], and [P] are given by Eqs. (B15 – B18) based on mass action rate law:

$$\frac{d[S]}{dt} = -k_f[S][E] + k_b[ES], \tag{B15}$$

$$\frac{d[E]}{dt} = -k_f[S][E] + (k_b + K_{cat})[ES], \tag{B16}$$

$$\frac{d[ES]}{dt} = k_f[S][E] - (k_b + K_{cat})[ES], \text{ and} \tag{B17}$$

$$\frac{d[P]}{dt} = K_{cat}[ES]. \tag{B18}$$

B.2.1 Equilibrium approximation

The original assumption taken by Michaelis and Menten to approximate the reaction rate of the production of P is that S, E and ES mix instantaneously to chemical equilibrium. i.e. $k_f[S][E] = k_b[ES]$. Therefore, [ES] is given by:

$$[ES] = {k_f}/{k_b}\,[S][E]. \tag{B19}$$

According to the mass conservation law: $[E] + [ES] = [E_T]$, where $[E_T]$ is the total concentration of the enzyme, Eq. (B19) can be modified to:

$$[ES] = \frac{1}{K_d}[S]([E_T] - [ES]), \tag{B20}$$

where $K_d = k_b / k_f$ is the dissociation constant of the ES formation. Rearrange Eq. (B20):

$$[ES] = \frac{[E_T][S]}{K_d + [S]}. \tag{B21}$$

Substituting equation (B21) into equation (B18), the reaction rate of the production of P, V, is given by Eq. (B22):

$$V = \frac{d[P]}{dt} = \frac{V_{\max}[S]}{K_d + [S]}, \tag{B22}$$

where $V_{max} = K_{cat}[E_T]$ is the maximum reaction rate when all the enzyme binds to the substrate (ES). When $[S] = K_d$, V is half of V_{max}.

The key of this approximation is that the reversible reaction is much faster than the irreversible reaction, i.e. $k_b \gg K_{cat}$, so that the irreversible reaction becomes the limiting factor of V.

B.2.2 Quasi-steady-state approximation

Briggs and Haldane (1925) approximate the reaction rate, V, by taking an assumption that there is no change in the concentration of the intermediate complex at all times, i.e. $k_f[S][E] = (k_b + K_{cat})[ES]$. Hence, $[ES]$ is given by:

$$[ES] = \frac{k_f}{k_b + K_{cat}}[S][E]. \tag{B23}$$

According to the mass conservation law, Eq. (B23) can be modified to:

$$[ES] = \frac{1}{K_m}[S]([E_T] - [ES]), \tag{B24}$$

where $K_m = \frac{k_b + K_{cat}}{k_f}$ is the Michaelis-Menten constant. Rearrange equation (B24):

$$[ES] = \frac{[E_T][S]}{K_m + [S]}. \tag{B25}$$

Substituting equation (B25) into equation (B18), V is:

$$V = \frac{d[P]}{dt} = \frac{V_{\max}[S]}{K_m + [S]}, \tag{B26}$$

Similar to equilibrium approximation, $V_{max} = K_{cat}[E_T]$ is the maximum reaction rate when all the enzyme is presented as complex with the substrate (ES). When $[S] = K_m$, V is half of V_{max}.

Eqs. (B22 and B26) are similar, but based on different constant, K_d and K_m, respectively. However, since $k_b \gg K_{cat}$ (assumption of the equilibrium approximation), so that $K_d \approx K_m$. Hence, the general behaviours of the two approximation are similar. As shown in Fig. B-4, there is a negligible difference between the two approximations.

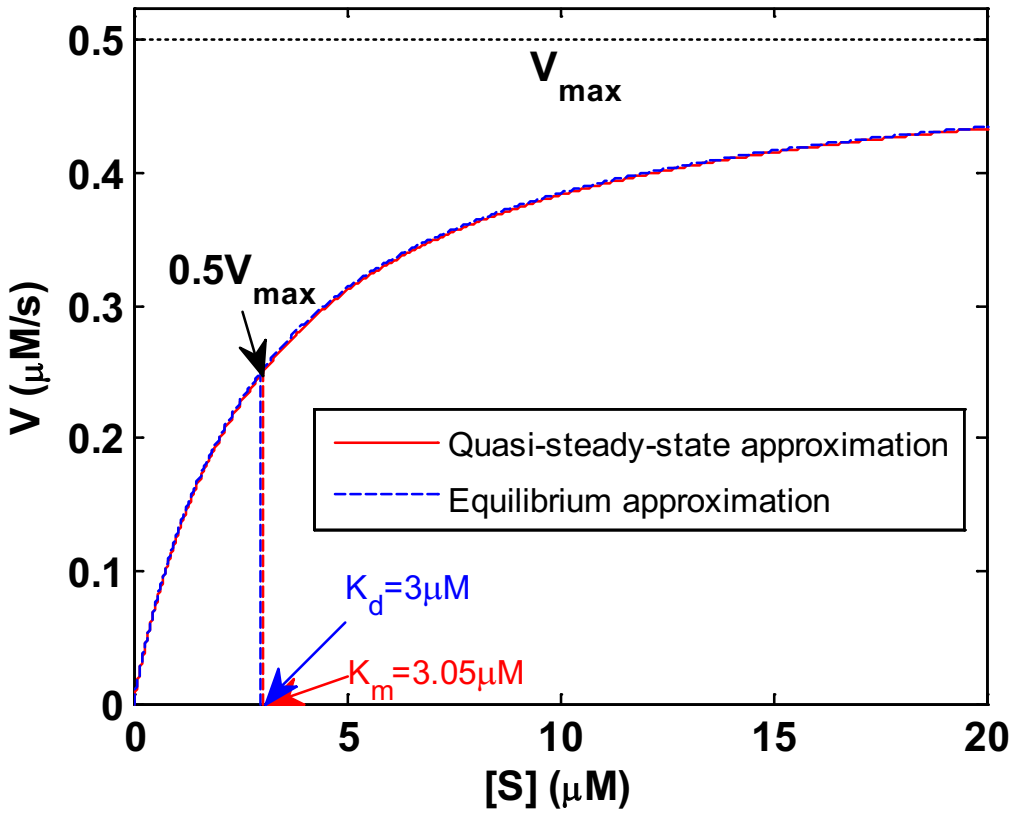

Figure B-4 The approxmiations of the reaction rate, V, of an enzyme-catalysed reaction by equilibrium approximation and quasi-steady-state approximation. The rate constants of the enzyme-catalysed reaction are, k_f = 2μM^{-1}s^{-1}, k_b = 6s^{-1} and K_{cat} = 0.1s^{-1}. [E_T] is 5μM. Hence, K_d = 3μM, K_m = 3.05μM, and V_{max} = 0.5μMs^{-1} .

B.3 Hill rate law

Hill rate law describes the cooperativity between two chemical species (Hill, 1910). The law is often applied to mathematically formulate the binding between ligands and receptors by expressing the fraction of the bound receptor as a function in terms of the ligand concentration (Weiss, 1997). Moreover, Hill rate law has shown advantage in describing the dependence between chemical substances and is extensively applied in modelling the cooperative activation and inhibition in complex biochemical systems. Consider the situation where a receptor contains two ligand binding sites and the binding between the receptor and ligands is shown as the following reaction scheme:

$$L + R \underset{k_{1b}}{\overset{k_{1f}}{\rightleftharpoons}} RL\,, \tag{B27}$$

$$RL + L \underset{k_{2b}}{\overset{k_{2f}}{\rightleftharpoons}} RL_2\,, \tag{B28}$$

where L is the ligand, R is the receptor, RL_n is the ligand-receptor complex occupying n binding sites. The ODEs of the dynamics of [*R*], [*L*], [*RL*] and [RL_2] are given by Eqs. (B29 – B32):

$$\frac{d[R]}{dt} = -k_{1f}[R][L] + k_{1b}[RL], \tag{B29}$$

$$\frac{d[L]}{dt} = -k_{1f}[R][L] + k_{1b}[RL] - k_{2f}[RL][L] + k_{2b}[RL_2], \tag{B30}$$

$$\frac{d[RL]}{dt} = k_{1f}[R][L] - k_{1b}[RL] - k_{2f}[RL][L] + k_{2b}[RL_2], \text{ and} \tag{B31}$$

$$\frac{d[RL_2]}{dt} = k_{2f}[RL][L] - k_{2b}[RL_2]. \tag{B32}$$

Now, if a final product, P, is produced at a rate proportional to [RL_2] (i.e. ions pass through open ion channels), and the reaction rate, *V*, is given by Eq. (B33):

$$V = \frac{d[P]}{dt} = k_3[RL_2]. \tag{B33}$$

To approximate *V*, we assume that the intermediate binding states (RL and RL_2) do not change on the timescale of *V* (quasi-steady-state approximation). Mathematically, this is given by Eqs. (B34 and B35):

$$k_{1f}[R][L]-k_{1b}[RL]=0\text{, and} \tag{B34}$$

$$k_{2f}[RL][L]-k_{2b}[RL_2]=0\text{.} \tag{B35}$$

Solving Eqs. (B34 and B35), we have:

$$[RL]=\frac{[L][R]}{K_1}\text{, and} \tag{B36}$$

$$[RL_2]=\frac{[L]^2[R]}{K_1K_2}\text{,} \tag{B37}$$

where $K_1=\frac{k_{1b}}{k_{1f}}$ and $K_2=\frac{k_{2b}}{k_{2f}}$. According to the mass conservation law, $[R] + [RL] + [RL_2] = [R_T]$, where $[R_T]$ is the total concentration of the receptor. Hence, the ratio of $[RL_2]$ to $[R_T]$ is given by Eq. (B38):

$$\begin{aligned}\frac{[RL_2]}{[R_T]}&=\frac{[RL_2]}{[R]+[RL]+[RL_2]}=\frac{[L]^2[R]}{K_1K_2\left([R]+\frac{[L][R]}{K_1}+\frac{[L]^2[R]}{K_1K_2}\right)},\\&=\frac{[L]^2}{K_1K_2+K_2[L]+[L]^2}.\end{aligned} \tag{B38}$$

Therefore, $[RL_2]$ is given as a function in terms of $[L]$ by Eq. (B39)

$$[RL_2]=\frac{[R_T][L]^2}{K_1K_2+K_2[L]+[L]^2}\text{.} \tag{B39}$$

If we assume that there is cooperativity between the bindings; the first binding is very slow, but once it is bound, the second binding is very fast, i.e. $k_{1f}\to 0$ and $k_{2f}\to\infty$. Therefore, $K_1\to\infty$, $K_2\to 0$, and K_1K_2 is a constant. Hence, Eq. (B39) is modified to:

$$[RL_2]=\frac{[R_T][L]^2}{{K_{0.5}}^2+[L]^2}\text{,} \tag{B40}$$

where $K_{0.5}^2=K_1K_2$. Therefore, V is given by Eq. (B41):

$$V=\frac{d[P]}{dt}=\frac{V_{\max}[L]^2}{{K_{0.5}}^2+[L]^2}\text{,} \tag{B41}$$

where $V_{max} = k_3[RT]$ is the maximum reaction rate occurred when all receptors are double-bound by ligands. Eq. (B41) is the general expression of Hill rate law. The law states that V is dependent on the concentration of the ligand. If $[L]$ is large ($[L] \gg K_{0.5}$), V approaches the maximum, V_{max}. If $[L] = K_{0.5}$, V is half of V_{max}. For a process involves n cooperative processes, Hill rate law becomes:

$$V = \frac{V_{\max}[L]^n}{K_{0.5}{}^n + [L]^n}, \tag{B42}$$

where n is called Hill coefficient indicating the degree of cooperativity. When n = 1, there is no cooperativity, and the equation is similar to Michaelis-Menten rate law.

An alternative form of Hill rate law describes the situation where V is inhibited by RL_n. That is, V decreases as $[RL_2]$ increases and is given by Eq. (B43):

$$V = V_{\max}\left(1 - \frac{[L]^n}{K_{0.5}{}^n + [L]^n}\right) = \frac{V_{\max}K_{0.5}{}^n}{K_{0.5}{}^n + [L]^n}. \tag{B43}$$

Here, V is maximum when $[L]$ is zero and deceases as $[L]$ increases. When $[L] = K_{0.5}$, V is half of V_{max}. As shown in Fig. B-5, the slope of V with respect to $[L]$ becomes steeper when the Hill coefficient increases. For n>1, V exhibits a switch like behaviour that is a good framework to describe the activation/inhibition of signalling pathway in cellular dynamics. For instance, Eq. (B42) is applied to describe the activation where a signalling pathway is turned on when the concentration of its controller protein passes the activating threshold, while Eq. (B43) is applied to describe the inhibition where a signalling pathway is turned off when the concentration of its controller protein passes the inhibiting threshold.

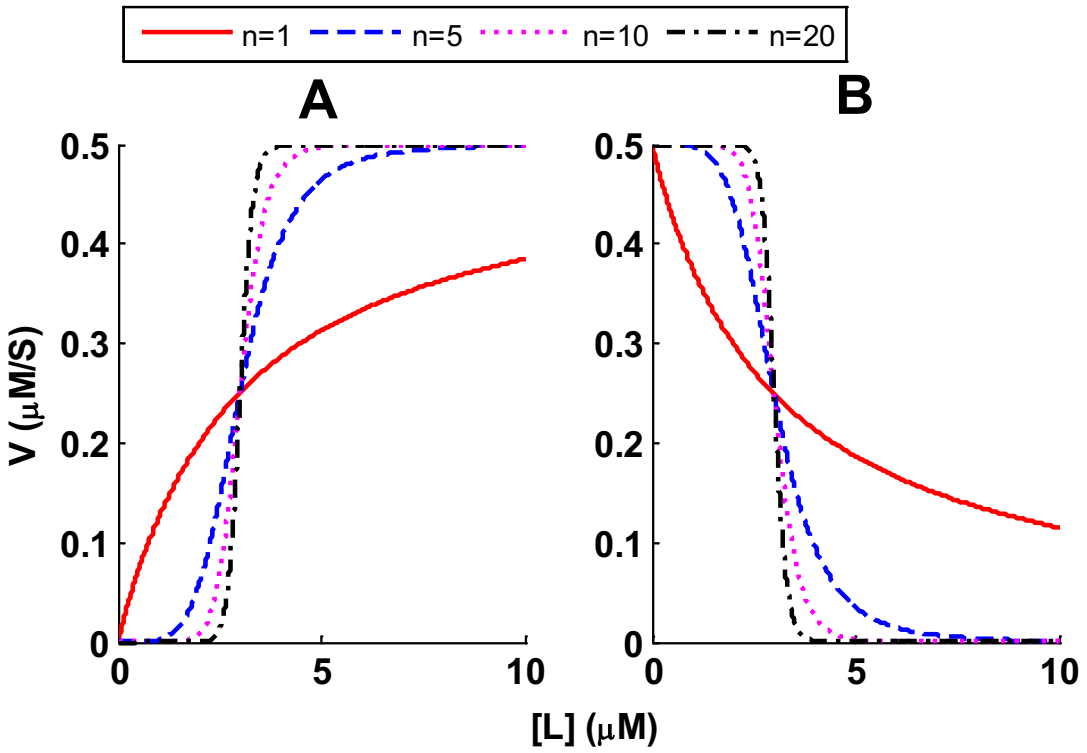

Figure B-5 The approxmiations of the reaction rate, V, by Hill rate law. The associated parameters are, $K_{0.5} = 3\mu M$ and $V_{\max} = 0.5\mu M s^{-1}$. Four values of Hill coefficients are tested: 1, 5, 10 and 20. The left figure shows the results of Hill rate law for the activation and the right figure show the result of Hill rate law for the inhibition.

Appendix C: Modelling Reaction Kinetics based on Molecular Numbers

Suppose a protein, x, is involved in three biological reactions within a compartment of volume, V. The three reactions include an irreversible first order reaction, an irreversible second order reaction to bind to another protein, y, and an enzymatic catalysis reaction by an enzyme, z. The first and second order reactions obey mass action kinetics and the enzymatic catalysis reaction is well characterised by Michaelis–Menten kinetics. Therefore, the time-dependent changes of the concentration of x, $[x]$, are determined by the following expression:

$$\frac{d[x]}{dt} = -k_1[x] - k_2[x][y] - \frac{K_{cat}[z][x]}{K_m + [x]}, \tag{C1}$$

where k_1 is reaction rate constant for the first order reaction, k_2 is the association rate constant between x and y, K_{cat} is the catalysis rate constant and K_m is the Michaelis constant. All these reactions kinetics are based on the corresponding concentrations of proteins: x, y and z.

Let $\#x$ be the molecular number of x, then:

$$\#x = [x] \cdot N_A \cdot V, \tag{C2}$$

where N_A is Avogadro constant with a value of 6.02214179×10^{23} mol^{-1}. Similarly, $\#y$ and $\#z$ are molecular numbers of y and z, respectively.

Hence, Eq. (C1) becomes:

$$\frac{d\left(\frac{\#x}{N_A V}\right)}{dt} = -k_1\left(\frac{\#x}{N_A V}\right) - k_2\left(\frac{\#x}{N_A V}\right)\left(\frac{\#y}{N_A V}\right) - \frac{K_{cat}\left(\frac{\#z}{N_A V}\right)\left(\frac{\#x}{N_A V}\right)}{K_m + \left(\frac{\#x}{N_A V}\right)}. \tag{C3}$$

Multiplying both sides of (C3) by $N_A V$, and simplification, Eq. (C3) becomes:

$$\frac{d\#x}{dt} = -k_1\#x - \frac{k_2}{N_A V}\#x\#y - \frac{K_{cat}\#z\#x}{K_m N_A V + \#x}. \tag{C4}$$

Let $k_{2\_new} = \frac{k_2}{N_A V}$, $K_{m\_new} = K_m N_A V$, then the time-dependent change of #*x* is shown in Eq. (C5),

$$\frac{d\#x}{dt} = -k_1 \#x - k_{2\_new} \#x \#y - \frac{K_{cat} \#z \#x}{K_{m\_new} + \#x} . \quad \text{(C5)}$$

Appendix D: Derivation of Probabilistic Binding between CaMKII and NMDAR

A NMDAR molecule binds a CaMKII holoenzyme which contains n pBSs. Given by assumption (7) in Chapter 4, a NMDAR molecule can bind to only one pBS, then what is the probability that the NMDAR molecule binds the CaMKII holoenzyme?

If the CaMKII holoenzyme contains only one pBS, there are two possible events, the NMDAR molecule binds to the pBS, *z*, or the NMDAR molecule does not bind to the pBS, $\overline{z}$. The probabilities for the events are defined as $P(Z)$ and $P(\overline{Z})$ as follows:

$$P(Z) = P_b, \text{ and} \tag{D1}$$

$$P(\overline{Z}) = 1 - P_b. \tag{D2}$$

As the CaMKII holoenzyme contains n pBSs, there are two possible events: (1) event 1 (E_1), the NMDAR molecule binds to one of the n pBSs; and (2) event 2 (E_2), the NMDAR molecule does not bind to any of the n pBSs. Therefore, the event space, *S*, is:

$$S = \{E_1, E_2\}, \text{ and}$$

$$P(S) = P(E_1 \cup E_2) = P(E_1) + P(E_2) = 1. \tag{D3}$$

Derivation 1:

Since the n pBSs are independent, so both events should be considered as the combinations of independent events occurring at the n pBSs: for example, E_1 is the situation that the NMDAR molecule binds to the j^{th} pBS (j=1…n), and does not bind to any other pBSs (A-j, where A = {1, 2, 3, … , n}). Therefore, the probability for the NMDAR molecule binding to the j^{th} pBS is $P(Z_j \cap \overline{Z_{A-j}})$. Because pBSs are independent,

so that $P\left(Z_j \cap \overline{Z_{A-j}}\right)$ is a product of the probabilities of the independent events occurring at the n pBSs. There are n choices of *j*, so $P\left(Z_j \cap \overline{Z_{A-j}}\right)$ is given by:

$$P\left(Z_j \cap \overline{Z_{A-j}}\right) = \sum_{j=1}^{n} P\left(Z_j\right) \cdot P\left(\overline{Z_{A-j}}\right), \tag{D4}$$

If *j*=2, then $P\left(\overline{Z_{A-j}}\right) = P\left(\overline{Z_1}\right) \cdot P\left(\overline{Z_3}\right) \cdot P\left(\overline{Z_4}\right) \cdot \ldots \cdot P\left(\overline{Z_n}\right)$. Combining Eqs. (D1, D2 and D4), $P\left(Z_j \cap \overline{Z_{A-j}}\right)$ is given by:

$$P\left(Z_j \cap \overline{Z_{A-j}}\right) = nP_b\left(1-P_b\right)^{n-1}. \tag{D5}$$

Similarly, E_2 is the situation that the NMDAR molecule does not bind to any of the n pBSs. So, the probability that the NMDAR does not bind to any of the n pBSs is $P\left(\overline{Z_A}\right)$ and expressed as:

$$P\left(\overline{Z_A}\right) = P\left(\overline{Z_1}\right) \cdot P\left(\overline{Z_2}\right) \cdot P\left(\overline{Z_3}\right) \cdot P\left(\overline{Z_4}\right) \ldots \cdot P\left(\overline{Z_n}\right). \tag{D6}$$

Combining Eqs. (D2 and D6), $P\left(\overline{Z_A}\right)$ is given by:

$$P\left(\overline{Z_A}\right) = \left(1-P_b\right)^n. \tag{D7}$$

The ratio of $P(E_1)$ to $P(E_2)$ is given by:

$$\frac{P\left(E_1\right)}{P\left(E_2\right)} = \frac{P\left(Z_j \cap \overline{Z_{A-j}}\right)}{P\left(\overline{Z_A}\right)} = \frac{nP_b\left(1-P_b\right)^{n-1}}{\left(1-P_b\right)^n} = \frac{nP}{1-P}. \tag{D8}$$

Therefore, $P(E_1)$ is given by:

$$P\left(E_1\right) = \frac{P\left(E_1\right)}{P\left(E_1\right)+P\left(E_2\right)} = \frac{1}{1+\dfrac{P\left(E_2\right)}{P\left(E_1\right)}} = \frac{1}{1+\dfrac{1-P}{nP}} = \frac{nP}{(n-1)P+1}, \tag{D9}$$

and $P(E_2)$ is given by:

$$P\left(E_2\right) = \frac{P\left(E_2\right)}{P\left(E_1\right)+P\left(E_2\right)} = \frac{1}{1+\dfrac{P\left(E_1\right)}{P\left(E_2\right)}} = \frac{1}{1+\dfrac{nP}{1-P}} = \frac{1-P}{(n-1)P+1}. \tag{D10}$$

Now, if S is the event space, $P(S) = P(E_1) + P(E_2) = \frac{(n-1)P_b + 1}{(n-1)P_b + 1} = 1$.

Derivation 2 (more elegantly):

Assume firstly that the NMDAR molecule can bind to up to nPBSs. Let X be the number of pBSs the NMDAR molecule binds to. Let P_b be the probability that the NMDAR molecule binds to a single pBS. Assuming the n pBSs are independent, we have

$$X \sim \text{Binomial}(n, P_b),$$

with probability function

$$P(X = x) = \binom{n}{x} P_b^x (1 - P_b)^{n-x} \quad for\ x = 0,1,...,n\,. \tag{D11}$$

From (D11) we have

$$P(X = 0) = (1 - P_b)^n\,, \text{ and} \tag{D12}$$

$$P(X = 1) = nP_b(1 - P_b)^{n-1}\,. \tag{D13}$$

Given by assumption (7), a NMDAR molecule can bind to only one pBS. Hence, we want to express the probabilities (D12 and D13) conditional on X$\leqslant$1 to give the probabilities of E_1 and E_2 in Eqs. (D14 and D15):

$$\begin{aligned} P(E_1) &= P(X = 0 \mid X \le 1) \\ &= \frac{P(X = 1)}{P(X \le 1)} \\ &= \frac{nP_b(1 - P_b)^{n-1}}{(1 - P_b)^n + nP_b(1 - P_b)^{n-1}}\,, \text{ and} \\ &= \frac{nP_b}{(n-1)P_b + 1} \end{aligned} \tag{D14}$$

$$P(E_2) = 1 - P(E_1) = \frac{1 - P_b}{(n-1)P_b + 1}\,. \tag{D15}$$

Appendix E: Parameter Estimation and Sensitivity

E.1 Parameter estimation using MCMC

Markov chain Monte Carlo (MCMC) is a sampling algorithm and is often applied to solve problems in large dimensional space (Andrieu et al., 2003). Parameter estimation is a optimisation problem over multiple dimensions, where each dimension corresponds to an unknown parameter. The estimation is very difficult to be sampled directly in large dimensions, but the goodness of a sample can be evaluated through calculating the error from the experimental data. MCMC generates samples for the parameters from a sample space, X , and the algorithm is constructed to draw samples from the most important regions (low error) which gives optimal parameters to describe the experimental data.

E.1.1 Markov chain

A chain here describes the evolution of a system/process among large but finite state spaces. The sampling process, x^i, (x^i denotes both the process and the i^{th} sample) draw samples from s discrete states $x^i \in X = \{x_1, x_2, ..., x_s\}$ according to a probability distribution, $P_i(X)$, which may be evolving over time. $P_i(X)$ evolution is a Markov chain only if the next state is dependent solely on the current state and a fixed probability governs the transitions among states as given by Eq. (E1) (Andrieu et al., 2003):

$$p\left(x^{i+1} = x_n \mid x^i = x_m, ..., x^1\right) = p\left(x_n \mid x_m\right), \quad (m, n = 1...s). \tag{E1}$$

where $p\left(x_n \mid x_m\right)$ determines the probability that the next sample is x_n given the current sample is x_m. A transition matrix, T, contains the transitional probabilites, such that $p\left(x_n \mid x_m\right) = T_{mn}$ and $\sum_{n=1}^{s} T_{mn} = 1$.

Considering a simple Markov chain as illustrated in Fig. (E-1), which has a sample space of three discrete states ($X = \{x_1, x_2, x_3\}$). The transition matrix for the Markov

chain is:

$$T = \begin{bmatrix} 0.2 & 0.8 & 0 \\ 0.4 & 0 & 0.6 \\ 0.9 & 0.1 & 0 \end{bmatrix}.$$

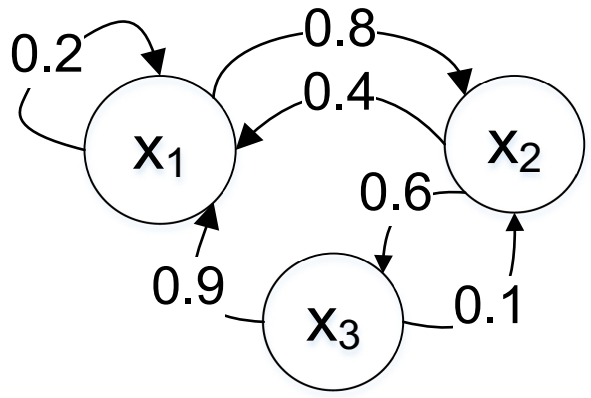

Figure E-1 A Markov chain with fixed transitional probability among the three states.

The chain is evolving from an initial distribution, $P_0(X)$= (P1, P2, P3) such that the chance of getting a sample of x_1, x_2 or x_3 is P1, P2, or P3, respectively. It follows that the $P_i(X)$ is evolved through the transformations by the transition matrix:

$$P_i(X) = P_{i-1}(X)T = P_{i-2}(X)T^2 = \ldots = P_0(X)T^i. \quad \text{(E2)}$$

If the size of the sampling is large enough, $\lim_{i\to\infty} T^i$ converges to approximately $\begin{bmatrix} 0.4234 & 0.3604 & 0.2162 \\ 0.4234 & 0.3604 & 0.2162 \\ 0.4234 & 0.3604 & 0.2162 \end{bmatrix}$. As a result, the distribution of the samples drawn converges to an invariant distribution, (0.4234 0.3604 0.2162), regardless of the initial distribution chosen.

The convergence is the central idea of MCMC and a Markov chain will converge to an invariant distribution, $P(X)$, if: (1) starting from any states, all other states are reachable in finite steps (irreducibility), and (2) the chain is aperiodic.

The invariant distribution of the convergence must satisfy the detailed balance condition as given by Eq. (E3) (Andrieu et al., 2003):

$$P(x_m)T_{mn} = P(x_n)T_{nm} \qquad (m,n = 1...s)\,. \tag{E3}$$

Summing both sides of Eq. (E3) over x_n:

$$P(x_m) = \sum\nolimits_{x_n} P(x_n)T_{nm}\,. \tag{E4}$$

Testing the sample Markov chain in Fig. (E1) with its invariant distribution, $P(X)$ = (0.4234, 0.3604, 0.2162). Let m=1, we have $P(x_1) = 0.4232 \approx \sum_{n=1}^{3} P(x_n)T_{n1} = 0.42322$.

E.1.2 The Metropolis-Hastings algorithm

If we can construct a Markov chain, which converges to the optimal distribution of parameters, then we can obtain the optimal distribution of parameters directly by drawing samples from the converged chain. The most popular MCMC algorithm for constructing the Markov chain is the Metropolis-Hastings algorithm (Hastings, 1970; Metropolis et al., 1953).

Supposing an aperiodic and irreducible Markov chain, C_1, with s discrete states of possible parameters space ($X = \{x_1, x_2, ..., x_s\}$) and a transition matrix, Q, given by Eq. (E5):

$$q\left(x^{i+1} = x_n \mid x^i = x_m\right) = Q_{mn}\,, \qquad (m,n = 1...s)\,, \tag{E5}$$

does not converge to the optimal distribution of optimal parameters, $P(X)$:

$$P(x_m)Q_{m,n} \neq P(x_n)Q_{n,m} \qquad . \tag{E6}$$

However, C_1 can be transformed by a function, A, in terms of x_m and x_n into C_2, so that C_2 safisfies the detailed balance condition:

$$P(x_m)Q_{m,n}A(x_m,x_n) = P(x_n)Q_{n,m}A(x_n,x_m)\,, \tag{E7}$$

and importantly, C_2 converges to $P(X)$. The simplest form of A is:

$$A(x_m,x_n) = P(x_n)Q_{n,m}\,, \text{ and } \quad A(x_n,x_m) = P(x_m)Q_{m,n}\,. \tag{E8}$$

Therefore, the transition matrix of C_2, Q', is

$$q'(x_n \mid x_m) = Q'_{mn} = Q_{m,n} Q_{n,m} P(x_n). \tag{E9}$$

A is called the aceptance probability, which declares the probability of accepting a state transition occuring in C_1 to occur in C_2 as well.

However, A may be so small that C_2 may take very long time (or samples) to explore the whole state space for converging to $P(X)$. Therefore, if we enlarge A by a factor, k, which satisfies the condition given by Eq. (E10):

$$kA(x_m, x_n) \le 1, kA(x_n, x_m) \le 1 \quad \text{and} \quad k \ge 1 \tag{E10}$$

then we have a new Markov chain, C_3, which converges (as given by Eq. (E11)) faster than C_2.

$$P(x_m) Q_{m,n} A(x_m, x_n) \times k = P(x_n) Q_{n,m} A(x_n, x_m) \times k, \tag{E11}$$

The speed of convergence becomes maximum when either $kA(x_m, x_n) = 1$ or $kA(x_n, x_m) = 1$, without breaking conditions given by Eq. (E10). Therefore, the maximum of $kA(x_m, x_n)$ is $\min\left\{ \frac{A(x_m, x_n)}{A(x_n, x_m)} \quad , \quad 1 \right\}$.

Now, the procedure of the Metropolis-Hastings algorithm is given as follows:

Step1: Initialise $x^0 \in X = \{x_1, x_2, ..., x_s\}$

Step2: For i = 0 to N-1

Generate a random number, u, from uniform distribution, $U(0,1)$. Then, take a sample, $y \in X = \{x_1, x_2, ..., x_s\}$, according to $Q_{x^i y}$.

If $u < \min\left\{ \frac{A(x^0, y)}{A(y, x^0)} \quad , \quad 1 \right\}$, $x^{i+1} = y$

Else, $x^{i+1} = x^i$

Although the Metropolis-Hastings algorithm may be inefficient for sampling over large

dimensions, the basic ideas of MCMC are well encapsulated in this algorithm and our discussion on the algorithms of MCMC ends here. For the details of more efficient algorithms of MCMC, we refer to Andrieu et al. (2003) and Haario (2006). We give an example of the application of MCMC in the next section.

E.1.3 Procedure of estimating the parameters of MoHST

The procedure of the parameter estimation is described as follows:

Step 1: Retrieve data points from experiments. We retrieve experimental data from Shen and Meyer (1999), which is the dynamics of CaMKII translocation normalised from the fluorescence intensity. The data comprises two dynamics, one is for the CaMKII translocation into PSD and one is for the CaMKII dissociation from PSD.

Step 2: Take a guess of the unknown parameters from the possible parameter spaces as given in Section 4.2.2. The guess becomes the initial sample x^0. Then, generate a Markov chain taking states from the possible parameter spaces.

Step 3: Calculate the dynamics of CaMKII translocation using the current sample x^i as discussed in Section 4.2.3.1 and calculate the mean square error (MSE) of the computed dynamics of CaMKII translocation from the experimental data. A likelihood function is defined as the probability density function of exponential distribution: $\lambda e^{-\lambda MSE}$ ($\lambda>0$), which samples parameters with low MSE more frequently. The target distribution is the integral taken from this likelihood function.

Step 4: Evolve the chain using MCMC algorithms and repeat Step 3 until the distribution of samples converges to an invariant distribution. We use Geweke's convergence diagnostic (Cowles and Carlin, 1996) to access the convergence of the chain (Fig. E2) and stop the sampling when Geweke's convergence diagnostic approaches 1.

Step 5: The target parameters are either the mean of the samples taken from step 4 or the particular parameters with the lowest MSE.

Step 6: Validate the estimated parameter with sets of separate data or observations. If

the validation fails, repeat from step 2. We validate the model with T286A mutant CaMKII data retrieved from the same experiment (Shen and Meyer, 1999).

We estimate the parameters of MoHST using MCMC toolbox for Matlab (http://helios.fmi.fi/~lainema/mcmc/), which automates the whole process (except the validation). Some examples of the results are shown in Fig. (E-2).

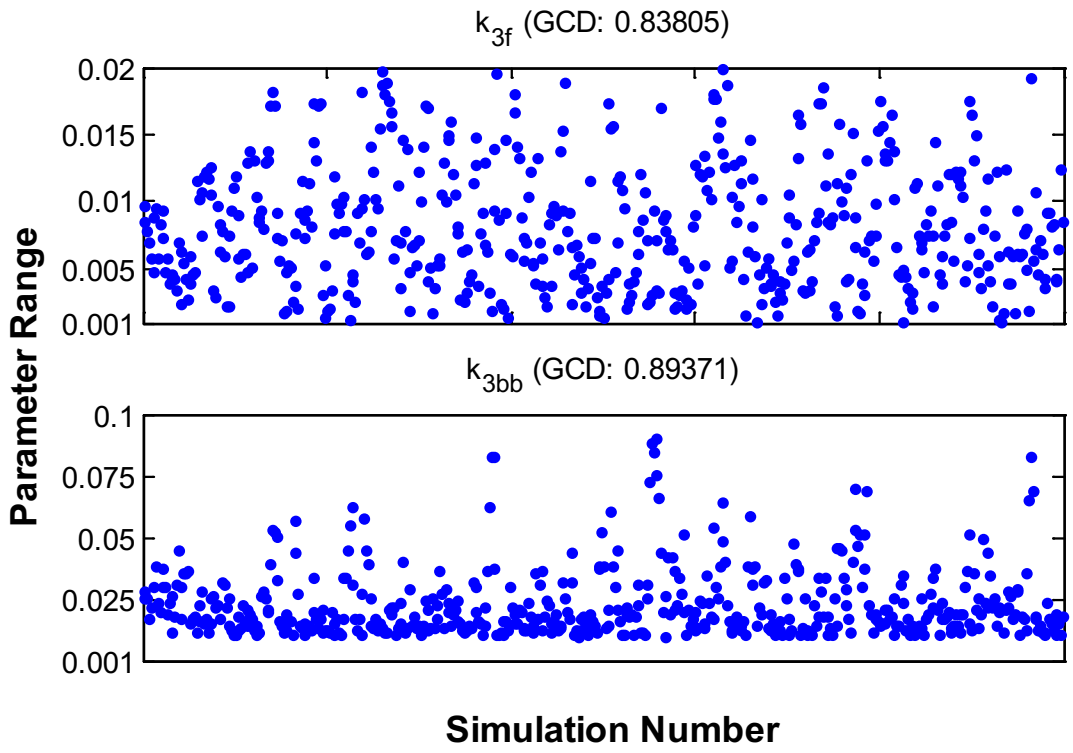

Figure E-2 The adaptation of k_{3f} and k_{3bb} through MCMC. We use Geweke's convergence diagnostic (GCD) to test the convergence of the simulations and the simulation is stopped when GCD is close to 1.

E.2 Parameter sensitivity using PRCC

The robustness of a biological system reflects its ability to retain normal functioning with a modest change to the working environment (Kitano, 2007) which may lead to highly variable parameters potentially resulting in undesirable levels of some species in the system. These stochastic effects are exacerbated due to the low copy numbers of proteins. Partial ranking correlation coefficient (PRCC) is a global sensitivity analysis method for quantifying the sensitivity of the model output with respect to the variation of parameters. PRCC is chosen for this study since it works better for nonlinear but monotonic relationships between outputs and inputs (Marino et al., 2008) (as shown in Fig. 4-6, the relationships between the formation of CaMKII-NMDAR complex and the chosen parameters are nonlinear but monotonic).

Sensitivity analysis methods rely on sampling algorithms, such as Latin hypercube sampling (LHS) (McKay et al., 1979), which feeds the model with a large number of sets of parameters that are varied within a realistic margin. To quantify the relation between a model output, y, and a particular parameter, x_j (j = 1..n), of n chosen parameters, correlation coefficient (CC), r_{yx_j}, is usually used and given by Eq. (E12):

$$r_{yx_j} = \frac{\sum_{i=1}^{N}\left(x_{ij}-\overline{x_j}\right)\left(y_i-\overline{y}\right)}{\sqrt{\sum_{i=1}^{N}\left(x_{ij}-\overline{x_j}\right)^2\sum_{i=1}^{N}\left(y_i-\overline{y}\right)^2}}, \tag{E12}$$

where N is the total number of sets of parameters, x_{ij} the value of i^{th} sample of x_j, which has y_i as the corresponding model output (Fig. E3), $\overline{x_j}$ and $\overline{y}$ are the means of samples of x_j and outputs, respectively. Correlated x_j and y have r_{yx_j} values close to -1 or 1, which means strong negative or positive correlation, while uncorrelated cases have r_{yx_j} values approaching 0. A p-value is calculated according to a null hypothesis, which states that x_j and y are uncorrelated. A small p-value (smaller than the significance level, which is normally set at 0.05) leads to rejection of the null hypothesis, and the conclusion is made that x_j and y are correlated.

CC has two major problems: (1) sampling algorithms like LHS perturbs all parameters simultaneously, hence, CC may be affected by the variation of parameters other than x_j; and (2) since parameters are usually sampled according to a percentage around their reference values, the magnitude of the reference value may have an impact on CC.

The solution for problem one is the partial correlation coefficient (PCC), which quantifies the relation between y and x_j after removing the linear effects on y of all parameters other than x_j. A linear regression model predicts y and x_j in terms of the n chosen parameters in a form given by Eq. (E13):

$$x_j = \varepsilon_1 + \sum_{\substack{i=1 \\ i \neq j}}^{n} \alpha_i x_i \text{ , and } \quad y = \varepsilon_2 + \sum_{\substack{i=1 \\ i \neq j}}^{n} \beta_i x_i \text{ ,} \tag{E13}$$

where α is the regression coefficients for x_j, β is the regression coefficients for y, ε_1 and ε_2 are error terms. The linear effects from parameters other than x_j can be removed to obtain two residue, $\hat{x}_j$ and $\hat{y}$ as given by Eq. (E14):

$$\hat{x}_j = x_j - \sum_{\substack{i=1 \\ i \neq j}}^{n} \hat{\alpha}_i x_i \text{ , and } \quad \hat{y} = y - \sum_{\substack{i=1 \\ i \neq j}}^{n} \hat{\beta}_i x_i \text{ .} \tag{E14}$$

PCC is the CC between $\hat{x}_j$ and $\hat{y}$.

The rank-transformed data (Fig. E-3) is the solution for problem two. The parameters and the output are first rank-transformed and then the PRCC is calculated by taking PCC between the ranked x_j and y. As a result, the parameters and the output are transferred from real values into ranks (integers 1 to N) so that the magnitude of the reference value is removed.

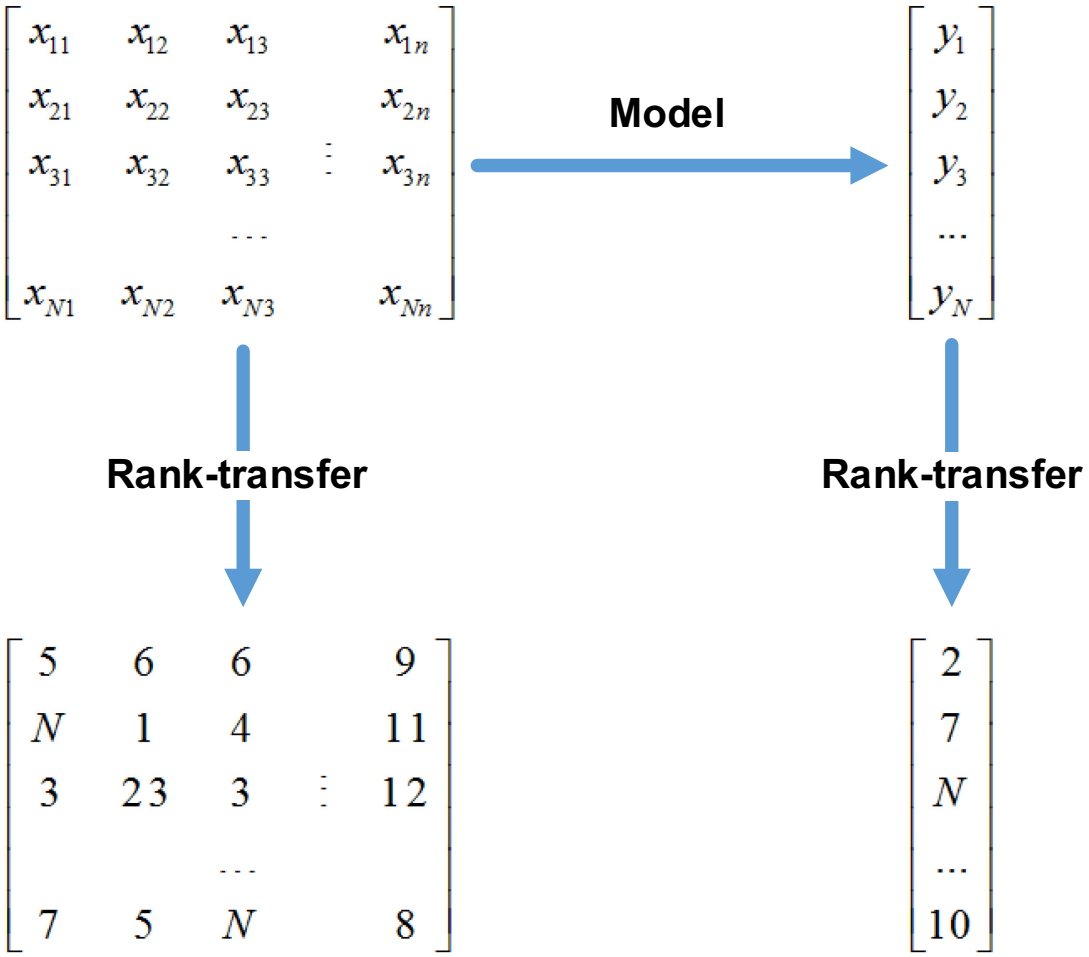

Figure E-3 Rank transfer of parameters and model output. A matrix, x, contains the LHS generated parameters. Each column of *x* compresises *N* samples of a parameter, and each row of *x* is a set of *n* parameters chosen. For each set of parameters, the model simulates an output and the output is stored into a vector, *y*, in the same raw as that set of parameters. The rank-transformation ranks each column of matrix *x* (*N* samples of a parameter) or vector y (small to large), so that each column of matrix *x* (or *y*) comprises *N* integers from 1 to *N* and each of the integers appears once.

The results of PRCC between the formation of CaMKII-NMDAR complex and the 8 parameter related to HSTs of CaMKII under rest level, 10Hz tetanus and 100Hz tetanus are shown in Figs. (E-4 to E-6), respectively. At rest, PRCCs of K_{m4} and k_{3bb} are very close to 0 and their associated p-values are very large which means their variations produce insignificant effects on the formation of CaMKII-NMDAR complex. These results can be seen visually from the figures that the two vertical bars (K_{m4} and k_{3bb}) indicating no relationship between the data in *x* and *y* axes (Fig. E-4). However, at 10Hz and 100Hz stimulation, both parameters have large PRCCs and low p-values, especially k_{3bb}. The figures also indicate negative correlated relationships between the variation of k_{m4} and k_{3bb} to the formation of CaMKII-NMDAR complex (Figs. E-5 and E-6).

The calculation and plots of PRCC are based on Matlab functions downloaded from http://malthus.micro.med.umich.edu/lab/usadata/ .

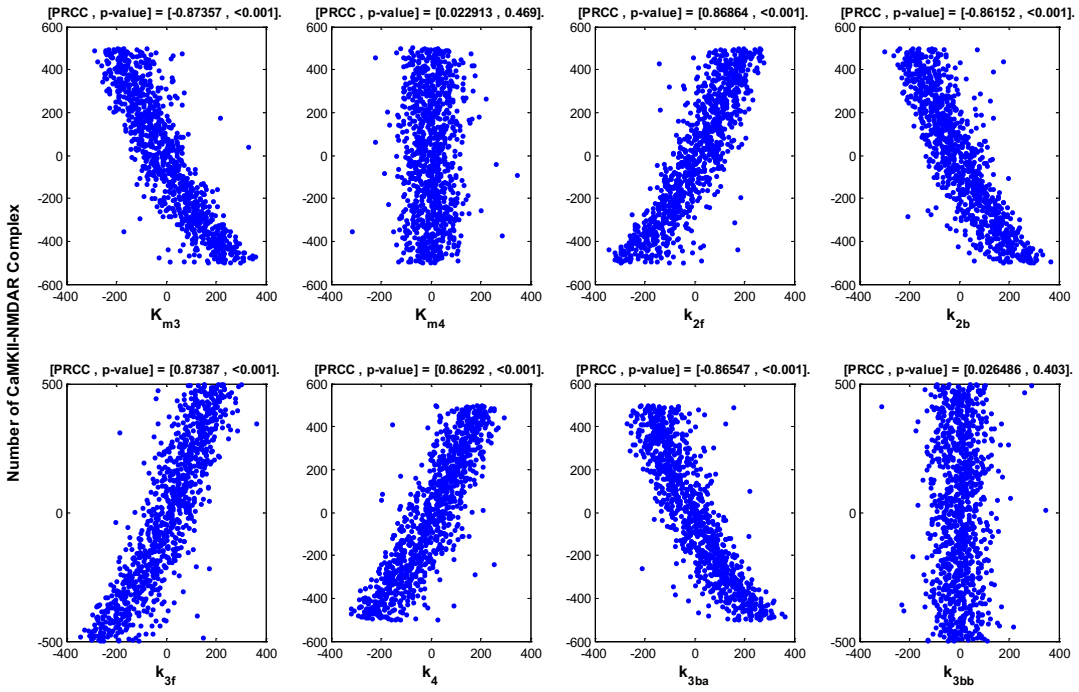

Figure E-4 PRCC and the associated p-values for the 8 chosen parameters at rest level. Axes of figures are residues as given in Eq. (E14). The title of each figure gives PRCC and p-value of the formation of CaMKII-NMDAR complex with respect to the corresponding parameter. Each simulation is run under the rest level of Ca^{2+} (70 nM).

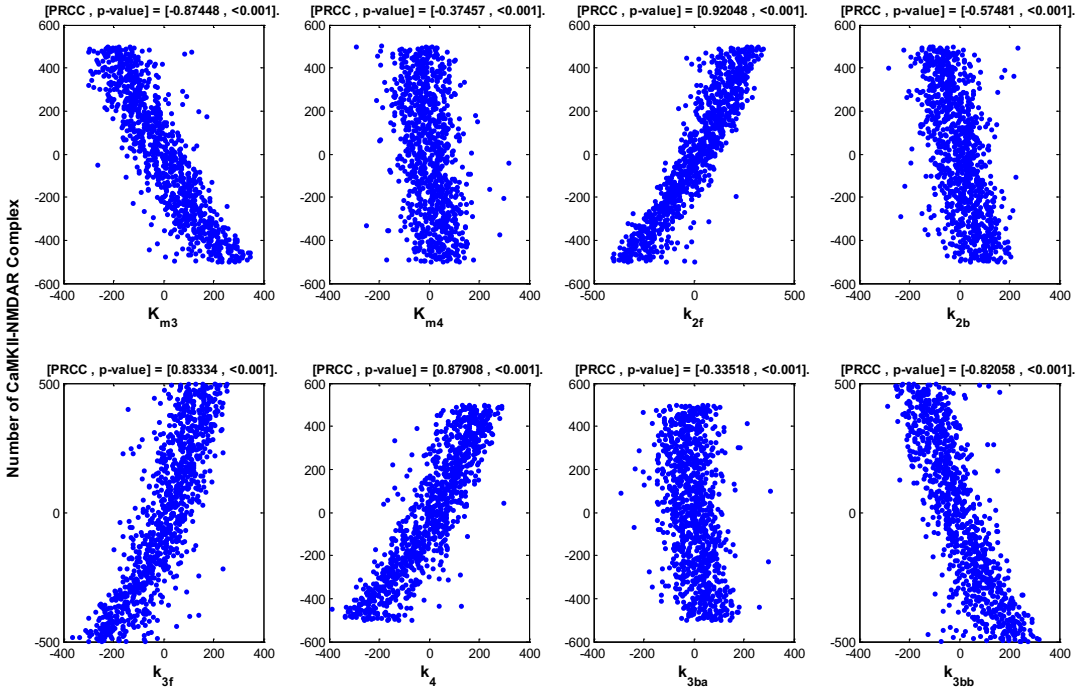

Figure E-5 PRCC and the associated p-values for the 8 chosen parameters at 10Hz tetanus. Axes of figures are residues as given in Eq. (E14). The title of each figure gives PRCC and p-value of the formation of CaMKII-NMDAR complex with respect to the corresponding parameter. Each simulation is run under 100 pulses of Ca^{2+} tetanus at 10Hz.

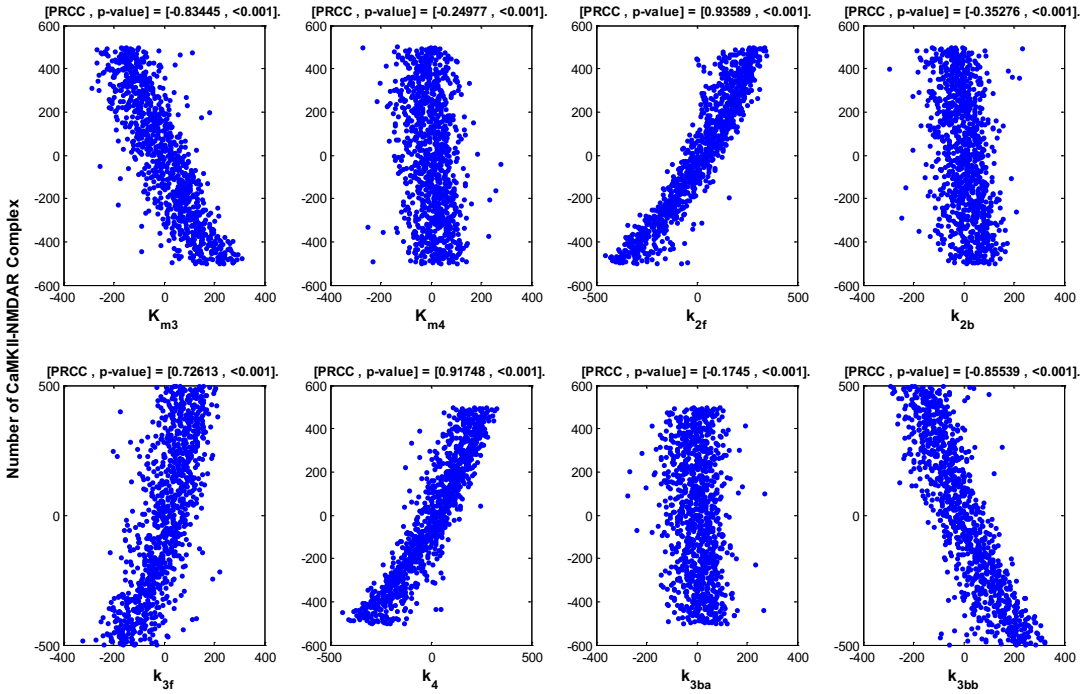

Figure E-6 PRCC and the associated p-values for the 8 chosen parameters at 100Hz tetanus. Axes of figures are residues as given in Eq. (E14). The title of each figure gives PRCC and p-value of the formation of CaMKII-NMDAR complex with respect to the corresponding parameter. Each simulation is run under 100 pulses of Ca^{2+} tetanus at 100Hz.

Appendix F: Complete Model of MoNP and Parameters

F.1 Reaction rates

Reactions rates (Unit: μM s^{-1}, R_1-R_{31}) of the activation of modulators and the interactions among modulators are given by Eqs. (F1 – F31). The biological meaning and parameters of the reaction rates are summarised in Table F-1 (see Chapters 2 and 3 for the explanation and derivation).

(5) Ca^{2+}/CaM complex formation:

$$R_1 = k_{1f}\left[Ca^{2+}\right][CaM] - k_{1b}[CaCaM], \tag{F1}$$

$$R_2 = k_{2f}\left[Ca^{2+}\right][CaCaM] - k_{2b}[Ca_2CaM], \tag{F2}$$

$$R_3 = k_{3f}\left[Ca^{2+}\right][Ca_2CaM] - k_{3b}[Ca_3CaM], \text{ and} \tag{F3}$$

$$R_4 = k_{4f}\left[Ca^{2+}\right][Ca_2CaM] - k_{4b}[Ca_3CaM]. \tag{F4}$$

(6) Activation cAMP and PKA:

$$R_5 = k_{c1f}[Ca_4CaM]\left(AC1_T - [CaMAC1]\right) - k_{c1b}[CaMAC1], \tag{F5}$$

$$R_6 = k_{c2f}[Ca_4CaM]\left(AC8_T - [CaMAC8]\right) - k_{c2b}[CaMAC8], \tag{F6}$$

$$R_7 = k_{c3f}[Ca_4CaM]\left(PDE1_T - [CaMPDE1]\right) - k_{c3b}[CaMPDE1], \tag{F7}$$

$$R_8 = K_{cat1}[CaMAC1], \tag{F8}$$

$$R_9 = K_{cat2}[CaMAC8], \tag{F9}$$

$$R_{10} = \frac{K_{cat3}[AC2_T]}{1 + K_1}, \tag{F10}$$

$$R_{11} = \frac{K_{cat4}PKAc\left([PDE4B_T] - \left[PDE4B^*\right]\right)}{K_{m1} + \left([PDE4B_T] - \left[PDE4B^*\right]\right)} - k_{5b}\left[PDE4B^*\right], \tag{F11}$$

$$R_{12} = \frac{K_{cat4} PKAc\left(\left[PDE4D_T\right] - \left[PDE4D^*\right]\right)}{K_{m1} + \left(\left[PDE4D_T\right] - \left[PDE4D^*\right]\right)} - k_{5b}\left[PDE4D^*\right], \tag{F12}$$

$$R_{13} = \frac{K_{cat5}\left[PDE1_T\right]\left[cAMP\right]}{K_{m2} + \left[cAMP\right]}\left(1 + \left(K_{cat6} \Big/ K_{cat5} - 1\right)\frac{\left[CaMPDE1\right]}{\left[PDE1_T\right]}\right), \tag{F13}$$

$$R_{14} = \frac{K_{cat7}\left[PDE4B_T\right]\left[cAMP\right]}{K_{m3} + \left[cAMP\right]}\left(1 + \left(K_{cat8} \Big/ K_{cat7} - 1\right)\frac{\left[PDE4B^*\right]}{\left[PDE4B_T\right]}\right), \tag{F14}$$

$$R_{15} = \frac{K_{cat9}\left[PDE4D_T\right]\left[cAMP\right]}{K_{m4} + \left[cAMP\right]}\left(1 + \left(K_{cat10} \Big/ K_{cat9} - 1\right)\frac{\left[PDE4D^*\right]}{\left[PDE4D_T\right]}\right), \tag{F15}$$

$$R_{16} = k_{6f}\left[R_2C_2\right]\left[cAMP\right]^2 - k_{6b}\left[R_2C_2cAMP_2\right], \tag{F16}$$

$$R_{17} = k_{7f}\left[R_2C_2cAMP_2\right]\left[cAMP\right]^2 - k_{7b}\left[R_2C_2cAMP_4\right], \text{ and} \tag{F17}$$

$$R_{18} = k_{8b}\left[R_2C_2cAMP_4\right] - k_{8f}\left[PKAc\right]^3 \Big/ 2 . \tag{F18}$$

(7) Activation of PP2b and PP1:

$$R_{19} = k_{c4f}\left[Ca_4CaM\right]\frac{\left(\left[\mathrm{PP}\,2b_T\right] - \left[CaMCaNA\right]\right)\left[Ca^{2+}\right]^{n1}}{K_{d1}{}^{n1} + \left[Ca^{2+}\right]^{n1}}, \tag{F19}$$

$$R_{20} = k_{c4b1}\left[CaMCaNA\right]\frac{\left[Ca^{2+}\right]^{n2}}{K_{d2}{}^{n2} + \left[Ca^{2+}\right]^{n2}}, \tag{F20}$$

$$R_{21} = k_{c4b2}\left[CaMCaNA\right]\left(1 - \frac{\left[Ca^{2+}\right]^{n2}}{K_{d2}{}^{n2} + \left[Ca^{2+}\right]^{n2}}\right), \tag{F21}$$

$$\left[PP1\right] = \left[PP1_T\right] - \left[I1^*PP1\right],$$

$$R_{22} = \frac{K_{cat11}\left[PKAc\right]\left(\left[I1_T\right] - \left[I1^*PP1\right]\right)}{K_{m5} + \left(\left[I1_T\right] - \left[I1^*PP1\right]\right)}, \tag{F22}$$

$$R_{23} = \frac{K_{cat12}\left[PP2a\right]\left[I1^*PP1\right]}{K_{m5} + \left[I1^*PP1\right]}, \text{ and} \tag{F23}$$

$$R_{24} = \frac{K_{cat13}\left(\left[CaMCaNA\right] + \frac{1}{20}\left[Ca_4CaNB\right]\right)\left[I1^* PP1\right]}{K_{m5} + \left[I1^* PP1\right]}. \quad \text{(F24)}$$

(8) Activation of CaMKII and autophosphorylation:

$$\left[iCaMKII\right] = \left[CaMKII_T\right] - \left[CaMCaMKII\right] - \left[CaMCaMKII^*\right] - \left[CaMKII^*\right],$$

$$R_{25} = k_{c5f}\left[iCaMKII\right]\left[Ca_4CaM\right] - k_{c5b1}\left[CaMCaMKII\right], \quad \text{(F25)}$$

$$R_{26} = k_{c5f}\left[CaMKII^*\right]\left[Ca_4CaM\right] - k_{c5b2}\left[CaMCaMKII^*\right], \quad \text{(F26)}$$

$$P = \left(1 - \frac{\left[iCaMKII\right]^2}{\left[CaMKII_T\right]^2}\right),$$

$$R_{27} = K_{cat14} P\left[CaMCaMKII\right], \quad \text{(F27)}$$

$$R_{28} = \frac{K_{cat15}\left[PP1\right]\left[CaMCaMKII^*\right]}{K_{m6} + \left[CaMCaMKII^*\right]}, \quad \text{(F28)}$$

$$R_{29} = \frac{K_{cat16}\left[PP2a\right]\left[CaMCaMKII^*\right]}{K_{m7} + \left[CaMCaMKII^*\right]}, \quad \text{(F29)}$$

$$R_{30} = \frac{K_{cat15}\left[PP1\right]\left[CaMKII^*\right]}{K_{m6} + \left[CaMKII^*\right]}, \text{ and} \quad \text{(F30)}$$

$$R_{31} = \frac{K_{cat16}\left[PP2a\right]\left[CaMKII^*\right]}{K_{m7} + \left[CaMKII^*\right]}. \quad \text{(F31)}$$

Table F-1

Reactions: their biological meaning and parameters

No.	***Biological Meaning***	k_f $\mu M^{-1}s^{-1}$	k_b s^{-1}	K_{cat} s^{-1}	K_m μM	K_d μM	*n/K*
1	*Formation of CaCaM*	2.5	50				
2	*Formation of Ca_2CaM*	88.25	50				
3	*Formation of Ca_2CaM*	12.5	1250				
3	*Formation of Ca^{2+}/CaM complex (Ca_4CaM)*	250	1250				
5	*Activation of AC1*	50	1				
6	*Activation of AC8*	20	1				
7	*Activation of PDE1*	100	1				
8	*Converting ATP into cAMP by AC1*			2.843			
9	*Converting ATP into cAMP by AC8*			2.843			
10	*Converting ATP into cAMP by AC2*			2			10
11	*Phosphorylation of PDE4B by PKA*		0.25	18	25		
12	*Phosphorylation of PDE4D by PKA*		0.25	18	25		
13	*Converting cAMP into AMP by PDE1*			1.7/10	10		
14	*Converting cAMP into AMP by PDE4B*			1.56/3.12	4.5		
15	*Converting cAMP into AMP by PDE4D*			5.4/10.8	1.5		
16	*Association of cAMP and PKA complex (1)*	8[a]	0.02				
17	*Association of cAMP and PKA complex (2)*	0.7[a]	0.2				
18	*Releasing of PKA catalytic subunit*	0.25[a]	0.0016				
19	*Full activation of PP2b*	46				0.5	1.8
20	*Dissociation of CaM from PP2b (high Ca^{2+})*		0.0012			0.6	3
21	*Dissociation of CaM from PP2b (low Ca^{2+})*		0.6			0.6	3
22	*Phosphorylation of I1by PKA*			1.4	5		
23	*Dephosphorylation of $I1^*$by PP2a*			2	16		
24	*Dephosphorylation of $I1^*$by PP2b*			2.8	3		
25	*Activation of CaMKII*	21	1.1				
26	*Association of Ca_4CaM and $CaMKII^*$*		0.0011				
27	*Autophosphorylation of CaMCaMKII*			1.2			
28	*Dephosphorylation of $CaMCaMKII^*$ by PP1*			1.72	11		
29	*Dephosphorylation of $CaMCaMKII^*$ by PP2a*			2	16		
30	*Dephosphorylation of $CaMKII^*$ by PP1*			1.72	11		
31	*Dephosphorylation of $CaMKII^*$ by PP2a*			2	16		

[a] unit: $\mu M^{-2}s^{-1}$

F.2 ODEs for dynamics of modulators

The ODEs for dynamics of the concentrations of modualtor are given by Eqs. (F32 – F51)

$$\frac{d[CaM]}{dt} = -R_1 + R_{21}, \tag{F32}$$

$$\frac{d[CaCaM]}{dt} = R_1 - R_2, \tag{F33}$$

$$\frac{d[Ca_2CaM]}{dt} = R_2 - R_3, \tag{F34}$$

$$\frac{d[Ca_3CaM]}{dt} = R_3 - R_4, \tag{F35}$$

$$\frac{d[Ca_4CaM]}{dt} = R_4 - R_5 - R_6 - R_7 - R_{19} + R_{20} - R_{25} - R_{26}, \tag{F36}$$

$$\frac{d[CaMAC1]}{dt} = R_5, \tag{F37}$$

$$\frac{d[CaMAC8]}{dt} = R_6, \tag{F38}$$

$$\frac{d[CaMPDE1]}{dt} = R_7, \tag{F39}$$

$$\frac{d[PDE4B^*]}{dt} = R_{11}, \tag{F40}$$

$$\frac{d[PDE4D^*]}{dt} = R_{12}, \tag{F41}$$

$$\frac{d[R_2C_2]}{dt} = -R_{16}, \tag{F42}$$

$$\frac{d[R_2C_2cAMP_2]}{dt} = R_{16} - R_{17}, \tag{F43}$$

$$\frac{d[R_2C_2cAMP_4]}{dt} = R_{17} - R_{18}, \tag{F44}$$

$$\frac{d[cAMP]}{dt} = R_8 + R_9 + R_{10} - R_{13} - R_{14} - R_{15} - 2R_{16} - 2R_{17}, \tag{F45}$$

$$\frac{d[PKAc]}{dt} = 2R_{18}, \tag{F46}$$

$$\frac{d\left[CaMCaNA\right]}{dt} = R_{19} - R_{20} - R_{21}\,, \tag{F47}$$

$$\frac{d\left[I1^{*}PP1\right]}{dt} = R_{22} - R_{23} - R_{24}\,, \tag{F48}$$

$$\frac{d\left[CaMCaMKII\right]}{dt} = R_{25} - R_{27} + R_{28} + R_{29}\,, \tag{F49}$$

$$\frac{d\left[CaMCaMKII^{*}\right]}{dt} = R_{26} + R_{27} - R_{28} - R_{29}\,, \text{ and} \tag{F50}$$

$$\frac{d\left[CaMKII^{*}\right]}{dt} = -R_{26} - R_{30} - R_{31}\,. \tag{F51}$$

F.3 Constants

We summarise the values of constants in used in MoNP in Table F-2 (see Chapter 3 for the source).

Table F-2

Values of constants

Const.	***Biological Meaning***	***Value (μM)***
$[AC1_T]$	*Total concentration of type 1 adenylyl cyclase*	*2.5*
$[AC8_T]$	*Total concentration of type 8 adenylyl cyclase*	*0.625*
$[AC2_T]$	*Total concentration of Ca^{2+} independent adenylyl cyclase*	*2.5*
$[PDE1_T]$	*Total concentration of type1 PDE*	*4*
$[PDE4B_T]$	*Total concentration of type4B PDE*	*1*
$[PDE4D_T]$	*Total concentration of type4D PDE*	*1*
$[R2C2_T]$	*Total concentration of PKA complex*	*1.2*
$[PP2b_T]$	*Total concentration of PP2b*	*2.1*
$[PP2a_T]$	*Total concentration of PP2a*	*0.11111*
$[PP1_T]$	*Total concentration of PP1*	*3.5*
$[I1_T]$	*Total concentration of I1*	*1.5*
$[CaMKII_T]$	*Total concentration of CaMKII*	*20*

Appendix G: Generating Ca^{2+} Signals

The Ca^{2+} elevation triggered by the tetanus is computed based on the exponential build-up and decay as described by Zhabotinsky (2000). For example, assume that a tetanus of *n* pulses at frequency *f* stimulates the hippocampal neuron where each pulse increases the intracellular Ca^{2+} level by A and the relaxation time of Ca^{2+} decay is τ. Then the resulting intracellular Ca^{2+} level, $\left[Ca^{2+}\right]$, following this tetanus can be described (Zhabotinsky, 2000):

$$\left[Ca^{2+}\right] = \left[Ca^{2+}\right]_{rest} + A\sum_{i=1}^{n}\exp\left(-i/(f\tau)\right), \tag{G1}$$

where $\left[Ca^{2+}\right]_{rest}$ is the rest Ca^{2+} level. The parameter values used by Zhabotinsky (2000) are: 0.4μM (1Hz), or 1μM (10Hz and 100Hz) for A and 0.2s for τ.

There are four patterns of Ca^{2+} signals used in this study: (1) tetanus contains 100 pulses at 100Hz (HFS), (2) tetanus contains 100 pulses at 10Hz, (3) tetanus contains 100/900 pulses at 1Hz (LFS), and (4) theta burst stimulation (TBS). The stimulation patterns are explained in Fig. (G-1). The intracellular Ca^{2+} concentrations following these stimulations are shown in Figs. (G-2 – G-5).

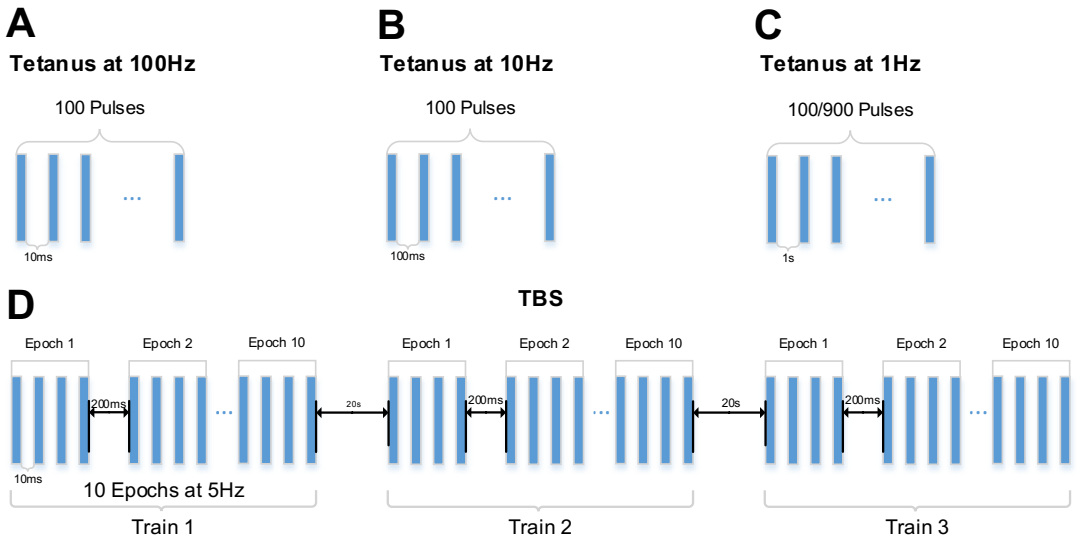

Figure G-1 Patterns of Ca^{2+} stimulation. Each pillar represents one pulse of the stiluation. (**A**) Tetanus at 100Hz contains 100 pulses delivered with 10ms separation. This pattern of stimulation is also refered as HFS for LTP induction. (**B**) Tetanus at 10Hz contains 100 pulses delivered with 100ms separation. (**C**) Tetanus at 1Hz contains 100 or 900 pulses delivered with 1s separation. This pattern of stimulation is also refered as LFS for LTD induction. (**D**) Theta burst stimulation contains 3 trains delivered with 20s separation. Each train contains 10 Epochs delivery at 5Hz (separate by 200ms). Each Epoch contains 4 pulses at 100Hz (separate by 10ms).

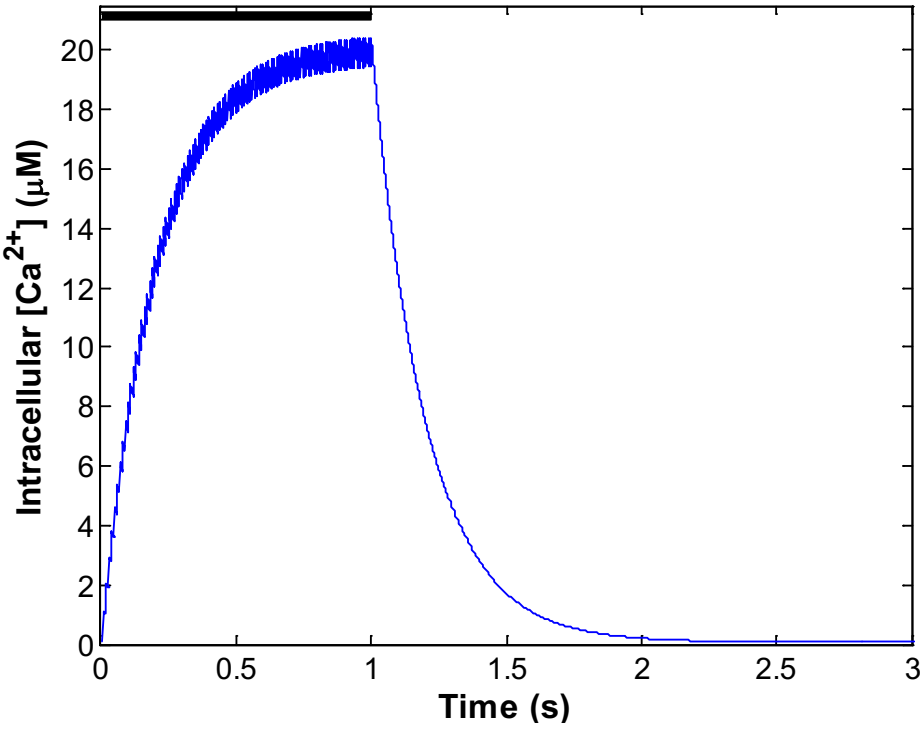

Figure G-2 Intracellular Ca^{2+} elevation in response to tetanus at 100Hz. The tetanus of 100 pulses is applied at t=0.01s and lasts for 1s (black bar). The intracellular Ca^{2+} level rises rapidly following the tetanus and reaches the maximum (around 20 μM). The intracellular Ca^{2+} level falls quickly (within a second) to the rest level after the disappearing of the tetanus at t=1s.

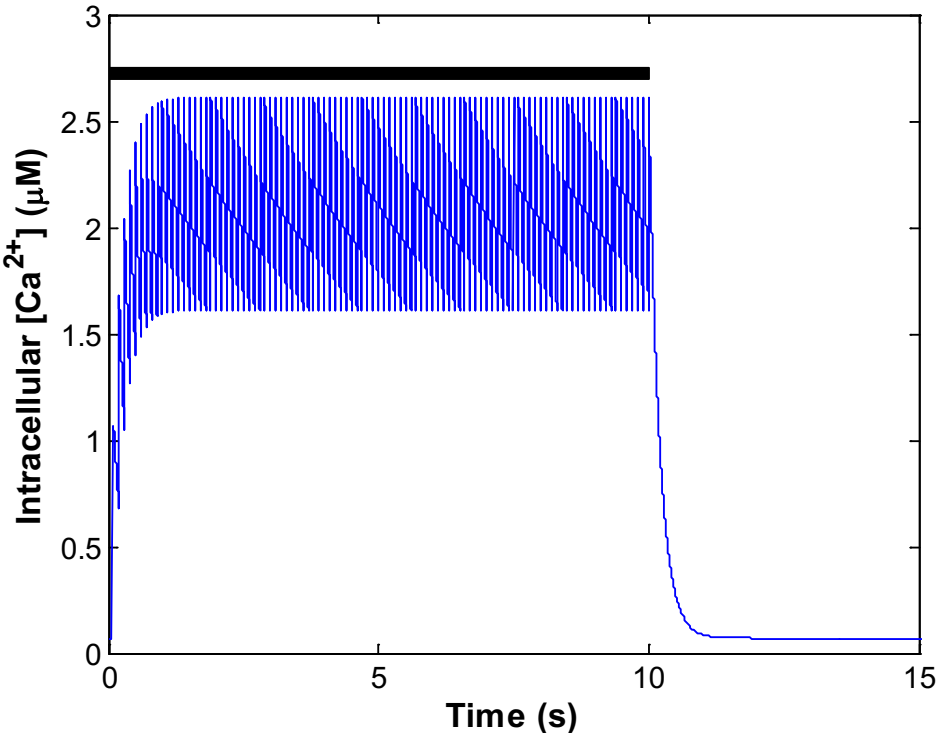

Figure G-3 Intracellular Ca^{2+} elevation in response to tetanus at 10Hz. The tetanus of 100 pulses is applied at t=0.1s and lasts for 10s (black bar). The intracellular Ca^{2+} level rises rapidly following the tetanus and reaches the maximum (around 2.55 μM). The intracellular Ca^{2+} level falls quickly (within a second) to the rest level after the disappearing of the tetanus at t=10s.

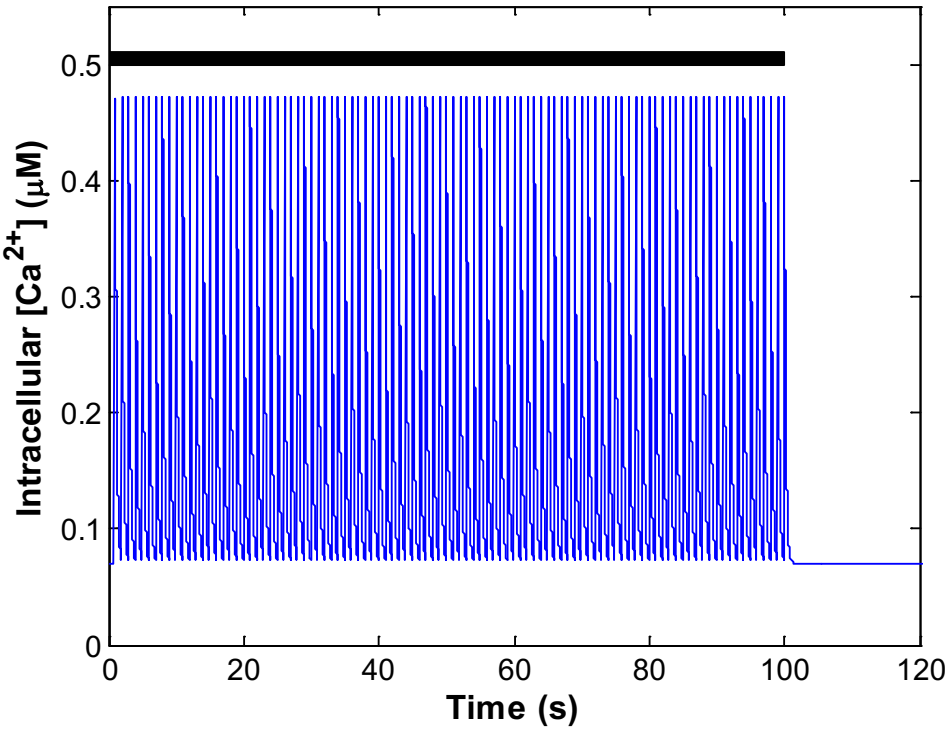

Figure G-4 Intracellular Ca^{2+} elevation in response to tetanus at 1Hz. The tetanus of 100 pulses is appied at t=1s and lasts for 100s (black bar). During the stimulation, the intracellular Ca^{2+} level fluctuates between the rest (0.07 μM) and 0.45 μM.

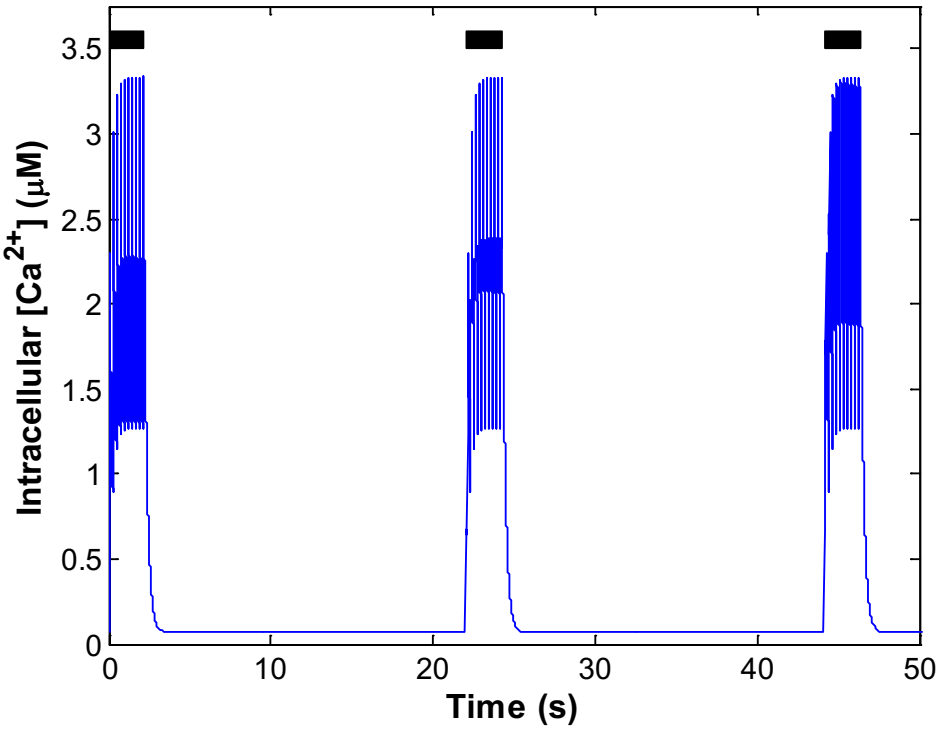

Figure G-5 Intracellular Ca^{2+} elevation in response to TBS. TBS is appied at t=0.01s. The stimulation contains 3 train (black bars) and each train elevates intracellular Ca^{2+} level to a peak of 3.25 μM. The intracellular Ca^{2+} level falls quickly after each train.

Reference

Abel, T., Nguyen, P. V, Barad, M., Deuel, T.A.S., Kandel, E.R., Bourtchouladze, R., 1997. Genetic demonstration of a role for PKA in the late phase of LTP and in hippocampus-based long-term memory. Cell 88, 615–626.

Ahmad, M., Polepalli, J.S., Goswami, D., Yang, X., Kaeser-Woo, Y.J., Südhof, T.C., Malenka, R.C., 2012. Postsynaptic complexin controls AMPA receptor exocytosis during LTP. Neuron 73, 260–267.

Anderson, J.R., 2000. Learning and memory. John Wiley New York.

Andrieu, C., Freitas, N. de, Doucet, A., Jordan, M.I., 2003. An Introduction to MCMC for Machine Learning. Mach. Learn. 50, 5–43. doi:10.1023/A:1020281327116

Appleby, V.J., Corrêa, S.A.L., Duckworth, J.K., Nash, J.E., Noël, J., Fitzjohn, S.M., Collingridge, G.L., Molnár, E., 2011. LTP in hippocampal neurons is associated with a CaMKII‐mediated increase in GluA1 surface expression. J Neurochem 116, 530–543.

Aslam, N., Kubota, Y., Wells, D., Shouval, H.Z., 2009. Translational switch for long-term maintenance of synaptic plasticity. Mol Syst Biol 5, 284.

Augustine, G.J., Santamaria, F., Tanaka, K., 2003. Local calcium signaling in neurons. Neuron 40, 331–346.

Banke, T.G., Bowie, D., Lee, H.-K., Huganir, R.L., Schousboe, A., Traynelis, S.F., 2000. Control of GluR1 AMPA Receptor Function by cAMP-Dependent Protein Kinase. J. Neurosci. 20, 89–102.

Barcomb, K., Coultrap, S.J., Bayer, K.U., 2013. Enzymatic Activity of CaMKII is not Required for its Interaction with the Glutamate Receptor Subunit GluN2B. Mol Pharmacol 84, 834–843.

Barria, A., Muller, D., Derkach, V., Griffith, L.C., Soderling, T.R., 1997. Regulatory Phosphorylation of AMPA-Type Glutamate Receptors by CaM-KII During Long-Term Potentiation. Science (80-.). 276, 2042–2045. doi:10.1126/science.276.5321.2042

Bastidas, A.C., Deal, M.S., Steichen, J.M., Keshwani, M.M., Guo, Y., Taylor, S.S., 2012. Role of N-terminal myristylation in the structure and regulation of cAMP-dependent protein kinase. J. Mol. Biol. 422, 215–29. doi:10.1016/j.jmb.2012.05.021

Baudier, J., Deloulme, J.C., Van Dorsselaer, A., Black, D., Matthes, H.W., 1991. Purification and characterization of a brain-specific protein kinase C substrate, neurogranin (p17). Identification of a consensus amino acid sequence between neurogranin and neuromodulin (GAP43) that corresponds to the protein kinase C phosphorylation si. J. Biol. Chem. 266, 229–237.

Bayer, K.U., LeBel, É., McDonald, G.L., O'Leary, H., Schulman, H., De Koninck, P., 2006. Transition from reversible to persistent binding of CaMKII to postsynaptic sites and NR2B. J. Neurosci. 26, 1164–1174.

Bayer, K.U., Paul De Koninck, A., Hell, J.W., Schulman, H., 2001. Interaction with the NMDA receptor locks CaMKII in an active conformation. Nature 411, 801–805.

Bear, M.F., Connor, B.W., Paradiso, M.A., 2007. Neuroscience: Exploring the Brain. Lippincott Williams & Wilkins.

Bear, M.F., Cooper, L.N., Ebner, F.F., 1987. A physiological basis for a theory of synapse modification. Science (80-.). 237, 42–48. doi:10.1126/science.3037696

Beattie, E.C., Carroll, R.C., Yu, X., Morishita, W., Yasuda, H., von Zastrow, M., Malenka, R.C., 2000. Regulation of AMPA receptor endocytosis by a signaling mechanism shared with LTD. Nat Neurosci 3, 1291–1300.

Bender, A.T., Beavo, J.A., 2006. Cyclic nucleotide phosphodiesterases: molecular regulation to clinical use. Pharmacol. Rev. 58, 488–520. doi:10.1124/pr.58.3.5

Benjamin, A.T., Quinn, J.J., 2003. Proofs that really count: the art of combinatorial proof. MAA.

Bhalla, U.S., 2013. Still Looking for the Memories: Molecules and Synaptic Plasticity, in: 20 Years of Computational Neuroscience. Springer, pp. 187–205.

Bhalla, U.S., Iyengar, R., 1999. Emergent properties of networks of biological signaling pathways. Science (80-.). 283, 381–387.

Bhattacharyya, S., Biou, V., Xu, W., Schlüter, O., Malenka, R.C., 2009. A critical role for PSD-95/AKAP interactions in endocytosis of synaptic AMPA receptors. Nat Neurosci 12, 172–181.

Bliss, T.V.P., Collingridge, G.L., 1993. A synaptic model of memory: long-term potentiation in the hippocampus. Nature 361, 31–39.

Bliss, T.V.P., Lømo, T., 1973. Long-lasting potentiation of synaptic transmission in the dentate area of the anaesthetized rabbit following stimulation of the perforant path. J Physiol 232, 331–356.

Blitzer, R.D., Connor, J.H., Brown, G.P., Wong, T., Shenolikar, S., Iyengar, R., Landau, E.M., 1998. Gating of CaMKII by cAMP-regulated protein phosphatase activity during LTP. Science (80-.). 280, 1940–1943.

Bourtchuladze, R., Frenguelli, B., Blendy, J., Cioffi, D., Schutz, G., Silva, A.J., 1994. Deficient long-term memory in mice with a targeted mutation of the cAMP-responsive element-binding protein. Cell 79, 59–68.

Bradshaw, J.M., Kubota, Y., Meyer, T., Schulman, H., 2003. An ultrasensitive Ca2+/calmodulin-dependent protein kinase II-protein phosphatase 1 switch facilitates specificity in postsynaptic calcium signaling. Proc. Natl. Acad. Sci. 100, 10512–10517.

Briggs, G.E., Haldane, J.B., 1925. A Note on the Kinetics of Enzyme Action. Biochem. J. 19, 338–9.

Buard, I., Coultrap, S.J., Freund, R.K., Lee, Y.-S., Dell'Acqua, M.L., Silva, A.J., Bayer, K.U., 2010. CaMKII "autonomy" is required for initiating but not for maintaining neuronal long-term information storage. J. Neurosci. 30, 8214–8220.

Cali, J.J., Zwaagstra, J.C., Mons, N., Cooper, D.M., Krupinski, J., 1994. Type VIII adenylyl cyclase. A Ca2+/calmodulin-stimulated enzyme expressed in discrete regions of rat brain. J. Biol. Chem. 269, 12190–5.

Carlier, M.-F., Pantaloni, D., 1997. Control of actin dynamics in cell motility. J Mol Biol 269, 459–467.

Carr, D.W., Stofko-Hahn, R.E., Fraser, I.D., Cone, R.D., Scott, J.D., 1992. Localization of the cAMP-dependent protein kinase to the postsynaptic densities by A-kinase anchoring proteins. Characterization of AKAP 79. J. Biol. Chem. 267, 16816–16823.

Carroll, R.C., Beattie, E.C., von Zastrow, M., Malenka, R.C., 2001. Role of AMPA receptor endocytosis in synaptic plasticity. Nat Rev Neurosci 2, 315–324.

Castellani, G.C., Quinlan, E.M., Bersani, F., Cooper, L.N., Shouval, H.Z., 2005. A model of bidirectional synaptic plasticity: from signaling network to channel conductance. Learn. Mem. 12, 423–432. doi:10.1101/lm.80705

Chang, H.P., Lindberg, F.P., Wang, H.L., Huang, A.M., Lee, E.H.Y., 1999. Impaired memory retention and decreased long-term potentiation in integrin-associated protein-deficient mice. Learn. Mem. 6, 448–457.

Chao, L.H., Stratton, M.M., Lee, I.-H., Rosenberg, O.S., Levitz, J., Mandell, D.J., Kortemme, T., Groves, J.T., Schulman, H., Kuriyan, J., 2011. A Mechanism for Tunable Autoinhibition in the Structure of a Human Ca< sup> 2+</sup>/Calmodulin-Dependent Kinase II Holoenzyme. Cell 146, 732–745.

Chen, H., Bernstein, B.W., Bamburg, J.R., 2000. Regulating actin-filament dynamics< i> in vivo</i>. Trends Biochem. Sci. 25, 19–23.

Chiba, H., Schneider, N.S., Matsuoka, S., Noma, A., 2008. A Simulation Study on the Activation of Cardiac CaMKII< i> δ</i>-Isoform and Its Regulation by Phosphatases. Biophys J 95, 2139–2149.

Cho, K.-O., Hunt, C.A., Kennedy, M.B., 1992. The rat brain postsynaptic density fraction contains a homolog of the Drosophila discs-large tumor suppressor protein. Neuron 9, 929–942.

Citri, A., Malenka, R.C., 2007. Synaptic plasticity: multiple forms, functions, and mechanisms. Neuropsychopharmacology 33, 18–41.

Coghlan, V.M., Perrino, B.A., Howard, M., Langeberg, L.K., Hicks, J.B., Gallatin, W.M., Scott, J.D., 1995. Association of protein kinase A and protein phosphatase 2B with a common anchoring protein. Science (80-.). 267, 108–111.

Colledge, M., Dean, R.A., Scott, G.K., Langeberg, L.K., Huganir, R.L., Scott, J.D., 2000. Targeting of PKA to glutamate receptors through a MAGUK-AKAP complex. Neuron 27, 107–119.

Coultrap, S.J., Barcomb, K., Bayer, K.U., 2012. A significant but rather mild contribution of T286 autophosphorylation to Ca2+/CaM-stimulated CaMKII activity. PLoS One 7, e37176.

Cowles, M.K., Carlin, B.P., 1996. Markov Chain Monte Carlo Convergence Diagnostics: A Comparative Review. J. Am. Stat. Assoc. 91, 883–904. doi:10.1080/01621459.1996.10476956

d'Alcantara, P., Schiffmann, S.N., Swillens, S., 2003. Bidirectional synaptic plasticity as a consequence of interdependent Ca2+ - controlled phosphorylation and dephosphorylation pathways. Eur. J. Neurosci. 17, 2521–2528. doi:10.1046/j.1460-9568.2003.02693.x

Davis, S., Butcher, S.P., Morris, R.G., 1992. The NMDA receptor antagonist D-2-amino-5-phosphonopentanoate (D-AP5) impairs spatial learning and LTP in vivo at intracerebral concentrations comparable to those that block LTP in vitro. J. Neurosci. 12, 21–34.

De Jong, A.P.H., Verhage, M., 2009. Presynaptic signal transduction pathways that modulate synaptic transmission. Curr Opin Neurobiol 19, 245–253. doi:10.1016/j.conb.2009.06.005

Dell'Acqua, M.L., Dodge, K.L., Tavalin, S.J., Scott, J.D., 2002. Mapping the Protein Phosphatase-2B Anchoring Site on AKAP79 Binding and Inhibition of Phosphatase Activity are Mediated by Residues 315–360. J. Biol. Chem. 277, 48796–48802.

Dell'Acqua, M.L., Faux, M.C., Thorburn, J., Thorburn, A., Scott, J.D., 1998. Membrane-targeting sequences on AKAP79 bind phosphatidylinositol-4, 5-bisphosphate. Embo J 17, 2246–2260.

Derkach, V., Barria, A., Soderling, T.R., 1999. Ca2+/calmodulin-kinase II enhances channel conductance of α-amino-3-hydroxy-5-methyl-4-isoxazolepropionate type glutamate receptors. Proc. Natl. Acad. Sci. 96, 3269–3274.

Dosemeci, A., Albers, R.W., 1996. A mechanism for synaptic frequency detection through autophosphorylation of CaM kinase II. Biophys J 70, 2493–2501. doi:10.1016/s0006-3495(96)79821-1

Dudek, S., Bear, M., 1993. Bidirectional long-term modification of synaptic effectiveness in the adult and immature hippocampus. J. Neurosci. 13, 2910–2918.

Dudek, S.M., Bear, M.F., 1992. Homosynaptic long-term depression in area CA1 of hippocampus and effects of N-methyl-D-aspartate receptor blockade. Proc. Natl. Acad. Sci. 89, 4363–4367.

Dupont, G., Houart, G., De Koninck, P., 2003. Sensitivity of CaM kinase II to the frequency of Ca2+ oscillations: a simple model. Cell Calcium 34, 485–497.

Efendiev, R., Samelson, B.K., Nguyen, B.T., Phatarpekar, P. V, Baameur, F., Scott, J.D., Dessauer, C.W., 2010. AKAP79 Interacts with Multiple Adenylyl Cyclase (AC) Isoforms and Scaffolds AC5 and-6 to α-Amino-3-hydroxyl-5-methyl-4-isoxazole-propionate (AMPA) Receptors. J. Biol. Chem. 285, 14450–14458.

Ehlers, M.D., 2000. Reinsertion or Degradation of AMPA Receptors Determined by Activity-Dependent Endocytic Sorting. Neuron 28, 511–525. doi:http://dx.doi.org/10.1016/S0896-6273(00)00129-X

Ehlers, M.D., 2003. Activity level controls postsynaptic composition and signaling via the ubiquitin-proteasome system. Nat Neurosci 6, 231–242.

Ehrlich, I., Klein, M., Rumpel, S., Malinow, R., 2007. PSD-95 is required for activity-driven synapse stabilization. Proc. Natl. Acad. Sci. 104, 4176–4181. doi:10.1073/pnas.0609307104

Elgersma, Y., Fedorov, N.B., Ikonen, S., Choi, E.S., Elgersma, M., Carvalho, O.M., Giese, K.P., Silva, A.J., 2002. Inhibitory autophosphorylation of CaMKII controls PSD association, plasticity, and learning. Neuron 36, 493–505.

Engert, F., Bonhoeffer, T., 1999. Dendritic spine changes associated with hippocampal long-term synaptic plasticity. Nature 399, 66–70. doi:http://www.nature.com/nature/journal/v399/n6731/suppinfo/399066a0_S1.html

Erreger, K., Dravid, S.M., Banke, T.G., Wyllie, D.J.A., Traynelis, S.F., 2005. Subunit‐specific gating controls rat NR1/NR2A and NR1/NR2B NMDA channel kinetics and synaptic signalling profiles. J Physiol 563, 345–358.

Esteban, J.A., Shi, S.-H., Wilson, C., Nuriya, M., Huganir, R.L., Malinow, R., 2003. PKA phosphorylation of AMPA receptor subunits controls synaptic trafficking underlying plasticity. Nat Neurosci 6, 136–143.

Ferguson, G.D., Storm, D.R., 2004. Why calcium-stimulated adenylyl cyclases? Physiology (Bethesda). 19, 271–6. doi:10.1152/physiol.00010.2004

Fong, Y.L., Taylor, W.L., Means, A.R., Soderling, T.R., 1989. Studies of the regulatory mechanism of Ca2+/calmodulin-dependent protein kinase II. Mutation of threonine 286 to alanine and aspartate. J. Biol. Chem. 264, 16759–16763.

Frey, U., Huang, Y.Y., Kandel, E.R., 1993. Effects of cAMP simulate a late stage of LTP in hippocampal CA1 neurons. Science (80-.). 260, 1661–1664.

Fukazawa, Y., Saitoh, Y., Ozawa, F., Ohta, Y., Mizuno, K., Inokuchi, K., 2003. Hippocampal LTP is accompanied by enhanced F-actin content within the dendritic spine that is essential for late LTP maintenance in vivo. Neuron 38, 447–460.

Gardoni, F., Caputi, A., Cimino, M., Pastorino, L., Cattabeni, F., Di Luca, M., 1998. Calcium/Calmodulin‐Dependent Protein Kinase II Is Associated with NR2A/B Subunits of NMDA Receptor in Postsynaptic Densities. J Neurochem 71, 1733–1741.

Garner, C.C., Nash, J., Huganir, R.L., 2000. PDZ domains in synapse assembly and signalling. Trends Cell Biol 10, 274–280.

Giese, K.P., Fedorov, N.B., Filipkowski, R.K., Silva, A.J., 1998. Autophosphorylation at Thr286 of the α calcium-calmodulin kinase II in LTP and learning. Science (80-.). 279, 870–873. doi:10.1126/science.279.5352.870

Goh, J.J., Manahan-Vaughan, D., 2014. Role of inhibitory autophosphorylation of Calcium/Calmodulin-dependent kinase II (αCAMKII) in persistent (> 24h) hippocampal LTP and in LTD facilitated by novel object-place learning and recognition in mice. Behav Brain Res.

Gold, M.G., Lygren, B., Dokurno, P., Hoshi, N., McConnachie, G., Taskén, K., Carlson, C.R., Scott, J.D., Barford, D., 2006. Molecular basis of AKAP specificity for PKA regulatory subunits. Mol. Cell 24, 383–95. doi:10.1016/j.molcel.2006.09.006

Goldberg, S., 1986. Probability: An Introduction. Dover Publications.

Gomez, L.L., Alam, S., Smith, K.E., Horne, E., Dell'Acqua, M.L., 2002. Regulation of A-kinase anchoring protein 79/150–cAMP-dependent protein kinase postsynaptic targeting by NMDA receptor activation of calcineurin and remodeling of dendritic actin. J. Neurosci. 22, 7027–7044.

Gomperts, B.D., Kramer, Ij.M., Tatham, P.E.R., 2009. Signal Transduction, Signal Transduction. Elsevier. doi:10.1016/B978-0-12-369441-6.00005-2

Gorski, J.A., Gomez, L.L., Scott, J.D., Dell'Acqua, M.L., 2005. Association of an A-kinase-anchoring protein signaling scaffold with cadherin adhesion molecules in neurons and epithelial cells. Mol Biol Cell 16, 3574–3590.

Grant, S.G.N., Silva, A.J., 1994. Targeting learning. Trends Neurosci 17, 71–75.

Graupner, M., Brunel, N., 2007. STDP in a bistable synapse model based on CaMKII and associated signaling pathways. PLoS Comput Biol 3, e221.

Haario, H., Laine, M., Mira, A., Saksman, E., 2006. DRAM: efficient adaptive MCMC. Stat. Comput. 16, 339–354.

Haario, H., Saksman, E., Tamminen, J., 2001. An adaptive Metropolis algorithm. Bernoulli 223–242.

Halt, A.R., Dallapiazza, R.F., Zhou, Y., Stein, I.S., Qian, H., Juntti, S., Wojcik, S., Brose, N., Silva, A.J., Hell, J.W., 2012. CaMKII binding to GluN2B is critical during memory consolidation. Embo J 31, 1203–1216.

Hastings, W.K., 1970. Monte Carlo sampling methods using Markov chains and their applications. Biometrika 57, 97–109. doi:10.1093/biomet/57.1.97

Hayashi, Y., Shi, S.-H., Esteban, J.A., Piccini, A., Poncer, J.-C., Malinow, R., 2000. Driving AMPA receptors into synapses by LTP and CaMKII: requirement for GluR1 and PDZ domain interaction. Sci. Signal. 287, 2262.

Hayer, A., Bhalla, U.S., 2005. Molecular switches at the synapse emerge from receptor and kinase traffic. PLoS Comput Biol 1, e20.

He, K., Song, L., Cummings, L.W., Goldman, J., Huganir, R.L., Lee, H.-K., 2009. Stabilization of Ca2+-permeable AMPA receptors at perisynaptic sites by GluR1-S845 phosphorylation. Proc. Natl. Acad. Sci. 106, 20033–20038.

He, Y., Kulasiri, D., Samarasinghe, S., 2014. Systems biology of synaptic plasticity: a review on N-methyl-D-aspartate receptor mediated biochemical pathways and related mathematical models. Biosystems. 122, 7–18. doi:10.1016/j.biosystems.2014.06.005

Hebb, D.O., 2002. The organization of behavior: A neuropsychological theory. Psychology Press.

Hemmings, H.C., Nairn, A.C., Greengard, P., 1984. DARPP-32, a dopamine- and adenosine 3':5'-monophosphate-regulated neuronal phosphoprotein. II. Comparison of the kinetics of phosphorylation of DARPP-32 and phosphatase inhibitor 1. J. Biol. Chem. 259, 14491–7.

Hill, A., 1910. The possible effects of the aggregation of the molecules of haemoglobin on its dissociation curves. J. Physiol. 40.

Hoffmann, R., Wilkinson, I.R., McCallum, J.F., Engels, P., Houslay, M.D., 1998. cAMP-specific phosphodiesterase HSPDE4D3 mutants which mimic activation and changes in rolipram inhibition triggered by protein kinase A phosphorylation of Ser-54: generation of a molecular model. Biochem. J. 333 (Pt 1, 139–49.

Hofmann, F., Bechtel, P.J., Krebs, E.G., 1977. Concentrations of cyclic AMP-dependent protein kinase subunits in various tissues. J. Biol. Chem. 252, 1441–1447.

Holcman, D., Triller, A., 2006. Modeling synaptic dynamics driven by receptor lateral diffusion. Biophys J 91, 2405–2415.

Holmes, W.R., 2000. Models of calmodulin trapping and CaM kinase II activation in a dendritic spine. J Comput Neurosci 8, 65–86.

Holmes, W.R., Levy, W.B., 1990. Insights into associative long-term potentiation from computational models of NMDA receptor-mediated calcium influx and intracellular calcium concentration changes. J Neurophysiol 63, 1148–1168.

Horne, E.A., Dell'Acqua, M.L., 2007. Phospholipase C is required for changes in postsynaptic structure and function associated with NMDA receptor-dependent long-term depression. J. Neurosci. 27, 3523–3534.

Huang, A.-M., Lee, E.H.Y., 1995. Role of hippocampal nitric oxide in memory retention in rats. Pharmacol. Biochem. Behav. 50, 327–332.

Huang, K.X., Paudel, H.K., 2000. Ser67-phosphorylated inhibitor 1 is a potent protein phosphatase 1 inhibitor. Proc. Natl. Acad. Sci. U. S. A. 97, 5824–9. doi:10.1073/pnas.100460897

Hudmon, A., Schulman, H., 2002. Structure–function of the multifunctional Ca2+/calmodulin-dependent protein kinase II. Biochem. J 364, 593–611.

Hulme, E.C., Trevethick, M.A., 2010. Ligand binding assays at equilibrium: validation and interpretation. Br. J. Pharmacol. 161, 1219–37. doi:10.1111/j.1476-5381.2009.00604.x

Huynh, Q.K., Pagratis, N., 2011. Kinetic mechanisms of Ca++/calmodulin dependent protein kinases. Arch. Biochem. Biophys. 506, 130–6. doi:10.1016/j.abb.2010.11.008

Irvine, E.E., Von Hertzen, L.S.J., Plattner, F., Giese, K.P., 2006. αCaMKII autophosphorylation: a fast track to memory. Trends Neurosci 29, 459–465.

Isaac, J.T.R., Nicoll, R.A., Malenka, R.C., 1995. Evidence for silent synapses: implications for the expression of LTP. Neuron 15, 427–434.

Kakiuchi, S., Yasuda, S., Yamazakiy, R., Teshima, Y., Kanda, K., Kakiuchi, R., Sobue, K., 1982. Quantitative Determinations of Calmodulin in the Supernatant and Particulate Fractions of Mammalian Tissues. J Biochem 92, 1041–1048.

Kandel, E.R., 2009. The biology of memory: a forty-year perspective. J. Neurosci. 29, 12748–12756. doi:10.1523/jneurosci.3958-09.2009

Keith, D.J., Sanderson, J.L., Gibson, E.S., Woolfrey, K.M., Robertson, H.R., Olszewski, K., Kang, R., El-Husseini, A., Dell'Acqua, M.L., 2012. Palmitoylation of A-kinase anchoring protein 79/150 regulates dendritic endosomal targeting and synaptic plasticity mechanisms. J. Neurosci. 32, 7119–7136.

Keller, C.H., Olwin, B.B., LaPorte, D.C., Storm, D.R., 1982. Determination of the free-energy coupling for binding of calcium ion and troponin I to calmodulin. Biochemistry 21, 156–162.

Kim, M., Huang, T., Abel, T., Blackwell, K.T., 2010. Temporal sensitivity of protein kinase a activation in late-phase long term potentiation. PLoS Comput. Biol. 6, e1000691. doi:10.1371/journal.pcbi.1000691

Kim, M., Park, A.J., Havekes, R., Chay, A., Guercio, L.A., Oliveira, R.F., Abel, T., Blackwell, K.T., 2011. Colocalization of protein kinase A with adenylyl cyclase enhances protein kinase A activity during induction of long-lasting long-term-potentiation. PLoS Comput. Biol. 7, e1002084. doi:10.1371/journal.pcbi.1002084

Kitagawa, Y., Hirano, T., Kawaguchi, S.Y., 2009. Prediction and validation of a mechanism to control the threshold for inhibitory synaptic plasticity. Mol. Syst. Biol. 5, 280.

Kitano, H., 2007. Towards a theory of biological robustness. Mol. Syst. Biol. 3.

Klauck, T.M., Faux, M.C., Labudda, K., Langeberg, L.K., Jaken, S., Scott, J.D., 1996. Coordination of three signaling enzymes by AKAP79, a mammalian scaffold protein. Science (80-.). 271, 1589–1592.

Klee, C.B., Ren, H., Wang, X., 1998. Regulation of the Calmodulin-stimulated Protein Phosphatase, Calcineurin. J. Biol. Chem. 273, 13367–13370. doi:10.1074/jbc.273.22.13367

Kotaleski, J.H., Blackwell, K.T., 2010. Modelling the molecular mechanisms of synaptic plasticity using systems biology approaches. Nat. Rev. Neurosci. 11, 239–251.

Kubota, Y., Bower, J.M., 2001. Transient versus asymptotic dynamics of CaM kinase II: possible roles of phosphatase. J Comput Neurosci 11, 263–279.

Kumar, A., 2011. Long-Term Potentiation at CA3-CA1 Hippocampal Synapses with Special Emphasis on Aging, Disease, and Stress. Front. Aging Neurosci. 3, 7. doi:10.3389/fnagi.2011.00007

LaPorte, D.C., Wierman, B.M., Storm, D.R., 1980. Calcium-induced exposure of a hydrophobic surface on calmodulin. Biochemistry 19, 3814–3819.

Lee, H.-K., Barbarosie, M., Kameyama, K., Bear, M.F., Huganir, R.L., 2000. Regulation of distinct AMPA receptor phosphorylation sites during bidirectional synaptic plasticity. Nature 405, 955–959.

Lee, H.-K., Takamiya, K., He, K., Song, L., Huganir, R.L., 2010. Specific Roles of AMPA Receptor Subunit GluR1 (GluA1) Phosphorylation Sites in Regulating Synaptic Plasticity in the CA1 Region of Hippocampus. J Neurophysiol 103, 479–489. doi:10.1152/jn.00835.2009

Lee, S.-J.J.R., Escobedo-Lozoya, Y., Szatmari, E.M., Yasuda, R., 2009. Activation of CaMKII in single dendritic spines during long-term potentiation. Nature 458, 299–304. doi:http://www.nature.com/nature/journal/v458/n7236/suppinfo/nature07842_S1.html

Leonard, A.S., Lim, I.A., Hemsworth, D.E., Horne, M.C., Hell, J.W., 1999. Calcium/calmodulin-dependent protein kinase II is associated with the N-methyl-D-aspartate receptor. Proc. Natl. Acad. Sci. 96, 3239–3244.

Li, S., Hong, S., Shepardson, N.E., Walsh, D.M., Shankar, G.M., Selkoe, D., 2009. Soluble oligomers of amyloid Beta protein facilitate hippocampal long-term depression by disrupting neuronal glutamate uptake. Neuron 62, 788–801. doi:10.1016/j.neuron.2009.05.012

Lin, J.W., Wyszynski, M., Madhavan, R., Sealock, R., Kim, J.U., Sheng, M., 1998. Yotiao, a novel protein of neuromuscular junction and brain that interacts with specific splice variants of NMDA receptor subunit NR1. J. Neurosci. 18, 2017–2027.

Ling, H., Kulasiri, D., Samarasinghe, S., 2010. Robustness of G1/S checkpoint pathways in cell cycle regulation based on probability of DNA-damaged cells passing as healthy cells. Biosystems 101, 213–221.

Lisman, J.E., 1989. A mechanism for the Hebb and the anti-Hebb processes underlying learning and memory. Proc Natl Acad Sci U S A 86, 9574–9578.

Lisman, J.E., McIntyre, C.C., 2001. Synaptic plasticity: a molecular memory switch. Curr. Biol. 11, R788–R791.

Lisman, J.E., Schulman, H., Cline, H., 2002. The molecular basis of CaMKII function in synaptic and behavioural memory. Nat. Rev. Neurosci. 3, 175–190.

Lisman, J.E., Yasuda, R., Raghavachari, S., 2012. Mechanisms of CaMKII action in long-term potentiation. Nat. Rev. Neurosci. 13, 169–182.

Lisman, J.E., Zhabotinsky, A.M., 2001. A model of synaptic memory: a CaMKII/PP1 switch that potentiates transmission by organizing an AMPA receptor anchoring assembly. Neuron 31, 191–201. doi:10.1016/s0896-6273(01)00364-6

Liu, L., Wong, T.P., Pozza, M.F., Lingenhoehl, K., Wang, Y., Sheng, M., Auberson, Y.P., Wang, Y.T., 2004. Role of NMDA receptor subtypes in governing the direction of hippocampal synaptic plasticity. Science (80-.). 304, 1021–1024.

Lou, L.L., Lloyd, S.J., Schulman, H., 1986. Activation of the multifunctional Ca2+/calmodulin-dependent protein kinase by autophosphorylation: ATP modulates production of an autonomous enzyme. Proc. Natl. Acad. Sci. 83, 9497–9501.

Lugnier, C., 2006. Cyclic nucleotide phosphodiesterase (PDE) superfamily: a new target for the development of specific therapeutic agents. Pharmacol. Ther. 109, 366–398.

Lüscher, C., Malenka, R.C., 2012. NMDA receptor-dependent long-term potentiation and long-term depression (LTP/LTD). Cold Spring Harb Perspect Biol 4.

Lüscher, C., Xia, H., Beattie, E.C., Carroll, R.C., von Zastrow, M., Malenka, R.C., Nicoll, R.A., 1999. Role of AMPA receptor cycling in synaptic transmission and plasticity. Neuron 24, 649–658.

Malenka, R.C., Kauer, J.A., Perkel, D.J., Mauk, M.D., Kelly, P.T., Nicoll, R.A., Waxham, M.N., 1989. An essential role for postsynaptic calmodulin and protein kinase activity in long-term potentiation. Nature 340, 554–557.

Manninen, T., Hituri, K., Kotaleski, J.H., Blackwell, K.T., Linne, M.-L., 2010. Postsynaptic signal transduction models for long-term potentiation and depression. Front. Comput. Neurosci. 4, 152. doi:10.3389/fncom.2010.00152

Marino, S., Hogue, I.B., Ray, C.J., Kirschner, D.E., 2008. A methodology for performing global uncertainty and sensitivity analysis in systems biology. J. Theor. Biol. 254, 178–196.

Mayer, M.L., Westbrook, G.L., Guthrie, P.B., 1984. Voltage-dependent block by Mg2+ of NMDA responses in spinal cord neurones. Nature 309, 261–3.

Mayford, M., Siegelbaum, S.A., Kandel, E.R., 2012. Synapses and memory storage. Cold Spring Harb Perspect Biol 4.

McKay, M.D., Beckman, R.J., Conover, W.J., 1979. A Comparison of three methods for selecting values of input variables in the analysis of output from a computer code. Technometrics 21, 239–245.

Metropolis, N., Rosenbluth, A.W., Rosenbluth, M.N., Teller, A.H., Teller, E., 1953. Equation of State Calculations by Fast Computing Machines. J. Chem. Phys. 21, 1087. doi:10.1063/1.1699114

Meyer, T., Hanson, P.I., Stryer, L., Schulman, H., 1992. Calmodulin trapping by calcium-calmodulin-dependent protein kinase. Science (80-.). 256, 1199–1202.

Michaelis, L., Menten, M., 1913. {Die kinetik der invertinwirkung}. Biochem. Z 49.

Miller, P., Zhabotinsky, A.M., Lisman, J.E., Wang, X.-J.J., 2005. The stability of a stochastic CaMKII switch: dependence on the number of enzyme molecules and protein turnover. PLoS Biol 3, e107.

Miller, S.G., Kennedy, M.B., 1986. Regulation of brain Type II Ca2+ calmodulin-dependent protein kinase by autophosphorylation: A Ca< sup> 2+</sup>-triggered molecular switch. Cell 44, 861–870.

Miller, S.G., Patton, B.L., Kennedy, M.B., 1988. Sequences of autophosphorylation sites in neuronal type II CaM kinase that control Ca 2+-independent activity. Neuron 1, 593–604.

Morgado-Bernal, I., 2011. Learning and memory consolidation: linking molecular and behavioral data. Neuroscience 176, 12–19.

Morris, R.G., 1989. Synaptic plasticity and learning: selective impairment of learning rats and blockade of long-term potentiation in vivo by the N-methyl-D-aspartate receptor antagonist AP5. J. Neurosci. 9, 3040–3057.

Morris, R.G.M., Garrud, P., Rawlins, J.N.P., O'Keefe, J., 1982. Place navigation impaired in rats with hippocampal lesions. Nature 297, 681–683.

Mulkey, R.M., Endo, S., Shenolikar, S., Malenka, R.C., 1994. Involvement of a calcineurin/ inhibitor-1 phosphatase cascade in hippocampal long-term depression. Nature 369, 486–488.

Mulkey, R.M., Herron, C.E., Malenka, R.C., 1993. An essential role for protein phosphatases in hippocampal long-term depression. Science (80-.). 261, 1051–1055.

Mullasseril, P., Dosemeci, A., Lisman, J.E., Griffith, L.C., 2007. A structural mechanism for maintaining the "on‐state"of the CaMKII memory switch in the post‐synaptic density. J Neurochem 103, 357–364.

Naoki, H., Sakumura, Y., Ishii, S., 2005. Local signaling with molecular diffusion as a decoder of Ca2+ signals in synaptic plasticity. Mol. Syst. Biol. 1.

Nowak, L., Bregestovski, P., Ascher, P., Herbet, A., Prochiantz, A., 1984. Magnesium gates glutamate-activated channels in mouse central neurones. Nature 307, 462–465. doi:10.1038/307462a0

Oh, M.C., Derkach, V.A., Guire, E.S., Soderling, T.R., 2006. Extrasynaptic membrane trafficking regulated by GluR1 serine 845 phosphorylation primes AMPA receptors for long-term potentiation. J. Biol. Chem. 281, 752–758.

Okamoto, K., Bosch, M., Hayashi, Y., 2009. The roles of CaMKII and F-actin in the structural plasticity of dendritic spines: a potential molecular identity of a synaptic tag? Physiology (Bethesda). 24, 357–66. doi:10.1152/physiol.00029.2009

Oliveira, R.F., Kim, M., Blackwell, K.T., 2012. Subcellular location of PKA controls striatal plasticity: stochastic simulations in spiny dendrites. PLoS Comput. Biol. 8, e1002383. doi:10.1371/journal.pcbi.1002383

Oliveria, S.F., Gomez, L.L., Dell'Acqua, M.L., 2003. Imaging kinase–AKAP79–phosphatase scaffold complexes at the plasma membrane in living cells using FRET microscopy. J Cell Biol 160, 101–112.

Olwin, B.B., Storm, D.R., 1985. Calcium binding to complexes of calmodulin and calmodulin binding proteins. Biochemistry 24, 8081–8086.

Opazo, P., Labrecque, S., Tigaret, C.M., Frouin, A., Wiseman, P.W., De Koninck, P., Choquet, D., 2010. CaMKII triggers the diffusional trapping of surface AMPARs through phosphorylation of stargazin. Neuron 67, 239–252.

Otmakhov, N., Tao-Cheng, J.-H., Carpenter, S., Asrican, B., Dosemeci, A., Reese, T.S., Lisman, J.E., 2004. Persistent accumulation of calcium/calmodulin-dependent protein kinase II in dendritic spines after induction of NMDA receptor-dependent chemical long-term potentiation. J. Neurosci. 24, 9324–9331.

Otmakhova, N.A., Otmakhov, N., Mortenson, L.H., Lisman, J.E., 2000. Inhibition of the cAMP Pathway Decreases Early Long-Term Potentiation at CA1 Hippocampal Synapses. J. Neurosci. 20, 4446–4451.

Pantaloni, D., Le Clainche, C., Carlier, M.-F., 2001. Mechanism of actin-based motility. Science (80-.). 292, 1502–1506.

Peersen, O.B., Madsen, T.S., Falke, J.J., 1997. Intermolecular tuning of calmodulin by target peptides and proteins: differential effects on Ca2+ binding and implications for kinase activation. Protein Sci. 6, 794–807.

Pepke, S., Kinzer-Ursem, T., Mihalas, S., Kennedy, M.B., 2010. A dynamic model of interactions of Ca2+, calmodulin, and catalytic subunits of Ca2+/calmodulin-dependent protein kinase II. PLoS Comput Biol 6, e1000675.

Polli, J.W., Kincaid, R.L., 1994. Expression of a calmodulin-dependent phosphodiesterase isoform (PDE1B1) correlates with brain regions having extensive dopaminergic innervation. J. Neurosci. 14, 1251–61.

Purves, D., Augustine, G.J., Fitzpatrick, D., Hall, W.C., LaMantia, A.S., McNamara, J.O., White, L.E., 2008. Neuroscience, Fourth. ed, De Boeck, Sinauer, Sunderland, Mass. Sinauer Associates © 2008 Sinauer Associates and Sumanas, Inc.

Puyal, J., Grassi, S., Dieni, C., Frondaroli, A., Demêmes, D., Raymond, J., Pettorossi, V.E., 2003. Developmental shift from long-term depression to long-term potentiation in the rat medial vestibular nuclei: role of group I metabotropic glutamate receptors. J Physiol 553, 427–443.

Quintana, A.R., Wang, D., Forbes, J.E., Waxham, M.N., 2005. Kinetics of calmodulin binding to calcineurin. Biochem. Biophys. Res. Commun. 334, 674–80. doi:10.1016/j.bbrc.2005.06.152

Ribrault, C., Sekimoto, K., Triller, A., 2011. From the stochasticity of molecular processes to the variability of synaptic transmission. Nat. Rev. Neurosci. 12, 375–387.

Robertson, H.R., Gibson, E.S., Benke, T.A., Dell'Acqua, M.L., 2009. Regulation of postsynaptic structure and function by an A-kinase anchoring protein–membrane-associated guanylate kinase scaffolding complex. J. Neurosci. 29, 7929–7943.

Robison, A.J., Bass, M.A., Jiao, Y., MacMillan, L.B., Carmody, L.C., Bartlett, R.K., Colbran, R.J., 2005. Multivalent interactions of calcium/calmodulin-dependent protein kinase II with the

postsynaptic density proteins NR2B, densin-180, and α-actinin-2. J. Biol. Chem. 280, 35329–35336. doi:10.1074/jbc.M502191200

Saitoh, T., Schwartz, J.H., 1985. Phosphorylation-dependent subcellular translocation of a Ca2+/calmodulin-dependent protein kinase produces an autonomous enzyme in Aplysia neurons. J Cell Biol 100, 835–842.

Sanderson, J.L., Dell'Acqua, M.L., 2011. AKAP signaling complexes in regulation of excitatory synaptic plasticity. Neurosci. 17, 321–336.

Sanderson, J.L., Gorski, J.A., Gibson, E.S., Lam, P., Freund, R.K., Chick, W.S., Dell'Acqua, M.L., 2012. AKAP150-anchored calcineurin regulates synaptic plasticity by limiting synaptic incorporation of Ca2+-permeable AMPA receptors. J. Neurosci. 32, 15036–15052.

Scozzari, R., Massaia, A., D'Atanasio, E., Myres, N.M., Perego, U.A., Trombetta, B., Cruciani, F., 2012. On the Mechanism of Synaptic Depression Induced by CaMKIIN, an Endogenous Inhibitor of CaMKII. PLoS One 7.

Shankar, G.M., Li, S., Mehta, T.H., Garcia-Munoz, A., Shepardson, N.E., Smith, I., Brett, F.M., Farrell, M.A., Rowan, M.J., Lemere, C.A., Regan, C.M., Walsh, D.M., Sabatini, B.L., Selkoe, D.J., 2008. Amyloid-beta protein dimers isolated directly from Alzheimer's brains impair synaptic plasticity and memory. Nat. Med. 14, 837–42. doi:10.1038/nm1782

Shapiro, M., 2001. Plasticity, Hippocampal Place Cells, and Cognitive Maps. Arch. Neurol. 58, 874. doi:10.1001/archneur.58.6.874

Sharma, R., Wang, J., 1986. Calmodulin and Ca2+-dependent phosphorylation and dephosphorylation of 63-kDa subunit-containing bovine brain calmodulin-stimulated cyclic nucleotide phosphodiesterase isozyme. J. Biol. Chem. 261, 1322–1328.

Shen, K., Meyer, T., 1999. Dynamic control of CaMKII translocation and localization in hippocampal neurons by NMDA receptor stimulation. Science (80-.). 284, 162–167.

Shen, K., Teruel, M.N., Connor, J.H., Shenolikar, S., Meyer, T., 2000. Molecular memory by reversible translocation of calcium/calmodulin-dependent protein kinase II. Nat Neurosci 3, 881–886.

Shen, K., Teruel, M.N., Subramanian, K., Meyer, T., 1998. CaMKIIβ functions as an F-actin targeting module that localizes CaMKIIα/β heterooligomers to dendritic spines. Neuron 21, 593–606.

Sheng, M., Hoogenraad, C.C., 2007. The postsynaptic architecture of excitatory synapses: a more quantitative view. Annu. Rev. Biochem. 76, 823–847.

Shinohara, Y., Hirase, H., Watanabe, M., Itakura, M., Takahashi, M., Shigemoto, R., 2008. Left-right asymmetry of the hippocampal synapses with differential subunit allocation of glutamate receptors. Proc. Natl. Acad. Sci. 105, 19498–19503.

Shoji-Kasai, Y., Ageta, H., Hasegawa, Y., Tsuchida, K., Sugino, H., Inokuchi, K., 2007. Activin increases the number of synaptic contacts and the length of dendritic spine necks by modulating spinal actin dynamics. J. Cell Sci. 120, 3830–7. doi:10.1242/jcs.012450

Silva, A.J., Paylor, R., Wehner, J.M., Tonegawa, S., 1992a. Impaired spatial learning in alpha-calcium-calmodulin kinase II mutant mice. Science (80-.). 257, 206–211. doi:10.1126/science.1321493

Silva, A.J., Stevens, C.F., Tonegawa, S., Wang, Y., 1992b. Deficient hippocampal long-term potentiation in alpha-calcium-calmodulin kinase II mutant mice. Science (80-.). 257, 201–206.

Smith, K.E., Gibson, E.S., Dell'Acqua, M.L., 2006. cAMP-dependent protein kinase postsynaptic localization regulated by NMDA receptor activation through translocation of an A-kinase anchoring protein scaffold protein. J. Neurosci. 26, 2391–2402.

Snyder, G.L., Galdi, S., Fienberg, A.A., Allen, P., Nairn, A.C., Greengard, P., 2003. Regulation of AMPA receptor dephosphorylation by glutamate receptor agonists. Neuropharmacology 45, 703–713.

Spiller, D.G., Wood, C.D., Rand, D.A., White, M.R.H., 2010. Measurement of single-cell dynamics. Nature 465, 736–745. doi:http://www.nature.com/nature/journal/v465/n7299/abs/nature09232.html#supplementary-information

Stanton, P.K., Bramham, C., Scharfman, H.E., 2005. Synaptic plasticity and transsynaptic signaling. Springer.

Stemmer, P., Klee, C.B., 1991. Serine/threonine phosphatases in the nervous system. Curr Opin Neurobiol 1, 53–64.

Stemmer, P.M., Klee, C.B., 1994. Dual Calcium Ion Regulation of Calcineurin by Calmodulin and Calcineurin B. Biochemistry 33, 6859–6866. doi:10.1021/bi00188a015

Stevens, C.F., 2004. Presynaptic function. Curr Opin Neurobiol 14, 341–345.

Strack, S., Colbran, R.J., 1998. Autophosphorylation-dependent targeting of calcium/calmodulin-dependent protein kinase II by the NR2B subunit of theN-methyl-D-aspartate receptor. J. Biol. Chem. 273, 20689–20692.

Strack, S., McNeill, R.B., Colbran, R.J., 2000. Mechanism and regulation of calcium/calmodulin-dependent protein kinase II targeting to the NR2B subunit of the N-methyl-D-aspartate receptor. J. Biol. Chem. 275, 23798–23806.

Stratton, M.M., Chao, L.H., Schulman, H., Kuriyan, J., 2013. Structural studies on the regulation of Ca< sup> 2+</sup>/calmodulin dependent protein kinase II. Curr. Opin. Struct. Biol. 23, 292–301.

Su, Q., Zhao, M., Weber, E., Eugster, H.P., Ryffel, B., 1995. Distribution and activity of calcineurin in rat tissues. Evidence for post-transcriptional regulation of testis-specific calcineurin B. Eur. J. Biochem. 230, 469–74.

Südhof, T.C., 2004. The synaptic vesicle cycle. Annu. Rev. Neurosci. 27, 509–547.

Tavalin, S.J., Colledge, M., Hell, J.W., Langeberg, L.K., Huganir, R.L., Scott, J.D., 2002. Regulation of GluR1 by the A-kinase anchoring protein 79 (AKAP79) signaling complex shares properties with long-term depression. J. Neurosci. 22, 3044–3051.

Thiagarajan, T.C., Piedras-Renteria, E.S., Tsien, R.W., 2002. α-and βCaMKII: inverse regulation by neuronal activity and opposing effects on synaptic strength. Neuron 36, 1103–1114.

Tomita, S., Stein, V., Stocker, T.J., Nicoll, R.A., Bredt, D.S., 2005. Bidirectional synaptic plasticity regulated by phosphorylation of stargazin-like TARPs. Neuron 45, 269–277.

Tsien, J.Z., Chen, D.F., Gerber, D., Tom, C., Mercer, E.H., Anderson, D.J., Mayford, M., Kandel, E.R., Tonegawa, S., 1996. Subregion- and Cell Type-Restricted Gene Knockout in Mouse Brain. Cell 87, 1317–1326. doi:10.1016/s0092-8674(00)81826-7

Vest, R.S., Davies, K.D., O'Leary, H., Port, J.D., Bayer, K.U., 2007. Dual mechanism of a natural CaMKII inhibitor. Mol Biol Cell 18, 5024–5033.

Waage, P., Gulberg, C.M., 1986. Studies concerning affinity. J. Chem. Educ. 63, 1044. doi:10.1021/ed063p1044

Wang, H., Peng, M.-S., Chen, Y., Geng, J., Robinson, H., Houslay, M.D., Cai, J., Ke, H., 2007. Structures of the four subfamilies of phosphodiesterase-4 provide insight into the selectivity of their inhibitors. Biochem. J. 408, 193–201. doi:10.1042/BJ20070970

Wang, H., Pineda, V. V, Chan, G.C.K., Wong, S.T., Muglia, L.J., Storm, D.R., 2003. Type 8 adenylyl cyclase is targeted to excitatory synapses and required for mossy fiber long-term potentiation. J. Neurosci. 23, 9710–8.

Wang, H., Strom, D.R., 2003. Calmodulin-Regulated Adenylyl Cyclases: Cross-Talk and Plasticity in the Central Nervous System. Mol. Pharmacol. 63, 463–468. doi:10.1124/mol.63.3.463

Waxham, M.N., Aronowski, J., Westgate, S.A., Kelly, P.T., 1990. Mutagenesis of Thr-286 in monomeric Ca2+/calmodulin-dependent protein kinase II eliminates Ca2+/calmodulin-independent activity. Proc. Natl. Acad. Sci. 87, 1273–1277.

Weiss, J., 1997. The Hill equation revisited: uses and misuses. FASEB J 11, 835–841.

Weng, G., Bhalla, U.S., Iyengar, R., 1999. Complexity in Biological Signaling Systems. Science (80-.). 284, 92–96. doi:10.1126/science.284.5411.92

Westphal, R.S., Tavalin, S.J., Lin, J.W., Alto, N.M., Fraser, I.D.C., Langeberg, L.K., Sheng, M., Scott, J.D., 1999. Regulation of NMDA receptors by an associated phosphatase-kinase signaling complex. Science (80-.). 285, 93–96.

Willoughby, D., Masada, N., Wachten, S., Pagano, M., Halls, M.L., Everett, K.L., Ciruela, A., Cooper, D.M.F., 2010. AKAP79/150 interacts with AC8 and regulates Ca2+-dependent cAMP synthesis in pancreatic and neuronal systems. J. Biol. Chem. 285, 20328–20342.

Wollmuth, L.P., Sobolevsky, A.I., 2004. Structure and gating of the glutamate receptor ion channel. Trends Neurosci 27, 321–328.

Xia, Z., Storm, D.R., 2005. The role of calmodulin as a signal integrator for synaptic plasticity. Nat. Rev. Neurosci. 6, 267–276.

Yang, E., Schulman, H., 1999. Structural examination of autoregulation of multifunctional calcium/calmodulin-dependent protein kinase II. J. Biol. Chem. 274, 26199–26208.

Yang, S., Tang, Y., Zucker, R.S., 1999. Selective Induction of LTP and LTD by Postsynaptic [Ca2+]i Elevation. J Neurophysiol 81, 781–787.

Yang, Y., Wang, X., Frerking, M., Zhou, Q., 2008. Delivery of AMPA receptors to perisynaptic sites precedes the full expression of long-term potentiation. Proc. Natl. Acad. Sci. 105, 11388–11393.

Yashiro, K., Philpot, B.D., 2008. Regulation of NMDA receptor subunit expression and its implications for LTD, LTP, and metaplasticity. Neuropharmacology 55, 1081–1094.

Zador, A., Koch, C., Brown, T.H., 1990. Biophysical model of a Hebbian synapse. Proc. Natl. Acad. Sci. 87, 6718–6722.

Zawadzki, K.M., Taylor, S.S., 2004. cAMP-dependent protein kinase regulatory subunit type IIbeta: active site mutations define an isoform-specific network for allosteric signaling by cAMP. J. Biol. Chem. 279, 7029–36. doi:10.1074/jbc.M310804200

Zhabotinsky, A.M., 2000. Bistability in the Ca2+/Calmodulin-Dependent Protein Kinase-Phosphatase System. Biophys J 79, 2211–2221. doi:10.1016/s0006-3495(00)76469-1

Zhang, M., Storm, D.R., Wang, H., 2011. Bidirectional synaptic plasticity and spatial memory flexibility require Ca2+-stimulated adenylyl cyclases. J. Neurosci. 31, 10174–83. doi:10.1523/JNEUROSCI.0009-11.2011

Zhang, P., Smith-Nguyen, E. V, Keshwani, M.M., Deal, M.S., Kornev, A.P., Taylor, S.S., 2012. Structure and allostery of the PKA RIIβ tetrameric holoenzyme. Science 335, 712–6. doi:10.1126/science.1213979

Zhang, Y.-P., Holbro, N., Oertner, T.G., 2008. Optical induction of plasticity at single synapses reveals input-specific accumulation of αCaMKII. Proc. Natl. Acad. Sci. 105, 12039–12044.

Zheng, Z., Keifer, J., 2009. PKA has a critical role in synaptic delivery of GluR1-and GluR4-containing AMPARs during initial stages of acquisition of in vitro classical conditioning. J Neurophysiol 101, 2539–2549. doi:10.1152/jn.91282.2008

Zhou, Y., Takahashi, E., Li, W., Halt, A., Wiltgen, B., Ehninger, D., Li, G.-D., Hell, J.W., Kennedy, M.B., Silva, A.J., 2007. Interactions between the NR2B receptor and CaMKII modulate synaptic plasticity and spatial learning. J. Neurosci. 27, 13843–13853.